

2016

The Role of Green Leafy Plants in Atmospheric Chemistry: Volatile Emissions and Secondary Organic Aerosol

Rebecca Harvey
University of Vermont

Follow this and additional works at: <https://scholarworks.uvm.edu/graddis>



Part of the [Atmospheric Sciences Commons](#), and the [Chemistry Commons](#)

Recommended Citation

Harvey, Rebecca, "The Role of Green Leafy Plants in Atmospheric Chemistry: Volatile Emissions and Secondary Organic Aerosol" (2016). *Graduate College Dissertations and Theses*. 556.
<https://scholarworks.uvm.edu/graddis/556>

This Dissertation is brought to you for free and open access by the Dissertations and Theses at ScholarWorks @ UVM. It has been accepted for inclusion in Graduate College Dissertations and Theses by an authorized administrator of ScholarWorks @ UVM. For more information, please contact donna.omalley@uvm.edu.

The Role of Green Leafy Plants in Atmospheric Chemistry:
Volatile Emissions and Secondary Organic Aerosol

A Dissertation Presented

by

Rebecca M. Harvey

to

The Faculty of the Graduate College

of

The University of Vermont

In Partial Fulfillment of the Requirements
for the Degree of Doctor of Philosophy
Specializing in Chemistry

May, 2016

Defense Date: March 23, 2016
Dissertation Examination Committee:

Giuseppe A. Petrucci, Ph.D., Advisor

Paul Bierman Ph.D., Chairperson

Matthew Liptak, Ph.D.

Joel Goldberg, Ph.D.

Cynthia J. Forehand, Ph.D., Dean of the Graduate College

ABSTRACT

Aerosols play important roles in atmospheric and environmental processes. Not only do they impact human health, they also affect visibility and climate. Despite recent advances made to understand their sources and fate, there remains a limited understanding of the mechanisms that lead to the formation of aerosols and their ultimate fate in the atmosphere. These knowledge gaps provide the crux of the research reported herein, which has focused on identifying novel sources of atmospheric aerosol, characterizing its physical and optical properties, and rationalizing these properties using an in-depth knowledge of the molecular level mechanisms that led to its formation.

Upon mowing, turfgrasses emit large amounts of green leaf volatiles which can then be oxidized by ozone to form secondary organic aerosol (SOA). Overall, the mowing of lawns has the potential to contribute nearly 50 μg SOA per m^2 of lawn mowed. This SOA contribution is on the same order of magnitude as other predominant SOA sources (isoprene, monoterpenes, sesquiterpenes).

Turfgrasses represent an interesting and potentially meaningful SOA source because they contribute to SOA and also because they cover large land areas in close proximity to oxidant sources. Another related SOA precursor is sugarcane, which is in the same family as turfgrass and is among the largest agricultural crops worldwide. Globally, the ozonolysis of sugarcane has the potential to contribute 16 Mg SOA to the atmosphere, compared to global estimates of SOA loading that range from 12-70 Tg SOA.

In order to fully understand the role of atmospheric SOA on the radiative budget (and therefore climate), it is also important to understand its optical properties; its ability to absorb vs scatter light. Turfgrass and sugarcane produced SOA that was weakly absorbing while its scatter efficiency was wavelength and size-dependent. Interestingly, SOA formed under both dry (10% RH) and wet (70% RH) conditions had the same bulk chemical properties, yet significantly different optical properties, which was attributed to differences in molecular-level composition.

The work presented herein represents a unique, inclusive study of SOA precursors. A complete understanding of the chemistry leading to SOA formation is used to understand its physical and optical properties and evaluate these large-scale effects of SOA from these precursors.

CITATIONS

Material from this dissertation has been published in the following form:

Harvey, R. M.; Zahardis, J.; Petrucci, G. A.. Establishing the contribution of lawn mowing to atmospheric aerosol levels in American suburbs. *Atmos. Chem. Phys.* **2014**, *14* (2), 797-812.

Harvey, R. M.; Petrucci, G. A.. Control of ozonolysis kinetics and aerosol yield by nuances in the molecular structure of volatile organic compounds. *Atmos Environ* **2015**, *122*, 188-195.

Material from this dissertation has been submitted for publication to Environmental Science and Technology on February 4, 2016 in the following form:

Harvey, R. M.; Bateman, A. P.; Jain, S.; Li, Y. J.; Petrucci, G. A.; Martin, S. T.. The optical properties of GLV-Derived SOA: Effect of chemical composition, humidity and phase. *Environ Sci Technol.*

ACKNOWLEDGEMENTS

Mom, Dad, and Ryan: Thank you for your guidance, heartfelt love and unwavering support through this journey. Thank you for your faith when I am in doubt and for pushing me to exceed my own expectations.

Luna and Jade the Dogs: Thank you for keeping me centered and grounded, for greeting me every day with whole-body wiggles, for being the zest in my life and for loving me regardless of test scores and manuscript reviews.

Steven: You have shown me what it's like to have a partner with whom to face the world. I look forward to taking the rest of it on with you by my side. Thank you for your love, support and a friendship like no other.

Joe: Your support and guidance have been essential to this work but also in shaping me into the scientist and person I am today. Thank you for encouraging me to try new things, chase new dreams and then finding the money to pay for it all.

Shash: You've been a strong constant and dear friend supporting me in this work and also in my life. From classes to research to personal life, your support and level-headedness have helped me reach my goals.

TABLE OF CONTENTS

CITATIONS	II
ACKNOWLEDGEMENTS	III
LIST OF TABLES	VIII
LIST OF FIGURES AND REACTION SCHEMES	IX
LIST OF ABBREVIATIONS	XII
CHAPTER 1. BACKGROUND AND OUTLINE OF DISSERTATION	1
1.1 A Brief Rationale for the Research	1
1.2 Specific Research Questions Addressed in this Dissertation	2
1.3 Thesis Outline	2
1.4 References	3
CHAPTER 2. REVIEW OF THE CURRENT LITERATURE.....	5
2.1 Atmospheric Aerosols	5
2.2 SOA Precursors	6
2.3 Oxidation Mechanisms.....	9
2.3.1 Oxidation of Alkenes by OH	10
2.3.2 Oxidation of Alkenes by NO _x	11
2.3.3 Oxidation of Alkenes by O ₃	11
2.4 Secondary Organic Aerosols.....	13
2.5 References	15
CHAPTER 3. INSTRUMENTAL INFRASTRUCTURE.....	19
3.1 VOC Analysis	21
3.1.1 Thermal Desorption GC/MS	21
3.1.2 Solid Phase Microextraction GC/MS	23
3.2 Wall Loss of VOCs	27
3.3 Wall Loss of SOA	29
3.4 Determining the Optical Properties of SOA	30
3.5 Determination of SOA Yield.....	31
3.6 Determination of Ozonolysis Rate Constant (k)	32
3.7 References	33

CHAPTER 4. ESTABLISHING THE CONTRIBUTION OF LAWN MOWING TO ATMOSPHERIC AEROSOL LEVELS IN AMERICAN SUBURBS	35
4.1 Introduction	35
4.2 Experimental	39
4.2.1 Grass Experiments	41
4.2.2 GLV Standard Experiments.....	44
4.3 Results	45
4.3.1 Grass Emissions.....	45
4.3.2 Ozonolysis of Individual GLVs.....	46
4.3.3 Two GLV Component Mixtures.....	53
4.3.4 Grass Ozonolysis	58
4.4 Contribution of Lawn Mowing to Atmospheric SOA.....	67
4.5 Conclusions	70
4.6 References	71
CHAPTER 5. OPTICAL PROPERTIES OF SECONDARY ORGANIC AEROSOL FROM CIS-3-HEXENOL AND CIS-3-HEXENYL ACETATE: EFFECT OF CHEMICAL COMPOSITION, HUMIDITY AND PHASE.....	76
5.1 Introduction	76
5.2 Experimental	78
5.3 Results and Discussion.....	81
5.3.1 Absorbance of CHA- vs HXL- SOA	81
5.3.2 Assignment of Spectral Features to Molecular Moieties.....	83
5.3.3 Effect of Humidity on the MAC of HXL SOA	86
5.3.4 Light Scatter by GLV-SOA	91
5.3.5 Scatter Enhancement and RH.....	92
5.3.6 Bounce Factor of GLV SOA	95
5.4 Future Implications:	95
5.5 References	97
CHAPTER 6. SUBTLITIES IN MOLECULAR-LEVEL DYNAMICS; VOC STRUCTURE, OZONOLYSIS KINETICS AND SOA YIELD	102
6.1 Introduction	102
6.2 Experimental	106
6.3 Results	111

6.3.1 SOA Yield of Cyclic vs. Linear Alkenes.	111
6.3.2 Ozonolysis rate constants (k) for linear and cyclic alkenes.....	116
6.3.3 SOA Yield for Oxygenated Linear Alkenes.....	122
6.3.4 Ozonolysis Kinetics for Oxygenated Linear Alkenes	123
6.4 Atmospheric Implications	125
6.5 References	127
CHAPTER 7. SUBTLETIES IN MOLECULAR-LEVEL DYNAMICS: ORDER OF	
INTRODUCTION	131
7.0 Introduction	131
7.1 Experimental	133
7.2 Data Treatment.....	133
7.3 Results and Discussion.....	134
7.4 Conclusions	137
7.5 References	138
CHAPTER 8. DETERMINATION OF THE VOLATILE EMISSIONS OF	
SUGARCANE AND THEIR ROLE IN ATMOSPHERIC CHEMISTRY	141
8.1 Introduction	141
8.2 Experimental	142
8.3 Results	144
8.3.1 VOC Emissions	144
8.3.2 VOCs and SOA Post Ozonolysis.....	148
8.4 Influence of Sugarcane on Global SOA and Further Conclusions.....	153
8.5 GLV SOA and Visibility.....	155
8.6 Conclusions	158
8.7 References	160
CHAPTER 9. CONCLUSIONS AND FUTURE WORK.....	162
9.1 General Conclusions	162
9.2 Expanding Research to Include Other Relevant Oxidants	164
9.3 Mie Theory to Further Characterize Optical Properties.....	166
9.4 Theoretical Study of Mechanisms and Kinetics of GLV Ozonolysis	167
9.5 Instrument Development.....	168

9.6 Factors Affecting New Particle Formation- Unanswered Questions Without Projected Answers (AKA future members' PhDs)	170
9.7 Final Thoughts.....	171
9.8 References	172
BIBLIOGRAPHY	174
APPENDIX I: PREPARATION OF HONO/ HIGH NO _x EXPERIMENTS.....	194
AI.1 Atmospheric NO _x and its Roles in SOA Formation	194
AI.2 Generation of NO _x	195
AI.3 References	196
APPENDIX II: CORRECTIONS FOR ERRONEOUS SMPS MEASUREMENTS	197
APPENDIX III: REPRINT OF “Establishing the Contribution of Lawn Mowing to Atmospheric Aerosol Levels in American Suburbs”	203
APPENDIX IV: REPRINT OF: “Control of ozonolysis kinetics and aerosol yield by nuances in the molecular structure of volatile organic compounds”	218

LIST OF TABLES

Table 3.1 Characteristics of reaction chambers used.....	20
Table 3.2 K-values for GLVs.....	26
Table 4.2 Summary of grass clipping experiments.....	66
Table 5.1 Experimental conditions for GLV ozonolysis experiments in HEC.....	79
Table 5.2 Physical and chemical characteristics of GLV-derived SOA.....	85
Table 6.1 Experimental conditions for kinetic and yield experiments	110
Table 6.2 SOA yield of cyclic, linear and oxygenated alkenes.....	115
Table 6.3 Ozonolysis rate constants (k) of alkenes.....	120
Table 7.1 Initial conditions for introduction order experiments.....	133
Table 8.1 Initial conditions for sugarcane experiments.....	144
Table 8.2 VOC emissions of sugarcane and volatile ozonolysis products.....	147
Table 8.3 Pre-ozonolysis concentration and emission rate of CHA and HXL from sugarcane samples	148
Table 8.4 Estimated Contribution of HXL and CHA to total sugarcane SOA loadings based on their emission rates and reported SOA Yields (for 1000 ppb GLV).....	150
Table 8.5 Estimated Contribution of HXL and CHA to total sugarcane SOA loadings based on their emission rates and reported SOA Yields (for 500 ppb GLV).....	151
Table 8.6 Mass extinction coefficients for CHA- and HXL-derived SOA.....	157
Table 9.1 The complex index of refraction of several atmospheric materials.....	167
Table A1.1 NO _x and NO conditions from HONO	196
Table AII.1 Initial reaction conditions for correction factor experiments.....	199
Table AII.2 Raw and corrected SOA mass concentrations in sugarcane experiments.....	201

LIST OF FIGURES AND REACTION SCHEMES

Figure 2.1 Molecular structures of commonly studied BVOCs.....	7
Scheme 2.1 General mechanism for the ozonolysis of alkenes.....	12
Figure 3.1 General schematic for experimental chambers.....	19
Figure 3.2 Structures of molecules studied in this work.....	21
Figure 3.3 Calibration curve for VOCs using TD GC/MS.....	22
Figure 3.4 Signal calibration for HXL in cyclohexane.....	24
Figure 3.5 Determination of equilibration time for HXL and CHA using SPME.....	25
Figure 3.6 HXL signal in blind experiment.....	27
Figure 3.7 Gaseous wall loss of GLVs.....	28
Figure 3.8 Loss of HXL-SOA to chamber walls.....	29
Figure 3.9 Schematic of Integrating Sphere UV/Vis.....	30
Figure 3.10 Reaction profile for the ozonolysis of 3-heptene under pseudo-first order conditions for rate constant experiments.....	32
Figure 3.11 A plot of $\ln([\text{Ozone}]_t/[\text{Ozone}]_0)$ vs time for 3-heptenal yields a straight line, which confirms that pseudo first order reactions conditions were met and can be used to determine the rate constant (k).....	33
Figure 4.1 Turfgrass in a suburban neighborhood in Essex, VT, USA.....	42
Figure 4.2 Reaction profile for grass clipping experiment.....	44
Figure 4.3 Chromatograms of volatile organic compounds emitted by (a) grass clippings and (b) as a result of the ozonolysis of grass clippings.....	47
Scheme 4.1 Simplified mechanism for the ozonolysis of (a) HXL and (b) CHA.....	49
Figure 4.4 Reaction profile for the ozonolysis of CHA.....	50
Figure 4.5 Reaction profile for the ozonolysis of HXL.....	50
Scheme 4.2 Reactive uptake of propanal by 3-oxylpropyl acetate.....	51
Figure 4.6 Reaction profile for the ozonolysis of propanal.....	52
Figure 4.7 Reaction profile for the ozonolysis of 1:1 mix of HXL and CHA.....	55
Figure 4.8 Reaction profile for the ozonolysis of 1:5 mix of HXL and CHA.....	55
Figure 4.9 Consumption of GLVs and evolution of SOA in grass headspace experiments.....	57
Figure 4.10 Evolution of volatile products from the ozonolysis of grass headspace.....	57

Figure 4.11 Reaction profile for 1-penten-3-ol ozonolysis.....	59
Figure 4.12 Photo of grass clippings in UVMEC for experiments.....	62
Scheme 4.3 Expected products from the ozonolysis of PTL.....	61
Figure 4.13 Reaction profile for the ozonolysis of grass clippings.....	63
Figure 4.14 Evolution of volatile products and SOA during grass clipping ozonolysis.....	63
Figure 5.1 MAC Values of GLV-SOA as a function of wavelength and RH.....	82
Figure 5.2 Absorbance spectrum of oxygenated standards.....	84
Figure 5.3 Mass spectra of HXL-SOA formed under dry (a) and wet (b) conditions.....	88
Scheme 5.1 Abbreviated mechanism for ozonolysis of HXL in the presence of water.....	90
Figure 5.3 Average MSC of GLV-SOA at 450 nm, 525 nm and 635 nm.....	91
Figure 5.4 Average ASE of GLV-SOA.....	92
Figure 5.5 Scatter enhancement for HXL-SOA.....	94
Scheme 6.1 Abbreviated ozonolysis mechanism for cyclic and linear alkenes.....	113
Figure 6.1 SOA yield of C ₅ -C ₇ linear and cyclic alkenes.....	115
Figure 6.2 Reaction profile for the ozonolysis of HXL used to determine k.....	117
Figure 6.3 Plots confirming kinetics experiments were pseudo-first order for VOC.....	119
Figure 7.1 Time dependent growth curves of limonene-SOA.....	135
Figure 7.2 Molecular structure of limonene.....	136
Figure 8.1 Sugarcane in 775 L reaction chamber for emission and SOA yield experiments.....	143
Figure 8.2 Chromatograms of sugarcane emissions (a) before and (b) after ozonolysis.....	145
Figure 8.3 GLV emissions from sugarcane in 11/4/2015 experiment.....	146
Figure 8.4 BVOC emissions from sugarcane in the 11/04/2015 experiment.....	148
Scheme 8.1 Abbreviated mechanism for the ozonolysis of OTL.....	153
Figure 8.5 The effect of particulate matter on visual range.....	156
Figure 8.6 Predicted visual range in air with 11 µg/m ³ SOA derived solely from CHA or HXL.....	158
Figure 9.1 Schematic of integrating sphere.....	169

Figure AI.1 Different reaction pathways under high and low NO _x conditions.....	172
Figure AII.1 Schematic of SMPS in operation.....	201
Figure AII.2 Particle distributions measured using SMPS.....	202
Figure AII.3 OTL-Derived SOA mass concentration monitored with SMPS using correct and incorrect flow settings.....	203
Figure AII.4 Size distribution of OTL-derived SOA using correct and incorrect SMPS settings are the same.....	204

LIST OF ABBREVIATIONS

1-HXN	1-hexene
3-HXN	3-hexene
σ_{ex}	Total light extinction
σ_{abs}	light extinction due to absorbance
σ_{scat}	light extinction due to scatter
AVOC	Anthropogenic volatile organic compound
ASE	Angstrom scatter exponent
ASOA	Anthropogenic secondary organic aerosol
BF	Bounce factor
b_v	Volume-normalized absorption coefficient
BVOC	Biogenic volatile organic compound
BSOA	Biogenic secondary organic aerosol
CCN	Cloud condensation nuclei
CHA	Cis-3-hexenyl acetate
CI	Creigee Intermediate
CO	Carbon monoxide
CPC	Condensation particle counter
ELPI	Electrostatic low pressure impactor
f(RH)	Scatter enhancement coefficient
GLV	Green leaf volatile
H:C	Hydrogen-to-carbon ratio
HEC	Harvard experimental chamber
HR-ToF-AMS	High-resolution time of flight mass spectrometer
HXL	Cis-3-hexenol
HXNDL	3-hexene-2,5-diol
K-value	Equilibrium constant
L_v	Visual Range
IN	Ice nuclei
IS- UV/Vis	integrating sphere UV/Vis spectrophotometer
IPCC	International Panel on Climate Control
MAC	Mass Absorption Coefficient
MSC	Mass Scatter Coefficient

NIR-LDI-AMS	Near IR laser desorption/ionization aerosol mass spectrometer
NO _x	Oxides of nitrogen (NO, NO ₂)
O ₃	Ozone
OA	Organic aerosol
O:C	Oxygen-to-carbon ratio
OH	Hydroxyl radical
ORVOC	Other reactive volatile organic compound
OTL	1-octene-3-ol
ppbv	Parts per billion by volume
POA	Primary organic aerosol
pptv	Parts per trillion by volume
PTL	1-pentene-3-ol
RH	Relative humidity
SAR	Structure-activity relationship
SM	Sampling manifold
SMPS	Scanning mobility particle sizer
SOA	Secondary organic aerosol
SPME-GC/MS	Solid phase microextraction gas chromatogram mass spectrometer
SVOC	Semi-volatile organic compound
TD- GC/MS	Thermal desorption gas chromatogram mass spectrometer
Tg C y ⁻¹	Terragrams of carbon per year
TIC	Total ion count
UVMEC	University of Vermont environmental chamber
VOC	Volatile organic compound
Y	Aerosol yield

CHAPTER 1. BACKGROUND AND OUTLINE OF DISSERTATION

1.1 A Brief Rationale for the Research

Aerosols are ubiquitous in the atmosphere and play important roles in atmospheric and environmental processes. Aerosol particles participate in heterogeneous chemical reactions in the atmosphere, affecting the distribution, abundance and transport of trace gases.^{1,2} Aerosols also influence the Earth's radiative budget by absorbing and scattering radiation (the direct effect) and by acting as nuclei for clouds (the indirect effect), which themselves absorb/scatter radiation and also contribute to local weather phenomena. It has been well accepted that atmospheric aerosols play a major role in the Earth's climate,³ yet there remain significant gaps in our understanding of the formation, ageing, physical and chemical properties, and removal of atmospheric aerosols. These knowledge gaps provide the crux of the research completed towards this dissertation, as I'm sure they will continue to do as atmospheric science grows.

Organic aerosols (OAs), aerosols that consist primarily of carbon, oxygen, hydrogen, sulfur, nitrogen and phosphorus, contribute 20-90% of total aerosol mass.⁴ Primary OA (POA) is emitted directly into the atmosphere as particles in processes like combustion and cooking. Secondary organic aerosol (SOA) is produced by gas-phase oxidation of volatile organic compounds (VOCs), which can be anthropogenic (AVOCs) or biogenic (BVOCs) in nature. In fact, the majority of SOA is derived from the oxidation of BVOCs. Despite improvements made to understand SOA, many of the basic processes governing its formation, growth, chemical and physical properties are still poorly understood. In fact, recent estimates of global SOA production rates have indicated that

there could be significant missing SOA precursors and/or a still poor understanding of the chemical processes that lead to SOA formation.⁵⁻⁷

Therefore, the main objective of this work was to identify potential sources of BVOC SOA precursors and to characterize the optical and physical properties of the resultant SOA. This work also included studies of structure-activity relationships to better understand, on a molecular level, the potential for VOCs to contribute to atmospheric aerosol. The fine level of understanding afforded by these studies will allow some generalizations to be made about specific functional groups in BVOCs and their influence on the kinetics of ozonolysis.

1.2 Specific Research Questions Addressed in this Dissertation

1. Do lawns and other leafy plants, such as sugarcane, represent a potential SOA source?
 - a. What are the predominant emissions of these grasses and are they SOA precursors?
2. How does SOA from these sources interact with light (absorbance vs scatter)?
3. What molecular-level subtleties of these classes of BVOCs drive SOA yield?

In the nature of scientific research, and much like a ‘write your own adventure’ story, the experiments and questions asked in this work evolved organically, building from each other. For your enjoyment, I hope to recreate this story in the chapters to follow.

1.3 Thesis Outline

The overall structure of this thesis is organized in nine chapters. Chapter 1 introduces the general background of the study, objective and significance of the work. Chapter 2 provides a more in-depth review of the current literature, providing pertinent

history of the field and further identifying the need for the work completed herein. Chapter 3 provides a general overview of the instruments and experimental protocols used throughout this work. In Chapter 4, I present and discuss results from an experimental campaign to establish the contribution of lawn mowing in atmospheric SOA loadings, which turns out to be minimal but significant. In order to fully understand the role of these lawn mowing induced SOA on climate, however, it's also important to understand their optical properties (whether they absorb or scatter light), which are presented in Chapter 5. In both Chapters 4 and 5, I present evidence suggesting that the molecular level composition of both VOC precursor and the resultant SOA itself have important roles in its atmospheric fate. Chapters 6 and 7 present a look into the molecular level nuances of ozonolysis reactions, including how the structure of parent VOC affects SOA yield (Chapter 6) and the nuanced behavior of chamber studies (Chapter 7). Chapter 8 revisits the goal of identifying novel sources of SOA and presents recent advances to understand the role of sugarcane horticulture on atmospheric SOA. Throughout this document, several important questions are addressed, yet in the true nature of research, more are posed. These additional questions and thoughts for future work are posed in Chapter 9, which also summarizes some key take-home messages of this work.

1.4 References

- (1) Haywood, J.; Boucher, O. *Rev Geophys* **2000**, *38*, 513.
- (2) Andreae, M. O.; Crutzen, P. J. *Science* **1997**, *276*, 1052.
- (3) Boucher, O.; Randall, D.; rtaxo, P.; Bretherton, C.; Feingold, G.; Forster, P.; Kerminen, V.-M.; Kondo, Y.; Liao, H.; Lohmann, U.; Rasch, P.; Satheesh, S. K.; Stevens, B.; Zhang, X. Y. *The Physical Science Basis. Contribution of Working Group I to the Fifth Assessment Report of the Intergovernmental Panel on Climate Change*, 2013.

- (4) Kanakidou, M.; Seinfeld, J. H.; Pandis, S. N.; Barnes, I.; Dentener, F. J.; Facchini, M. C.; Van Dingenen, R.; Ervens, B.; Nenes, A.; Nielsen, C. J.; Swietlicki, E.; Putaud, J. P.; Balkanski, Y.; Fuzzi, S.; Horth, J.; Moortgat, G. K.; Winterhalter, R.; Myhre, C. E. L.; Tsigaridis, K.; Vignati, E.; Stephanou, E. G.; Wilson, J. *Atmos. Chem. Phys.* **2005**, *5*, 1053.
- (5) Goldstein, A. H.; Galbally, I. E. *Environ Sci Technol* **2007**, *41*, 1514.
- (6) Carlton, A. G.; Wiedinmyer, C.; Kroll, J. H. *Atmos. Chem. Phys.* **2009**, *9*, 4987.
- (7) Shilling, J. E.; Zaveri, R. A.; Fast, J. D.; Kleinman, L.; Alexander, M. L.; Canagaratna, M. R.; Fortner, E.; Hubbe, J. M.; Jayne, J. T.; Sedlacek, A.; Setyan, A.; Springston, S.; Worsnop, D. R.; Zhang, Q. *Atmos. Chem. Phys.* **2013**, *13*, 2091.

CHAPTER 2. REVIEW OF THE CURRENT LITERATURE

There is growing evidence that the Earth's climate is changing. According to the International Panel on Climate Control's (IPCC) 2014 report, human activities have shifted the global loading and distribution of atmospheric greenhouse gases, clouds, and aerosol.¹ This shift can significantly modify the Earth's energy balance resulting in a warming or cooling of the climate system and dramatic changes in weather.

Despite our realization that anthropogenic activities have shifted the Earth's energy balance, there remains significant uncertainty in our understanding of the environmental impact of atmospheric aerosol, owing to a still-limited knowledge of its sources, composition, properties, and the mechanisms that lead to its formation and ageing.²⁻⁴ In fact, recent estimates of global SOA production rates largely under-predict measured loadings, indicating that there could be significant missing SOA precursors and/or a still poor understanding of the chemical processes that lead to SOA formation.^{2,4,5} Therefore, identifying the sources, interactions and reactivity of VOCs is integral to understanding their impact on the formation of SOA and, consequently, on regional air quality and climate patterns, and is among the primary foci of the work reported herein.

2.1 Atmospheric Aerosols

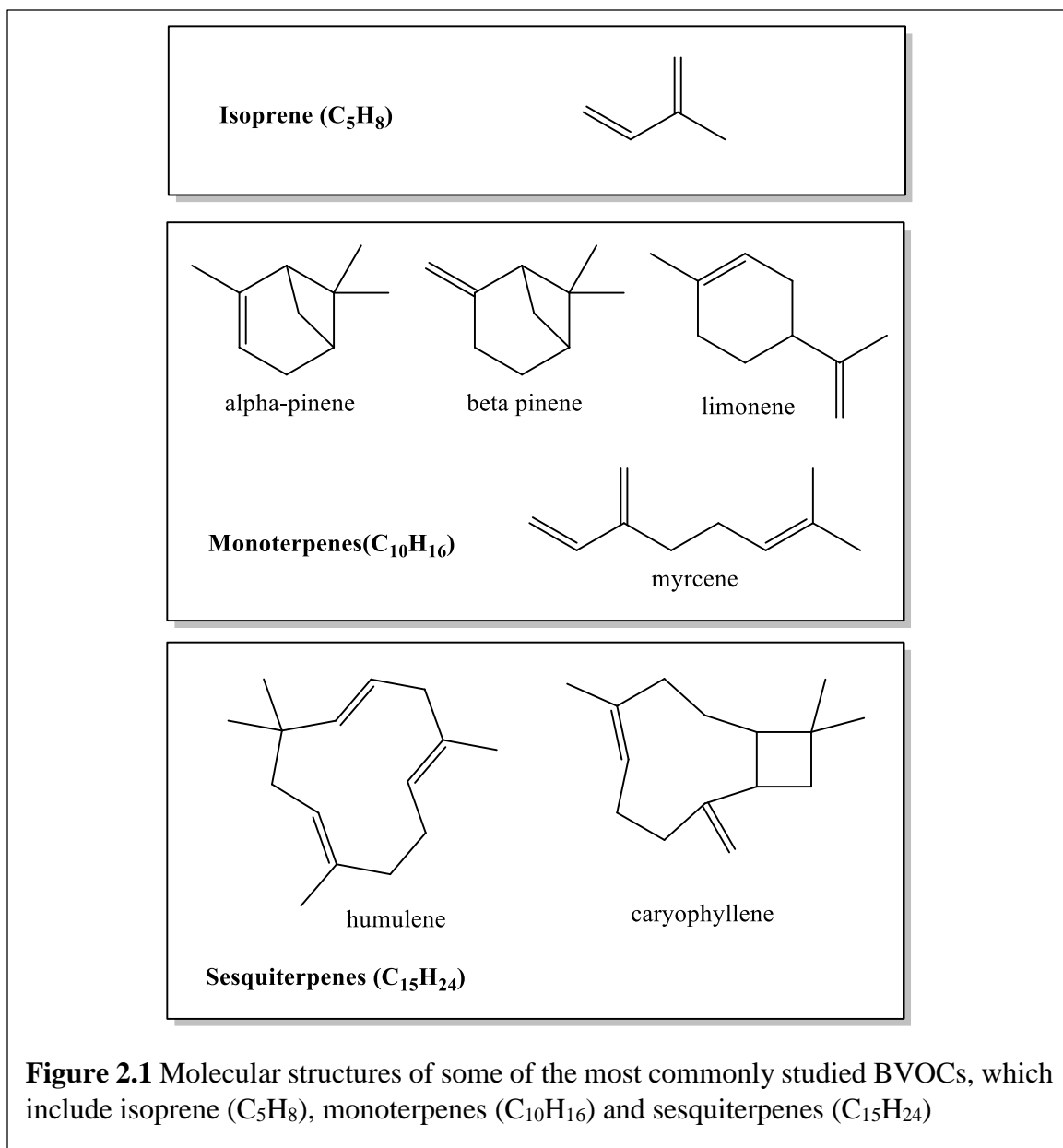
Atmospheric aerosol is a mixture of liquid or solid particles (or particulate matter) suspended in the air. These particles have both anthropogenic (biomass burning, fossil fuel combustion/exhaust, food cooking) and natural (sea spray, gas-to-particle conversion, mineral dust) sources and can be inorganic or organic in composition. Aerosol sizes range

from about 0.01 μm to 10 μm . The wide range in sizes and chemical composition of aerosols make them an interesting and challenging system to study.

Organic aerosol (OA) contributes 20-90% of the total mass of fine atmospheric aerosol^{6,7} and 70-90% of OA is secondary in nature (SOA), being formed by the oxidation of volatile organic compounds (VOCs) in the atmosphere.⁸ The remaining fraction of OA consists of primary OA (POA), which is emitted directly to the atmosphere as particles and of a smaller subset of compounds that are emitted as gases, that then condense to form particles (without reacting).

2.2 SOA Precursors

The VOCs that lead to SOA originate from both anthropogenic (AVOC) and biogenic (BVOC) sources. Isoprene (Figure 2.1) is the most dominant non-methane BVOC, accounting for about half of all BVOC emissions (estimated global emissions range between 250 and 750 Tg C y^{-1} , about half of which is from tropical broadleaf trees and the remainder primarily from shrubs).^{9,10} The oxidation of isoprene yields relatively little SOA (on a mass basis, only about 1% of oxidized isoprene is converted to SOA: the SOA yield is 1%) yet has such a large global source strength that its global SOA contribution is significant, corresponding to $\sim 2\text{-}6 \text{ Tg y}^{-1}$ SOA² compared to global estimates of OA ranging between 12-70 Tg y^{-1} .⁷



Monoterpenes and sesquiterpenes are plant emissions defined by the number of isoprene units they contain, where monoterpenes contain two isoprene units and have the general formula C₁₀H₁₆, and sesquiterpenes contain 3 isoprene units with the general formula C₁₅H₂₄. Monoterpenes and sesquiterpenes also contribute to global SOA loadings, not because they are emitted in large quantities (global emission rates estimated

at $\sim 130 \text{ Tg C y}^{-1}$),¹¹ but because they have considerably larger aerosol yields (average of about 15% but up to 100% for some sesquiterpenes).¹² These VOC emissions rates, aerosol yield measurements and an understanding of the chemical mechanisms leading to SOA formation are then coupled in atmospheric models to achieve global SOA loading estimates. As indicated above, though, current models largely under-predict the measured SOA loadings in the atmosphere, suggesting that there are missing SOA precursors and/or a still poor understanding of the chemical processes that lead to SOA formation.^{2,4,5}

Green leaf volatiles (GLVs) represent another potentially important SOA precursor. These C₅ and C₆ oxygenated BVOCs are emitted by leafy green plants and grasses, where their main role is as protective antioxidants.^{13,14} Upon wounding (mechanical or chemical), however, these emissions are enhanced and participate in interesting plant-plant and plant-insect communication channels.^{13,15} The mowing of turfgrasses stimulates enhanced emission of GLVs from turfgrasses, contributing to the “freshly mowed lawn” smell that many of us are familiar with.¹⁴⁻²² The most documented GLVs include the compounds cis-3-hexenal, cis-3-hexenol (HXL), cis-3-hexenyl acetate (CHA), and trans-2-hexenal. More recently, cis-2-penten-1-ol and 1-penten-3-ol have also been identified in the wound-induced emissions of plants.^{15,17,23} Not only do these compounds have interesting roles in plant protection and plant-plant/plant-animal communication, GLVs also actively take part in atmospheric chemistry.^{3,24-26}

The contribution of GLV-derived SOA to bulk atmospheric loadings may be especially impactful at the urban-suburban interface (so-called peri-urban region), where urban hubs provide a source of anthropogenic oxidants and SOA, while suburban

neighborhoods have the potential to emit large quantities of reactive, mow-induced GLVs. Hamilton et al. (2007, 2009)^{3,24} established the importance of GLV oxidation to global SOA using single-component systems, with one oxidant being introduced to each GLV separately; however, these GLVs do not exist in isolation. In fact, recent work by Shilling et al. (2013)⁴ in the CARES campaign indicates that VOC *mixtures* have a significant impact on SOA formation. Briefly, Shilling et al. (2013)⁴ found that the oxidation of a mixture of anthropogenic and biogenic VOCs produced more OA than the components alone,⁴ highlighting the importance of understanding mixed VOC systems.

Therefore, this work will extend our understanding of the role of GLVs in atmospheric chemistry by representing the multi-component system experienced in the environment. This approach provides a unique opportunity to study aerosol formation in a multi-component system and at a regionally relevant scale.^{15,22,27-29}

2.3 Oxidation Mechanisms

The reactivity of most BVOCs stems from the fact that they contain one or more double bonds. These electron rich regions are highly reactive with electron seeking atmospheric oxidants, including the hydroxyl radical (OH), NO_x and O₃.³⁰ These reactions have been reviewed extensively by Calvert et al., (2000) and by the Petrucci Group (2007)^{30,31} and ultimately result in the formation of low volatility products that subsequently condense (either onto seed particles or homogeneously) to form SOA and also contribute to the self-propagation of oxidants (O₃ and OH radicals) in the atmosphere.

2.3.1 Oxidation of Alkenes by OH

The OH radical is a major oxidant for alkenes in the atmosphere, largely due to its ubiquitous nature and because OH oxidation reactions are very fast (rate constants on the order of $10^{-10} \text{ cm}^3 \text{ molecule}^{-1} \text{ s}^{-1}$).³² Photolysis of ozone by ultraviolet light in the presence of water is the main source of OH yet it is also produced as a side product in the ozonolysis of VOCs. Due to its high reaction rates, atmospheric OH is difficult to measure but concentrations in pristine environments are on the order of 0.04 pptv and those in polluted regions are closer to 0.4 pptv³²⁻³⁴

The primary reaction pathway for OH oxidation of an alkene proceeds via the addition of OH to the double bond to form an intermediate that either decomposes back to the reactants (a very minor pathway, only becoming significant for very small alkenes) or stabilizes and continues to react.³² Specifically, the new C-OH bond is formed via charge transfer from the π -bond of the alkene to the OH radical, with the position of the OH moiety favoring the less substituted carbon. The remaining unpaired π -bond electron becomes localized on the adjacent carbon atom, forming a radical. In an oxygen-rich environment, the radicals formed in OH addition readily react with O_2 to form peroxy radicals, which themselves continue to react in the atmosphere to form several different oxidized products that may (or may not) condense to form SOA.³⁰

This work does not include experiments with strictly OH-driven oxidation of VOCs, but OH radicals are coproduced by the ozonolysis of VOCs and are then available to participate in the oxidation. OH scrubbers (cyclohexane and butanol) can be used to scavenge OH radicals, but were seldom used in this work.

2.3.2 Oxidation of Alkenes by NO_x

Oxides of nitrogen (NO₂, NO, collectively termed NO_x) play important roles in atmospheric chemistry.³⁵ Not only do they contribute to acid rain, but NO_x enhances the SOA yield of other oxidation reactions, particularly photooxidation reactions (which are OH driven).³⁶⁻³⁸ In the presence of NO_x peroxy radicals formed via the photooxidation of VOCs react virtually entirely with NO, leading to the formation of large alkoxy radicals that isomerize (rather than fragment) to yield large, multifunctional products with low volatility, enhancing SOA yield.³⁸

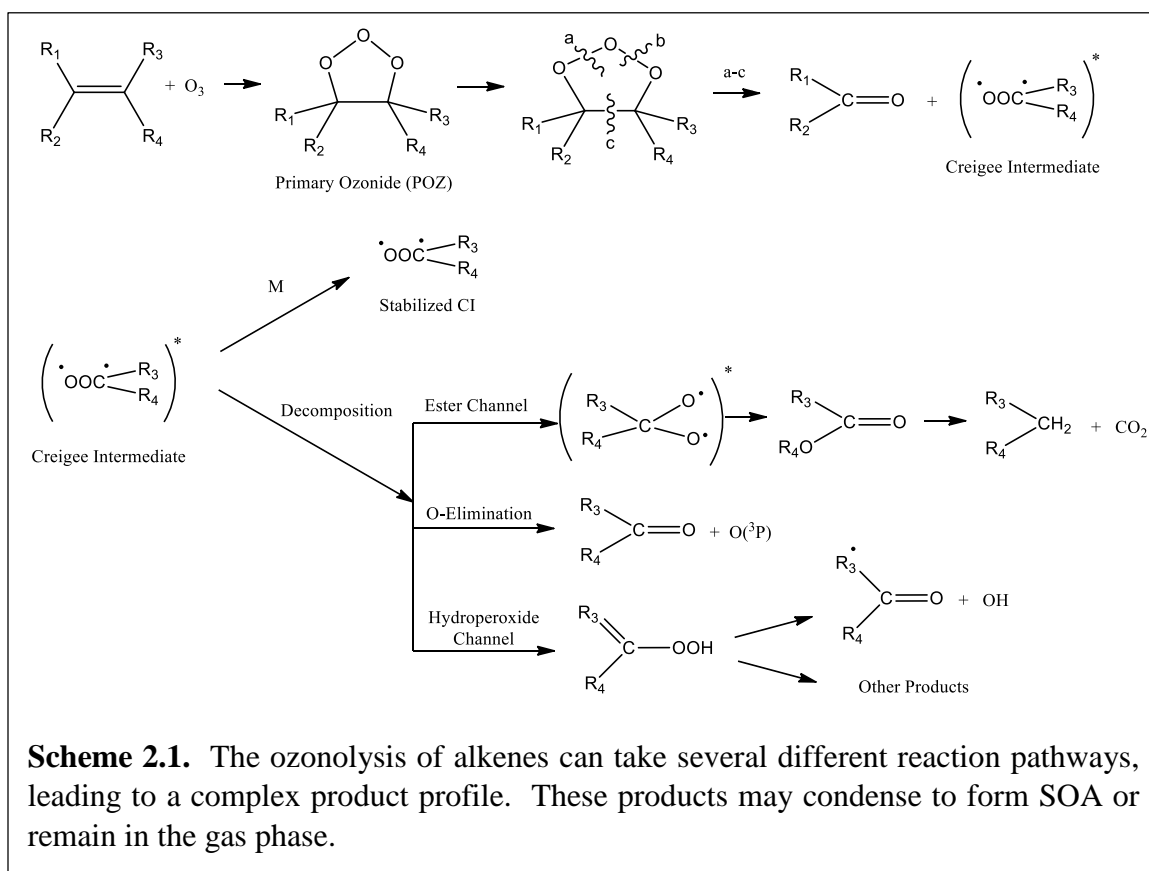
The pathways leading to NO_x in the atmosphere are varied and complex, with many feedback loops with O₃, O₂ and OH and a detailed discussion is beyond the scope of this project. Overall, however, anthropogenic sources (including cars, power plants, and incinerators) contribute about 90% of NO_x in the atmosphere. Biogenic sources include lightning, forest/grass fires, and yeasts.³⁹ NO_x is rapidly photolysed, resulting in lifetimes on the order of 5 s and making its role in daytime chemistry relatively minor.⁴⁰ Night time NO_x chemistry, however, is particularly important (and interesting). Of course, under highly polluted conditions it is possible for NO_x to persist during the day.⁴⁰

This work does not include oxidation via NO_x, but standard operating procedures to generate NO_x in the laboratory were developed and could be implemented in future work. The specifics of this method can be found in Appendix 1.

2.3.3 Oxidation of Alkenes by O₃

Ozone is a naturally occurring gas that can be found throughout the atmosphere. While stratospheric ozone shields us from ultraviolet radiation, tropospheric ozone is often

considered “bad” ozone due to its negative impacts on human health and plants. Tropospheric ozone is produced in situ by photochemical reactions between NO_x and VOCs, methane, or CO.⁴¹ These O₃ precursors originate from natural sources including wildfires, biogenic hydrocarbon and NO_x emissions, and lightning but also from anthropogenic fossil fuel and biofuel combustion, or crop burning.⁴² In rural areas, ozone concentrations typically range between 20 and 80 ppbv, while in urban areas ozone concentrations range between 40 and 120 ppbv, with maxima usually occurring on warm, sunny days during rush hour (due to photolysis reactions).⁴²



The mechanism for the ozonolysis of a general alkene is given in Scheme 2.1. Briefly, the reaction proceeds by electrophilic addition of O₃ across the C-C double bond,

leading to an energy-rich 1,2,3,-trioxolane adduct, also called the primary ozonide (POZ). The POZ then rapidly decomposes, cleaving the C-C bond and one of the O-O bonds (shown in Scheme 2.1 as the a-c cleavage, but a-b cleavage is also possible) to form energy rich carbonyl and carbonyl oxide biradical products, also known as the Creigee Intermediates (CI) that can rearrange to form low-volatility carboxylic acids and/or participate in multigenerational chemistry. These reactions have been studied extensively; Calvert et al. (2000) provides a comprehensive review of their mechanisms and kinetics.³⁰ The take-away, however, is that they can result in the formation of product molecules with sufficiently low vapor pressures that they condense (homogeneously or onto existing particulate matter) to form SOA.

2.4 Secondary Organic Aerosols

The oxidation mechanisms described above can lead to the formation of products with sufficiently low vapor pressures that they condense to form a particle. These particles can coagulate, forming larger, mixed-system particles, undergo additional oxidation reactions in the atmosphere (chemical ageing), transport across landscapes or throughout the atmosphere or be deposited onto surfaces. Depending on the type of air mass (urban, marine, free troposphere, remote) and its size, the time a particle spends in each of these modes can vary significantly, ranging from just a few hours to several weeks.³²

Organic aerosols (OAs), including SOA, are a major component of fine aerosols and influence climate through direct and indirect effects, although there is an expressed high degree of uncertainty about the magnitude of these effects.^{43,44} The direct effect of SOA includes its ability to absorb or scatter radiation (either from the sun or from the Earth

itself), which ultimately affects the Earth's radiative budget. Much like a dark sweater on a sunny day warming your body, atmospheric particles that are efficient light absorbers contribute to positive radiative effect, warming the planet. Most SOA particles are efficient scatterers of visible light, though, and generally have a net negative radiative effect, helping to keep the planet cool, at least initially. As SOA undergoes secondary reactions in the atmosphere (is chemically aged), it can become more oxidized, and thereby contribute to light absorption. These secondary reactions, then, become very important when considering the direct effect of SOA. Incidentally, SOA is a major component of fine aerosol and has a long atmospheric lifetime, giving it ample opportunity to participate in secondary chemistry and interact with light. The impact of SOA, therefore has the potential to have a greater impact on atmospheric chemistry and climate forcing than other particulate matter.

The indirect effect of SOA includes its ability to act as cloud condensation nuclei (CCN) and/or ice nuclei (IN), which contribute to cloud formation throughout the atmosphere. Clouds play an important role in climate through absorption of terrestrial infrared radiation and reflection of solar radiation (albedo). Depending on the type of cloud and where it is found in the atmosphere, cloud water can be in the form of liquid droplets, solid ice crystals, or a mix of the two. The phase, composition, size and shape of cloud water play important roles in determining the clouds' effect on climate.⁴ Liquid clouds are found in the lower troposphere and have a predominantly cooling effect due to their ability to reflect shortwave solar radiation off their bright tops and into space.⁵ Ice clouds are found in the upper troposphere and also contribute to cooling by reflecting solar radiation

into space. Additionally, however, ice clouds trap longwave radiation emitted by the Earth back towards its surface, contributing a warming effect. The CCN or IN activity of SOA depends largely on its size, phase (liquid or solid) and chemical composition.

SOA also impacts local weather patterns and has been associated with deleterious impacts on human health, though this is well outside the scope of this project.^{45,46}

Currently, there remains significant uncertainty in our understanding of the environmental impact of SOA, owing to a still limited knowledge of its sources, composition, properties, and the mechanisms that lead to its formation.^{4,47,48} Herein, results from several different, yet related, experimental campaigns designed to fill these knowledge gaps will be presented and discussed. This work focuses primarily on identifying novel SOA precursors and characterizing the chemical, physical and optical properties of the resultant SOA. This work contributes significantly to an enhanced understanding of the molecular-level dynamics involved in the formation of atmospheric aerosol.

2.5 References

- (1) Boucher, O.; Randall, D.; rtaxo, P.; Bretherton, C.; Feingold, G.; Forster, P.; Kerminen, V.-M.; Kondo, Y.; Liao, H.; Lohmann, U.; Rasch, P.; Satheesh, S. K.; Stevens, B.; Zhang, X. Y. *The Physical Science Basis. Contribution of Working Group I to the Fifth Assessment Report of the Intergovernmental Panel on Climate Change*, 2013.
- (2) Carlton, A. G.; Wiedinmyer, C.; Kroll, J. H. *Atmos. Chem. Phys.* **2009**, *9*, 4987.
- (3) Hamilton, J. F.; Lewis, A. C.; Carey, T. J.; Wenger, J. C.; Borrás i Garcia, E.; Muñoz, A. *Atmos. Chem. Phys.* **2009**, *9*, 3815.
- (4) Shilling, J. E.; Zaveri, R. A.; Fast, J. D.; Kleinman, L.; Alexander, M. L.; Canagaratna, M. R.; Fortner, E.; Hubbe, J. M.; Jayne, J. T.; Sedlacek, A.; Setyan, A.; Springston, S.; Worsnop, D. R.; Zhang, Q. *Atmos. Chem. Phys.* **2013**, *13*, 2091.
- (5) Goldstein, A. H.; Galbally, I. E. *Environ Sci Technol* **2007**, *41*, 1514.

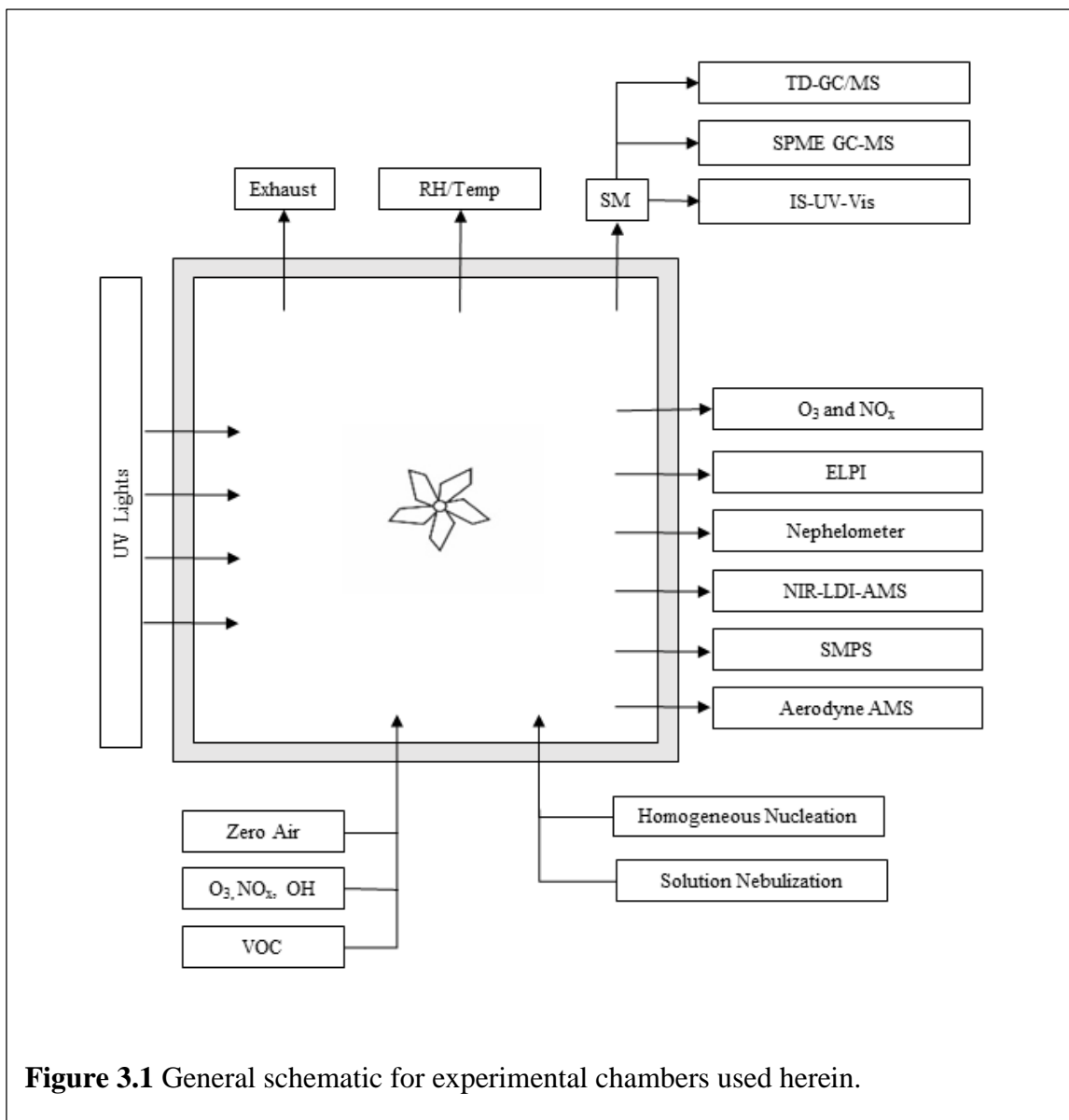
- (6) Kim, H.; Barkey, B.; Paulson, S. E. *J Phys Chem A* **2012**, *116*, 6059.
- (7) Kanakidou, M.; Seinfeld, J. H.; Pandis, S. N.; Barnes, I.; Dentener, F. J.; Facchini, M. C.; Van Dingenen, R.; Ervens, B.; Nenes, A.; Nielsen, C. J.; Swietlicki, E.; Putaud, J. P.; Balkanski, Y.; Fuzzi, S.; Horth, J.; Moortgat, G. K.; Winterhalter, R.; Myhre, C. E. L.; Tsigaridis, K.; Vignati, E.; Stephanou, E. G.; Wilson, J. *Atmos. Chem. Phys.* **2005**, *5*, 1053.
- (8) Hallquist, M.; Wenger, J. C.; Baltensperger, U.; Rudich, Y.; Simpson, D.; Claeys, M.; Dommen, J.; Donahue, N. M.; George, C.; Goldstein, A. H.; Hamilton, J. F.; Herrmann, H.; Hoffmann, T.; Iinuma, Y.; Jang, M.; Jenkin, M. E.; Jimenez, J. L.; Kiendler-Scharr, A.; Maenhaut, W.; McFiggans, G.; Mentel, T. F.; Monod, A.; Prévôt, A. S. H.; Seinfeld, J. H.; Surratt, J. D.; Szmigielski, R.; Wildt, J. *Atmos. Chem. Phys.* **2009**, *9*, 5155.
- (9) Wiedinmyer, C.; Guenther, A.; Harley, P.; Hewitt, N.; Geron, C.; Artaxo, P.; Steinbrecher, R.; Rasmussen, R. In *Emissions of Atmospheric Trace Compounds*; Granier, C., Artaxo, P., Reeves, C., Eds.; Kluwer Academic Publishers: Dordrecht, The Netherlands, 2004, p 115.
- (10) Guenther, A.; Karl, T.; Harley, P.; Wiedinmyer, C.; Palmer, P. I.; Geron, C. *Atmos. Chem. Phys.* **2006**, *6*, 3181.
- (11) Guenther, A.; Hewitt, C. N.; Erickson, D.; Fall, R.; Geron, C.; Graedel, T.; Harley, P.; Klinger, L.; Lerdau, M.; McKay, W. A.; Pierce, T.; Scholes, B.; Steinbrecher, R.; Tallamraju, R.; Taylor, J.; Zimmerman, P. *Journal of Geophysical Research: Atmospheres* **1995**, *100*, 8873.
- (12) Yu, J.; Cocker, D. R.; Griffin, R. J.; Flagan, R. C.; Seinfeld, J. H. *J Atmos Chem*, *34*, 207.
- (13) Scala, A.; Allmann, S.; Mirabella, R.; Haring, M. A.; Schuurink, R. C. *Int J Mol Sci* **2013**, *14*, 17781.
- (14) Brilli, F.; Hörtnagl, L.; Bamberger, I.; Schnitzhofer, R.; Ruuskanen, T. M.; Hansel, A.; Loreto, F.; Wohlfahrt, G. *Environ Sci Technol* **2012**, *46*, 3859.
- (15) Karl, T.; Harren, F.; Warneke, C.; de Gouw, J.; Grayless, C.; Fall, R. *J Geophys Res-Atmos* **2005**, *110*.
- (16) Kirstine, W. V.; Galbally, I. E. *J Air Waste Manage* **2004**, *54*, 1299.
- (17) Jardine, K.; Barron-Gafford, G. A.; Norman, J. P.; Abrell, L.; Monson, R. K.; Meyers, K. T.; Pavao-Zuckerman, M.; Dontsova, K.; Kleist, E.; Werner, C.; Huxman, T. E. *Photosynth Res* **2012**, *113*, 321.
- (18) Hatanaka, A. *Phytochemistry* **1993**, *34*, 1201.
- (19) Kirstine, W.; Galbally, I.; Ye, Y.; Hooper, M. *Journal of Geophysical Research: Atmospheres* **1998**, *103*, 10605.
- (20) Brilli, F.; Ruuskanen, T. M.; Schnitzhofer, R.; Müller, M.; Breitenlechner, M.; Bittner, V.; Wohlfahrt, G.; Loreto, F.; Hansel, A. *Plos One* **2011**, *6*, e20419.

- (21) Ormeño, E.; Gentner, D. R.; Fares, S.; Karlik, J.; Park, J. H.; Goldstein, A. H. *Environ Sci Technol* **2010**, *44*, 3758.
- (22) de Gouw, J. A.; Howard, C. J.; Custer, T. G.; Fall, R. *Geophysical Research Letters* **1999**, *26*, 811.
- (23) Hartikainen, K.; Riikonen, J.; Nerg, A.-M.; Kivimäenpää, M.; Ahonen, V.; Tervahauta, A.; Kärenlampi, S.; Mäenpää, M.; Rousi, M.; Kontunen-Soppela, S.; Oksanen, E.; Holopainen, T. *Environ Exp Bot* **2012**, *84*, 33.
- (24) Hamilton, J. F.; Lewis, A. C.; Carey, T. J.; Wenger, J. C. *Anal Chem* **2007**, *80*, 474.
- (25) Pinto, D. M.; Nerg, A. M.; Holopainen, J. K. *J Chem Ecol* **2007**, *33*, 2218.
- (26) Uchida, R.; Sato, K.; Imamura, T. *Chemistry Letters* **2015**, *advpub*.
- (27) Nemitz, E.; Dorsey, J. R.; Flynn, M. J.; Gallagher, M. W.; Hensen, A.; Erisman, J. W.; Owen, S. M.; Dämmgen, U.; Sutton, M. A. *Biogeosciences* **2009**, *6*, 1627.
- (28) Guenther, A. B.; Jiang, X.; Heald, C. L.; Sakulyanontvittaya, T.; Duhl, T.; Emmons, L. K.; Wang, X. *Geosci. Model Dev.* **2012**, *5*, 1471.
- (29) Steinbrecher, R.; Klauer, M.; Hauff, K.; R. Stockwell, W.; Jaeschke, W.; Dietrich, T.; Herbert, F. *Atmos Environ* **2000**, *34*, 3779.
- (30) Calvert, J. G.; Atkinson, R.; Kerr, J. A.; Madronich, S.; Moortgat, G.; Wallington, T. J.; Yarwood, G. *The Mechanisms of Atmospheric Oxidation of the Alkenes*; Oxford University Press: New York, Oxford, 2000.
- (31) Zahardis, J.; Petrucci, G. A. *Atmos. Chem. Phys.* **2007**, *7*, 1237.
- (32) Finnlaysen-Pitts, B. J. a. J. N. P. J. *Chemistry of the Upper and Lower Atmosphere*; Academic Press: San Diego, CA, 2000.
- (33) Seinfeld, J. H. a. S. N. P. *Atmospheric Chemistry and Physics: From Air Pollution to Climate Change*; 2 ed.; John Wiley and Sons, INC: Hoboken, N.J., 2006.
- (34) Jacob, D. J. *Introduction to Atmospheric Chemistry*; Princeton University Press: Princeton University, NJ, Chichester, West Sussex, United Kingdom, 1999.
- (35) Rollins, A. W.; Browne, E. C.; Min, K. E.; Pusede, S. E.; Wooldridge, P. J.; Gentner, D. R.; Goldstein, A. H.; Liu, S.; Day, D. A.; Russell, L. M.; Cohen, R. C. *Science* **2012**, *337*, 1210.
- (36) Xu, L.; Kollman, M. S.; Song, C.; Shilling, J. E.; Ng, N. L. *Environ Sci Technol* **2014**, *48*, 2253.
- (37) Ng, N. L.; Chhabra, P. S.; Chan, A. W. H.; Surratt, J. D.; Kroll, J. H.; Kwan, A. J.; McCabe, D. C.; Wennberg, P. O.; Sorooshian, A.; Murphy, S. M.; Dalleska, N. F.; Flagan, R. C.; Seinfeld, J. H. *Atmos. Chem. Phys.* **2007**, *7*, 5159.
- (38) Ng, N. L.; Chhabra, P. S.; Chan, A. W. H.; Surratt, J. D.; Kroll, J. H.; Kwan, A. J.; McCabe, D. C.; Wennberg, P. O.; Sorooshian, A.; Murphy, S. M.; Dalleska, N. F.; Flagan, R. C.; Seinfeld, J. H. *Atmos Chem Phys* **2007**, *7*, 5159.

- (39) (MD-12), U. E. P. A. C. A. T. C. *Nitrogen Oxides (NO_x), Why and How They Are Controlled*, US Environmental Protection Agency 1999.
- (40) Monks, P. S. *Chem Soc Rev* **2005**, *34*, 376.
- (41) Monks, P. S.; Granier, C.; Fuzzi, S.; Stohl, A.; Williams, M. L.; Akimoto, H.; Amann, M.; Baklanov, A.; Baltensperger, U.; Bey, I.; Blake, N.; Blake, R. S.; Carslaw, K.; Cooper, O. R.; Dentener, F.; Fowler, D.; Fragkou, E.; Frost, G. J.; Generoso, S.; Ginoux, P.; Grewe, V.; Guenther, A.; Hansson, H. C.; Henne, S.; Hjorth, J.; Hofzumahaus, A.; Huntrieser, H.; Isaksen, I. S. A.; Jenkin, M. E.; Kaiser, J.; Kanakidou, M.; Klimont, Z.; Kulmala, M.; Laj, P.; Lawrence, M. G.; Lee, J. D.; Liousse, C.; Maione, M.; McFiggans, G.; Metzger, A.; Mieville, A.; Moussiopoulos, N.; Orlando, J. J.; O'Dowd, C. D.; Palmer, P. I.; Parrish, D. D.; Petzold, A.; Platt, U.; Pöschl, U.; Prévôt, A. S. H.; Reeves, C. E.; Reimann, S.; Rudich, Y.; Sellegri, K.; Steinbrecher, R.; Simpson, D.; ten Brink, H.; Theloke, J.; van der Werf, G. R.; Vautard, R.; Vestreng, V.; Vlachokostas, C.; von Glasow, R. *Atmos Environ* **2009**, *43*, 5268.
- (42) Cooper, O. R.; Parrish, D. D.; Ziemke, J.; Balashov, N. V.; Cuperio, M.; Galbally, I. E.; Gilge, S.; Horowitz, L.; Jensen, N. R.; Lamarque, J. F.; Naik, V.; Oltmans, S. J.; Schwab, J.; Shindell, D.; Thompson, A. M.; Thouret, V.; Wang, Y.; Zbinden, R. M. *Elementa Science of the Anthropocene* **July 10, 2014**, *2*.
- (43) Kanakidou, M.; Seinfeld, J. H.; Pandis, S. N.; Dentener, F. J.; Facchini, M. C.; Van Dingenen, R.; Ervens, B.; Nenes, A.; Nielson, C. J.; Swietlicki, E.; Putaud, J. P.; Balkanski, Y.; Fuzzi, S.; Horth, J.; Moortgat, G. K.; Winterhalter, R.; Myhre, C. E. L.; Tsigaridis, K.; Vignati, E.; Stephanou, E. G.; Wilson, J. *Atmos. Chem. Phys.* **2005**, *5*, 1053.
- (44) *Climate Change 2007: The Physical Science Basis: Contribution of Working Group I to the Fourth Assessment Report of the Intergovernmental Panel on Climate Change*; Solomon, S.; Qin, D.; Manning, M.; Chen, Z.; Marquis, M.; Averyt, K. B.; Tignor, M.; Miller, H. L., Eds.; Cambridge University Press: Cambridge, United Kingdom and New York City, NY, USA, 2007.
- (45) Miller-Schulze, J. P.; Shafer, M. M.; Schauer, J. J.; Solomon, P. A.; Lantz, J.; Artamonova, M.; Chen, B.; Imashev, S.; Sverdlik, L.; Carmichael, G. R.; Deminter, J. T. *Atmospheric Environment* **2011**, *45*, 6955.
- (46) Diaz, E. A.; Lemos, M.; Coull, B.; Long, M. S.; Rohr, A. C.; Ruiz, P.; Gupta, T.; Kang, C. M.; Godleski, J. J. *Inhal Toxicol* **2011**, *23*, 42.
- (47) Hamilton, J. F.; Lewis, A. C.; Carey, T. J.; Wenger, J. C.; Garcia, E. B. I.; Munoz, A. *Atmospheric Chemistry and Physics* **2009**, *9*, 3815.
- (48) Carlton, A. G.; Wiedinmyer, C.; Kroll, J. H. *Atmospheric Chemistry and Physics* **2009**, *9*, 4987.

CHAPTER 3. INSTRUMENTAL INFRASTRUCTURE

The following instrumental infrastructure was used to characterize and understand the yield and properties of SOA generated via the ozonolysis of GLVs. A schematic representation of the general operating mode is given in Figure 3.1 with more detailed descriptions of experimental protocols in subsequent chapters.



All experiments were performed at ambient pressure and temperature (~23°C) in Teflon chambers. A summary of the chamber characteristics can be found in Table 3.1. Between experiments, chambers were passivated overnight with 1-2 ppm O₃ and flushed with particle, VOC and oxidant-free air (zero air) to attain background aerosol mass loadings < 0.1 µg m⁻³.

Table 3.1 Characteristics of reaction chambers used in this work.

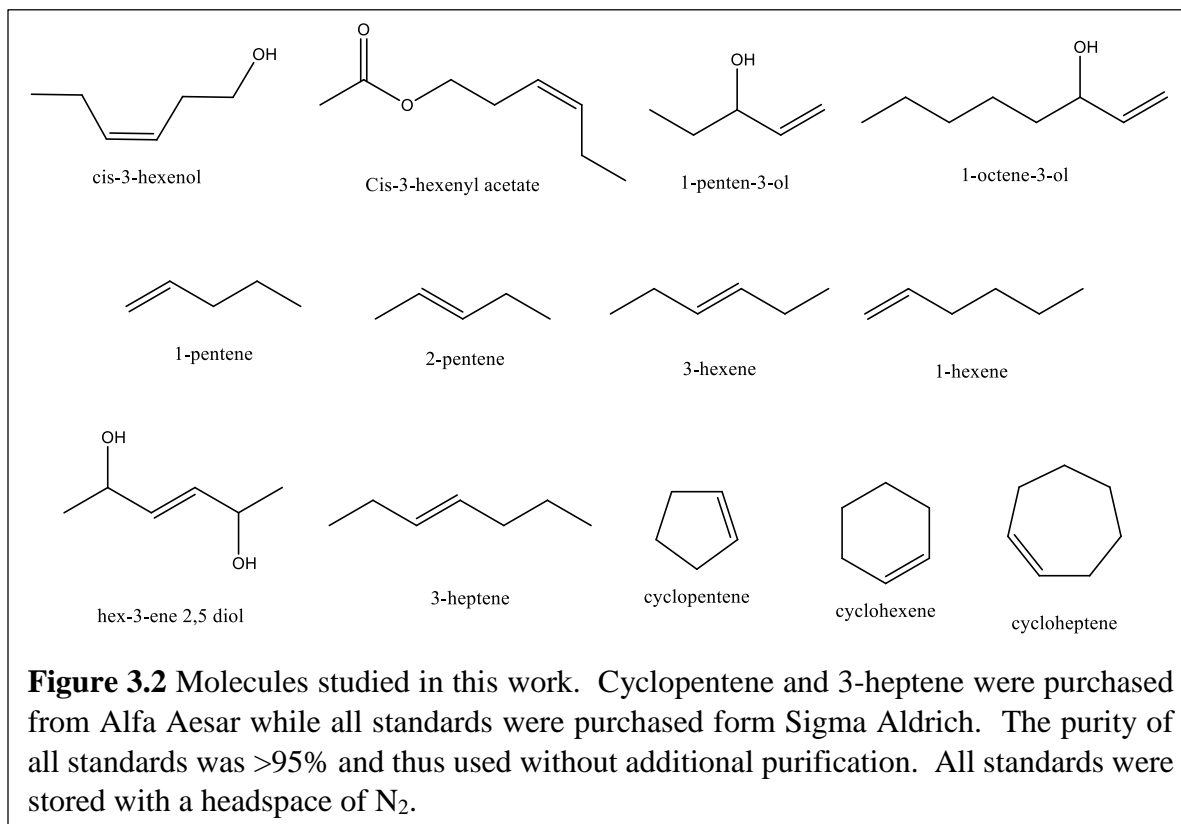
	UVM Pillow Reactor	UVM Environmental Chamber (UVMEC)	Harvard Environmental Chamber (HEC)
Material	Teflon	Teflon	Teflon
Operation Mode	Batch	Batch	Continuous Flow
Volume	775 L	8000 L	4700 L

Standards (all >95%) were purchased from suppliers and used without further purification. A complete list of all standards used can be found in Table 3.2 below. Standards were introduced to the experimental chambers via a heated bulb under steady flow of dry, zero air, which was produced by passing compressed air sequentially through silica, activated carbon and HEPA filters.

Zero air was also used to generate ozone using a commercial corona discharge ozone generator (OLSOA/DLS OzoneLab), which was injected into reaction chambers as a quick burst and was then monitored with an American Ecotech Serinus O₃ Monitor (model E020010).

Aerosol particle size distributions, as well as total aerosol mass loadings were measured continuously with a scanning mobility particle sizer (SMPS, model 3080, TSI Inc., Shoreview, MN). A multi stage electrical low pressure impactor (ELPI+, Dekati

Kangasala, Finland) was also used to measure particle size distributions and to measure particle Bounce Factor (BF) in accordance with Jain et al. 2015.¹



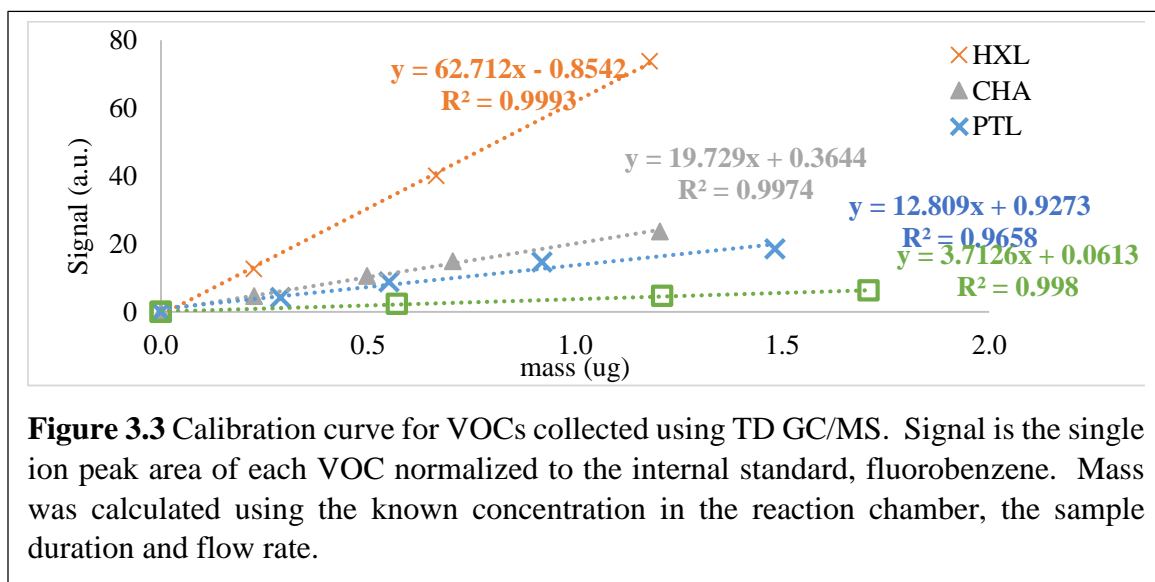
3.1 VOC Analysis

3.1.1 Thermal Desorption GC/MS

Thermal desorption gas chromatography mass spectrometry (TD-GC/MS, Perkin Elmer Turbomatrix TD coupled with a Perkin Elmer Clarus 600 GC and a Perkin Elmer Clarus 600 T mass spectrometer) was used to monitor VOC concentrations. Briefly, air samples are drawn through a TD tube packed with a (or several) sorbent bed, where VOCs are trapped. Samples are then transferred from the sorbent tubes by thermal two-step desorption directly onto the analytical column (Stabilwax 30 m 0.32 mm i.d., Restek) of a

gas chromatograph, effectively concentrating the sample. Prior to desorption, an internal standard (fluorobenzene) was automatically injected onto the TD tubes by the Turbomatrix TD. Calibration of the TD-GC/MS was done by injecting a known mass of pure VOC standard directly into the reaction chamber to reach a known concentration (since the chamber volume was known). Samples were then collected at a known flow rate and duration, allowing for a volume and thereby a theoretical mass of standard to be calculated. The signal of this known mass was then quantified via peak area in single ion monitoring mode and repeated for a range of different masses. Representative calibration curves for GLVs are given in Figure 3.3.

New calibration curves were used each day to limit errors due to instrument drift. Ozone was then injected into the reaction chamber as a brief burst and sampling continued. Standard experiments were carried out at a 1:1 and 1:2 GLV to O₃ molar ratio to determine aerosol yields and measure reaction products. High GLV mass loadings were used to ensure sufficient SOA mass and volatile product evolution for analysis.



3.1.2 Solid Phase Microextraction GC/MS

One of the most common methods used to measure the VOC emission profile of plants is solid phase microextraction (SPME) coupled with gas chromatography mass spectrometry (GC/MS).²⁻⁵ SPME consists of a small polymer-coated fiber to which, in the presence of a gas sample, VOCs adsorb. After a suitable period of time, the fiber is extracted from the sample gas and injected directly into a GC/MS for analysis.^{2,5,6} One advantage of this method is that analytes can be quantified without the need for calibration curves (critically important if the analyte is not available commercially in pure form).

One limitation of SPME is its poor trapping efficiency for high volatility compounds (SPME is more efficient at sampling semi-VOCs).⁴ TD-GC/MS, however has shown great utility to measure plant volatiles⁷⁻¹⁰ and compliments SPME in its ability to efficiently sample very volatile compounds. The combination of these two sampling methods is important to sampling VOCs with a wide range of volatilities. Furthermore, the ability of both methods to pre-concentrate samples greatly enhances the sensitivity of the analysis.

As mentioned above, one advantage to using SPME for VOC emission analysis is that it is a “calibration-free” method. This feature stems from the fact that sampling is an equilibrium process, where analytes establish equilibrium between the fiber and the surrounding matrix. If the fiber is exposed to the sample until an equilibrium point is reached, then the extracted analyte is proportional to the initial concentration in the matrix. This equilibrium can be expressed using the equilibrium constant K , which is the ratio of the concentration of a given analyte in the gas phase (C_g) and on the fiber (C_f):

$$K = \frac{c_f}{c_g} \quad (3.1)$$

K is a constant for a given analyte and a given fiber phase and, once determined, can be used to estimate the concentration of analyte in a gas without performing calibrations.

We determined K for HXL, CHA, and 1-octene-3-ol. First, the signal response from the GC/MS (peak area) was calibrated using standards in cyclohexane (1 μL injections). Figure 3.4 shows a calibration curve for HXL in cyclohexane. Triplicate measurements were made at each concentration, giving a linear response with a good R^2 value of 0.999.

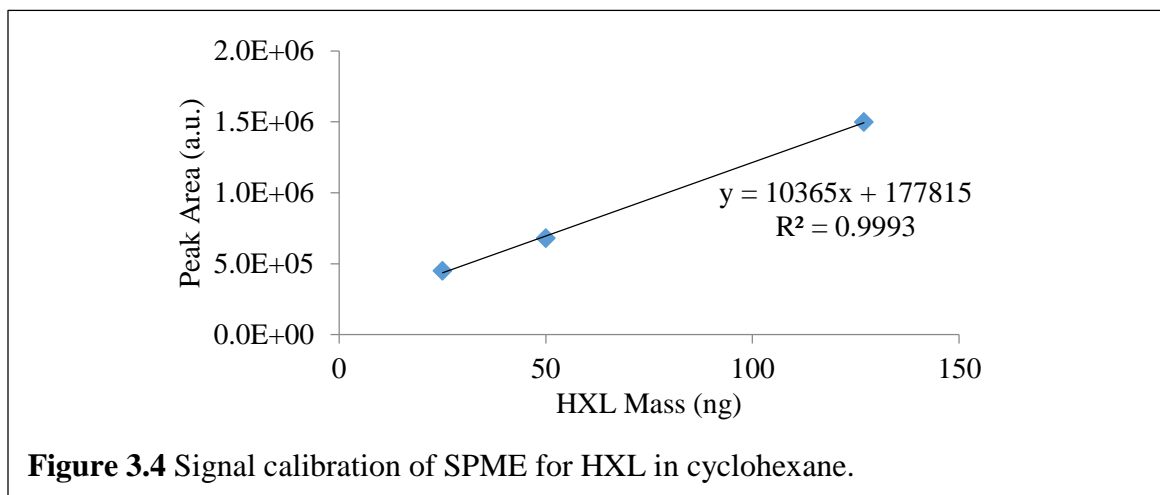


Figure 3.4 Signal calibration of SPME for HXL in cyclohexane.

We then needed to determine the equilibration time, or how long the fiber needed to be exposed to the matrix in order to ensure equilibrium was reached. In separate experiments, single analyte solutions of HXL and CHA in cyclohexane were injected into the 775 L Teflon Pillow Chamber to reach a final gaseous concentration of 5.5×10^{-4} ng/ μL HXL and 5.8×10^{-4} ng/ μL CHA. Samples were then collected for varying amounts of time until the analyte signal no longer increased as a function of sampling time. As shown in Figure 3.5, the signal for HXL plateaued after only 20 min of sampling time, indicating

that HXL reaches equilibrium with SPME fiber and gas phase in that amount of time. Even after 60 min of sampling, however, gaseous CHA did not reach equilibration with the SPME fiber. In fact, CHA signal increased with sample time up to 1 hour of sample time, shown in Figure 3.5.

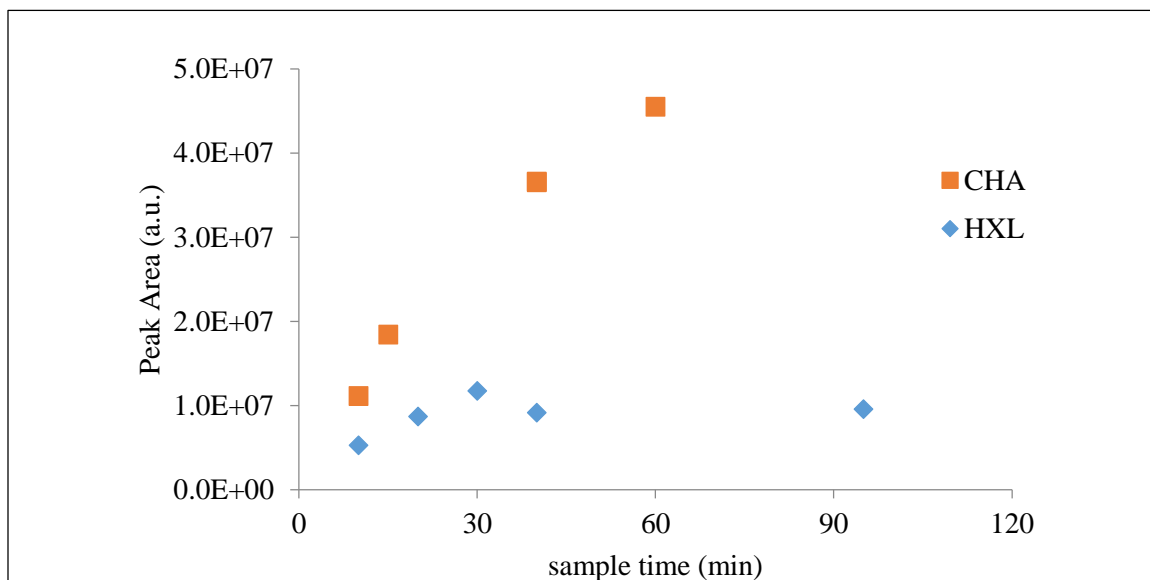


Figure 3.5 Determination of equilibration time for HXL and CHA. The HXL signal did not increase after 20 min sample time, indicating that equilibration is reached within 20 min. CHA however, did not equilibrate with the fiber, even after 60 min, and in fact appears to have a logarithmic trend.

For logistical reasons, a 60 + minute sampling time was not feasible for this research. Instead, we took advantage of the fact that, before equilibrium is reached, the mass of analyte adsorbed onto the fiber is linearly proportional to the sampling time and the mass of analyte in the sample gas.¹¹ So by determining K for a specific sampling time, and then maintaining that sampling time in experiments, gaseous concentrations could be determined.

Therefore, SPME samples were collected for 40 (± 0.25) min and analyzed via

GC/MS. Signal response was converted to mass using instrument calibrations (Fig 3.4). K was then determined using Equation 3.1, where C_f was determined by dividing the average mass of HXL in the fiber by the SPME fiber volume (V_f), which was given by the manufacturer to be 0.418 μL :

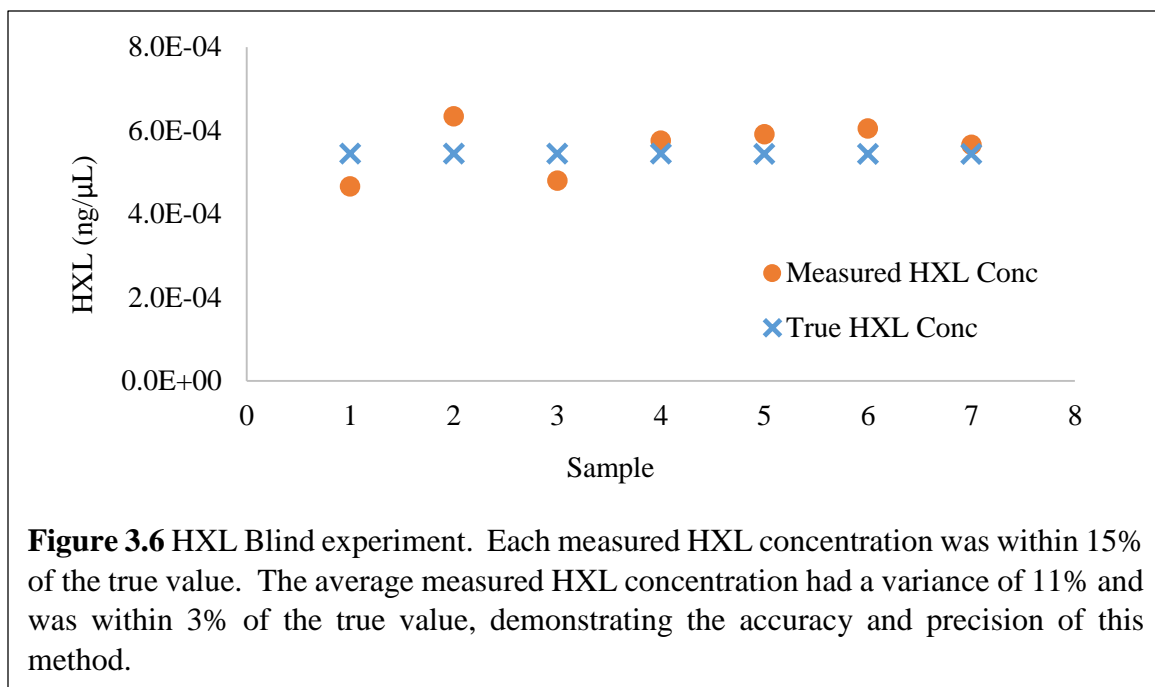
$$C_f = \frac{\text{HXL mass (ng)}}{V_f (\mu\text{L})} \quad (3.2)$$

C_g (Equation 3.1) was known in these experiments, as a known mass of VOC was injected into the reaction chamber with a known volume. The K -values for the GLVs studied are given in Table 3.2

Table 3.2 K -values for GLVs

GLV	Sample Time (min)	Mass on Fiber (ng)	K	Log(K)
HXL	40	297	1.29×10^6	6.11
CHA	40	173	7.16×10^5	5.85
1-octene-3-ol	40	80	3.51×10^5	5.54

To validate this methodology, we used these K -values to accurately predict gas-phase concentrations of HXL in a “blind experiment,” where a known mass of HXL was injected into the reaction chamber and then the concentration was measured using SPME and the K -values determined experimentally. As shown in Figure 3.6, the measured HXL concentration for each sample was within 15% of the theoretically calculated value. Averaged across all seven samples, the measured HXL concentration was within 3% of the expected theoretical value and the variation between measurements was 11%, confirming that this method for determining gas-phase concentration of VOCs is both accurate and precise.



3.2 Wall Loss of VOCs

Gaseous wall-loss of standards was determined by monitoring VOC concentration using TD-GC/MS within the 775-L reaction chamber for six hours (Figure 3.7). A 3- μ L aliquot of an equimolar mix of GLVs was injected into the reaction chamber and monitored for 3 hours. The absence of any downward trend in GLV signal indicates that no GLVs partitioned onto the chamber walls and there was little or no gaseous wall loss for any of the species within this time frame.

At time 14:40 (as indicated by a black line in Figure 3.7), an additional \sim 175 mL of zero air was added to dilute the chamber air and the GLVs were monitored for an additional 3 hours to investigate if any observed wall loss was reversible. If a GLV had shown loss to the reaction chamber walls within the first 3 hours (as evidenced by a decrease in concentration), then remained constant or increased in concentration after the

dilution step, it would demonstrate *reversible* wall losses as described by Loza et al. (2010)¹² However, as stated above, we saw no evidence of wall loss of our gaseous GLVs, and therefore no reversible wall loss either.

Despite being injected at an equimolar ratio, the measured concentration for CHA and HXL was less than that for 1-penten-3-ol. The disparity may be a result of the incomplete transfer of GLV into the reaction chamber (sorption to tubing from bulb to reaction chamber), or differences in sampling efficiency by the TD, although these would be expected to have occurred in calibration measurements as well, which would have accounted for losses. The reason for the difference in signal is not clear, but is inconsequential to conclusions that can be made from this experiment.

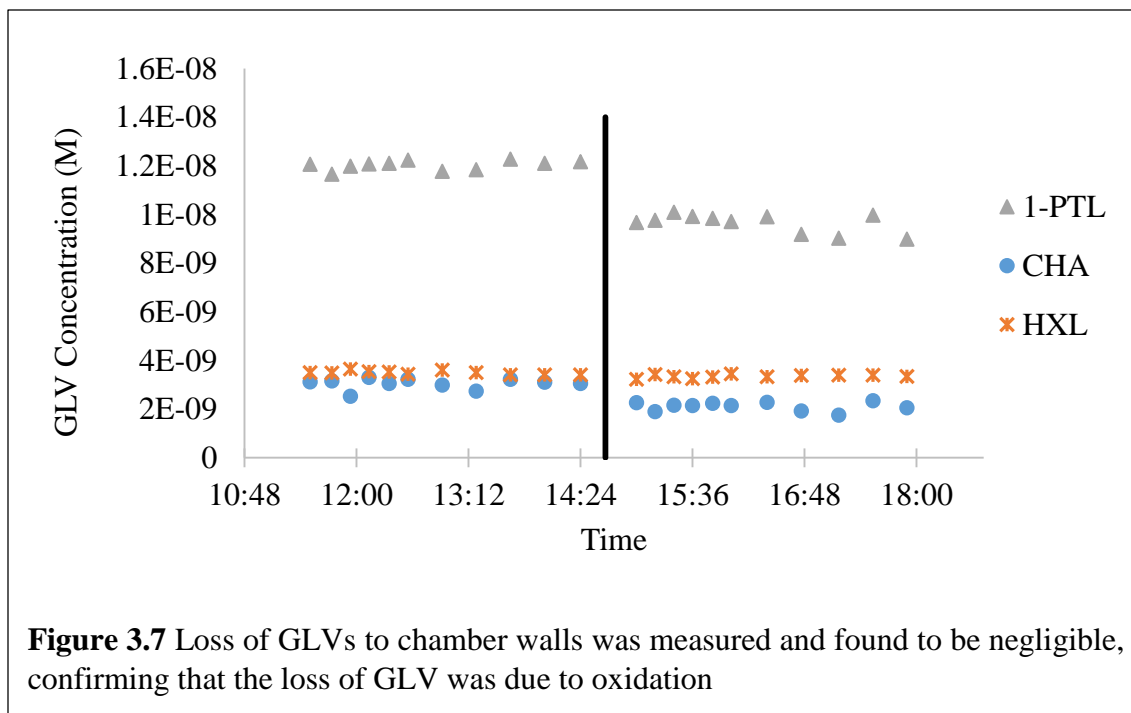


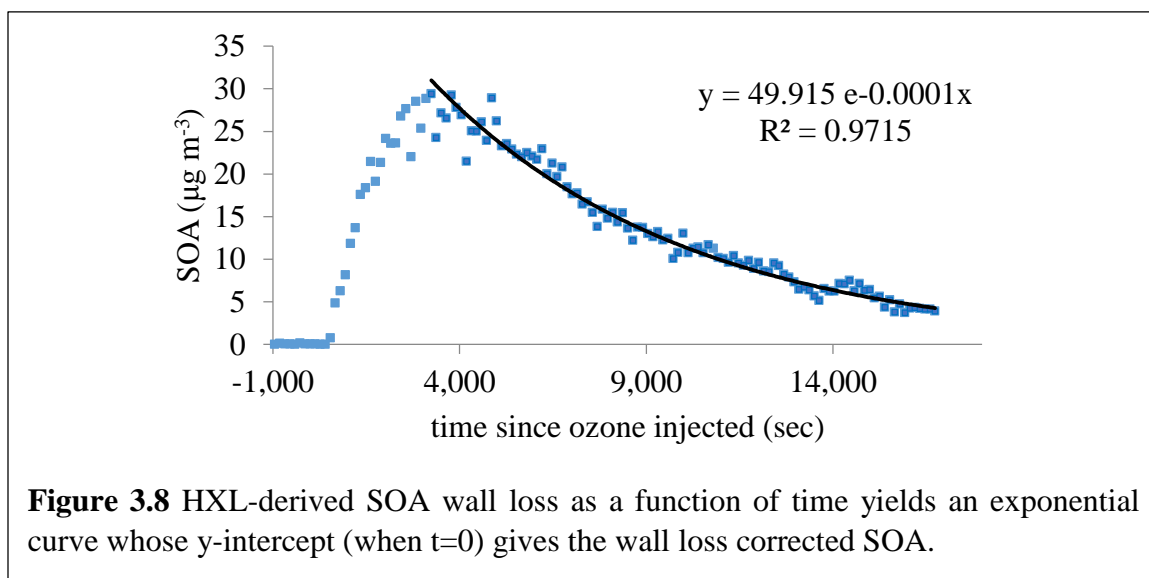
Figure 3.7 Loss of GLVs to chamber walls was measured and found to be negligible, confirming that the loss of GLV was due to oxidation

3.3 Wall Loss of SOA

The partitioning of particles to chamber walls is a significant loss mechanism for SOA in these chamber studies, and results in erroneously low SOA concentrations as measured by SMPS. To account for this loss, the decay of SOA signal as a function of time in GLV ozonolysis experiments was monitored and extrapolated back to time zero, the time at which ozone was injected into the chamber. For example, a HXL ozonolysis experiment gave the SOA profile in Figure 3.8. The HXL-derived SOA decay fits the exponential equation:

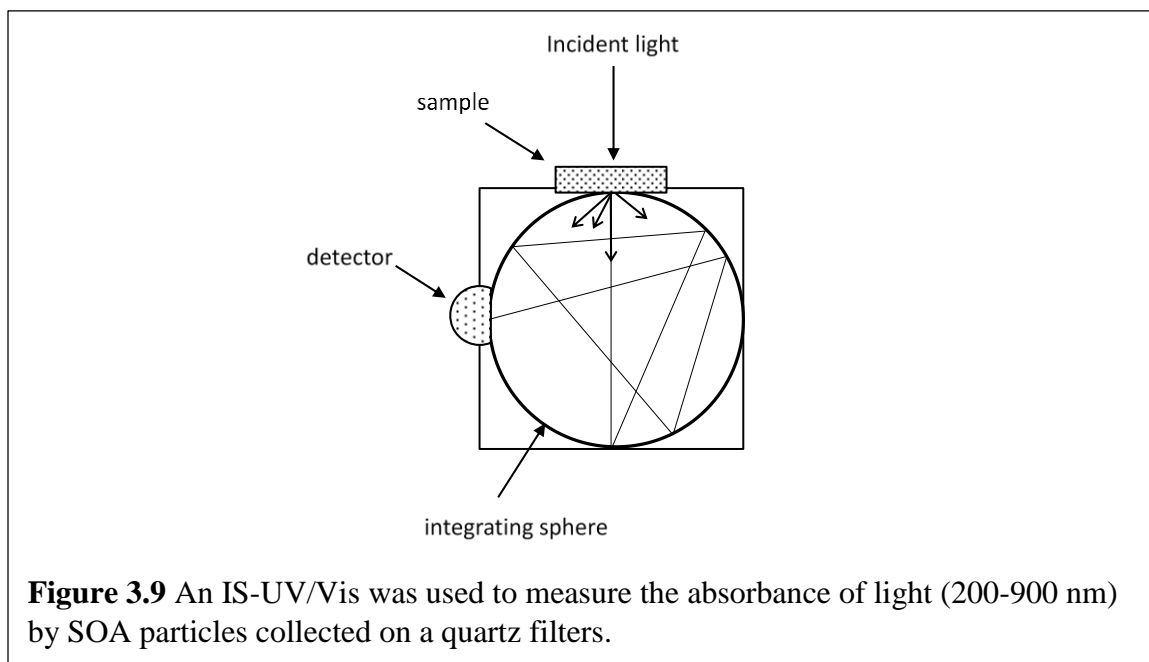
$$y = 49.915e^{-1E-04x} \quad (3.3)$$

Extrapolation to time zero yields a SOA_{max} of $49.9 \mu\text{g}/\text{m}^3$, which represents the wall loss-corrected maximum SOA concentration, as compared to the maximum SOA measured; $29.4 \mu\text{g}/\text{m}^3$. These plots and analyses were used for each experiment herein to report the “wall loss corrected SOA” mass concentration.



3.4 Determining the Optical Properties of SOA

SOA was collected on to quartz filters and absorbance was measured via integrating sphere UV-Vis spectroscopy from 200 nm to 900 nm at 1-nm resolution (IS-UV-Vis, Shimadzu UV-2450 with ISR 2200) (Figure 3.9). Filters with collected SOA are placed at the inlet of the IS. A detector measures the percent transmitted light through the sample and determines absorbance by the sample (correcting for absorbance by a clean quartz filter). A more detailed sampling protocol is described in Chapter 5.0.



A three-wavelength integrating nephelometer (Aurora 3000, Ecotech) was used to measure the scatter of light by particles (forward and backward) at 450 nm, 525 nm and 635 nm. An extensive review of integrating nephelometers has been given by Heintzenberg and Charlson (1996),¹³ and a review of the performance of the Aurora 3000 specifically is given by Muller et al. (2011).¹⁴ Briefly, integrating nephelometers are

widely used to measure the light scattering coefficient of both ambient and laboratory-generated particles. They can be calibrated with gases of known scattering coefficients, require no assumptions about particle composition, size or shape and the Aurora 3000 has detection limits on the order of 0.1 Mm^{-1} and uncertainties on the order of 5-10%.¹⁴ Nephelometer measurements do however, introduce truncation errors that influence the measured scatter values.¹⁵ For particles with diameters greater than $1 \text{ }\mu\text{m}$, these errors can be as large 20%-50%. For accumulation-mode particles (diameters between 200 and 400 nm), however, truncation errors are limited to $\sim 10\%$.¹⁵ Since the particles being studied in this work are in the accumulation-mode, truncation errors represent a lower bound of measurement errors in this work and thus no attempts to quantify and/or correct this error were made

3.5 Determination of SOA Yield

The aerosol yield (Y) quantifies the conversion efficiency with which a VOC produces SOA on a mass basis. Y for GLVs were calculated according to equation (3.4) where $\Delta[\text{SOA}]$ is the maximum SOA concentration ($\mu\text{g}/\text{mL}$, assuming a particle density of $1.2 \text{ }\mu\text{g}/\text{m}^3$) and $\Delta[\text{GLV}]$ is the total amount of GLV consumed ($\mu\text{g}/\text{mL}$) at that SOA maximum.¹⁶

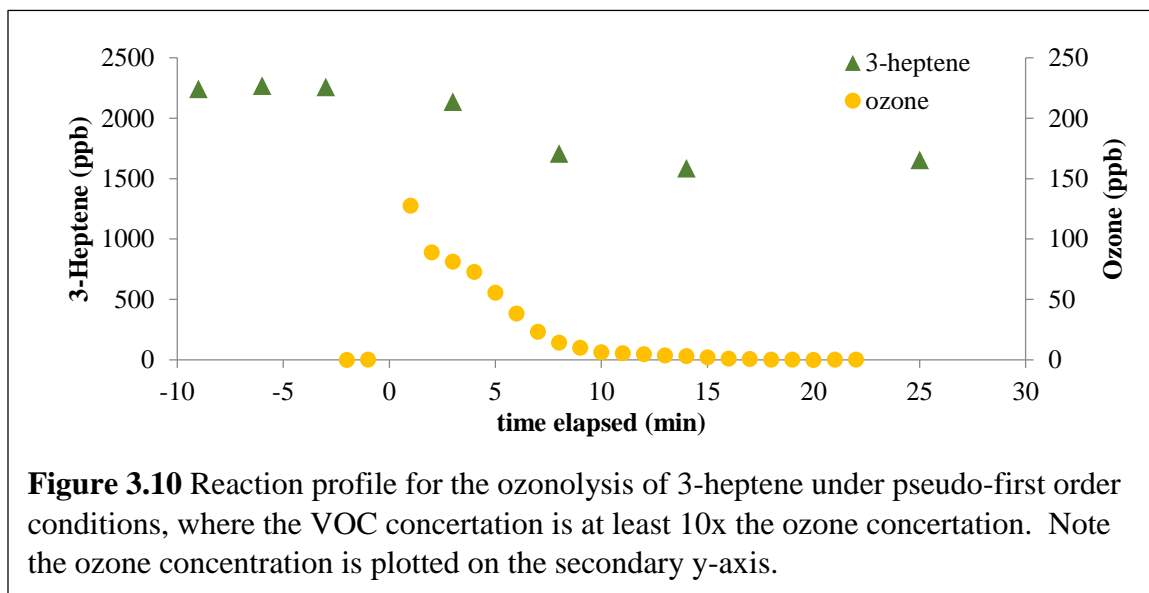
$$Y = \frac{\Delta[\text{SOA}]}{\Delta[\text{GLV}]} \times 100\% \quad (3.4)$$

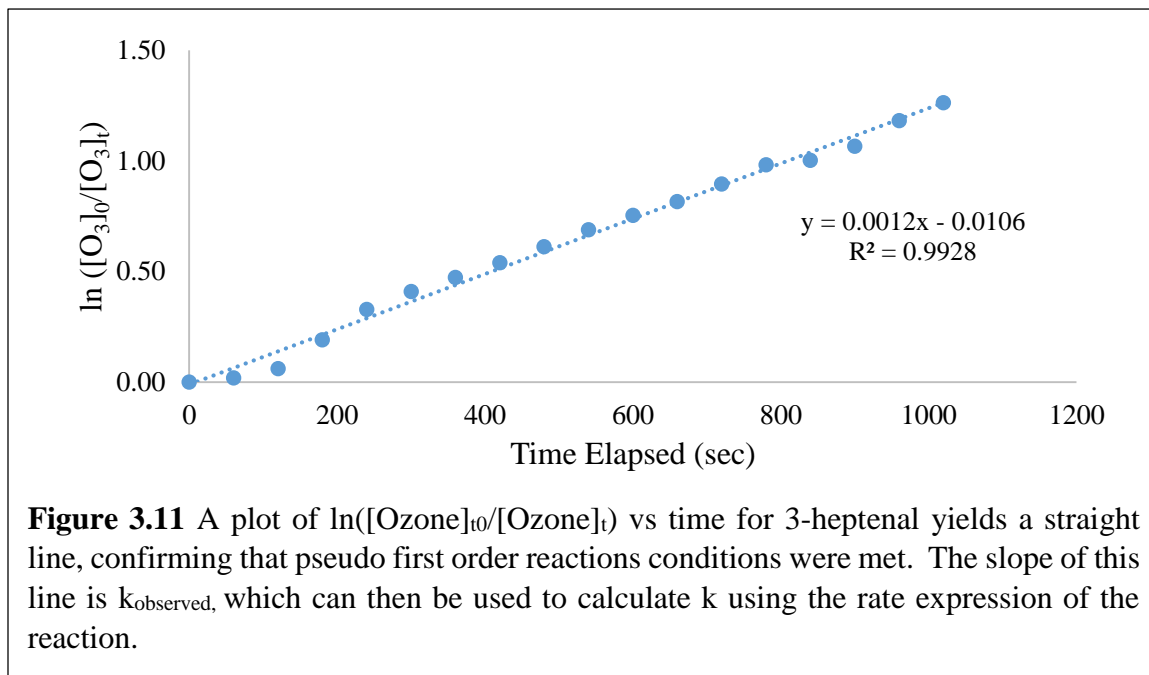
Aerosol yield scales with VOC loading, where higher loadings result in greater yield. The aerosol yields used herein were determined at VOC loadings of 1000 ppb.

3.6 Determination of Ozonolysis Rate Constant (k)

Reaction rate constants (k) for the ozonolysis of VOCs were determined using the experimental protocol described elsewhere.^{17,18} Briefly, pseudo-first-order reaction conditions were induced, whereby the VOC was present in at least a 10 times excess of ozone. Ozone was injected as a quick burst and monitored throughout the reaction, while the GLV was monitored periodically to ensure pseudo-first order conditions were maintained (Figure 3.10).

A plot of $\ln([O_3]_0/[O_3]_t)$, where $[O_3]_0$ is the initial ozone concentration and $[O_3]_t$ is the ozone concentration at time (t), against time (seconds) yields a straight line, confirming that pseudo-first order reaction conditions were met (Figure 3.11). The slope of this line is the observed rate constant (k_{obs})(sec^{-1}). The rate constant is then found using the rate expression of the reaction, $k = k_{observed}/[VOC]_0$, where $[VOC]_0$ is the initial concentration of the VOC in units of molecules cm^{-3} , which gives k in units of $cm^3sec^{-1}molecule^{-1}$.





3.7 References

- (1) Jain, S.; Petrucci, G. A. *Aerosol Sci Tech* **2015**, *49*, 390.
- (2) Baker, B.; Sinnott, M. *J Chromatogr A* **2009**, *1216*, 8442.
- (3) Risticvic, S.; Lord, H.; Gorecki, T.; Arthur, C. L.; Pawliszyn, J. *Nat. Protocols* **2010**, *5*, 122.
- (4) Koziel, J. A.; Pawliszyn, J. *J Air Waste Manage* **2001**, *51*, 173.
- (5) Cornu, A.; Carnat, A.-P.; Martin, B.; Coulon, J.-B.; Lamaison, J.-L.; Berdagué, J.-L. *J Agr Food Chem* **2001**, *49*, 203.
- (6) Bouvier-Brown, N. C.; Holzinger, R.; Palitzsch, K.; Goldstein, A. H. *J Chromatogr A* **2007**, *1161*, 113.
- (7) Esteban, J. L.; MartinezCastro, I.; Morales, R.; Fabrellas, B.; Sanz, J. *Chromatographia* **1996**, *43*, 63.
- (8) Vallat, A.; Gu, H. N.; Dorn, S. *Phytochemistry* **2005**, *66*, 1540.
- (9) Kallenbach, M.; Oh, Y.; Eilers, E. J.; Veit, D.; Baldwin, I. T.; Schuman, M. C. *Plant J* **2014**, *78*, 1060.
- (10) Harvey, R. M.; Zahardis, J.; Petrucci, G. A. *Atmos Chem Phys* **2014**, *14*, 797.

- (11) Bouvier-Brown, N. C.; Holzinger, R.; Palitzsch, K.; Goldstein, A. H. *J Chromatogr A* **2007**, *1161*, 113.
- (12) Loza, C. L.; Chan, A. W. H.; Galloway, M. M.; Keutsch, F. N.; Flagan, R. C.; Seinfeld, J. H. *Environ Sci Technol* **2010**, *44*, 5074.
- (13) Heintzenberg, J.; Charlson, R. J. *J Atmos Ocean Tech* **1996**, *13*, 987.
- (14) Müller, T.; Laborde, M.; Kassell, G.; Wiedensohler, A. *Atmos. Meas. Tech.* **2011**, *4*, 1291.
- (15) Moosmüller, H.; Arnott, W. P. *Review of Scientific Instruments* **2003**, *74*, 3492.
- (16) Odum, J. R.; Hoffmann, T.; Bowman, F.; Collins, D.; Flagan, R. C.; Seinfeld, J. H. *Environ. Sci. Technol.* **1996**, *30*, 2580.
- (17) Grosjean, D.; Grosjean, E.; Williams, E. L. *Int J Chem Kinet* **1993**, *25*, 783.
- (18) Grosjean, E.; Grosjean, D. *Int J Chem Kinet* **1994**, *26*, 1185.

CHAPTER 4. ESTABLISHING THE CONTRIBUTION OF LAWN MOWING TO ATMOSPHERIC AEROSOL LEVELS IN AMERICAN SUBURBS

The following is an expansion upon a manuscript, submitted and accepted for publication in *Atmospheric Physics and Chemistry*. The full reference follows and a reprint of the published manuscript can be found in the Appendix.

Harvey, R. M.; Zahardis, J.; Petrucci, G. A., Establishing the contribution of lawn mowing to atmospheric aerosol levels in American suburbs. *Atmos. Chem. Phys.* 2014, *14* (2), 797-812.

4.1 Introduction

Volatile organic compounds (VOCs) are emitted by both biogenic (BVOCs) and anthropogenic (AVOCs) sources and play an important role in the chemistry of the atmosphere. The photooxidation of VOCs can lead to the formation of ozone, with which other VOCs can react (along with other atmospheric oxidants) to produce secondary organic aerosol (SOA).^{1,2} Organic aerosols, including SOA are a major component of fine aerosols and influence climate through direct and indirect effects, although there is an expressed high degree of uncertainty about the magnitude of these effects.^{3,4} SOA also impacts local weather patterns and has been associated with deleterious impacts on human health.^{5,6} Currently, there remains significant uncertainty in our understanding of the environmental impact of SOA, owing to a still limited knowledge of its sources, composition, properties, and the mechanisms that lead to its formation.⁷⁻⁹ Identifying the

sources, interactions and reactivity of VOCs is integral to understanding their impact on the formation of SOA and consequently on regional air quality and climate patterns.

Globally, biogenic SOA (BSOA) predominates over anthropogenic SOA (ASOA).¹ Though our understanding of the mechanisms that lead to SOA formation has improved, significant gaps exist in our understanding of SOA formation and ageing, namely our understanding of systems with competing reactive pathways. Several recent studies have stressed the potential importance of interactions between AVOCs, BVOCs and oxidants in SOA formation and ageing, and yet these interactions remain largely uncharacterized.⁹⁻¹³ Of special interest to our group is SOA production and ageing at the interface of urban and suburban/rural landscapes. This interface offers the unique opportunity to study atmospherically relevant mixtures of anthropogenic and biogenic VOCs and SOA, as will be discussed.

Characterized by a ‘freshly mowed lawn’ smell, the cutting of turfgrass enhances emission of a complex mixture of C₅ and C₆ BVOCs, along with other low molecular weight oxygenated BVOCs.¹⁴⁻²² Together these BVOCs are termed green leaf volatiles (GLVs).²³ The most documented GLVs include the C₆ compounds *cis*-3-hexenal, *cis*-3-hexenol (HXL), *cis*-3-hexenyl acetate (CHA), and *trans*-2-hexenal. More recently, C₅ compounds (*cis*-2-penten-1-ol and 1-penten-3-ol) have also been identified in the wound-induced emissions of plants.^{21,23,24} Not only do these compounds have interesting roles in plant protection and plant-plant/plant-animal communication, GLVs also actively take part in atmospheric chemistry.^{19,25,26}

Though individual VOCs differ greatly in their reactivity and consequently their SOA-forming potential, many grass-GLVs contain unsaturated double bonds, which are readily oxidized by ozone, hydroxyl radicals and nitrate radicals, providing important potential pathways to the generation of photochemical smog and SOA.^{7,20,24,27-30} Brill et al.¹⁹ estimate that grassland ecosystems emit up to 130 Mg C m⁻² GLVs annually. Several other studies have reported GLV emission rates on the same order of magnitude for mowed grasses.^{14,22,31} Lawn coverage in the US is estimated at 10-16 million ha, which corresponds to a total of ~13-21 Gg C yr⁻¹ of GLVs emitted by lawns in the US alone.³² Omitting methanol and other low molecular weight GLVs, which account for ~70% of total GLV emissions and are not readily oxidized in the atmosphere, reactive lawn-GLV emissions can be estimated at between 3.9 and 6.3 Gg C annually. Annual non-methane VOCs in North America are estimated at 84 Tg C.^{19,20,33,34}

The role reactive GLVs play in global SOA levels, however is not straightforward. Reports of GLV aerosol yields are varied. CHA is reported to have 8.5-24% aerosol yield from ozonolysis and less than 1% aerosol yield from photooxidation, while HXL has been reported to have 9.6% and 3.1% aerosol yield from ozonolysis and photooxidation, respectively.^{7,28,35} Based on GLV emission rates and SOA yield efficiencies, lawns in the US alone therefore have the potential to contribute ~1.5 Gg C of SOA to the atmosphere annually. Hamilton et al.⁷ estimated that photooxidation of the predominant C₆ GLVs HXL and CHA contribute as much as 1-5 Tg C yr⁻¹ SOA to global emissions, which current models estimate to be between 25-300 Tg C yr⁻¹.^{1,7,36,37} *Photooxidation* of these two GLVs alone could contribute a significant fraction of global SOA. The *ozonolysis* of GLVs,

however, having greater aerosol yields than photooxidation, is likely to be an additional, significant SOA source to the atmosphere with important contributions to climate forcing and air quality at the airshed.

Hamilton et al.⁷ established the importance of GLV oxidation to global SOA using single-component systems, with one oxidant being introduced to each GLV separately. We extend this work by representing the multi-component system experienced in the environment, especially at the urban/suburban interface. At this interface, traffic and industry located in urban hubs provide a source of anthropogenic oxidants and ASOA, while suburban neighborhoods, with their sprawling monocultural lawns and recreational fields, have the potential to emit large quantities of mow-induced GLVs and BSOA. This scenario provides a unique opportunity to study aerosol formation in a multi-component system and at a regionally relevant scale.^{22,23,38-42} Since grass mowing typically occurs on hot sunny days in a regionally, seasonally and sometimes temporally coordinated fashion, emission of reactive GLVs is expected to occur in large-scale bursts. Simultaneously, tropospheric ozone is present at elevated concentrations on hot sunny days.⁴² In urban and suburban environments, GLV bursts into oxidizing atmospheric conditions therefore, provide an opportunity for concerted bursts of SOA into an airshed.^{20,23} The interface between urban and suburban landscapes provides the opportunity to study SOA formation in a multi-component system at a small spatial and temporal scale, where ASOA can exceed BSOA and where processes leading to SOA formation could be different from those in largely forested regions.^{10,42-45}

Although the GLV-emission profile of several grass and clover species has been characterized^{14,15,19,20,22,23,31,34,46} and the SOA yields of several individual GLVs have been estimated,^{7,27,28,30} to the best of our knowledge there is no reported work on GLV mixtures with respect to their aerosol yields or the characterization of the resultant SOA. In this work, a holistic approach to understanding GLV oxidation and SOA evolution has been used to characterize the contribution of lawn mowing to local SOA levels. Thermal desorption gas chromatography mass spectrometry (TD-GC/MS) was used to characterize the VOC profile of mowed grass. TD-GC/MS was also used to monitor the consumption of GLVs upon ozonolysis and the subsequent evolution of gas phase products, while aerosol size distributions and mass loadings were continuously measured using a scanning mobility particle sizer.

We show that the mow-induced GLV emission profile from turfgrass in a suburban neighborhood in Vermont, USA is dominated by CHA and HXL, which readily undergo oxidation by ozone to form SOA. Aerosol yields were determined for each GLV individually and used to predict SOA evolution for simple, atmospherically relevant mixtures of HXL and CHA and for grass clippings collected from the field. An apparent disparity between predicted and measured SOA production, along with the volatile product profile of each chemical system are discussed herein, highlighting the need to understand more fully the dynamic chemical interactions posed at the urban/suburban interface.

4.2 Experimental

Cis-3-hexenyl acetate (> 98%) and *cis*-3-hexenol (99%) were purchased from Sigma Aldrich and were used without further purification. Dry, zero air was produced by

passing compressed air sequentially through silica, activated carbon and HEPA filters. This zero air was also used to generate ozone using a commercially available corona discharge ozone generator (OLSOA/DLS OzoneLab). Ozone concentrations were monitored with an American Ecotech Serinus O₃ Monitor (model E020010).

All experiments were performed in a 775-L Teflon chamber at ambient temperature (~ 23°C) and atmospheric pressure. Between experiments, the chamber was passivated with O₃ at high concentrations (1-2 ppm) and flushed with zero air to attain background aerosol mass loadings below 0.1 µg/m³.

Air samples were collected from the reaction chamber onto AirToxics glass sorption tubes (Perkin Elmer N9307008) that had been previously conditioned at 310°C for 20 min and stored with Swagelok caps. Air was drawn through the sorption tubes using a personal sampler pump (SKC Airchek Sampler, model 224-44XR) at a constant rate of approximately 100 ml min⁻¹ (actual flow rate monitored by a F&J Specialty Products mini calibrator, model MC-500cc) for a known duration of time, allowing the total volume of air sampled to be determined. Typical sample volumes ranged between 0.6 L and 3.6 L. Ozone scrubbers were not used because some have been shown to retain ozonolysis products.^{47,48}

Air samples were then transferred from the sorbent tubes by thermal two-step desorption (TurboMatrix TD 350, Perkin Elmer) to a gas chromatograph (Clarus 600, Perkin Elmer) equipped with a mass spectrometer (Clarus 600 T Perkin Elmer) detector. Prior to desorption, an internal standard of fluorobenzene (AirLiquide) was injected by the Turbomatrix TD directly onto the sorption tubes. During the first step of desorption, the

sorbent tubes were heated to 330°C for 8 min to desorb and cryo-focus GLVs onto a AirMonitoring trap held at -10°C. The trap was then heated at a rate of 40°Cs⁻¹ to a final temperature of 310°C, where it was held for 8 min. The GLVs were transferred to a GC analytical column (Stabilwax 30 m, 0.32 mm i.d., Restek) via a heated transfer line (250°C). The GC oven was programmed as follows: held at 35°C for 4 min, increasing 10°C min⁻¹ to a final temperature of 220°C. The total run time per sample was 22.5 min. The head pressure of the helium carrier gas was 1.8 psi, which resulted in a flow rate of 1.52 ml/min. Electron impact ionization (70 eV) was used and masses were scanned from 15 to 300 m/z. Chromatographic peaks were identified by comparison of retention times to those of known standards and by spectral matching with the NIST 2005 mass spectral library. Compounds were quantified on an area basis using single ion monitoring.

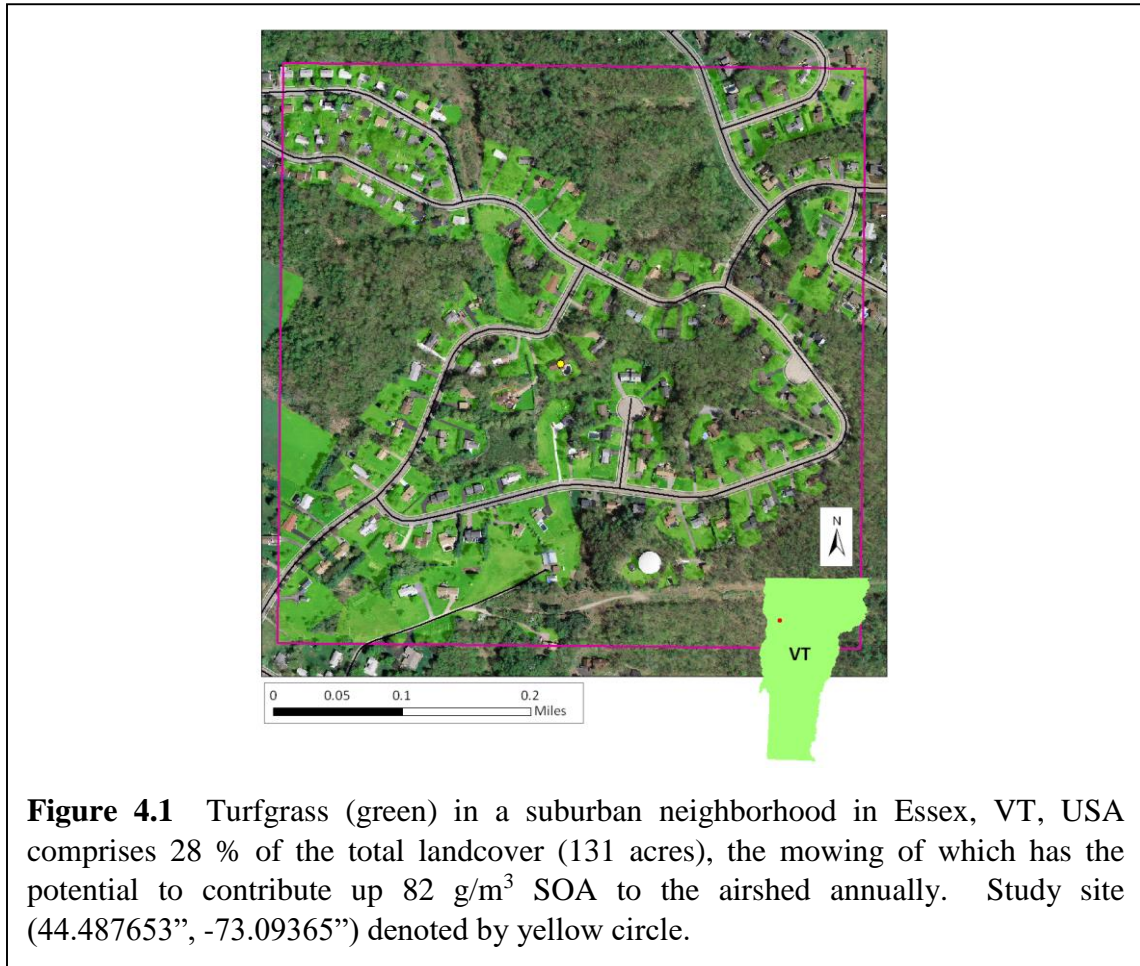
Aerosol particle number and mass size distributions, as well as total aerosol mass loadings, were measured continuously with a scanning mobility particle sizer (SMPS, model SMPS 3080, TSI Inc., Shoreview, MN).

The vapor pressure of several organic ozonolysis products was estimated using structure based estimators courtesy of the Dortmund Data Bank found in the online database by Clegg et al.^{49,50} Estimates were made at 298K and are reported as an average of three estimates determined using methods described in references⁵¹⁻⁵⁵.

4.2.1 Grass Experiments

The grass collection site chosen was located in a residential neighborhood in Essex Junction, VT (44.487653, -73.09365), approximately 10 miles east of Burlington, VT (Figure 4.1). A geospatial analysis of the study site was performed using ArcGIS 9.0 software. Aerial photographs taken in 2004 were obtained from the Vermont Center for

Geographic Information. ⁵⁶ The resolution of these photos was sufficient to visually identify residential turfgrass, ArcGIS software was used to quantify the area of turfgrass (36 acres) along with the total site area (131 acres).

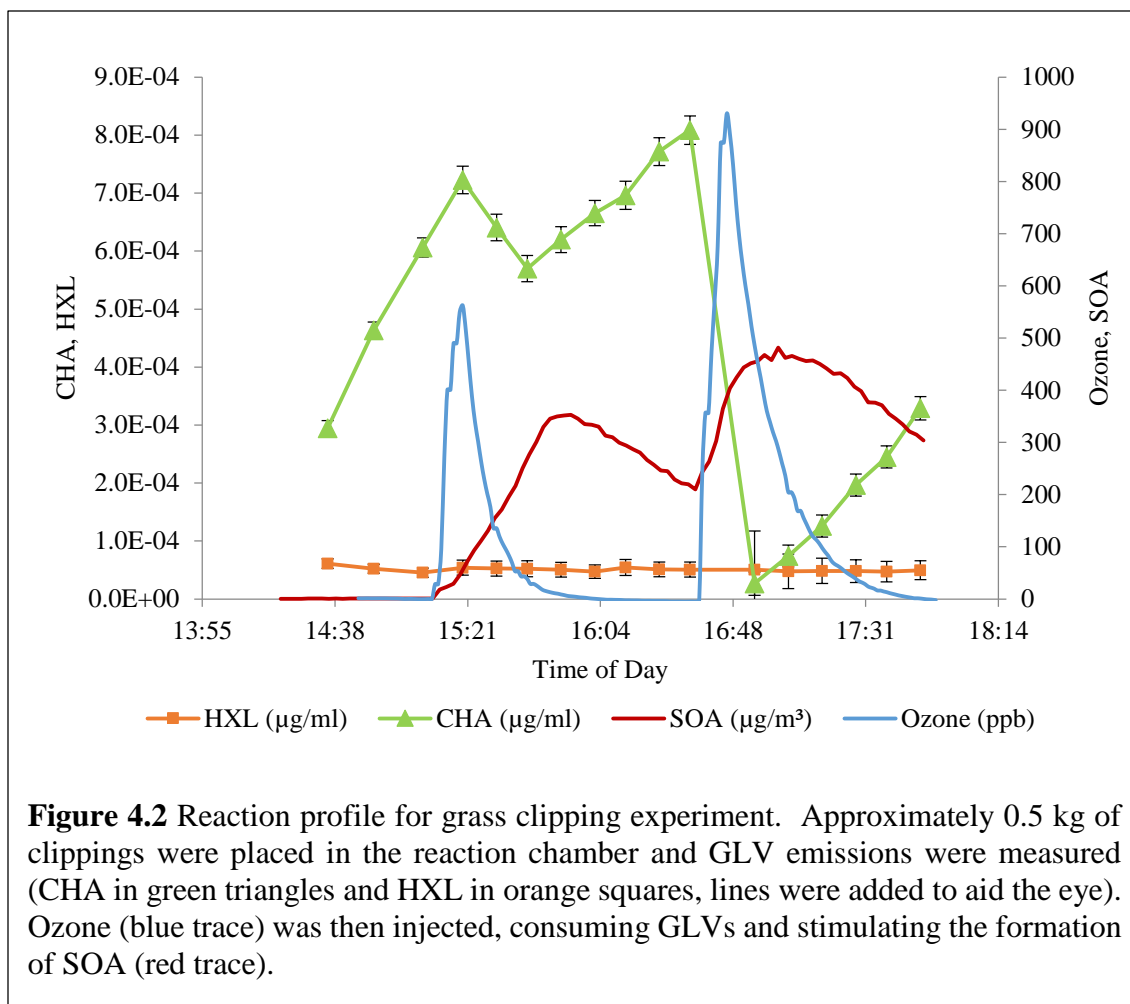


A section of representative turfgrass comprised predominantly of genera *Festuca*, *Lolium* and *Poa* was mowed using a commercially available, residential lawn mower. Clippings were collected and transported in sealed paper bags to the University of Vermont, Burlington VT for analysis. Total time elapsed between mowing and sampling

in the Teflon chamber was between 60 – 90 min. Samples were collected from nine mowing events between September and November of 2012 and one event in May of 2013.

In grass “clipping” experiments, approximately 0.5 kg of grass clippings (wet weight) were placed directly inside the experimental chamber, which was then filled with zero air. Ozone was injected as a brief burst directly into the chamber. A representative reaction profile is given in Figure 4.2.

Grass clipping experiments were designed to represent environmentally relevant conditions, where ozone was allowed to interact with volatile species in the gas phase along with any reactive species contained within or on the blades of grass themselves. Whereas in “headspace” experiments, only volatile species within the headspace of grass clippings were flushed into the reaction chamber, to which ozone was then introduced. For the headspace experiments, approximately 150 grams of grass clippings (wet weight) were placed in a 0.4 L conical flask. Zero air was flushed through the conical flask for ~20 min into the reaction chamber, carrying the GLVs with it. Headspace experiments represented a simplified version of the chemical system of interest, where only the volatile species emitted by cut grass were oxidized by ozone. In general, initial CHA and HXL concentrations were greater in headspace experiments than in clipping experiments. This difference is likely due to experimental design; grass clippings were allowed to equilibrate in the experimental chamber for 20-30 minutes before ozone was injected while grass headspace was allowed to build up in the paper sampling bag for up to two hours before being flushed into the chamber. Grass clippings, however, continuously emitted CHA and HXL.



4.2.2 GLV Standard Experiments

GLV standards experiments were designed to further simplify headspace experiments and were used to determine whether SOA produced as the result of grass ozonolysis could be modeled by a single GLV or a two-component mixture of GLVs. Standards of CHA or HXL were introduced to the experimental chamber by evaporation via injection into a 3-neck flask over a warm water bath. A zero air carrier flow was flushed through the flask and into the reaction chamber for at least 15 minutes. Gaseous wall-loss of GLV standards was determined by monitoring GLV concentration within the reaction

chamber for six hours. GLV concentration did not decrease over the course of this experiment, however and gaseous wall-loss was found to be insignificant (Section S2 material). Calibration was completed by collecting a known volume and thereby known mass of GLV standards from the experimental chamber onto TD tubes. Ozone was then injected as a brief burst and sampling continued. Standard experiments were carried out at a 1:1 and 1:2 GLV to O₃ molar ratio to determine aerosol yields and measure reaction products. High GLV mass loadings were used to ensure sufficient SOA mass and volatile product evolution for analysis.

Reaction rate constants (*k*) for the ozonolysis of CHA and HXL were determined using the experimental protocol described elsewhere.^{57,58} Briefly, pseudo-first-order reaction conditions were induced, whereby the GLV was present in excess of ozone, which was monitored throughout the reaction. A plot of $\ln([\text{Ozone}]_{t_0}/[\text{Ozone}]_t)$ vs time yields a straight line with slope *k*_{observed}. From the rate expression of the reaction, $k = k_{\text{observed}}/[\text{GLV}]_{t_0}$.

4.3 Results

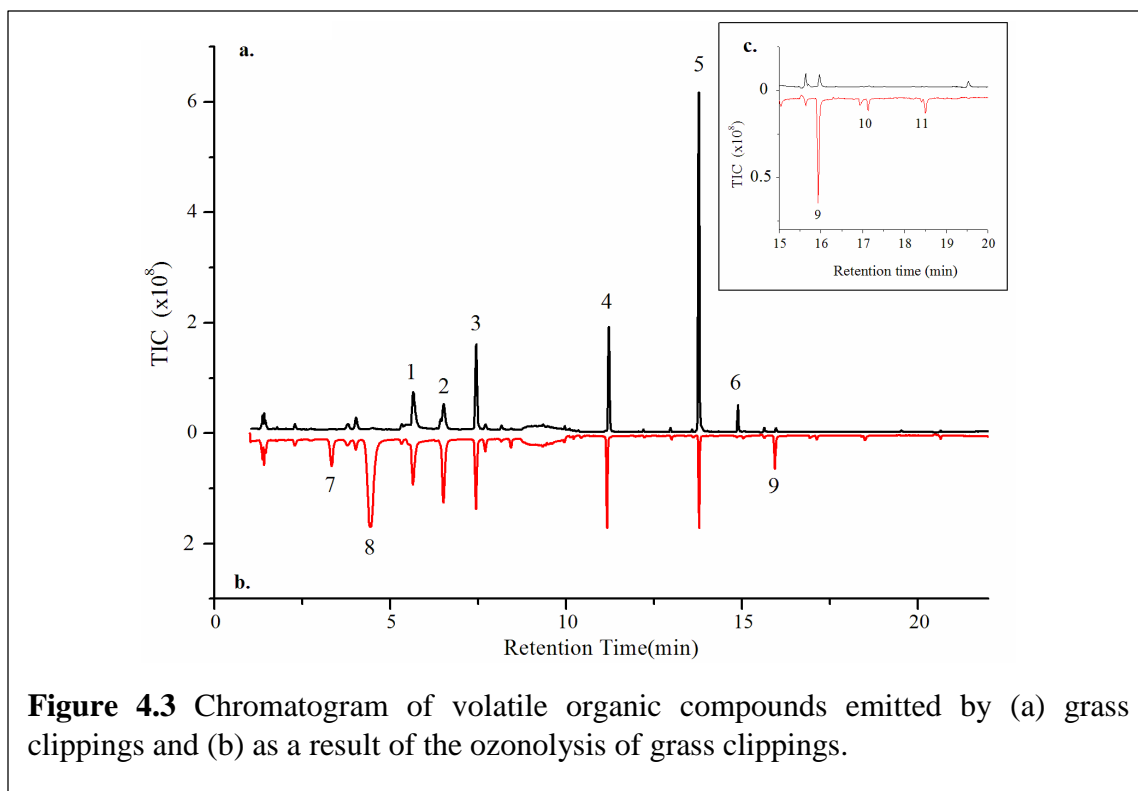
4.3.1 Grass Emissions

The total ion chromatogram (TIC) of GLVs emitted by cut grass (Figure 4.3a) shows a relatively complex mixture of volatile organics, dominated by CHA, 1-penten-3-ol and 2-pentanone (peaks 5, 4 and 3, respectively). Also present is a significant amount of HXL (peak 6), which, along with CHA, is a SOA precursor when subjected to ozone (Scheme 1). This reactivity is clearly demonstrated by the TIC of the GLV mixture post-ozonolysis (Figure 4.3b). 2-pentanone contains no chemical unsaturations and is therefore nonreactive

with ozone. 1-penten-3-ol, despite its double bond, does not appear to be highly reactive with ozone either. This interesting observation is the crux of Chapter 6, which focuses on the control of ozonolysis kinetics and aerosol yield by nuances in the molecular structure of parent volatile organic compounds.

4.3.2 Ozonolysis of Individual GLVs

To better understand the ozonolysis mechanisms for CHA and HXL, each system was studied individually using standards. The ozonolysis of CHA (Scheme 4.1b) is predicted to produce 3-oxopropyl acetate and propanal, along with two stabilized Criegee intermediates (CI-3 and CI-4) that produce propanoic acid and 3-acetoxy propanoic acid, respectively upon isomerization and hydration.^{35,59} Upon ozonolysis of CHA, we observed the evolution of propanal and propanoic acid using TD GC/MS, but not 3-oxopropyl acetate or 3-acetoxy propanoic acid. The estimated vapor pressure of 3-acetoxy propanoic acid (4×10^{-5} atm) is sufficiently low as to indicate that it is non-volatile and would exist primarily in the particle phase. The relatively high vapor pressure of 3-oxopropyl acetate (5×10^{-3} atm), however, is on the same order of magnitude as that of propanal and propanoic acid (0.4 atm and 4×10^{-3} atm, respectively), suggesting that it should be found in the gas phase. Nonetheless, it was not observed in this work and experimental identification of 3-oxopropyl acetate by others has been tentative at best.^{35,60,61}

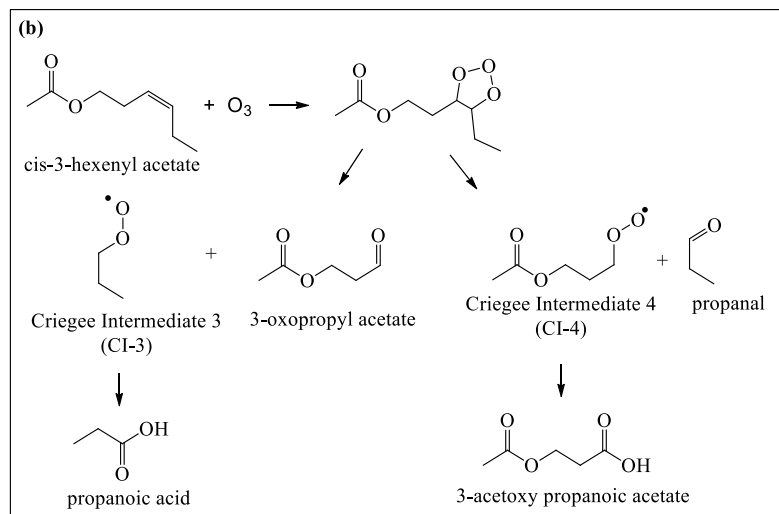
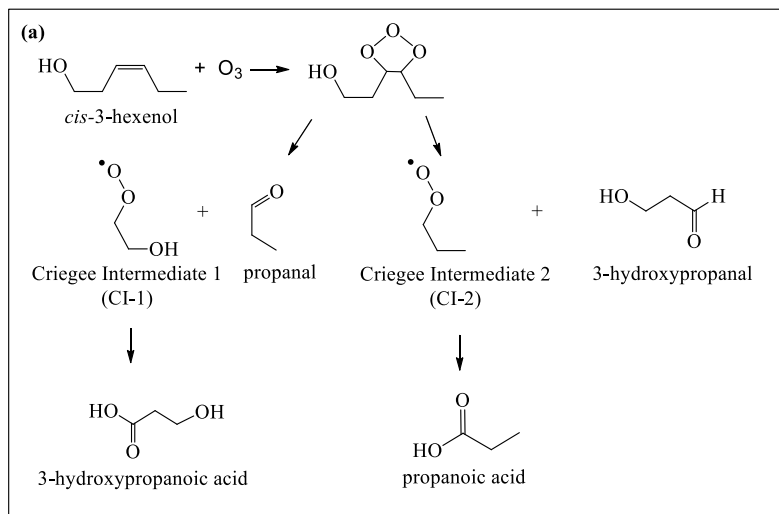


According to Scheme 4.1a, propanal, propanoic acid, 3-hydroxypropanal and 3-hydroxypropanoic acid are expected products of the ozonolysis of HXL, of which we observed the evolution of both propanal and propanoic acid in the gas phase. 3-hydroxypropanal and 3-hydroxypropanoic were not observed. In accord with the estimated vapor pressures of these species (1×10^{-7} atm and 2×10^{-5} atm, respectively), these species would likely contribute to SOA in the particle phase.

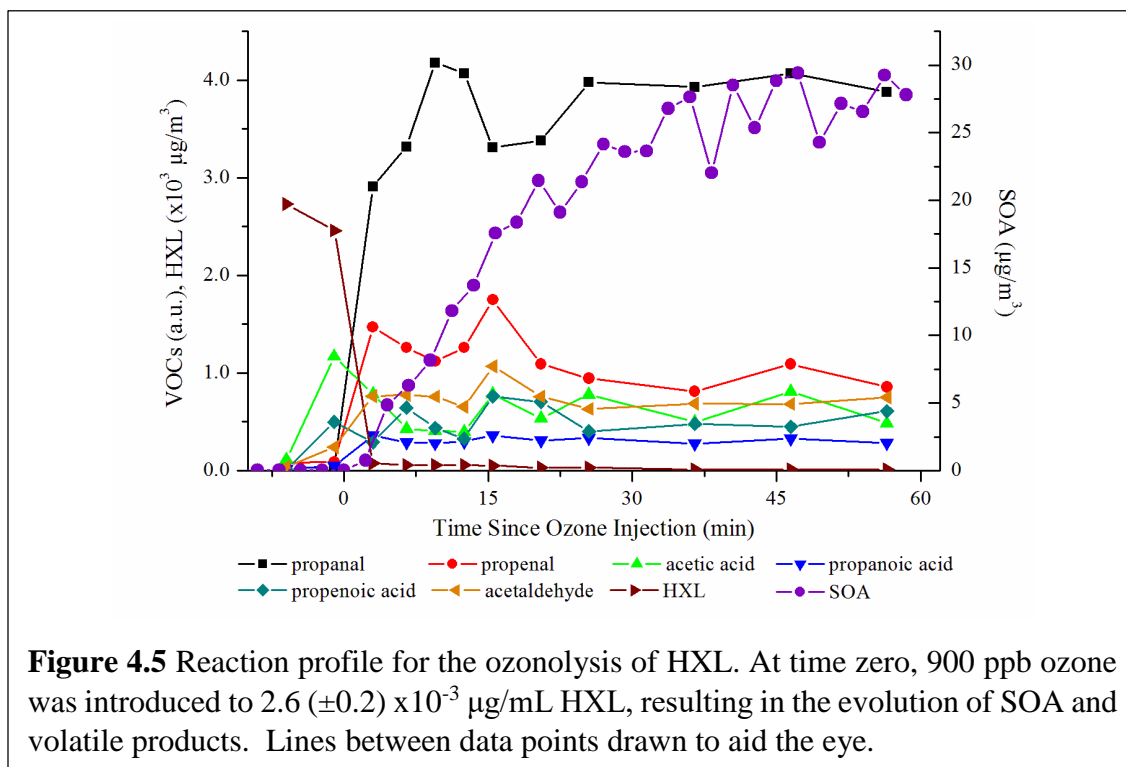
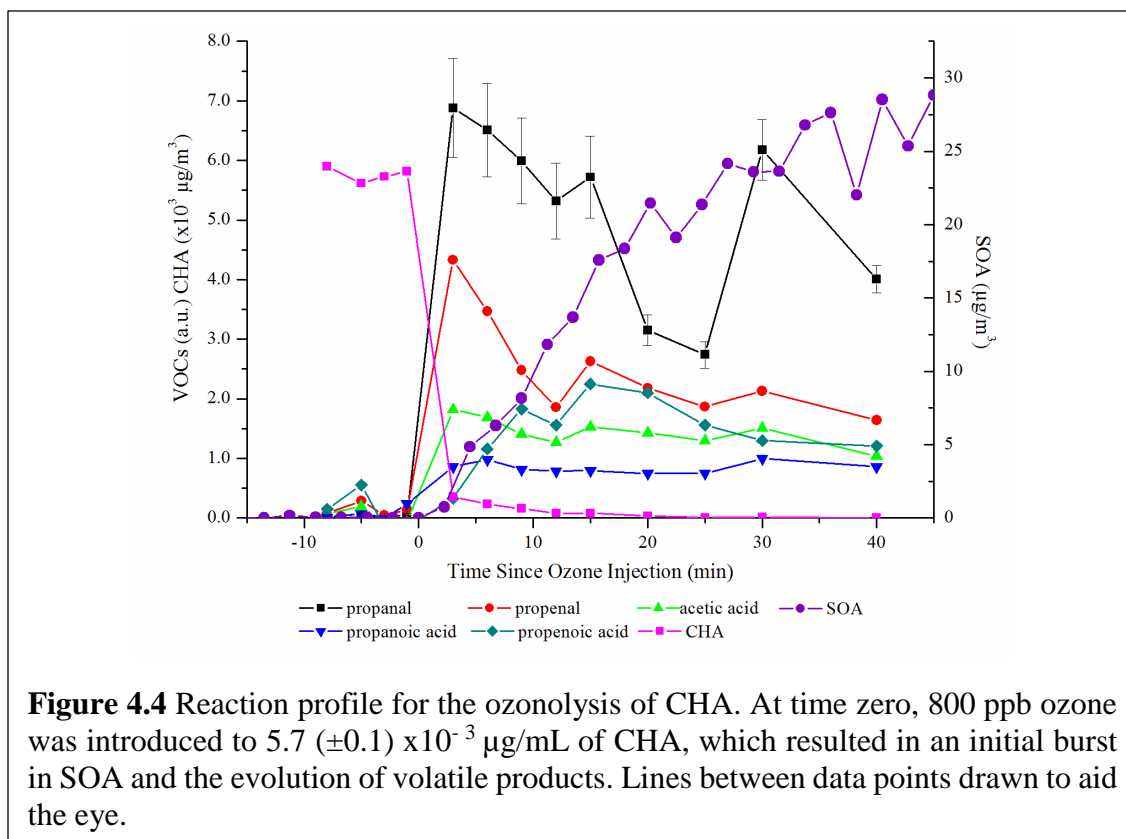
In addition to the predicted ozonolysis products, we also observed the evolution of 2-propenal and propenoic acid from both CHA and HXL. We also observed the production of acetic acid from CHA and acetaldehyde from HXL. Considerable work has been done by Hamilton et al.⁷ to identify the oxidation products of CHA and HXL, and though they identify acetic acid, it is attributed to fragmentation of other species during their mass

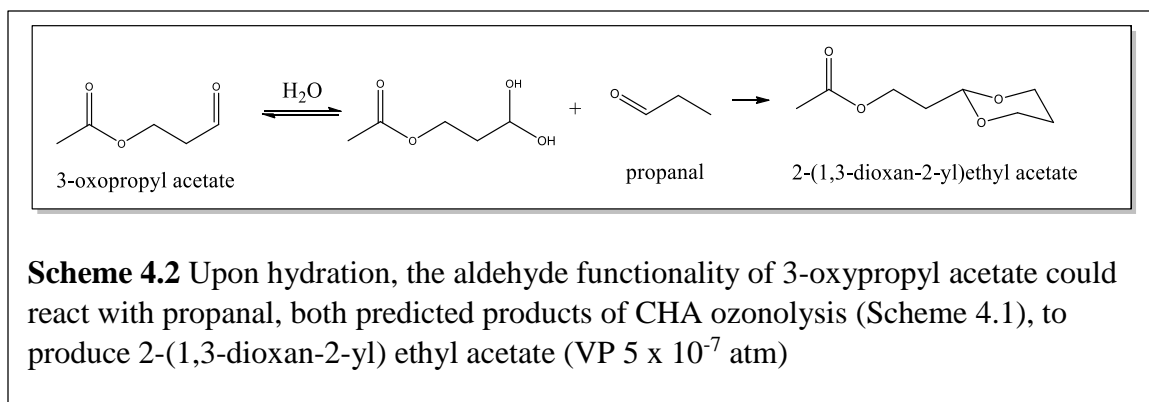
spectrometry ionization process. To our knowledge, this is the first known observation of these species as CHA and/or HXL ozonolysis products, however a full understanding of the mechanism leading to their formation is not clear and warrants additional work. Albeit, Scheme 4.1 is a simple representation of the ozonolysis via the Criegee mechanism and does not take into account the many competing reaction pathways likely occurring simultaneously, however these alternative reaction pathways are discussed elsewhere yet still do not account for these products.^{7,61}

The evolution of volatile ozonolysis products occurred as a concerted burst in both GLV systems, after which the signal for most products remained steady. In the ozonolysis of CHA, however, the propanal signal decreased over the course of ~25 min before peaking again 30 minutes post ozonolysis (Figure 4.4). This valley/peaked response suggests the presence of secondary reactions resulting in the consumption/production of propanal in the CHA system. While propanal was also measured as a product of HXL ozonolysis, the valley/peaked response was not observed for that system (Figure 4.5). Hamilton et al.⁷ propose a mechanism for the uptake of propanal by 3-hydroxypropanal, (product of HXL ozonolysis). Although we did not see evidence to support the uptake of propanal by HXL, the mechanism proposed by Hamilton et al.⁷ could apply to the CHA system, where the valley/peak response in propanal provides evidence for its reactive uptake. In the CHA system, the aldehyde in 3-oxopropyl acetate could react with propanal to produce 2-(1,3-dioxan-2-yl)ethyl acetate (Scheme 4.2), which based on its estimated vapor pressure (5×10^{-7} atm) would likely exist in the particle phase.²⁹ This secondary reaction may also explain why 3-oxopropyl acetate was not observed in CHA ozonolysis experiments.



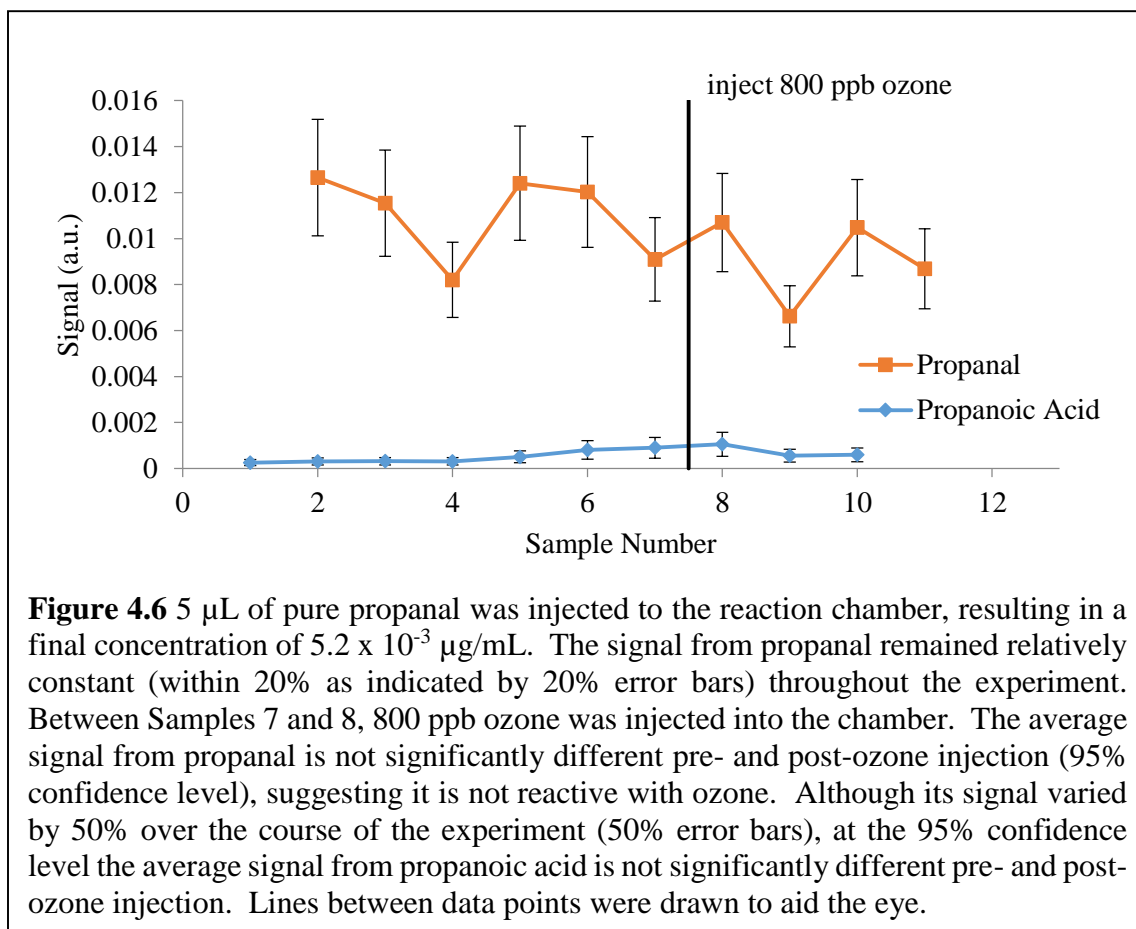
Scheme 4.1 The ozonolysis of HXL (a) is predicted to produce hydroxyl acetic-acid and propanal along with the stabilized Creigee Intermediates CI-1 and CI-2, which produce propanoic acid and hydroxypropanal respectively upon isomerization and hydration. The ozonolysis of CHA (b) is predicted to produce 3-oxopropyl acetate and propanal, along with two stabilized Criegee intermediates (CI-3 and CI-4) that produce propanoic acid and 3-acetoxy propanoic acid, respectively.





In the general mechanism shown in Scheme 4.1, propanoic acid is produced by ozonolysis of CHA. According to Li et al.⁶¹, the evolution of propanoic acid is a result of the α -addition of water to CI-3 to form 1-hydroperoxypropan-1-ol, which further decomposes to produce propanoic acid. Li et al.⁶¹ also performed a kinetic investigation of the mechanism for CHA ozonolysis that confirmed that formation of 1-hydroperoxypropan-1-ol is the favored reaction pathway for CI-3.⁶¹ However, they found that the subsequent decomposition of 1-hydroperoxypropan-1-ol to propanoic acid and water has an energy barrier of 45.57 kcal mol⁻¹ and is, therefore, not likely.⁶¹ Nevertheless, we observed propanoic acid as a product of CHA ozonolysis (Figure 4.4) and this is the only proposed pathway leading to its formation. The oxidizing environment in which these reactions were performed could lead to further oxidation of propanal, which was observed as a major ozonolysis product of both GLVs, to produce propanoic acid. However, we saw no evidence of the consumption of propanal coinciding with the production of propanoic acid in the reaction profile of CHA or HXL. Additionally, separate experiments showed that a propanal standard did not oxidize to form propanoic acid when injected into the experimental chamber in the presence of high ozone (Figure

4.6). The decomposition pathway leading to the formation of propanoic acid, therefore, appears relevant, despite being energetically disfavored.



During the ozonolysis of each GLV, SOA evolution began immediately upon introduction of ozone and reached a maximum concentration in ~60-90 minutes before decreasing slowly, likely due to particle loss to the chamber walls. Aerosol yields, Y , for CHA and HXL were calculated according to Equation 3.4 in Chapter 3.

Ozonolysis of CHA and HXL individually resulted in measured aerosol yields of $0.5 (\pm 0.4) \%$ and $0.3 (\pm 0.2) \%$, respectively. Particle loss to chamber walls was estimated according to Presto et al.⁶³ and proved to be significant, with an average wall deposition

rate of $5.76 \times 10^{-4} \mu\text{gm}^{-3}\text{sec}^{-1}$, which is greater than that reported for experimental chambers used by others (2.5×10^{-5} and 1.0×10^{-4}).⁶³⁻⁶⁶ Given the large surface-to-volume ratio of our chamber, however (5.3 m^{-1}), compared to that of others (2.12 m^{-1} to 2.8 m^{-1}), a greater deposition rate is expected.^{63,67} Unless otherwise noted, all subsequent reports of ‘measured’ or ‘observed’ SOA concentrations account for wall-losses.

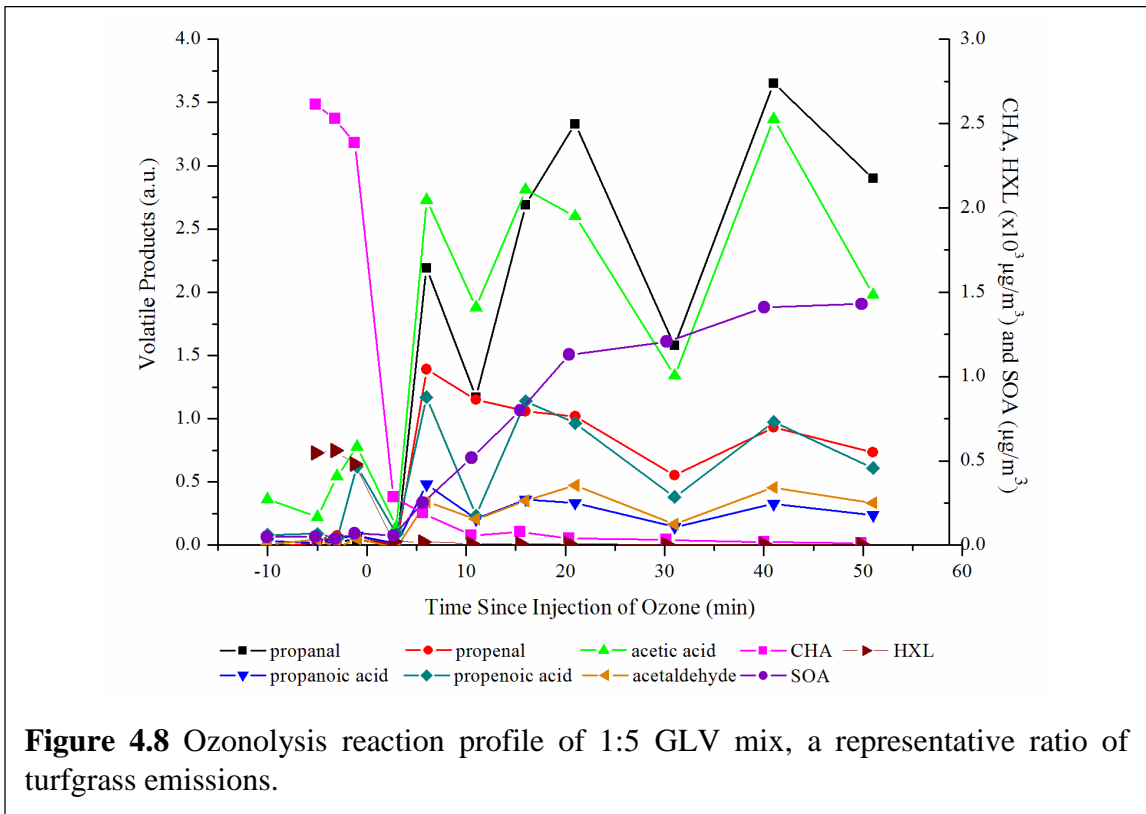
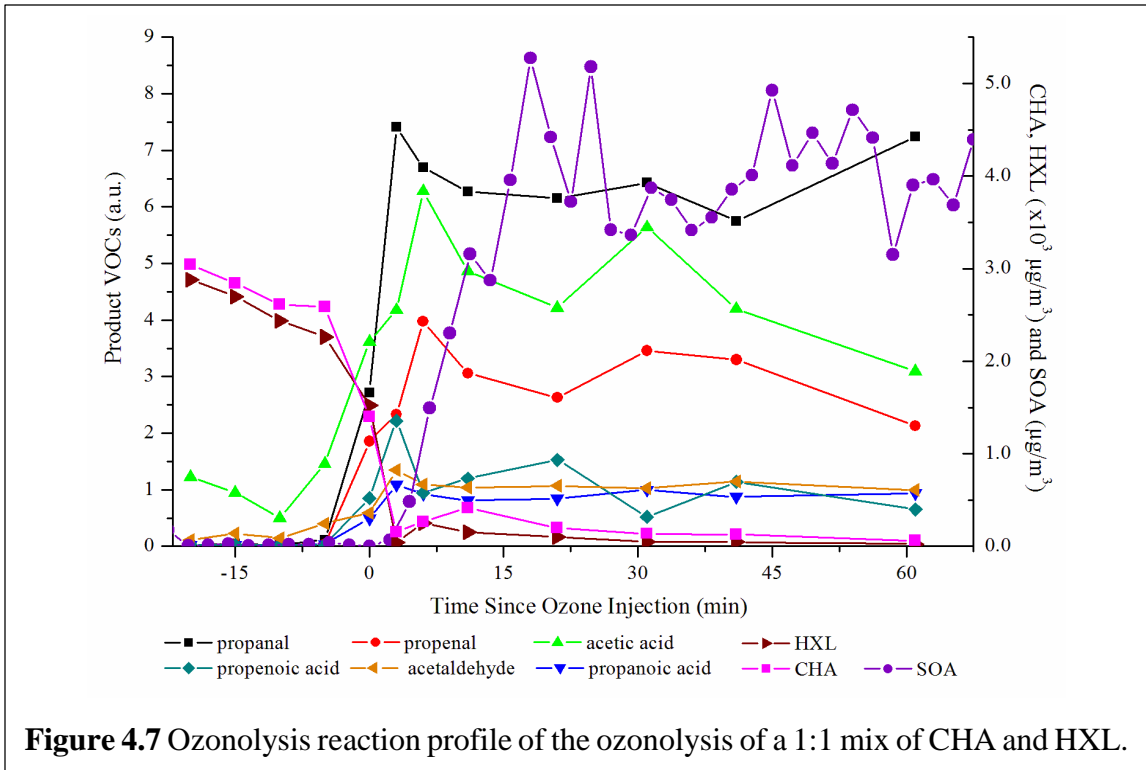
Our wall-loss coefficient was used to correct aerosol yield from GLV standard experiments. The corrected aerosol yields from ozonolysis of CHA and HXL were $1.2 (\pm 1.1) \%$ and $3.3 (\pm 3.1) \%$ respectively. The error associated with these yields is due to the variability in the amount SOA formed in experiments. Our aerosol yield values are lower than the wall-loss-corrected aerosol yields reported by Hamilton et al., which were on the order of magnitude of prevalent monoterpenes; $9.5 - 24 \%$ for CHA and 8.6% for HXL.^{7,35} The ozonolysis of the endocyclic double bond of monoterpenes, as is the case in α -pinene, terpinolene and limonene, however, results in the formation of oxygenated species with higher molecular weights than the parent hydrocarbon that likely partition into the particle phase and contribute to SOA, resulting in relatively high aerosol yields. Alternatively, CHA and HXL are linear alkenes that, upon oxidative cleavage via ozonolysis, produce species with relatively low molecular weight and, thereby, high volatility, likely contributing to the gaseous phase and, subsequently, should result in a lower aerosol yield than their cyclic counterparts.

4.3.3 Two GLV Component Mixtures

As stated above, we measured several different, potentially reactive compounds in the complex mixture of GLVs emitted by grass clippings. Recent work by Shilling et al.⁹ in the CARES campaign indicates that VOC mixtures have a significant impact on SOA

formation. With the goal of better understanding SOA formation and yield under environmentally relevant conditions (where VOCs exist as a mixture), we performed two-component ozonolysis experiments with CHA and HXL. In one experiment, ozone was introduced to a GLV mixture containing a 1:1 (mole ratio) mix of the two components, while a second experiment was designed to represent the ozonolysis of environmentally relevant GLV mixtures, containing a 1:5 mole ratio of HXL to CHA, analogous to that measured from real grass clippings.

The reaction profile for the ozonolysis of the 1:1 GLV mixture (Figure 4.7) shows that the majority of both CHA and HXL is consumed within the first five minutes of the reaction. SOA and volatile product evolution occurred immediately, reaching maxima less than 20 min into the reaction. SOA and volatile product concentrations remained relatively constant post-maxima; propanal did not exhibit the peak/valley trend observed in the CHA-only ozonolysis experiments. Qualitatively, the 1:1 GLV mix reaction profile bears a strong semblance to that of the HXL-only ozonolysis profile (Figure 4.5), suggesting HXL in an equimolar concentration, is more reactive to ozonolysis than CHA. The reaction rate constants we calculated also indicate that HXL ($k = 6.7 \times 10^{-17} \text{ cm}^3 \text{ sec}^{-1} \text{ molecule}^{-1}$) is more reactive to ozone than CHA ($3.6 \times 10^{-17} \text{ cm}^3 \text{ sec}^{-1} \text{ molecule}^{-1}$) (Section S6). These reaction rates agree well with those found by Kirstine et al.²⁰ ($5.4 \times 10^{-17} \text{ cm}^3 \text{ sec}^{-1} \text{ molecule}^{-1}$ for CHA and $6.4 \times 10^{-17} \text{ cm}^3 \text{ sec}^{-1} \text{ molecule}^{-1}$ for HXL), who used the relative reaction rate method and also found that HXL was more reactive to ozonolysis. Using the aerosol yields measured in this work and the initial mass of GLVs injected into



the chamber, total SOA production for the 1:1 mix was expected to reach $125 (\pm 85) \mu\text{g}/\text{m}^3$. However, the maximum observed SOA concentration was $9.8 \mu\text{g}/\text{m}^3$.

The ozonolysis of 1:5 GLV mix also resulted in the rapid consumption of GLVs and the immediate evolution of SOA and volatile products (Figure 4.8). This reaction profile more closely approximates the CHA-only reaction profile (Figure 4.5), with both propanal and acetic acid exhibiting the valley/peak trend, which suggests the occurrence of the same secondary reactions observed in the CHA-only system. Wall-loss corrected aerosol yields predicted the formation of $50 (\pm 17) \mu\text{g}/\text{m}^3$ SOA, much more than the SOA maximum observed; $5.3 \mu\text{g}/\text{m}^3$.

The disparity between the measured and predicted SOA concentrations in mixture experiments could suggest the presence of secondary chemistry that resulted in the consumption of GLVs without the production of SOA, which may have also been the case in grass clipping experiments.

Figures 4.9 and 4.10 show reaction profiles for the ozonolysis of grass headspace. Again, in these experiments, zero air was passed through the grass clippings and into the reaction chamber, carrying emissions with it. Maximum concentrations of CHA and HXL ($12 (\pm 1) \times 10^{-4} \mu\text{g}/\text{mL}$ and $2.05 (\pm 0.01) \times 10^{-4} \mu\text{g}/\text{mL}$, respectively) were measured post ozonolysis, which we believe was due to incomplete mixing within the experimental chamber before ozone injection. At time zero, ~ 470 ppb ozone was injected (indicated by the vertical line) and within 20 minutes the HXL concentration dropped below the instrument detection limit while SOA reached its maximum wall-loss corrected concentration ($15.7 \mu\text{g}/\text{m}^3$). CHA remained relatively constant after the first 20 minutes

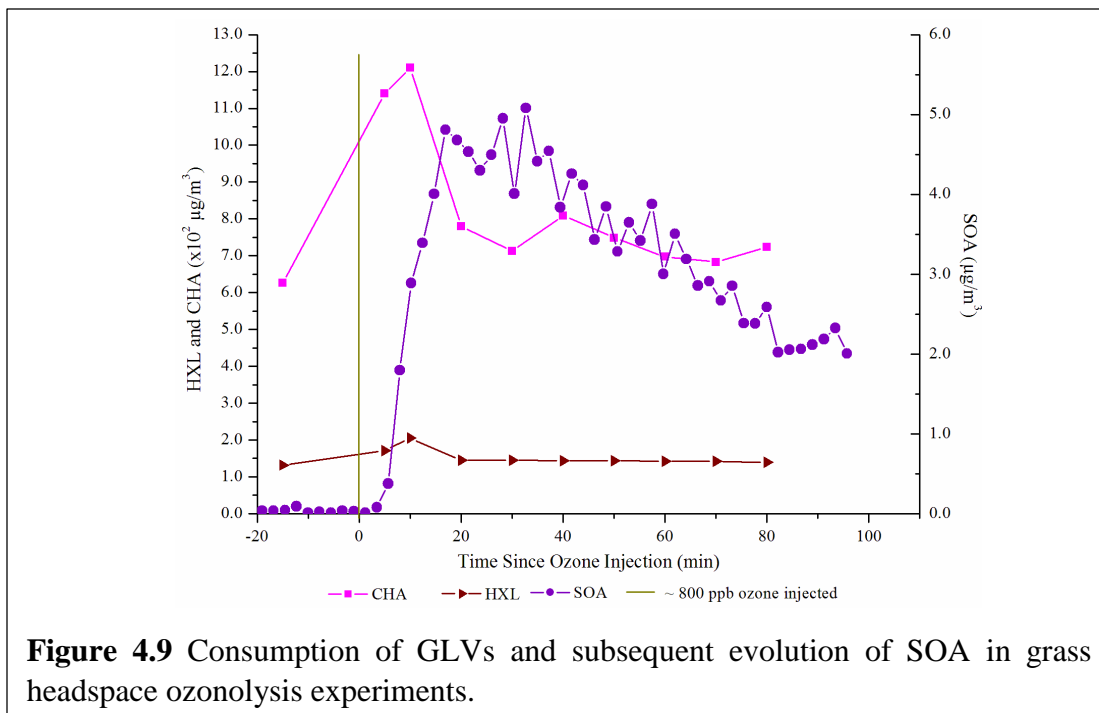


Figure 4.9 Consumption of GLVs and subsequent evolution of SOA in grass headspace ozonolysis experiments.

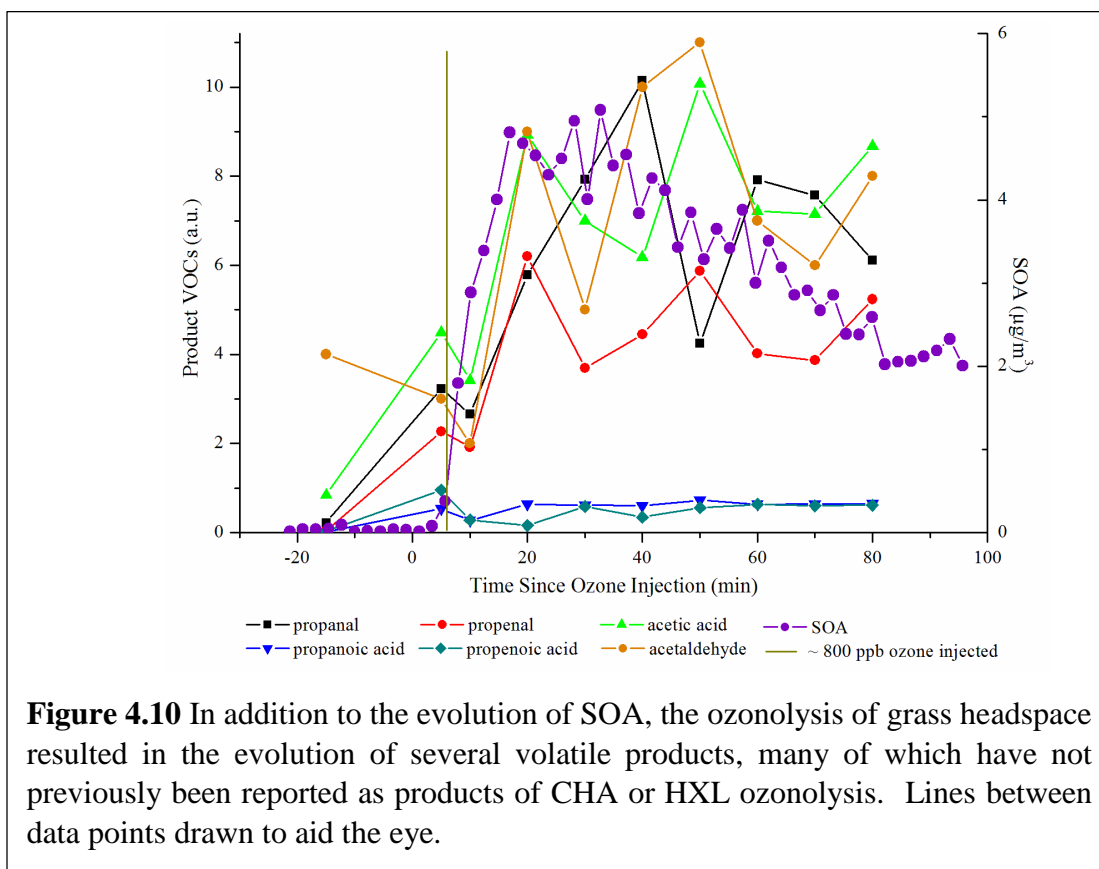


Figure 4.10 In addition to the evolution of SOA, the ozonolysis of grass headspace resulted in the evolution of several volatile products, many of which have not previously been reported as products of CHA or HXL ozonolysis. Lines between data points drawn to aid the eye.

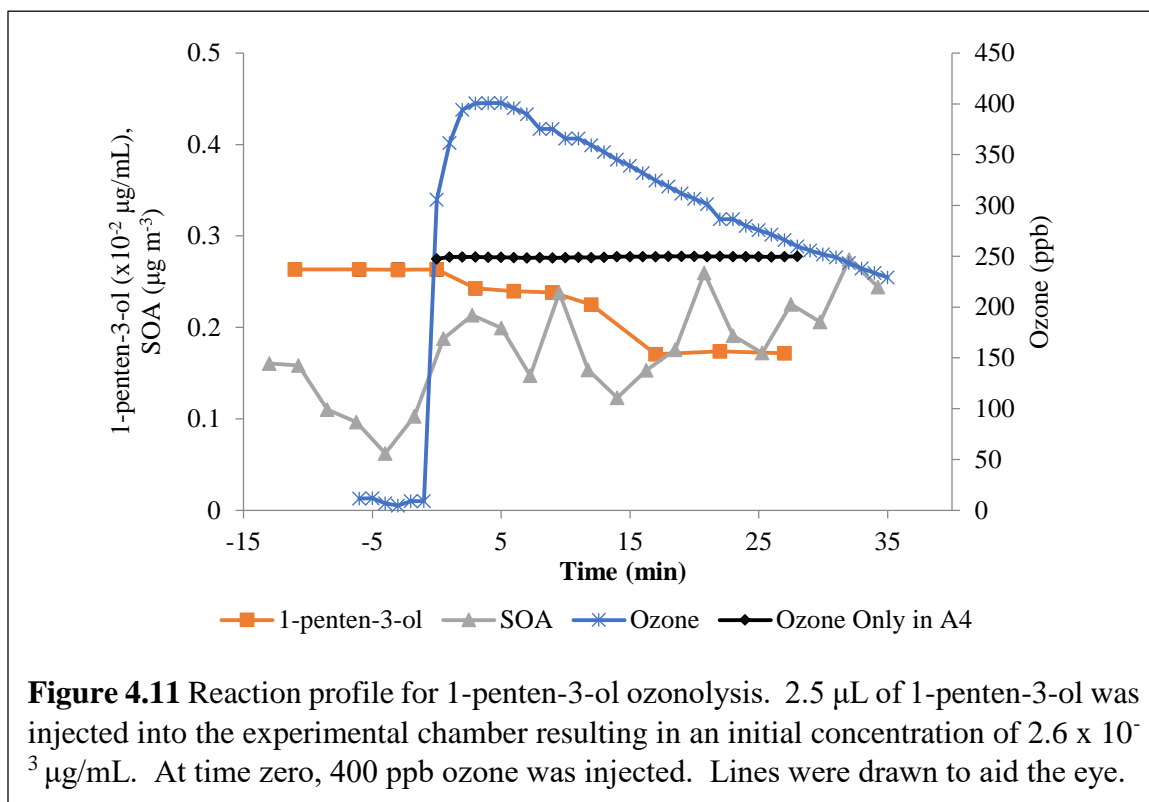
of the reaction ($0.74 (\pm 0.05) \times 10^{-3} \mu\text{g/mL}$) and was never completely consumed. SOA evolution begins immediately post ozonolysis and reaches a wall-loss corrected maximum of $15.7 \mu\text{g/m}^3$ within 20 minutes before beginning to decrease, which coincides with the complete consumption of HXL, supporting our hypothesis that HXL has an important role in SOA formation in the mixture. CHA also decreases throughout the reaction but is never completely consumed and there is no corresponding SOA growth even with continued consumption of the CHA, suggesting that CHA plays a minor role in the evolution of SOA in the mixture, as compared to HXL, but is being consumed to produce more volatile compounds.

In addition to the evolution of SOA, the ozonolysis of grass headspace resulted in the evolution of several volatile products (Figure 4.10), including propanal, propenal, propenoic acid, acetic acid, propanoic acid, acetaldehyde, several of which have not previously been reported as products of CHA or HXL ozonolysis.

4.3.4 Grass Ozonolysis

As stated above, although grass clippings emitted several volatile species, the GLV profile was dominated by CHA, HXL and 1-penten-3-ol (PTL), all of which are unsaturated and thereby have the potential to undergo oxidation by ozone as predicted by Scheme 4.1. Despite its unsaturation, however, PTL showed limited reactivity with ozone. To further characterize the ozonolysis kinetics and aerosol yield of PTL, we performed ozonolysis reactions with standards (Figure 4.11). $2.5 \mu\text{L}$ of PTL was injected into the experimental chamber resulting in an initial concentration of $2.6 \times 10^{-3} \mu\text{g mL}^{-1}$. At time zero, 400 ppb ozone was injected. Initial aerosol concentration was about $0.15 \mu\text{g m}^{-3}$ and, though it

showed an increasing trend over the course of the experiment (final concentration of about $0.25 \mu\text{g m}^{-3}$), it never exceeded $0.3 \mu\text{g m}^{-3}$.

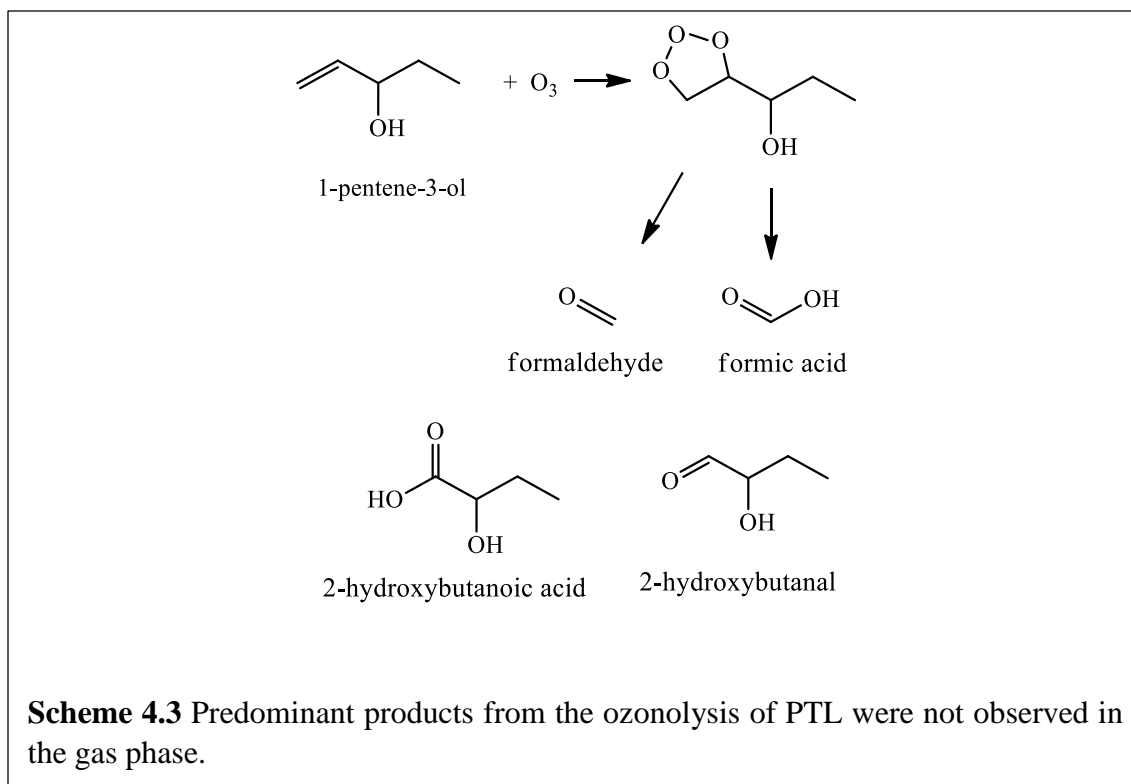


At a 95% confidence level, the average PTL concentration pre- and post-ozonolysis (2.6×10^{-3} and $2.2 \times 10^{-3} \mu\text{g/mL}$, respectively) are statistically different, about 50% lower post ozonolysis. However, upon injection of ozone, 1-penten-3-ol concentration did not show a dramatic drop in concentration, suggesting that any reactivity with ozone is very slow, or that ozonolysis is not the loss mechanism for PTL. Ozone concentration fell to about from 400 ppb to 225 ppb by the end of the experiment, but did not show the second order consumption (exponential decrease) that is indicative of the alkene-ozone reaction. In a separate experiment, 250 ppb ozone was injected into the reaction chamber alone and

remained constant ($251 \pm 0.5\%$ ppb) for over 5 hours, which suggests some degree of chemical reactivity for ozone in the PTL ozonolysis experiment.

According to Scheme 4.3, the predominant ozonolysis products of PTL include 2-hydroxybutanal, 2-hydroxybutanoic acid, formaldehyde and formic acid. These products were not observed using TD-GC/MS, supporting our hypothesis that PTL has limited (no) reactivity with ozone. These products, however may need derivatization for detection by GC/MS. It is, therefore, unclear what the loss mechanism for PTL is in this experiment. Though, as described in Chapter 3 Section 2, loss of VOCs to the chamber walls is expected to be negligible. These interesting observations stimulated a series of questions regarding the molecular level control of ozonolysis kinetics and aerosols yield. For example, why did CHA and HXL show considerable reactivity with ozone and produce SOA, while PTL, which has a similar molecular structure, show no (or limited) reactivity with ozone? Chapter 6 focuses on addressing this questions.

Revisiting the more well-behaved GLVs, the initial CHA, HXL, and ozone concentrations for several grass clipping and headspace experiments are listed in Table 4.2 and are on the same order of magnitude and mole ratio as the ‘1:5 standard mixture’ experiment above (Figure 4.7). In the ozonolysis of both grass headspace and grass clippings, these GLVs decreased in signal, while that of their corresponding gas-phase oxidation products, propanal, propanoic acid, and acetic acid increased. As in the GLV standard reactions, we also observed the evolution of propanal, propenoic acid, acetic acid



and acetaldehyde, which have not previously been observed as products of grass ozonolysis.

A typical reaction profile for the ozonolysis of grass clippings is shown in Figures 4.13 and 4.14. Several of these experiments were completed, where approximately 0.5 kg of grass clippings were placed in the experimental chamber, which was then filled with zero air (Figure 4.12 is a photograph from a different but analogous emissions experiment done in the UVMEC). Initial concentrations of CHA and HXL were monitored before ozone (~800 ppb) was injected, resulting in an initial burst of SOA. High ozone loadings were used to ensure a complete oxidation of all GLVs and to model GLV standard ozonolysis experiments (Table 4.2), but do not represent atmospherically relevant conditions, as discussed below. In several headspace and grass clipping experiments, the

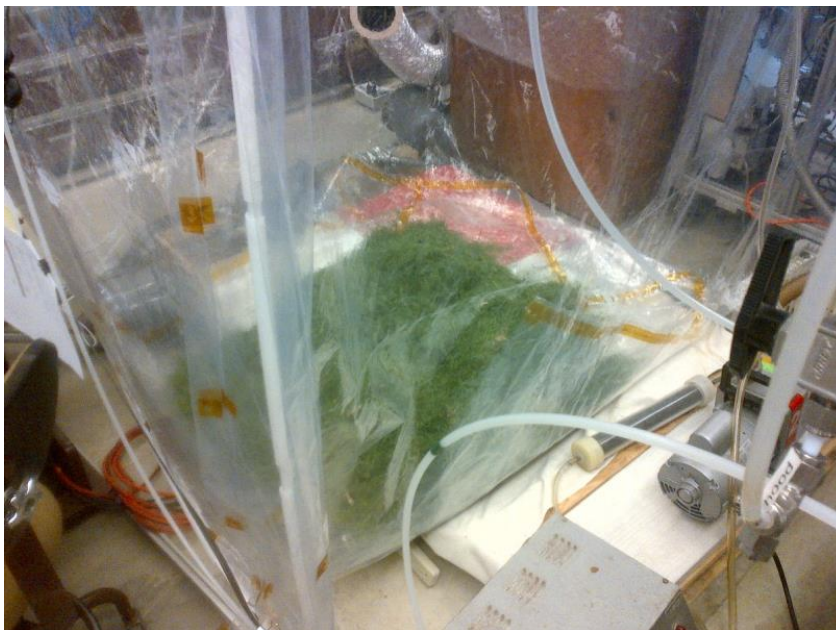
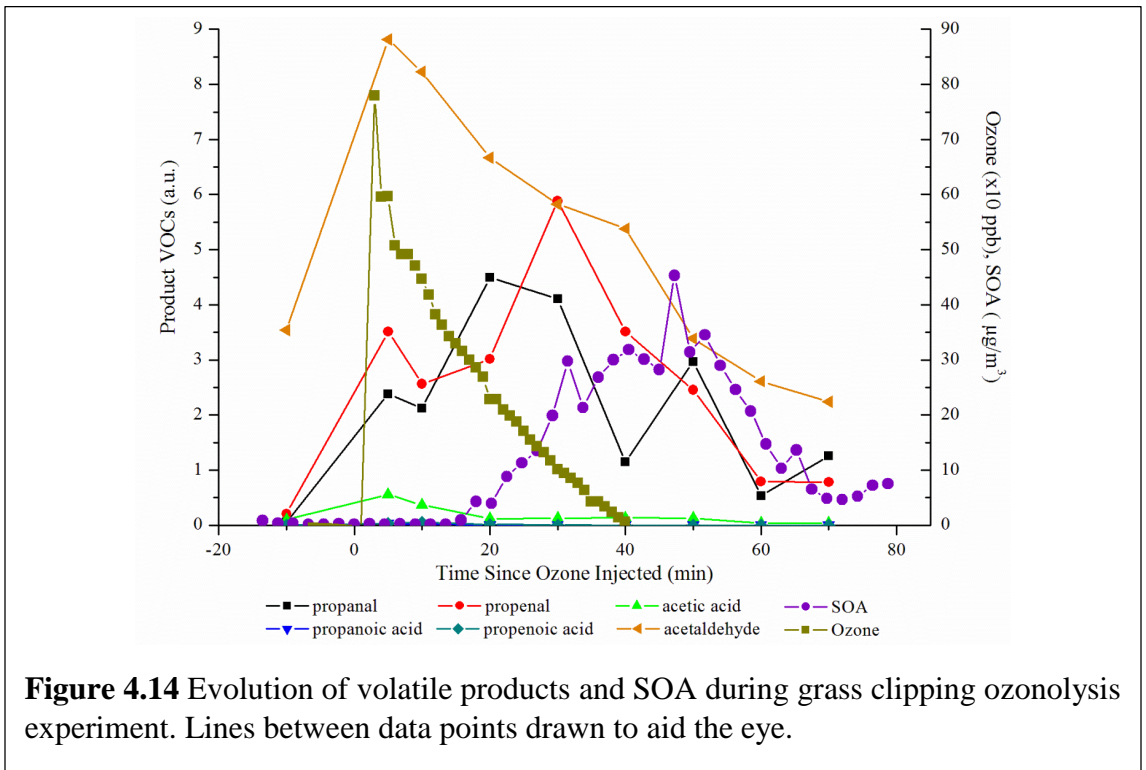
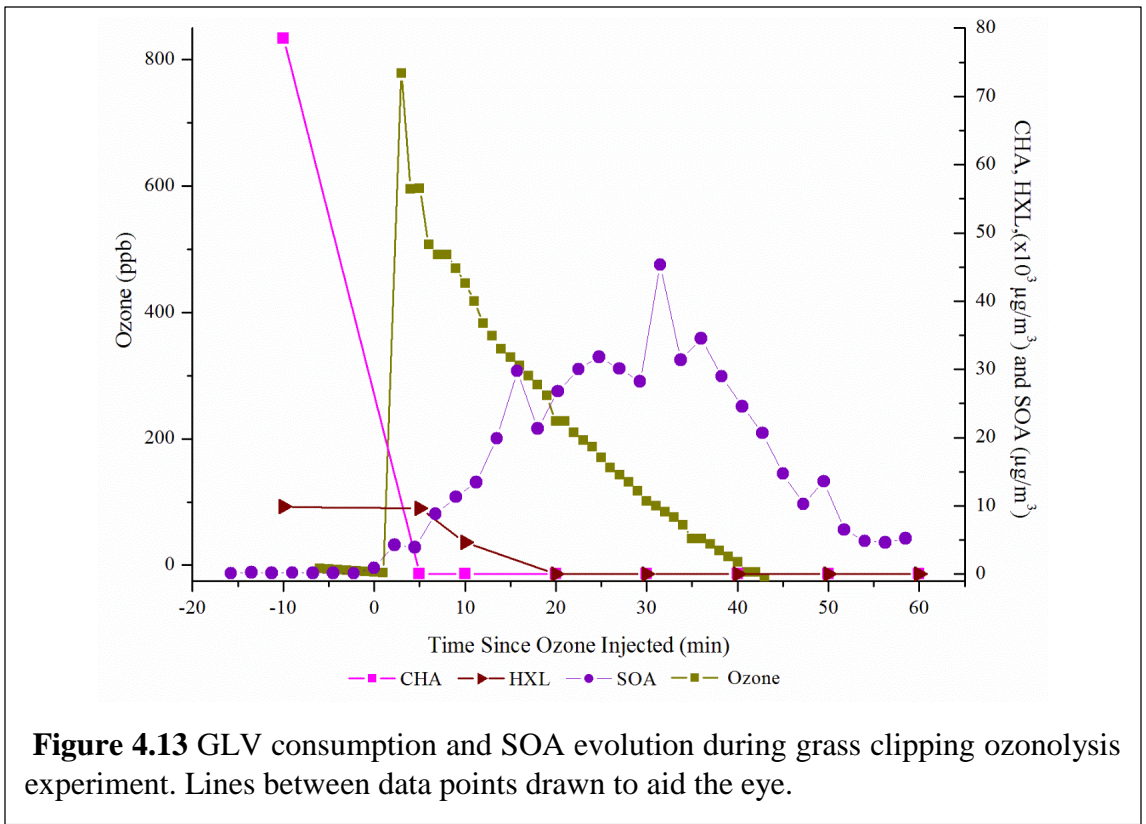


Figure 4.12 Grass emission profiles were measured by placing grass clippings directly inside the reaction chamber and filling with zero air. Here, ~6.5 kg of clippings were placed inside UVMEC.

resultant SOA concentration increased to maxima ($\sim 50 \mu\text{g m}^{-3}$ and $\sim 215 \mu\text{g m}^{-3}$ in headspace and clipping experiments, respectively) approximately 20-30 minutes post-ozonolysis before decreasing rapidly to background levels. We also observed a SOA concentration drop in grass headspace experiments (i.e., no grass clippings in the reaction chamber), suggesting that the rapid decrease in SOA concentration in clipping experiments is not due to sorption to the grass clippings. The mechanism for SOA loss in grass clipping and headspace experiments is not understood but may involve secondary reactions that *increase* the volatility of SOA as it ages (ie additional oxidation by hydroxyl radicals). These loss mechanisms may have important roles in determining the atmospheric lifetime of GLV-SOA, therefore understanding these dynamics warrants additional work.



In both headspace and clipping experiments, volatile products increased as a concerted burst within the first 10 minutes post ozone injection (Figure 4.10 and Figure 4.13, respectively). In the first 40 minutes of headspace experiments, 50% of CHA, and HXL was consumed, while more than 90% of the ozone was consumed. CHA concentration decreased then remained constant once ozone had been depleted. Propenal and acetaldehyde increased steadily post ozonolysis. Propanal increased, but exhibited a peak-valley behavior similar to that in GLV standards experiments. All other VOC products decreased post ozonolysis.

In grass clipping experiments, CHA and HXL were completely consumed within the first 10 minutes of the reaction, while ozone concentration fell to background levels 35 minutes post ozonolysis. GLV concentrations were lower in grass clipping experiments than in headspace experiments, but this may have been a result of experimental design, as grass clippings were not allowed to equilibrate in the reaction chamber for more than a few minutes before ozone was injected. Acetic acid, propanoic acid and propenoic acid signal fell after an initial burst, while propanal remained steady after its post-ozonolysis increase (similar to HXL standard experiments).

Applying the calculated aerosol yields above to the measured GLV emission rates in both headspace and clipping experiments, theoretical SOA production could be estimated (Table 4.2). The observed SOA production in grass headspace experiments was less than that predicted by aerosol yields with a -120% difference. This difference was similar to the degree of disparity in the 1:1 mix ozonolysis experiment (-115% difference), suggesting the 1:1 mix may model SOA production from grass headspace to some degree.

The observed SOA production in grass clipping experiments was much *greater* than what aerosol yields predicted (+170%). The ozonolysis of neither the 1:1 mix nor the 1:5 GLV mix resulted in the over-production of SOA, as was seen in grass clippings. In fact, based on the corrected SOA yields, HXL and CHA account for only a small fraction of observed SOA (15(\pm 13)%), suggesting that neither accurately models grass clippings. Because GLVs are continuously emitted by grass clippings, they likely represent a continuous source of SOA, rather than a one-time burst, which may contribute to the observed disparity between predicted and measured SOA. This disparity may also suggest that other, potentially important, processes are contributing to SOA evolution by the mowing and subsequent oxidation of grass, as will be discussed below.

As demonstrated by the disparity between predicted and actual SOA production, the ozonolysis of HXL or CHA alone does not accurately represent SOA from the ozonolysis of grass clippings or grass headspace. Mixtures of the two dominant reactive GLVs are more representative of the grass headspace system than the grass clippings, and produce similar *trends* in SOA growth and volatile product evolution. Therefore, predictions of atmospheric SOA mass loading using even these two predominant GLVs underestimate actual SOA loading resulting from lawn mowing.

Table 4.2. Summary of grass clipping and headspace experiments

Date	SOA (#/cm ³)	SOA (µg/m ³)	Wall Loss Corrected SOA (µg/m ³)	Predicted SOA (µg/m ³)	RSD	HXL (x10 ⁻⁵ µg/mL)	RSD	HXL per m ² lawn (µg/m ²)	RSD	CHA (x10 ⁻⁵ µg/mL)	RSD	CHA per m ² lawn (µg/m ²)	RSD
Clippings													
10/23/2012	11835	39	55	9.55	2.51	13.7	0.09	0.14	0.04	210	0.04	2.29	0.04
10/27/2012	6077	16	27	1.21	1.12	3.14	0.49	0.022	0.19	7.57	0.87	0.05	0.87
11/06/2012	46102	82	113	10.05	4.12	3.92	0.39	0.033	0.18	365	0.04	3.10	0.04
05/28/2013	73630	120	153	3.74	2.41	5.66	0.30	0.0079	0.03	78.5	0.04	0.11	0.04
Headspace													
10/23/2012	1190	5.9	8.8	43.56	1.58	88.5	0.03	1.7	0.02	606	0.04	11.36	0.42
10/27/2012	348.42	2.9	3.8	13.34	3.34	12.0	0.13	0.19	0.12	392	0.04	6.35	0.49
11/06/2012	1422	5.2	16	9.66	1.44	20.5	0.22	0.089	0.16	122	0.04	0.53	0.39
05/08/2013	793.657	6.8	12	5.59	1.60	11.3	0.11	0.23	0.11	78.8	0.03	1.60	0.35

4.4 Contribution of Lawn Mowing to Atmospheric SOA

The site area chosen for this study was a residential, suburban neighborhood in close proximity to an industrial, urban landscape. A geospatial analysis of the 131-acre area around the study site showed that lawns and turfgrass comprise 27.5% of the total landcover in this suburban neighborhood (36 acres). Remaining landcover was comprised of wooded lots, scrub-brush and impervious surfaces such as roads, driveways and rooftops. Lawn mowing has been estimated to produce $\sim 1.3 \times 10^3$ gdw/m²/yr of clippings (where gdw is grams dry weight).⁶⁷ Stevenson⁶⁸ estimated that New England homeowners mow their lawn 20 times annually, and so we predict that approximately 66 gdw/m²/mowing of grass clippings are produced by New England lawns. We estimate that lawns in this typical suburban neighborhood have the capacity to emit 8.66 (± 0.08) $\mu\text{g}/\text{m}^2$ CHA and 1.21 (± 0.06) $\mu\text{g}/\text{m}^2$ HXL as a concerted burst upon mowing. Based on our corrected aerosol yields, these GLVs have the capacity, therefore, to contribute 177 mg SOA to the neighborhood airshed, annually.

However, as shown above, the actual SOA measured due to the ozonolysis of grass clippings is much greater than predicted by our yields, so the estimate above is not truly representative of the potential contribution of lawn mowing to SOA levels. Based on the measured SOA as a function of the area of lawn mowed, *each mowing event* could contribute 27.5 $\mu\text{g}/\text{m}^3$ SOA per m² of lawn or 425 $\mu\text{g}/\text{m}^2$ annually. Based on their reported emissions from forested landscapes and the fraction of forested landscape in the region of the study area, isoprene and monoterpenes are estimated to contribute 2,500 and 2,000 $\mu\text{g}/\text{m}^2$ annually, respectively.^{69,70} Lawn mowing, therefore, has the potential to emit a

significant amount of SOA, comparable to the two predominant SOA sources, as a concerted burst to the local airshed.

As stated above, ozone was introduced to the experimental chamber as a one-time burst that resulted in concentrations of about 800 ppb, which is much greater than average ozone levels in Chittenden County, VT (~60 ppb).⁷¹ 800 ppb ozone was used in preliminary grass clipping experiments to ensure a sufficient concentration to result in SOA growth and was used in subsequent GLV standard and grass experiments for the sake of consistency. Though ambient ozone concentrations are lower than the experimental ones used herein, they *are* expected to be elevated on warm, sunny days, the same time lawn mowing is expected to occur. Additionally, ozone plumes can be transported several hundred kilometers from industrial or urban sources to rural sites where they can interact with BVOCs.⁷²⁻⁷⁴ For example, plumes originating in New York City, NY can extend 600 km and contain up to 160 ppb ozone.⁷⁵ The prevailing winds in Essex Junction, VT are from the west, putting the study site five miles downwind from the City of Burlington, VT and many industrial areas, which may introduce an additional source of ozone. Therefore, it is possible that local ozone levels in rural landscapes could be elevated during mowing events. Additionally, in the field, any consumed ozone is expected to be replenished by other sources that are prevalent in the atmosphere, whereas in our experiments ozone was injected as a single burst.⁴² Exposure to a concerted burst of 800 ppb ozone is admittedly different than an exposure to 100 ppb over the course of 8 hours, which would be a more representative exposure scenario, but such exposures will require use of a continuous flow reaction chamber.

Though our aerosol yields under-estimate the actual SOA produced by the ozonolysis of grass clippings and atmospheric ozone levels are less than those used in this study, our work demonstrates that mowing of lawns in this neighborhood could contribute a localized burst of up to $27.5 \mu\text{g m}^{-3}\text{m}^{-2}$ SOA to the atmosphere per mowing event, whereas the ambient particulate matter concentration in this region is $\sim 6 \mu\text{g m}^{-3}$.⁷⁶ During any given mowing event, $\text{PM}_{2.5}$ (particulate matter with diameter less than $2.5 \mu\text{m}$, the average diameter of SOA produced by the ozonolysis of grass clippings and headspace is $0.125 \mu\text{m}$) levels in suburban neighborhoods could approach or exceed the suggested guideline value for annual mean and 24-hour mean guidelines ($10 \mu\text{g m}^{-3}$ and $25 \mu\text{g m}^{-3}$, respectively) set by the World Health Organizations and the $\text{PM}_{2.5}$ standard set by the US Environmental Protection Agency ($12 \mu\text{g m}^{-3}$), representing an episode of acute exposure to potentially harmful PM.^{77,78}

Despite our efforts to model real world conditions in our experiments, the atmosphere offers additional complexities that may lead to additional SOA evolution as a result of lawn mowing. Work done by Kirstine et al.,²⁰ Orlando et al.,²⁴ and Papagani et al.⁷⁹ have shown that grass GLVs have considerable reactivity with nitrate and hydroxyl radicals, on the same order of magnitude as common anthropogenic VOCs. Hamilton et al. predicted aerosol yields of 3.1% and 0.9% from the photooxidation of HXL and CHA, respectively.⁷ Given the established reactivity of GLVs with other atmospheric oxidants, additional work should be done to characterize the volatile products and SOA produced from the photooxidation of GLVs.

This work focused on the interaction of two predominant GLVs and their roles in SOA formation, however there is also growing evidence to indicate that the presence of anthropogenic organic aerosol and AVOC in conjunction with BVOC synergistically enhances the production of SOA.^{9,10,80} The relatively large ratio of landcover encompassed by lawns in suburban neighborhoods represent a source of BVOCs, which, by definition are in close proximity to urban and industrial sources of BVOCs and BSOA, as well as elevated concentrations of oxidants. There are several sources of A/BVOCs and A/BSOA at the urban/suburban interface that provides ample opportunity for interaction. For example, the emissions of lawn mowers themselves have been found to contribute as much as $4 \mu\text{g m}^{-3}$ aerosol during a mowing event, likely from unspent fuel emissions and agitated plant debris and soil.⁸¹ Additional work is needed to determine whether an anthropogenic enhancement effect drives additional SOA production from the ozonolysis of grass clippings, not seen in headspace or GLV standard experiments. These experiments should include the ozonolysis of GLVs in the presence of seed aerosols, which would serve as a proxy to ambient atmospheric particulate matter or primary organic aerosols and should also involve GLV oxidation in the presence of AVOCs and oxidants.

4.5 Conclusions

Though many volatile species are emitted by grass clippings, the profile is dominated by CHA and HXL, which are easily oxidized by ozone to produce significant amounts of SOA, in addition to a suite of oxygenated volatile products. Herein we report the first known observation of propenal and propenoic acid as ozonolysis products of both CHA and HXL, as well as support other products previously reported in the literature.^{7,27-}

^{29,61} We found that the mowing of lawns has the potential to contribute up to $27.5 \mu\text{g m}^{-3} \text{ m}^{-2}$ SOA, which cannot be modeled solely by the ozonolysis of CHA or HXL. While these two GLVs were found to produce SOA upon ozonolysis, they each largely under-predict SOA mass loading from ozonolysis of grass clippings or simple binary mixtures of the two. The disparity between measured and predicted SOA mass loading may be rectified by incorporating additional oxidation sources, BVOCs, AVOCs and ASOA, which may contribute to an anthropogenic enhancement effect in grass clipping oxidation.

The ozonolysis of two-component mixtures of CHA and HXL begins to suggest that the chemical processes leading to SOA formation could be better modeled by mixtures, than by single-component systems. However, the chemical processes involved are not well understood and warrant additional work.

4.6 References

- (1) Hallquist, M.; Wenger, J. C.; Baltensperger, U.; Rudich, Y.; Simpson, D.; Claeys, M.; Dommen, J.; Donahue, N. M.; George, C.; Goldstein, A. H.; Hamilton, J. F.; Herrmann, H.; Hoffmann, T.; Iinuma, Y.; Jang, M.; Jenkin, M. E.; Jimenez, J. L.; Kiendler-Scharr, A.; Maenhaut, W.; McFiggans, G.; Mentel, T. F.; Monod, A.; Prevot, A. S. H.; Seinfeld, J. H.; Surratt, J. D.; Szmigielski, R.; Wildt, J. *Atmospheric Chemistry and Physics* **2009**, *9*, 5155.
- (2) Kroll, J. H.; Seinfeld, J. H. *Atmos Environ* **2008**, *42*, 3593.
- (3) Kanakidou, M.; Seinfeld, J. H.; Pandis, S. N.; Dentener, F. J.; Facchini, M. C.; Van Dingenen, R.; Ervens, B.; Nenes, A.; Nielson, C. J.; Swietlicki, E.; Putaud, J. P.; Balkanski, Y.; Fuzzi, S.; Horth, J.; Moortgat, G. K.; Winterhalter, R.; Myhre, C. E. L.; Tsigaridis, K.; Vignati, E.; Stephanou, E. G.; Wilson, J. *Atmos. Chem. Phys.* **2005**, *5*, 1053.
- (4) *Climate Change 2007: The Physical Science Basis: Contribution of Working Group I to the Fourth Assessment Report of the Intergovernmental Panel on Climate Change*; Solomon, S.; Qin, D.; Manning, M.; Chen, Z.; Marquis, M.; Averyt, K. B.; Tignor, M.; Miller, H. L., Eds.; Cambridge University Press: Cambridge, United Kingdom and New York City, NY, USA, 2007.

- (5) Miller-Schulze, J. P.; Shafer, M. M.; Schauer, J. J.; Solomon, P. A.; Lantz, J.; Artamonova, M.; Chen, B.; Imashev, S.; Sverdlik, L.; Carmichael, G. R.; Deminter, J. T. *Atmospheric Environment* **2011**, *45*, 6955.
- (6) Diaz, E. A.; Lemos, M.; Coull, B.; Long, M. S.; Rohr, A. C.; Ruiz, P.; Gupta, T.; Kang, C. M.; Godleski, J. J. *Inhal Toxicol* **2011**, *23*, 42.
- (7) Hamilton, J. F.; Lewis, A. C.; Carey, T. J.; Wenger, J. C.; Garcia, E. B. I.; Munoz, A. *Atmospheric Chemistry and Physics* **2009**, *9*, 3815.
- (8) Carlton, A. G.; Wiedinmyer, C.; Kroll, J. H. *Atmospheric Chemistry and Physics* **2009**, *9*, 4987.
- (9) Shilling, J. E.; Zaveri, R. A.; Fast, J. D.; Kleinman, L.; Alexander, M. L.; Canagaratna, M. R.; Fortner, E.; Hubbe, J. M.; Jayne, J. T.; Sedlacek, A.; Setyan, A.; Springston, S.; Worsnop, D. R.; Zhang, Q. *Atmos. Chem. Phys.* **2013**, *13*, 2091.
- (10) Emanuelsson, E. U.; Hallquist, M.; Kristensen, K.; Glasius, M.; Bohn, B.; Fuchs, H.; Kammer, B.; Kiendler-Scharr, A.; Nehr, S.; Rubach, F.; Tillmann, R.; Wahner, A.; Wu, H. C.; Mentel, T. F. *Atmos. Chem. Phys.* **2013**, *13*, 2837.
- (11) Glasius, M.; la Cour, A.; Lohse, C. *J Geophys Res-Atmos* **2011**, *116*.
- (12) Spracklen, D. V.; Jimenez, J. L.; Carslaw, K. S.; Worsnop, D. R.; Evans, M. J.; Mann, G. W.; Zhang, Q.; Canagaratna, M. R.; Allan, J.; Coe, H.; McFiggans, G.; Rap, A.; Forster, P. *Atmospheric Chemistry and Physics* **2011**, *11*, 12109.
- (13) Hoyle, C. R.; Boy, M.; Donahue, N. M.; Fry, J. L.; Glasius, M.; Guenther, A.; Hallar, A. G.; Hartz, K. H.; Petters, M. D.; Petaja, T.; Rosenoern, T.; Sullivan, A. P. *Atmospheric Chemistry and Physics* **2011**, *11*, 321.
- (14) Kirstine, W.; Galbally, I.; Ye, Y. R.; Hooper, M. *J Geophys Res-Atmos* **1998**, *103*, 10605.
- (15) Brilli, F.; Ruuskanen, T. M.; Schnitzhofer, R.; Muller, M.; Breitenlechner, M.; Bittner, V.; Wohlfahrt, G.; Loreto, F.; Hansel, A. *Plos One* **2011**, *6*.
- (16) Karl, T.; Harren, F.; Warneke, C.; de Gouw, J.; Grayless, C.; Fall, R. *J Geophys Res-Atmos* **2005**, *110*.
- (17) Ormeno, E.; Gentner, D. R.; Fares, S.; Karlik, J.; Park, J. H.; Goldstein, A. H. *Environ Sci Technol* **2010**, *44*, 3758.
- (18) Hatanaka, A. *Phytochemistry* **1993**, *34*, 1201.
- (19) Brilli, F.; Hortnagl, L.; Bamberger, I.; Schnitzhofer, R.; Ruuskanen, T. M.; Hansel, A.; Loreto, F.; Wohlfahrt, G. *Environ Sci Technol* **2012**, *46*, 3859.
- (20) Kirstine, W. V.; Galbally, I. E. *J Air Waste Manage* **2004**, *54*, 1299.
- (21) Jardine, K.; Barron-Gafford, G. A.; Norman, J. P.; Abrell, L.; Monson, R. K.; Meyers, K. T.; Pavao-Zuckerman, M.; Dontsova, K.; Kleist, E.; Werner, C.; Huxman, T. E. *Photosynth Res* **2012**, *113*, 321.

- (22) de Gouw, J. A.; Howard, C. J.; Custer, T. G.; Fall, R. *Geophys Res Lett* **1999**, *26*, 811.
- (23) Karl, T.; Fall, R.; Jordan, A.; Lindinger, W. *Environ Sci Technol* **2001**, *35*, 2926.
- (24) Orlando, J. J.; Tyndall, G. S.; Ceazan, N. *Journal of Physical Chemistry A* **2001**, *105*, 3564.
- (25) Pinto, D. M.; Nerg, A. M.; Holopainen, J. K. *Journal of Chemical Ecology* **2007**, *33*, 2218.
- (26) Hartikainen, K.; Riikonen, J.; Nerg, A. M.; Kivimaenpaa, M.; Ahonen, V.; Tervahauta, A.; Karenlampi, S.; Maenpaa, M.; Rousi, M.; Kontunen-Soppela, S.; Oksanen, E.; Holopainen, T. *Environ Exp Bot* **2012**, *84*, 33.
- (27) Aschmann, S. M.; Shu, Y. H.; Arey, J.; Atkinson, R. *Atmospheric Environment* **1997**, *31*, 3551.
- (28) O'Dwyer, M. A.; Carey, T. J.; Healy, R. M.; Wenger, J. C.; Picquet-Varrault, B.; Doussin, J. F. *Z Phys Chem* **2010**, *224*, 1059.
- (29) Reisen, F.; Aschmann, S. M.; Atkinson, R.; Arey, J. *Environ Sci Technol* **2003**, *37*, 4664.
- (30) Joutsensaari, J.; Loivamaki, M.; Vuorinen, T.; Miettinen, P.; Nerg, A. M.; Holopainen, J. K.; Laaksonen, A. *Atmospheric Chemistry and Physics* **2005**, *5*, 1489.
- (31) Olofsson, M.; Ek-Olausson, B.; Ljungstrom, E.; Langer, S. *J Environ Monitor* **2003**, *5*, 963.
- (32) Robbins, P.; Birkenholtz, T. *Land Use Policy* **2003**, *20*, 181.
- (33) Guenther, A.; Geron, C.; Pierce, T.; Lamb, B.; Harley, P.; Fall, R. *Atmos Environ* **2000**, *34*, 2205.
- (34) Kirstine, W., Galbally, I., Hooper, M. In *16th International Clean Air Conference* Christchurch, New Zealand, 2002.
- (35) Hamilton, J. F.; Lewis, A. C.; Carey, T. J.; Wenger, J. C. *Anal Chem* **2008**, *80*, 474.
- (36) Cahill, T. M.; Seaman, V. Y.; Charles, M. J.; Holzinger, R.; Goldstein, A. H. *J Geophys Res-Atmos* **2006**, *111*.
- (37) Solomon, S. D.; Qin, M. M.; Chen, Z.; Marquis, M.; Averyt, K. B.; Tignor, M.; Miller, H. L. e. *Contribution of Working Group I to the Fourth Assessment Report of the Intergovernmental Panel on Climate Change, 2007*; Cambridge University Press.: Cambridge, United Kingdom and New York, NY, USA., 2007.
- (38) Nemitz, E.; Dorsey, J. R.; Flynn, M. J.; Gallagher, M. W.; Hensen, A.; Erisman, J. W.; Owen, S. M.; Dämmgen, U.; Sutton, M. A. *Biogeosciences* **2009**, *6*, 1627.
- (39) Gulden, L. E.; Yang, Z. L.; Niu, G. Y. *J Geophys Res-Atmos* **2007**, *112*.
- (40) Lefohn, A. S.; Shadwick, D.; Oltmans, S. J. *Atmospheric Environment* **2010**, *44*, 5199.

- (41) Guenther, A. B.; Jiang, X.; Heald, C. L.; Sakulyanontvittaya, T.; Duhl, T.; Emmons, L. K.; Wang, X. *Geosci Model Dev* **2012**, *5*, 1471.
- (42) Steinbrecher, R.; Klauer, M.; Hauff, K.; Stockwell, W. R.; Jaeschke, W.; Dietrich, T.; Herbert, F. *Atmospheric Environment* **2000**, *34*, 3779.
- (43) Fushimi, A.; Wagai, R.; Uchida, M.; Hasegawa, S.; Takahashi, K.; Kondo, M.; Hirabayashi, M.; Morino, Y.; Shibata, Y.; Ohara, T.; Kobayashi, S.; Tanabe, K. *Environ Sci Technol* **2011**, *45*, 6784.
- (44) Starn, T. K.; Shepson, P. B.; Bertman, S. B.; Riemer, D. D.; Zika, R. G.; Olszyna, K. *Journal of Geophysical Research: Atmospheres* **1998**, *103*, 22437.
- (45) Aiken, A. C.; Salcedo, D.; Cubison, M. J.; Huffman, J. A.; DeCarlo, P. F.; Ulbrich, I. M.; Docherty, K. S.; Sueper, D.; Kimmel, J. R.; Worsnop, D. R.; Trimborn, A.; Northway, M.; Stone, E. A.; Schauer, J. J.; Volkamer, R. M.; Fortner, E.; de Foy, B.; Wang, J.; Laskin, A.; Shutthanandan, V.; Zheng, J.; Zhang, R.; Gaffney, J.; Marley, N. A.; Paredes-Miranda, G.; Arnott, W. P.; Molina, L. T.; Sosa, G.; Jimenez, J. L. *Atmos. Chem. Phys.* **2009**, *9*, 6633.
- (46) Watkins, E.; Gianfagna, T. J.; Sun, R. Q.; Meyer, W. A. *Crop Sci* **2006**, *46*, 2575.
- (47) Uchiyama, S.; Inaba, Y.; Kunugita, N. *Journal of chromatography. A* **2012**, *1229*, 293.
- (48) Helmig, D. *Atmospheric Environment* **1997**, *31*, 3635.
- (49) Clegg, S. L.; Kleeman, M. J.; Griffin, R. J.; Seinfeld, J. H. *Atmos. Chem. Phys.* **2008**, *8*, 1087.
- (50) Clegg, S. L.; Brimblecombe, P.; Wexler, A. S. Vapor Pressures of Pure Liquid Organic Compounds. [Online Early Access]. <http://www.aim.env.uea.ac.uk/aim/aim.php> (accessed 1 January 2013).
- (51) Moller, B.; Rarey, J.; Ramjugernath, D. *J Mol Liq* **2008**, *143*, 52.
- (52) Myrdal, P. B.; Yalkowsky, S. H. *Ind Eng Chem Res* **1997**, *36*, 2494.
- (53) Nannoolal, Y.; Rarey, J.; Ramjugernath, D. *Fluid Phase Equilib* **2008**, *269*, 117.
- (54) Nannoolal, Y.; Rarey, J.; Ramjugernath, D.; Cordes, W. *Fluid Phase Equilib* **2004**, *226*, 45.
- (55) Stein, S. E.; Brown, R. L. *J Chem Inf Comp Sci* **1994**, *34*, 581.
- (56) Brotzman, D.; Pelch, L. 2013.
- (57) Grosjean, D.; Grosjean, E.; Williams, E. L. *Int J Chem Kinet* **1993**, *25*, 783.
- (58) Grosjean, E.; Grosjean, D. *Int J Chem Kinet* **1994**, *26*, 1185.
- (59) Grosjean, E.; Grosjean, D. *J Atmos Chem* **1997**, *27*, 271.
- (60) Grosjean, E.; Grosjean, D. *J Atmos Chem* **1999**, *32*, 205.
- (61) Li, J.; Sun, Y.; Cao, H.; Han, D.; He, M. *Struct Chem* **2013**, *1*.

- (62) Odum, J. R.; Hoffmann, T.; Bowman, F.; Collins, D.; Flagan, R. C.; Seinfeld, J. H. *Environ. Sci. Technol.* **1996**, *30*, 2580.
- (63) Presto, A. A.; Huff Hartz, K. E.; Donahue, N. M. *Environ Sci Technol* **2005**, *39*, 7036.
- (64) Cocker, D. R.; Flagan, R. C.; Seinfeld, J. H. *Environ Sci Technol* **2001**, *35*, 2594.
- (65) Carter, W. P. L.; Cocker Iii, D. R.; Fitz, D. R.; Malkina, I. L.; Bumiller, K.; Sauer, C. G.; Pisano, J. T.; Bufalino, C.; Song, C. *Atmospheric Environment* **2005**, *39*, 7768.
- (66) Wu, S.; Lu, Z. F.; Hao, J. M.; Zhao, Z.; Li, J. H.; Hideto, T.; Hiroaki, M.; Akio, Y. *Adv Atmos Sci* **2007**, *24*, 250.
- (67) Wu, J. D.; Bauer, M. E. *Remote Sens-Basel* **2012**, *4*, 849.
- (68) Stevenson, N., Plymouth State University, 2010.
- (69) Guenther, A.; Zimmerman, P.; Wildermuth, M. *Atmospheric Environment* **1994**, *28*, 1197.
- (70) Zheng, D. L.; Ducey, M. J.; Heath, L. S. *Urban for Urban Gree* **2013**, *12*, 61.
- (71) US_Environmental_Protection_Agency 2013; Vol. 2013.
- (72) Mao, H. T.; Talbot, R.; Troop, D.; Johnson, R.; Businger, S.; Thompson, A. M. *J Geophys Res-Atmos* **2006**, *111*.
- (73) Bertschi, I. T.; Jaffe, D. A. *J Geophys Res-Atmos* **2005**, *110*.
- (74) Wang, T.; Ding, A. J.; Gao, J.; Wu, W. S. *Geophys Res Lett* **2006**, *33*.
- (75) Lee, S. H.; Kim, S. W.; Trainer, M.; Frost, G. J.; McKeen, S. A.; Cooper, O. R.; Flocke, F.; Holloway, J. S.; Neuman, J. A.; Ryerson, T.; Senff, C. J.; Swanson, A. L.; Thompson, A. M. *Atmos. Chem. Phys.* **2011**, *11*, 7375.
- (76) van Donkelaar, A.; Martin, R. V.; Brauer, M.; Kahn, R.; Levy, R.; Verduzco, C.; Villeneuve, P. J. *Environ Health Persp* **2010**, *118*, 847.
- (77) Agency, U. S. E. P. 2012.
- (78) Organization, W. H. 2011.
- (79) Papagni, C.; Arey, J.; Atkinson, R. *Int J Chem Kinet* **2001**, *33*, 142.
- (80) Hildebrandt, L.; Henry, K. M.; Kroll, J. H.; Worsnop, D. R.; Pandis, S. N.; Donahue, N. M. *Environ Sci Technol* **2011**, *45*, 6329.
- (81) Drewnick, F.; Dall'Osto, M.; Harrison, R. M. *Atmospheric Environment* **2008**, *42*, 3006.

CHAPTER 5. OPTICAL PROPERTIES OF SECONDARY ORGANIC AEROSOL FROM CIS-3-HEXENOL AND CIS-3-HEXENYL ACETATE: EFFECT OF CHEMICAL COMPOSITION, HUMIDITY AND PHASE

The following is an expansion upon a manuscript, submitted (Feb, 2016) and under review for publication in Environmental Science and Policy. The full reference is as follows:

Harvey, R. M.; Bateman, A. P.; Jain, S.; Li, Y. J.; Petrucci, G. A.; Martin, S. T.. The optical properties of GLV-Derived SOA: Effect of chemical composition, humidity and phase. . *Environ Sci Technol* (**under review**).

5.1 Introduction

The absorption and scatter of light by atmospheric aerosols plays an important role in Earth's radiative balance. However, the magnitude of absorption and scatter has proven difficult to pin down, largely due to challenges associated with measuring aerosol optical properties, which are size, composition and wavelength dependent. Organic aerosol (OA) contributes 20-90% of the total mass of atmospheric aerosol^{1,2} and 70-90% of OA is secondary in nature (SOA), being formed by the oxidation of volatile organic compounds (VOCs) in the atmosphere.³ There is growing evidence to suggest that SOA contributes to light attenuation (by both absorbance and scatter) in the atmosphere and may play an important role in the radiative budget.⁴⁻¹² Green leaf volatiles (GLVs) are a class of wound-induced VOCs emitted by several plant species. The most dominant and ozone-reactive GLVs include cis-3-hexenyl acetate (CHA) and cis-3-hexenol (HXL), which have been

shown to react with ozone to produce SOA at comparable levels to predominant biogenic SOA sources, yet the optical properties of these SOA are not understood.¹³

The optical properties of SOA can be characterized by the extinction coefficient (σ_{ext}), which describes total light attenuation; the mass absorbance/scatter coefficient (MAC, MSC), which describe the mass-normalized contribution of light absorbance/scatter to the total extinction; and the Angstrom Scatter Exponent (ASE), which describes the wavelength dependence of scatter.^{7,14-17} These optical properties are closely related to particle size, phase and chemical composition, which are themselves dependent on the parent VOC, type of oxidation (by ozone, NO_x, OH etc.) and environmental conditions (i.e., temperature, humidity). Over long time scales, particle-phase reactions and chemical aging also contribute to optical properties.¹⁸ Bulk chemical properties such as the oxygen-to-carbon ratio (O:C) of SOA have been used to predict or rationalize SOA optical properties.^{2,4,9,18-22} For example, a greater O:C has been shown to correlate to greater light absorption.^{17,23,24} However, recent studies have also shown no correlation between O:C and optical properties, or even the opposite trend.^{18,25}

In this work, we measure the optical properties and phase state of SOA as a function of chemical system (CHA vs HXL) and environmental conditions (relative humidity, RH). We further demonstrate that a molecular-level understanding of SOA chemical composition is important to understand its optical properties and predict its role in radiative forcing.

5.2 Experimental

All experiments were performed in the Harvard Environmental Chamber (HEC) operated in continuous-flow mode.^{26,27} The HEC consists of a 4.7-m³ PFA Teflon bag housed in a temperature and humidity-controlled room. Dry, clean, hydrocarbon-free air was produced with a pure air generator (Aadco 737). A syringe pump was used to continuously introduce standards of CHA or HXL (both >98 %, Sigma-Aldrich) into a secondary chamber. A constant flow of zero air was used to sweep volatilized compounds from the secondary chamber into the HEC. Neither seed particles nor OH scavengers were used in these experiments. Ozone was produced by passing air around an ultraviolet lamp (Jelight 600) and then monitored in the chamber using a Teledyne 400 E. Humidity was controlled by passing zero air through a water bubbler (18 M Ω cm) followed by a HEPA filter and into the chamber, where it was monitored with a Rotronics humidity sensor (Hygroclip SC05). Bulk chemical properties (O:C, H:C) were measured using an Aerodyne high-resolution time of flight mass spectrometer (HR-ToF-AMS),^{28,29} according to Chen et al. (2011).³⁰ Molecular level chemical analysis of SOA was performed using Near-IR Laser Desorption/Ionization Aerosol Mass Spectrometry (NIR-LDI AMS).^{31,32}

An integrating sphere UV-Vis spectrometer (IS-UV-Vis, Shimadzu UV-2450 with ISR 2200) was used to measure the wavelength-dependent light absorption of SOA.⁹ SOA was collected on 25 mm diameter quartz filters (Pall Tissuquartz PN 7200) at 4.95 ± 0.05 L min⁻¹ for a known duration of time (See Table 5.1). Filters were individually wrapped in aluminum foil and stored in a desiccator at room temperature until analysis (<2 weeks). The volume-normalized absorption coefficient (b_v , m⁻¹) was determined by measuring the absorbance (Abs) of SOA on a filter according to:

$$b_v = \frac{A}{V} \times Abs \times \ln(10) \quad (5.1)$$

where A is filter area (m^2) and V is the volume of air sampled (m^3). All samples were blank corrected using clean filters. To compare the absorption coefficients of SOA from different precursors, the mass normalized absorption coefficient (MAC, m^2g^{-1}) was calculated by:

$$MAC = \frac{b_v}{M_v} \quad (5.2)$$

where M_v is the average SOA mass concentration ($g\ m^{-3}$), which was measured using a multi stage electrical low pressure impactor (ELPI+, Dekati). Size distribution was also measured using a scanning mobility particle sizer (SMPS) and condensation particle counter (CPC). Typical SOA mass loading on filters was approximately $50\ \mu g$. Where SOA mass concentrations were sufficiently high, the collection of several filters was possible, in which case MAC values are reported as the average ± 1 standard deviation.

Table 5.1 Experimental conditions for GLV ozonolysis experiment in HEC.

Experiment	HXL 1	HXL 2	CHA 1
Date	11/3/2015	11/4/2015	11/12/2015
[HXL] (ppb)	500	500	0
[CHA] (ppb)	0	0	500
[Ozone] (ppb)	200	200	200
RH %	10	70	10
SOA Mass Conc. ($\mu g\ m^{-3}$)	80	30	15
Filter 1 Sample Volume (L)	440	300	630
Filter 2 Sample Volume (L)	325	330	550
Filter 3 Sample Volume (L)	330	530	n/a
Filter 4 Sample Volume (L)	n/a	540	n/a
Approximate Reaction Time (hr)*	4	7.25	2.5

* reaction time corresponds to time over which experimental conditions were stable (SOA mass concentration, RH, $[O_3]$, and [VOC]).

The scattering coefficient (σ_{scat}) of the bulk aerosol was measured directly using a three-wavelength integrating nephelometer (Aurora 3000, Ecotech), which was then used to determine the mass scattering coefficient (MSC, m^2g^{-1}) by normalizing to the average SOA mass concentration (M_v , g m^{-3}):

$$MSC = \frac{\sigma_{\text{scat}}}{M_v} \quad (5.3)$$

Nephelometer measurements introduce truncation errors that influence the measured scatter values.³³ For particles with diameters greater than 1 μm , these errors can be as large 20%-50%. For accumulation mode particles (diameter between 200 and 400 nm), however, truncation errors are limited to $\sim 10\%$.³³ Truncation errors represent a lower bound of measurement errors in this work and, thus, we did not attempt to quantify and/or correct for this error.

The ozonolysis of CHA was performed under dry conditions only (at 10% RH) while that of HXL was performed under both dry and wet conditions (10% RH and 70% RH, respectively). Upon completion of dry HXL ozonolysis experiments (i.e. experiment “HXL 1” in Table 5.1), RH was slowly increased from 10% to 70% over the course of 13 hours. Recall that the HEC was operated in continuous flow mode, where VOC and oxidant were continuously injected into the chamber as RH was increased. During this period, σ_{scat} was continuously monitored, allowing for the determination of $f(\text{RH})$, the scatter enhancement coefficient:

$$f(\text{RH}) = \frac{MSC(\text{RH}, \lambda)}{MSC(\text{RH}_{\text{dry}}, \lambda)} \quad (5.4)$$

where $MSC(\text{RH}, \lambda)$ and $MSC(\text{RH}_{\text{dry}}, \lambda)$ are the mass normalized scattering coefficients at wavelength (λ) for a given RH and under dry conditions (10% RH), respectively.³⁴

Particle bounce factor (BF) was measured using the ELPI+ operating with either smooth or sintered impaction plates.³⁵ Briefly, the method assumes that solid particles bounce from upper stages of the smooth impaction plates (where they should be counted) to lower levels designed to count smaller particles, shifting the particle size distribution compared to that measured using sintered plates, which measures the true size distribution (i.e., no bounce). The BF is calculated by comparing the raw current measured on each stage of the smooth/sintered plates for the same bulk aerosol:

$$BF = \frac{I_{Filter(smooth)}^{(bounce)} - I_{Filter(sintered)}^{(no\ bounce)}}{\sum I_{impactor\ stage > filter}^{(no\ bounce)}} \quad (5.5)$$

where $I_{Filter(smooth)}^{(bounce)}$ and, $I_{Filter(sintered)}^{(no\ bounce)}$ are the raw currents measured at the smallest diameter channel of the smooth and sintered plates (the filter), respectively.

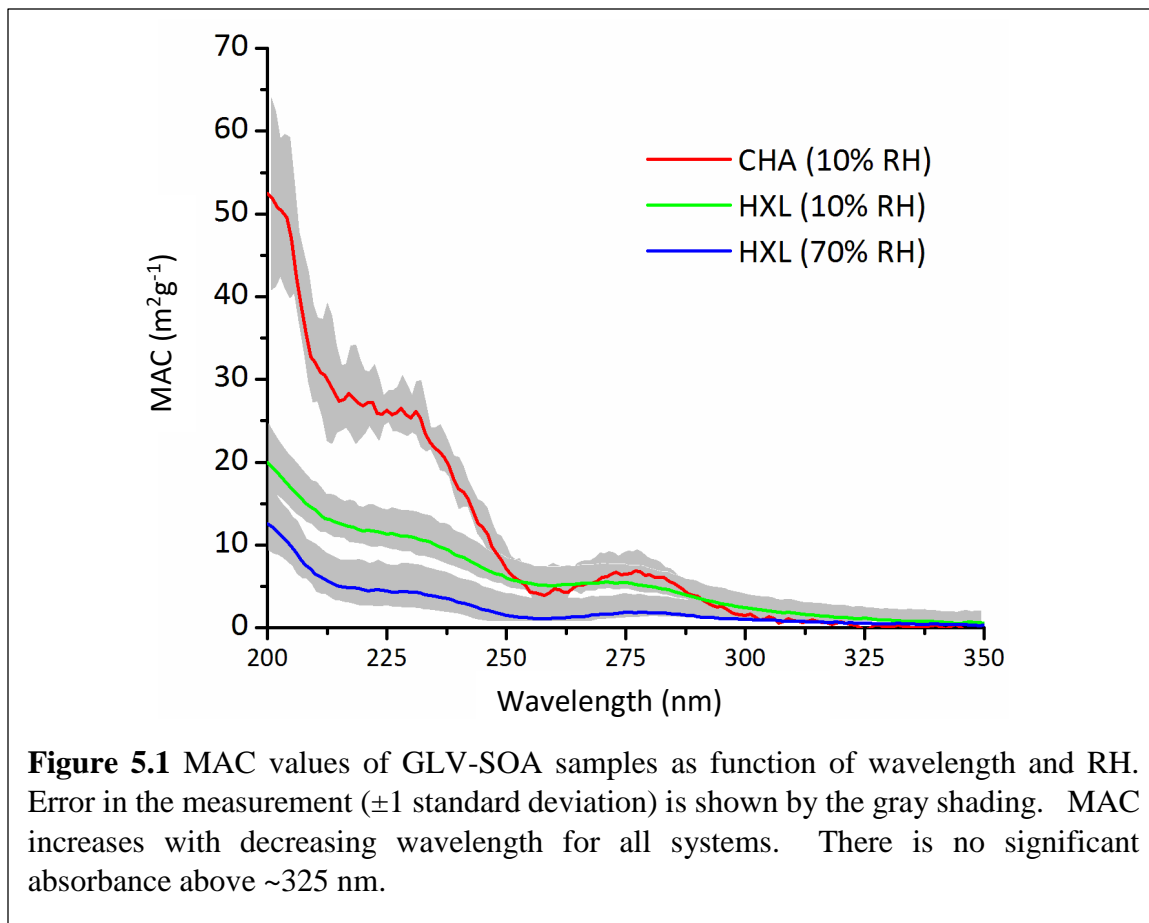
$\sum I_{impactor\ stage > filter}^{(no\ bounce)}$ is the sum of the raw currents obtained from all stages of the sintered plates except the smallest, filter stage. By this method, liquid particles result in $BF = 0$.

5.3 Results and Discussion

5.3.1 Absorbance of CHA- vs HXL- SOA

Integrating spheres (by design) are prone to over-estimating aerosol absorption relative to the same particles in suspension; scattering by the filter allows for multiple opportunities for absorption. The magnitude of this error depends on the filter type and method of sample deposition.²² There is some evidence to suggest that the use of nucleopore filters may limit this error,³⁶ yet does not eliminate it completely.³⁷ We used

quartz filters, which are commonly used by others in the field⁹ in order to maintain internal consistency of the measurements and to allow for comparison with existing literature reports. No corrections for multiple scatter events were made herein, but the measured MAC values are internally consistent and allow for a discussion of the different chemical systems studied.



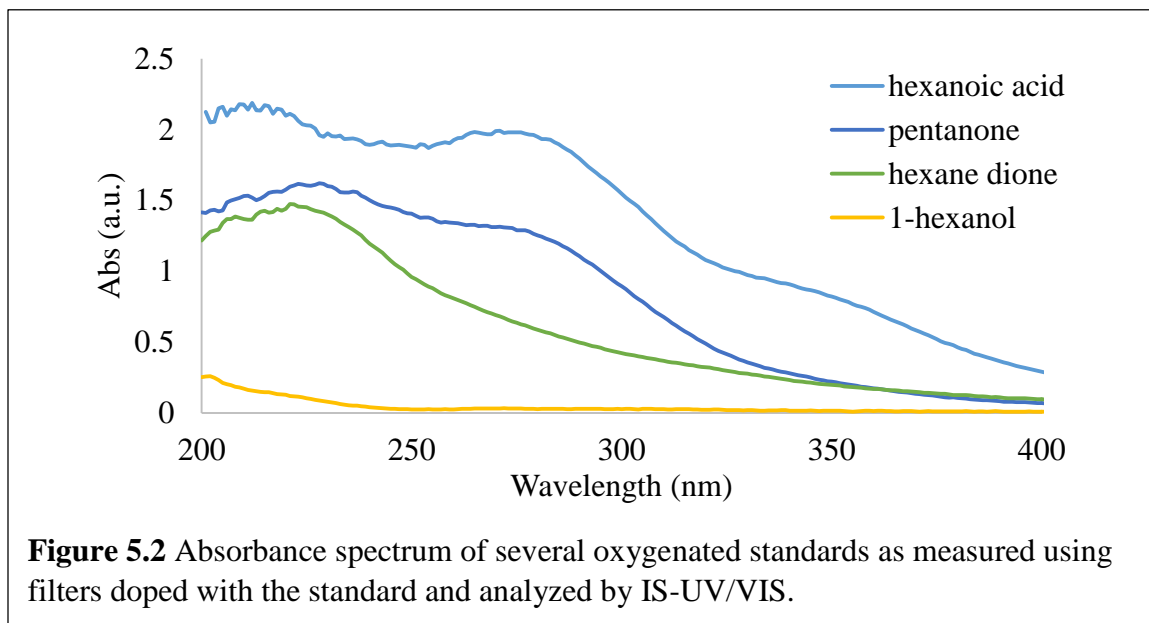
Both CHA- and HXL-SOA show negligible MAC values at wavelengths greater than ~ 350 nm (< 0.2 m² g⁻¹, which is within one standard deviation of zero in our measurements) (Figure 5.1). At wavelengths shorter than 350 nm, MAC increases with decreasing wavelength to a maximum of 50 m²g⁻¹ and 20 m²g⁻¹ at 200 nm for CHA-SOA

and HXL-SOA, respectively. Both CHA and HXL have broad absorption bands at ~ 275 nm and ~ 225 nm, but CHA-SOA shows more distinct spectral features and greater overall MAC, suggesting it contains a greater relative amount of absorbing species. Only a small fraction of actinic light overlaps with the absorption by GLV-SOA, which may limit its overall impact in radiative forcing. However, when absorbing species exist at a high enough concentration, small MAC values can translate to significant light attenuation, effectively impacting the Earth's radiative budget.³⁸ For example, humic-like substances (HULIS) have much lower MAC values in the visible region than GLVs ($\sim 0.03 \text{ m}^2\text{g}^{-1}$), yet HULIS accounts for roughly 8.5-11.5 % of light attenuation between 300-700 nm and between 6.4-8.6% across the entire tropospherically relevant solar spectrum, largely due to their ubiquitous nature.³⁸ HULIS mass concentrations of about $15 \mu\text{g m}^{-3}$ were used to estimate this light attenuation.³⁸ Analogously, the mowing of lawns alone has the capacity to release enough GLVs to yield roughly $50 \mu\text{g}$ of SOA per square meter of grass as a concerted burst.¹³ At GLV-derived SOA levels this high, the MAC values we measured could result in significant light attenuation.

5.3.2 Assignment of Spectral Features to Molecular Moieties

GLV-SOA contains significant amounts of non-conjugated carbonyl, carboxylic acid and hydroxyl substituted products,³⁹⁻⁴¹ for which the $n \rightarrow \pi^*$ absorption occurs in the region 280-300 nm,^{9,15,42} as confirmed in our lab for several oxygenated standards (ketone, carboxylic acid, alcohol) on filters (Figure 5.2). Analogous to GLV-derived SOA, the ketone (2-pentanone) showed broad absorbance bands at both 275 nm and 230 nm, while the carboxylic acid moiety (1-hexanoic acid) showed absorbance bands at 275 nm and at 215 nm.¹⁵ The alcohol standard we measured (1-hexanol) showed no distinct spectral

features but did increase in absorbance at wavelengths less than ~250 nm, echoing the trend we see in CHA and HXL-derived SOA and those seen for SOA known to contain hydroxyl groups.⁴³



The relative intensities of these bands in the two GLV-SOA systems suggest that CHA-SOA contains a greater fraction of carbonyl moieties than HXL-SOA. Using NIR-LDI AMS,^{31,32} the relative abundance of these species was compared between chemical systems. By summing the area of each spectral peak corresponding to carbonyl-containing species (as identified by Jain et al. (2014)⁴¹) and normalizing to the total area of the mass spectrum, the ‘carbonyl contribution’ to CHA-SOA (3.7 ± 0.8 %) was found to be statistically greater than that of HXL-SOA (2.1 ± 0.5 %) (Table 5.2). These estimates are in keeping with recent observations that, upon ozonolysis, HXL readily undergoes oligomerization reactions to yield high molecular-weight products containing predominantly alcohol moieties.⁴¹ Alternatively, the acetate functionality in CHA limits

oligomerization and the dominant pathway in CHA-ozonolysis is the hydroperoxide channel, yielding predominantly carbonyl functionalities.³⁹⁻⁴¹

Table 5.2 Physical and chemical properties of GLV-derived SOA

Experiment	HXL 1	HXL 2	CHA 1
Average b_v (Mm^{-1}) (450 nm)	39.1	14.5	1.8
Average b_v (Mm^{-1}) (525 nm)	36.9	16.5	6.0
Average b_v (Mm^{-1}) (635 nm)	34.6	13.8	8.4
Carbonyl Contribution (%)	2.1 ± 0.5	1.2 ± 0.2	3.7 ± 0.8
Bounce Factor (BF)	0.15 ± 0.08	0.02 ± 0.01	n/a
O:C	0.68 ± 0.05	0.70 ± 0.02	0.55 ± 0.06
Mass Extinction Coefficient (MEC, m^2g^{-1}) (450 nm)	0.73	0.83	3.9
Mass Extinction Coefficient (MEC, m^2g^{-1}) (525 nm)	1.1	0.95	2.4
Mass Extinction Coefficient (MEC, m^2g^{-1}) (635 nm)	0.9	1.58	2.0
Relative Contribution of MSC to MEC * (450 nm)	64%	79%	86%
Relative Contribution of MSC to MEC * (525 nm)	77%	80%	70%
Relative Contribution of MSC to MEC * (635 nm)	84%	85%	68%

* Relative contribution of MSC to MEC = $MSC/MEC \times 100\%$

The O:C ratio measured for HXL-SOA (0.68 ± 0.05) was greater than that for CHA-SOA (0.55 ± 0.06). In some cases, the degree of oxidative ageing (for which the O:C ratio serves as proxy) of SOA has been directly correlated to light absorption of SOA.^{4,6,9,15,18,23,44,45} Despite being more oxygenated (having a greater O:C), however,

HXL-SOA was less absorbing than CHA-SOA, which we attributed to a smaller fraction of carbonyl functionalities. To determine and explain the optical properties of SOA, therefore, it is important to know not only the O:C ratio, but also the oxidation state of the oxygen (i.e., its chemical form), highlighting the need for a molecular-level understanding of SOA composition.

5.3.3 Effect of Humidity on the MAC of HXL SOA

For the HXL system, low RH (10%) produced SOA with a greater MAC than high RH (70%) (Figure 5.1). The absorbance features at ~280 nm and ~230 nm are present in both cases, however, suggesting the same general classes of chemical products are present but are at higher concentrations under the dry environment (assuming the absorbance follows Beer's Law). The impact of excess water on product distribution has been shown previously for the case of aqueous phase *versus* gas phase oxidation of several VOCs.⁴⁶⁻⁵⁰ We ascertain that as RH increases, and water becomes more available, aqueous phase ozonolysis mechanisms may start to occur/become prevalent for reactions in the particle phase. While the mass spectra for HXL-SOA formed under dry (Figure 5.3a) and wet (Figure 5.3b) conditions generally show the same dominant product peaks (73 m/z, 89 m/z, 103 m/z), their relative intensities differ, suggesting different relative product yields. For example, peaks at 103 m/z and 89 m/z dominate the spectrum for dry HXL-SOA, but the peak at 133 m/z becomes major for wet HXL-SOA. We also found that the carbonyl contribution in SOA formed by HXL ozonolysis at 70% RH (1.2 ± 0.2 %) was less than that formed at 10% RH (2.1 ± 0.5 %) (Table 5.2), which agrees with our observed trend of enhanced MAC value at low RH. Interestingly, the O:C ratio for HXL-SOA was found to be independent of RH within experimental error (0.68 ± 0.05 at 10% RH and 0.70 ± 0.02

at 70% RH), which would suggest the same MAC values for the two systems. However, we measured significantly different MAC values (Figure 5.1), further reinforcing the need for molecular-level characterization of SOA in order to understand its contribution to light absorption.

HXL-SOA readily undergoes oligomerization via several mechanisms, many of which are affected by ambient water (i.e., esterification and aldol condensation) to produce or consume carbonyl-containing chromophores.^{39-41,51} Several of these oligomerization reaction pathways are acid catalyzed, (i.e., aldol condensation), and can be particularly sensitive to changes in RH. As RH increases, water dilutes the SOA, decreasing particle ‘acidity’ and inhibiting the production of chromophores. This phenomenon was also observed by Nguyen et al. (2012),⁵² where high RH conditions resulted in reduced light absorbance by limonene-SOA. Song et al. (2013)⁵³ found similar results for SOA generated from α -pinene in the presence of acidic seed aerosol; the MAC of this SOA at RH > ~30% was negligible, as compared to 2% RH, where MAC increased significantly. It is possible that the presence of excess water effectively dilutes the particle acidity, limiting acid-catalyzed reactions that produce chromophores, and resulting in reduced MAC. The absence of acidic seed particles in our work suggests also that RH would play a correspondingly bigger role on the total acidity of the SOA produced.

As described above, the mass spectrum of HXL-SOA formed under wet conditions presents a prominent peak at 133 m/z , whereas it is only a minor feature in the spectrum recorded under dry conditions (Figure 5.3).

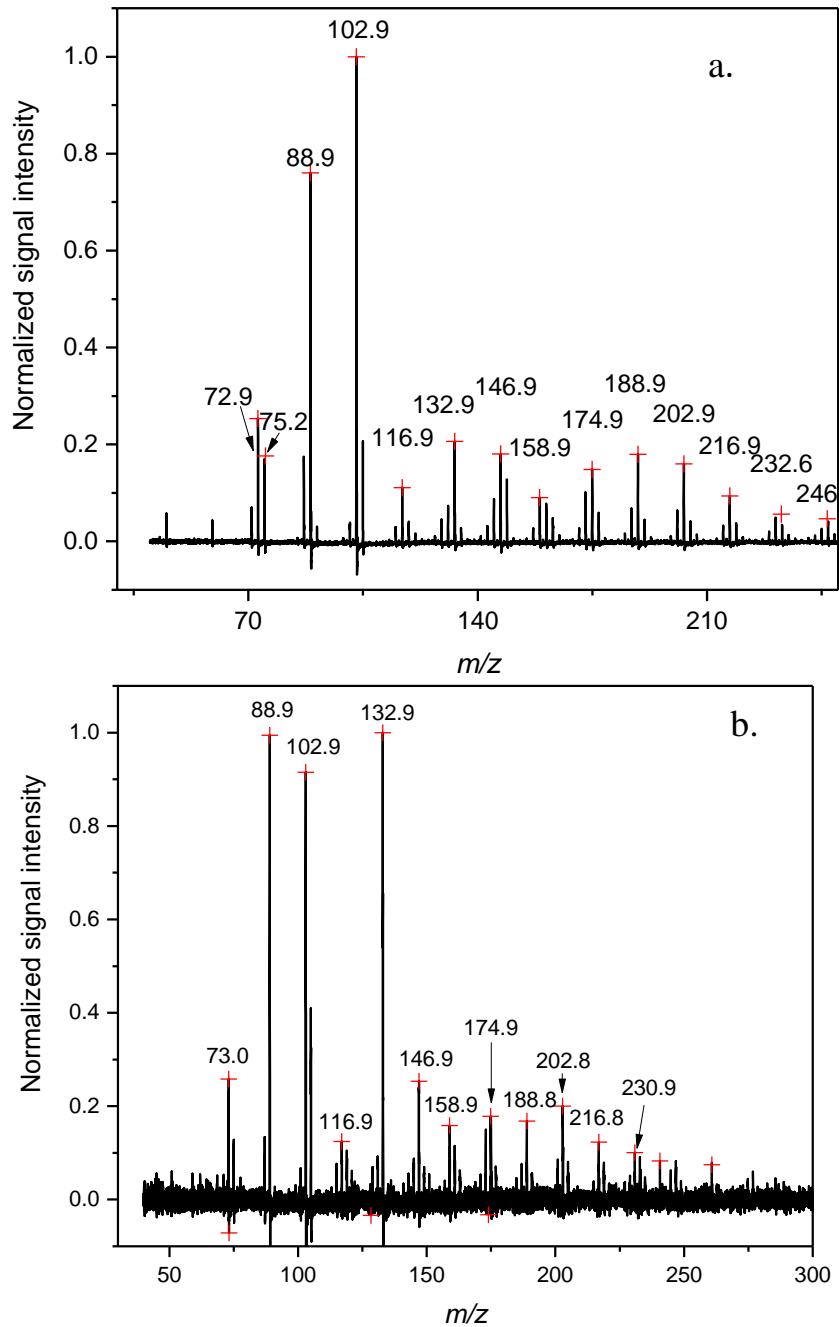
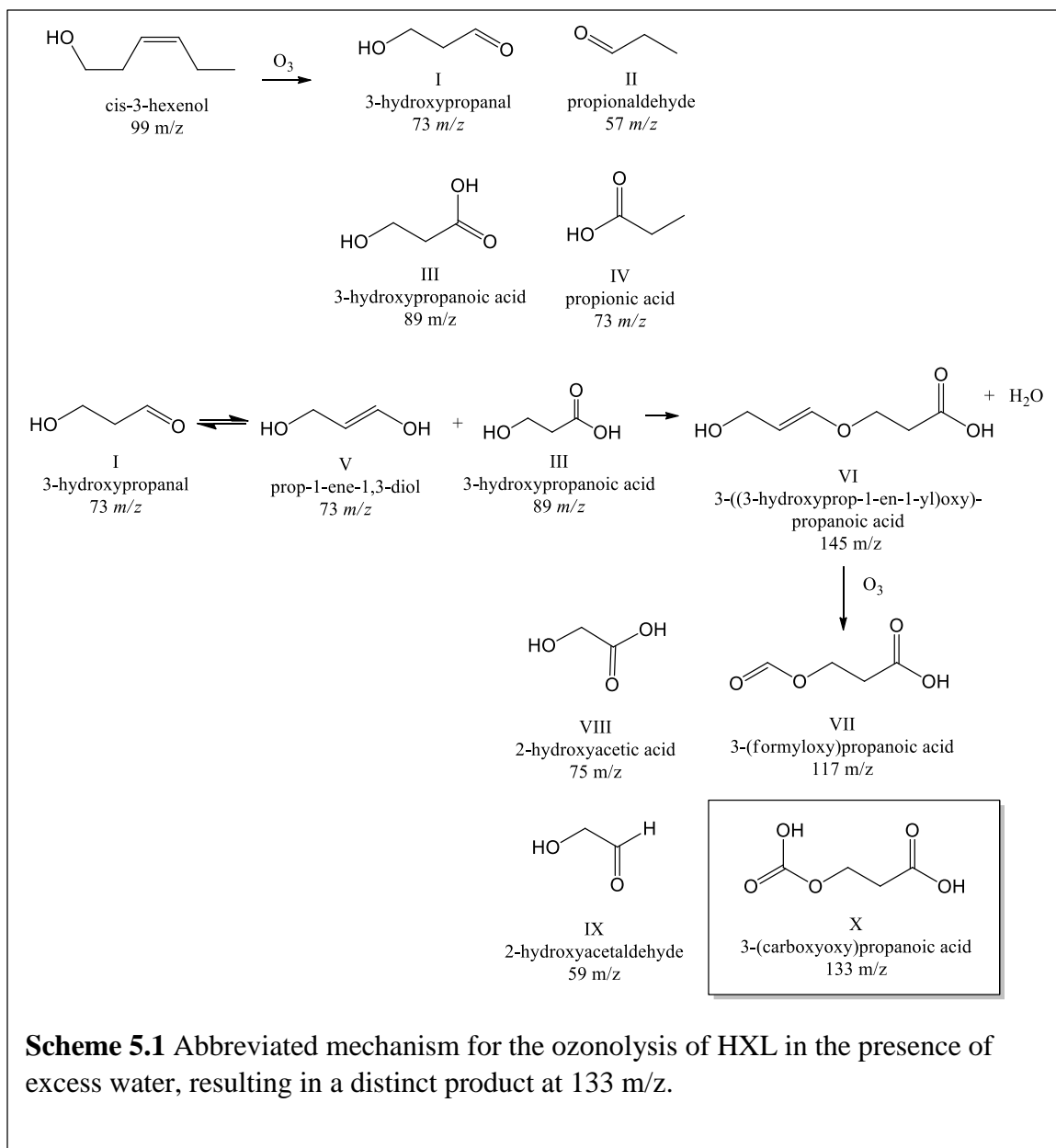
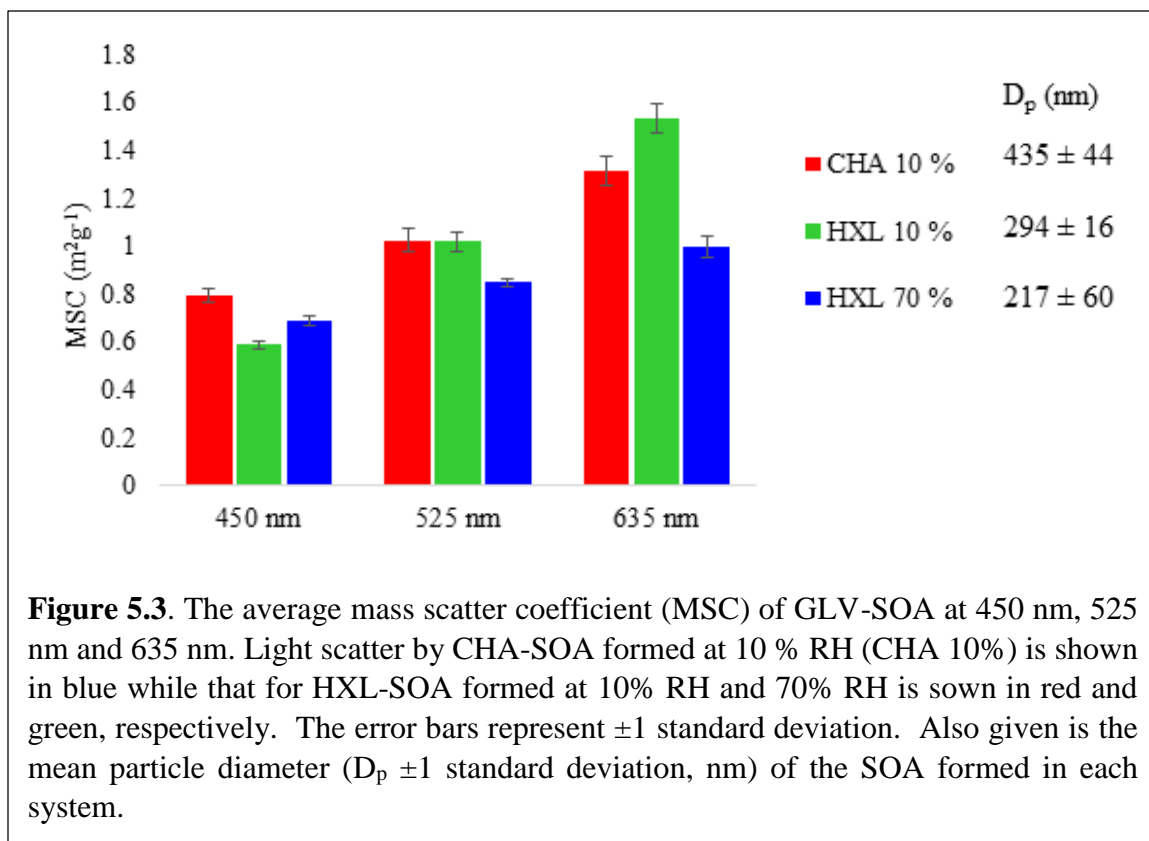


Figure 5.3. Mass spectra of HXL-SOA formed under dry (a, 10 % RH) and wet (b, 70% RH) conditions show a very similar product profile, with the same predominant peaks at 73 m/z , 89 m/z and 103 m/z . The main differences are the relative intensity of each peak in the two spectra and the intensity of the peak at 133 m/z .

Ozonolysis mechanisms for HXL^{39-41,54} have not yet accounted for a product of this molar mass, although Hamilton et al.(2009)⁴⁰ tentatively assigned this mass peak to 3-(2-hydroxyethoxy)-propanoic acid. Herein, we propose a different structure and accompanying mechanism for this product that rationalizes its observed RH-driven enhancement (Scheme 5.1).

Briefly, nucleophilic attack by ozone on HXL produces 3-hydroxy propanal (3-HPA, I), propionaldehyde (II) and two stabilized Criegee Intermediates, which, through further reaction, yield 3-hydroxypropanoic acid (III, 89 m/z) and propionic acid (IV, 73 m/z). 3-HPA undergoes keto-enol tautomerization to form prop-1-ene-1,3-diol (V, 73 m/z), which then reacts with III⁴⁰ to yield 3-((3-hydroxyprop-1-en-1-yl)oxy)propanoic acid (VI, 145 m/z). Further oxidation of VI by ozone yields 3-(formyloxy)propanoic acid (VII 117 m/z), 2-hydroxyacetic acid (VIII, 75 m/z), 2-hydroxyacetaldehyde (IX, 59 m/z) and the molecule of interest, 3-(carboxyoxy)propanoic acid (X, 133 m/z). This reaction pathway could also occur at low RH, as evidenced by the presence of the 133 m/z peak in Figure 5.3a. However, it has been shown that, in the presence of excess water, organic acids like 3-HPA (I), are found predominantly in their enol form (V in this case),⁵⁵ which would promote the formation of VI, VII, IX and X under high RH while decreasing the signal from III and V, as they are consumed. We see clear enhancement of X at high RH (nearly 2-fold increase in signal). The peaks at 73 m/z (IV) and 89 m/z (III) do not, however, decrease at high RH as anticipated. This, however, could be due to production of isobaric products,⁴¹ two of which we propose in this discussion (I and IV).



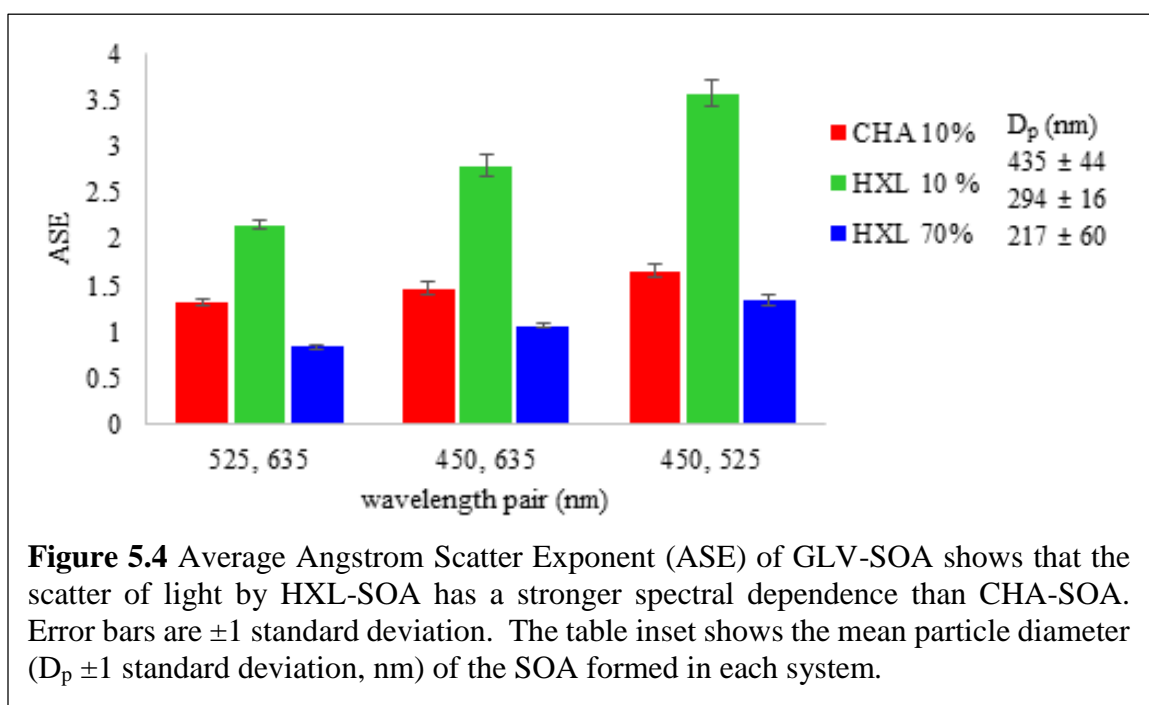


5.3.4 Light Scatter by GLV-SOA

The scatter of light by particles plays a crucial role in both climate forcing and visibility. Scatter efficiency depends on the competitive effect of aerosol mass concentration, chemical composition, size/shape and RH.^{56,57} The mass scattering coefficient, (MSC) for CHA-SOA and HXL-SOA show a strong and unique wavelength dependence (Figure 5.3). CHA-SOA is a more efficient scatterer at 450 nm, while an inversion is observed between 525 nm and 635 nm, where HXL-SOA becomes the more efficient scatterer. The wavelength dependence of scatter is generally represented by the Angstrom Scatter Exponent (ASE):

$$ASE = \frac{\ln(\sigma(\lambda_1)) - \ln(\sigma(\lambda_2))}{\ln(\lambda_1) - \ln(\lambda_2)} \quad (5.6)$$

where $\sigma(\lambda_1)$ and $\sigma(\lambda_2)$ are the scatter coefficients (in Mm^{-1}) measured at two different wavelengths (λ_1 and λ_2). The MSC increases at a greater rate for HXL-SOA than CHA-SOA, suggesting a stronger spectral dependency in scatter by HXL-SOA, which is also shown in as a greater ASE (Figure 5.4). ASE is inversely dependent on particle size.⁵⁸ Therefore, since HXL-SOA was smaller ($D_p = 294 \pm 16$ nm) than CHA-SOA ($D_p = 435 \pm 44$ nm), it follows that HXL-SOA should have a greater ASE than CHA, in agreement with our results.



5.3.5 Scatter Enhancement and RH

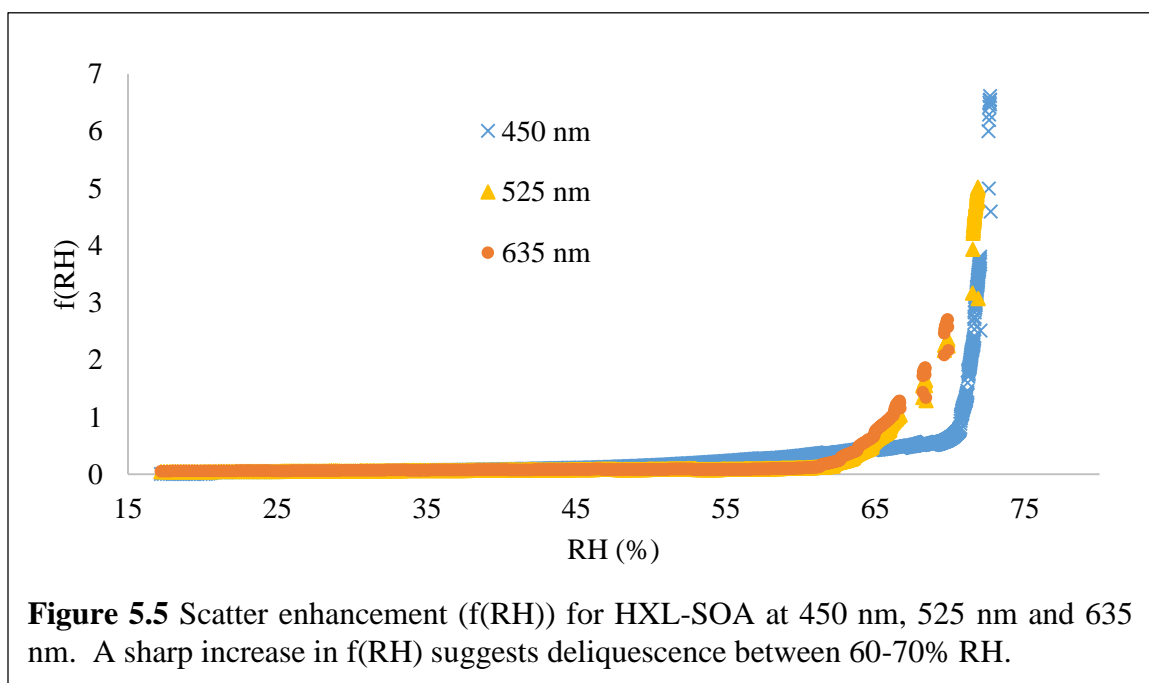
Aerosol light scatter is also dependent on RH, due to the hygroscopic growth of particles controlled by RH, which enhances scatter efficiency.^{19,34,56,59-63} Again, we see a wavelength dependency in the MSC of HXL-SOA formed under both wet and dry conditions (Figure 5.3), where scatter increases with increasing wavelength. Despite originating from the same VOC, however, light scatter by “wet HXL-SOA” (formed at

70% RH) and “dry HXL-SOA” (formed at 10% RH) have different wavelength dependencies. As discussed above, ASE is inversely related to particle size. Therefore, the wet HXL-SOA measured herein (with its smaller diameter) is expected to have a greater ASE than dry HXL-SOA. However, the ASE for wet HXL-SOA is considerably less than that for dry HXL-SOA (Figure 5.4). The reason for this discrepancy is unclear but may be related to the fact that the experimental design used herein results in the formation of SOA with distinct chemical properties under the two RH regimes (additional discussion in Section 5.4). This change in chemical composition may be driving trends in ASE, rather than particle size. It should also be noted that RH within the SMPS (where particle size distributions were measured) was not known during these particle size measurements but was probably less than 70% RH. This lower RH could have caused water within the wet HXL-SOA particles to evaporate, thereby reducing their apparent size.

The scattering enhancement factor ($f(\text{RH})$) describes the effect of RH on the light scattering efficiency of SOA. Also called the ‘optical growth factor,’⁶⁴ $f(\text{RH})$ is similar to the growth factor ($g(\text{RH})$) in that it can be related to a change in particle size as a function of RH, and can thus shed light on particles’ hygroscopic properties and can be used to infer its potential role in cloud formation.^{64,65} Whereas $g(\text{RH})$ describes the behavior of one given particle (or size regime of particle), $f(\text{RH})$ describes bulk aerosol properties.

Figure 5.5 is a plot of $f(\text{RH})$ (according to Equation 5.4) versus RH for HXL-SOA. For the 450 nm light, we observed a very small change in scatter from 10% to about 65% RH followed by a sharp increase at 70% RH, indicative of deliquescence.⁶² At deliquescence RH, a particle undergoes phase transformation from a solid particle to a

semi-solid or liquid droplet, causing the distinct enhancement in light scatter.^{34,66} We saw the same trend for $f(\text{RH})$ at 525 nm and 635 nm, however deliquescence appeared to occur at ~65% RH at 525 nm and 60% RH at 635 nm. Recall that different wavelengths of light interact more efficiently with different size regimes (450 nm with fine and ultrafine, 525 nm with accumulation mode, 635 nm with large, coarse mode PM). Since $f(\text{RH})$ is a bulk measurement, it is possible that the different deliquescence RH that we observed for different wavelengths of light may be a result of different sized particles having different affinities for water and thus deliquescing at different RH values.⁶⁷



Ultimately, the size dependency of particle hygroscopicity is related to differences in chemical composition, where smaller particles may be enriched with oxygenated products as compared to larger particles.⁶⁷ The enhanced oxidation state of these smaller particles enhances their hygroscopicity, contributing to the greater deliquescence RH observed at 450 nm. Understanding the hygroscopic behavior and deliquescence RH of

particles is important in understanding their roles as cloud condensation nuclei and ice nuclei, which have important roles in indirect climate forcing.⁶⁸ Although these indirect climate effects were not among the foci of this work, $f(\text{RH})$ represents an interesting characteristic that warrants additional research.

5.3.6 Bounce Factor of GLV SOA

To confirm whether these particles experience a phase change at elevated RH, we measured the bulk bounce factor (BF , Equation 5.6) of GLV-SOA. All other factors being equal, BF should scale with particle viscosity, particles with a BF near 1 are assumed to be solid whereas those with BF of 0 are considered liquid, with a range of viscosities between. We measured the BF for dry HXL-SOA and wet HXL-SOA to be 0.15 ± 0.08 and 0.02 ± 0.01 , respectively (Table 5.2). For comparison, the BF of ammonium sulfate, a model solid particle, is 0.5 (using this method) while oleic acid, a model liquid particle, has no significant bounce ($BF = 0$).³⁵ We observe a significantly greater BF for dry HXL-SOA as compared to wet HXL-SOA, supporting a change in viscosity and chemistry of HXL-SOA as a function of RH at particle genesis.

5.4 Future Implications:

The chemical, physical and optical properties of GLV-SOA (O:C, molecular level composition, MAC, MSC, $f(\text{RH})$, BF , etc.) vary as a function of chemical system (CHA vs HXL) and environmental conditions (RH). To our knowledge, this is the first extensive and inclusive study of these properties for GLV-SOA. Although the total extinction of HXL- and CHA-SOA is relatively small (MEC values between $0.7\text{-}4 \text{ m}^2\text{g}^{-1}$, Table 5.2), GLV-SOA can exist in concentrations great enough to contribute to the Earth's radiative

budget. Since the scatter of light plays a more significant role than absorbance for GLV-SOA (accounting for 70-90% of total extinction at 450nm, 525nm and 635nm Table 5.2) it is likely that these systems contribute a net negative impact on climate, at least initially.

We have found that SOA formed under different RH conditions can have different chemical, optical and physical properties. This observation is particularly important as we compare the numerous studies on the hygroscopic properties of SOA and their role in radiative forcing. Several studies involve the formation of particles under dry conditions, followed by particle wetting via the introduction of humid air.^{64,69-72} Upon wetting *via* this method, particles increase in size (driving scatter enhancement) and/or may undergo a phase transition. This conventional method mimics the formation of a particle in a dry atmosphere, which is then transported into a damp body of air. Our methodology involves particle *genesis* under varying RH conditions and paints an equally relevant picture that has received little attention⁷³ yet should be explored further. For example, we observed that particles generated under elevated RH had unique chemical and physical properties. We ascertain that water molecules play an important role in the chemical mechanisms leading to SOA growth, resulting in unique physical properties. To our knowledge, there has not been a comprehensive assessment of the impact of water *during particle formation* on optical and physical properties.

We have also demonstrated the importance of understanding the molecular-level composition of SOA to accurately predict its role in climate forcing. SOA with the same apparent bulk properties can have different optical properties and thereby elicit different impacts on the Earth's radiative budget. This observation suggests that bulk chemical

properties may be insufficient to fully describe/predict the optical properties of SOA and also provides an interesting launching point for future research designed to understand the fundamental chemical processes leading to SOA with unique physical properties.

5.5 References

- (1) Kim, H.; Barkey, B.; Paulson, S. E. *J Phys Chem A* **2012**, *116*, 6059.
- (2) Kanakidou, M.; Seinfeld, J. H.; Pandis, S. N.; Barnes, I.; Dentener, F. J.; Facchini, M. C.; Van Dingenen, R.; Ervens, B.; Nenes, A.; Nielsen, C. J.; Swietlicki, E.; Putaud, J. P.; Balkanski, Y.; Fuzzi, S.; Horth, J.; Moortgat, G. K.; Winterhalter, R.; Myhre, C. E. L.; Tsigaridis, K.; Vignati, E.; Stephanou, E. G.; Wilson, J. *Atmos. Chem. Phys.* **2005**, *5*, 1053.
- (3) Hallquist, M.; Wenger, J. C.; Baltensperger, U.; Rudich, Y.; Simpson, D.; Claeys, M.; Dommen, J.; Donahue, N. M.; George, C.; Goldstein, A. H.; Hamilton, J. F.; Herrmann, H.; Hoffmann, T.; Iinuma, Y.; Jang, M.; Jenkin, M. E.; Jimenez, J. L.; Kiendler-Scharr, A.; Maenhaut, W.; McFiggans, G.; Mentel, T. F.; Monod, A.; Prévôt, A. S. H.; Seinfeld, J. H.; Surratt, J. D.; Szmigielski, R.; Wildt, J. *Atmos. Chem. Phys.* **2009**, *9*, 5155.
- (4) Li, K.; Wang, W.; Ge, M.; Li, J.; Wang, D. *Sci. Rep.* **2014**, *4*.
- (5) Nakayama, T.; Matsumi, Y.; Sato, K.; Imamura, T.; Yamazaki, A.; Uchiyama, A. *Journal of Geophysical Research: Atmospheres* **2010**, *115*, D24204.
- (6) Bones, D. L.; Henricksen, D. K.; Mang, S. A.; Gonsior, M.; Bateman, A. P.; Nguyen, T. B.; Cooper, W. J.; Nizkorodov, S. A. *Journal of Geophysical Research: Atmospheres* **2010**, *115*, D05203.
- (7) Liu, P.; Zhang, Y.; Martin, S. T. *Environ Sci Technol* **2013**, *47*, 13594.
- (8) Kim, H.; Paulson, S. E. *Atmos. Chem. Phys.* **2013**, *13*, 7711.
- (9) Zhong, M.; Jang, M. *Atmos Environ* **2011**, *45*, 4263.
- (10) Scott, C. E.; Rap, A.; Spracklen, D. V.; Forster, P. M.; Carslaw, K. S.; Mann, G. W.; Pringle, K. J.; Kivekäs, N.; Kulmala, M.; Lihavainen, H.; Tunved, P. *Atmos. Chem. Phys. Discuss.* **2013**, *13*, 16961.
- (11) Laskin, J.; Laskin, A.; Roach, P. J.; Slysz, G. W.; Anderson, G. A.; Nizkorodov, S. A.; Bones, D. L.; Nguyen, L. Q. *Anal Chem* **2010**, *82*, 2048.
- (12) Hecobian, A.; Zhang, X.; Zheng, M.; Frank, N.; Edgerton, E. S.; Weber, R. J. *Atmos. Chem. Phys.* **2010**, *10*, 5965.
- (13) Harvey, R. M.; Zahardis, J.; Petrucci, G. A. *Atmos. Chem. Phys.* **2014**, *14*, 797.
- (14) Hinds, W. *Aerosol Technology, Properties Behavior and Measurement of Airborne Particles*; John Wiley and Sons, 1982.

- (15) Lambe, A. T.; Cappa, C. D.; Massoli, P.; Onasch, T. B.; Forestieri, S. D.; Martin, A. T.; Cummings, M. J.; Croasdale, D. R.; Brune, W. H.; Worsnop, D. R.; Davidovits, P. *Environ Sci Technol* **2013**, *47*, 6349.
- (16) Yee, L. D.; Kautzman, K. E.; Loza, C. L.; Schilling, K. A.; Coggon, M. M.; Chhabra, P. S.; Chan, M. N.; Chan, A. W. H.; Hersey, S. P.; Crounse, J. D.; Wennberg, P. O.; Flagan, R. C.; Seinfeld, J. H. *Atmos. Chem. Phys.* **2013**, *13*, 8019.
- (17) Cappa, C. D.; Che, D. L.; Kessler, S. H.; Kroll, J. H.; Wilson, K. R. *Journal of Geophysical Research: Atmospheres* **2011**, *116*, D15204.
- (18) Kim, H.; Liu, S.; Russell, L. M.; Paulson, S. E. *Aerosol Sci Tech* **2014**, *48*, 498.
- (19) Titos, G.; Lyamani, H.; Cazorla, A.; Sorribas, M.; Foyo-Moreno, I.; Wiedensohler, A.; Alados-Arboledas, L. *2014* **2014**.
- (20) Lin, Y.-H.; Budisulistiorini, S. H.; Chu, K.; Siejack, R. A.; Zhang, H.; Riva, M.; Zhang, Z.; Gold, A.; Kautzman, K. E.; Surratt, J. D. *Environ Sci Technol* **2014**, *48*, 12012.
- (21) Utry, N.; Ajtai, T.; Filep, Á.; Dániel Pintér, M.; Hoffer, A.; Bozoki, Z.; Szabó, G. *Atmos Environ* **2013**, *69*, 321.
- (22) Bond, T. C.; Bergstrom, R. W. *Aerosol Sci Tech* **2006**, *40*, 27.
- (23) Flores, J. M.; Zhao, D. F.; Segev, L.; Schlag, P.; Kiendler-Scharr, A.; Fuchs, H.; Watne, Å. K.; Bluvshstein, N.; Mentel, T. F.; Hallquist, M.; Rudich, Y. *Atmos. Chem. Phys.* **2014**, *14*, 5793.
- (24) Nakayama, T.; Sato, K.; Matsumi, Y.; Imamura, T.; Yamazaki, A.; Uchiyama, A. *Atmos. Chem. Phys.* **2013**, *13*, 531.
- (25) Nakayama, T.; Sato, K.; Matsumi, Y.; Imamura, T.; Yamazaki, A.; Uchiyama, A. *SOLA* **2012**, *8*, 119.
- (26) Seinfeld, J. H.; Kleindienst, T. E.; Edney, E. O.; Cohen, J. B. *Aerosol Sci Tech* **2003**, *37*, 728.
- (27) Shilling, J. E.; Chen, Q.; King, S. M.; Rosenoern, T.; Kroll, J. H.; Worsnop, D. R.; McKinney, K. A.; Martin, S. T. *Atmos. Chem. Phys.* **2008**, *8*, 2073.
- (28) Jayne, J. T.; Leard, D. C.; Zhang, X.; Davidovits, P.; Smith, K. A.; Kolb, C. E.; Worsnop, D. R. *Aerosol Sci Tech* **2000**, *33*, 49.
- (29) DeCarlo, P. F.; Slowik, J. G.; Worsnop, D. R.; Davidovits, P.; Jimenez, J. L. *Aerosol Sci Tech* **2004**, *38*, 1185.
- (30) Chen, Q.; Liu, Y. J.; Donahue, N. M.; Shilling, J. E.; Martin, S. T. *Environ Sci Technol* **2011**, *45*, 4763.
- (31) Geddes, S.; Nichols, B.; Flemer, S.; Eisenhauer, J.; Zahardis, J.; Petrucci, G. A. *Anal Chem* **2010**, *82*, 7915.
- (32) Geddes, S.; Nichols, B.; Todd, K.; Zahardis, J.; Petrucci, G. A. *Atmos. Meas. Tech.* **2010**, *3*, 1175.

- (33) Moosmüller, H.; Arnott, W. P. *Review of Scientific Instruments* **2003**, *74*, 3492.
- (34) Fierz-Schmidhauser, R.; Zieger, P.; Wehrle, G.; Jefferson, A.; Ogren, J. A.; Baltensperger, U.; Weingartner, E. *Atmos. Meas. Tech.* **2010**, *3*, 39.
- (35) Jain, S.; Petrucci, G. A. *Aerosol Sci Tech* **2015**, *49*, 390.
- (36) Martins, J. V.; Artaxo, P.; Kaufman, Y. J.; Castanho, A. D.; Remer, L. A. *Geophysical Research Letters* **2009**, *36*, L13810.
- (37) Clarke, A. D.; Noone, K. J.; Heintzenberg, J.; Warren, S. G.; Covert, D. S. *Atmos Environ* **1987**, *21*, 1455.
- (38) Hoffer, A.; Gelencsér, A.; Guyon, P.; Kiss, G.; Schmid, O.; Frank, G. P.; Artaxo, P.; Andreae, M. O. *Atmos. Chem. Phys.* **2006**, *6*, 3563.
- (39) Hamilton, J. F.; Lewis, A. C.; Carey, T. J.; Wenger, J. C. *Anal Chem* **2007**, *80*, 474.
- (40) Hamilton, J. F.; Lewis, A. C.; Carey, T. J.; Wenger, J. C.; Borrás i Garcia, E.; Muñoz, A. *Atmos. Chem. Phys.* **2009**, *9*, 3815.
- (41) Jain, S.; Zahardis, J.; Petrucci, G. A. *Environ Sci Technol* **2014**.
- (42) Ofner, J.; Krüger, H. U.; Grothe, H.; Schmitt-Kopplin, P.; Whitmore, K.; Zetzsch, C. *Atmos. Chem. Phys.* **2011**, *11*, 1.
- (43) Aimanant, S.; Ziemann, P. J. *Aerosol Sci Tech* **2013**, *47*, 581.
- (44) Flores, J. M.; Washenfelder, R. A.; Adler, G.; Lee, H. J.; Segev, L.; Laskin, J.; Laskin, A.; Nizkorodov, S. A.; Brown, S. S.; Rudich, Y. *Phys Chem Chem Phys* **2014**, *16*, 10629.
- (45) Updyke, K. M.; Nguyen, T. B.; Nizkorodov, S. A. *Atmos Environ* **2012**, *63*, 22.
- (46) Wang, H. L.; Huang, D.; Zhang, X.; Zhao, Y.; Chen, Z. M. *Atmos. Chem. Phys.* **2012**, *12*, 7187.
- (47) Gäb, S.; Turner, W. V.; Wolff, S.; Becker, K. H.; Ruppert, L.; Brockmann, K. J. *Atmos Environ* **1995**, *29*, 2401.
- (48) Sauer, F.; Schäfer, C.; Neeb, P.; Horie, O.; Moortgat, G. K. *Atmos Environ* **1999**, *33*, 229.
- (49) Chen, Z. M.; Wang, H. L.; Zhu, L. H.; Wang, C. X.; Jie, C. Y.; Hua, W. *Atmos. Chem. Phys.* **2008**, *8*, 2255.
- (50) Zhang, X.; Chen, Z.; Wang, H.; He, S.; Huang, D. *Atmos Environ* **2009**, *43*, 4465.
- (51) Nguyen, T. B.; Roach, P. J.; Laskin, J.; Laskin, A.; Nizkorodov, S. A. *Atmos. Chem. Phys.* **2011**, *11*, 6931.
- (52) Nguyen, T. B.; Lee, P. B.; Updyke, K. M.; Bones, D. L.; Laskin, J.; Laskin, A.; Nizkorodov, S. A. *Journal of Geophysical Research: Atmospheres* **2012**, *117*, D01207.
- (53) Song, C.; Gyawali, M.; Zaveri, R. A.; Shilling, J. E.; Arnott, W. P. *Journal of Geophysical Research: Atmospheres* **2013**, *118*, 11.

- (54) Aschmann, S. M.; Shu, Y.; Arey, J.; Atkinson, R. *Atmos Environ* **1997**, *31*, 3551.
- (55) Ghorai, S.; Laskin, A.; Tivanski, A. V. *The Journal of Physical Chemistry A* **2011**, *115*, 4373.
- (56) Denjean, C.; Formenti, P.; Picquet-Varrault, B.; Pangui, E.; Zapf, P.; Katrib, Y.; Giorio, C.; Tapparo, A.; Monod, A.; Temime-Roussel, B.; Decorse, P.; Mangeney, C.; Doussin, J. F. *Atmos. Chem. Phys. Discuss.* **2014**, *14*, 10543.
- (57) Covert, D. S.; Charlson, R. J.; Ahlquist, N. C. *Journal of Applied Meteorology* **1972**, *11*, 968.
- (58) Seinfeld, J. H. a. S. N. P. *Atmospheric Chemistry and Physics: From Air Pollution to Climate Change*; 2 ed.; John Wiley and Sons, INC: Hoboken, N.J., 2006.
- (59) Zieger, P.; Fierz-Schmidhauser, R.; Weingartner, E.; Baltensperger, U. *Atmos Chem Phys* **2013**, *13*, 10609.
- (60) Zieger, P.; Weingartner, E.; Henzing, J.; Moerman, M.; de Leeuw, G.; Mikkilä, J.; Ehn, M.; Petäjä, T.; Clémer, K.; van Roozendaal, M.; Yilmaz, S.; Frieß, U.; Irie, H.; Wagner, T.; Shaiganfar, R.; Beirle, S.; Apituley, A.; Wilson, K.; Baltensperger, U. *Atmos. Chem. Phys.* **2011**, *11*, 2603.
- (61) Arnott, W. P.; Moosmüller, H.; Sheridan, P. J.; Ogren, J. A.; Raspet, R.; Slaton, W. V.; Hand, J. L.; Kreidenweis, S. M.; Collett, J. L. *Journal of Geophysical Research: Atmospheres* **2003**, *108*, 4034.
- (62) Denjean, C.; Formenti, P.; Picquet-Varrault, B.; Pangui, E.; Zapf, P.; Katrib, Y.; Giorio, C.; Tapparo, A.; Monod, A.; Temime-Roussel, B.; Decorse, P.; Mangeney, C.; Doussin, J. F. *Atmos Chem Phys* **2015**, *15*, 3339.
- (63) Tijjani, B. I.; Aliyu, A.; Shuaibu, F. *Open Journal of Applied Sciences* **2013**, *Vol.03No.06*, 12.
- (64) Ervens, B.; Cubison, M.; Andrews, E.; Feingold, G.; Ogren, J. A.; Jimenez, J. L.; DeCarlo, P.; Nenes, A. *Journal of Geophysical Research: Atmospheres* **2007**, *112*, D10S32.
- (65) Chen, J.; Zhao, C. S.; Ma, N.; Yan, P. *Atmos. Chem. Phys.* **2014**, *14*, 8105.
- (66) Tang, I. N.; Munkelwitz, H. R. *Atmospheric Environment. Part A. General Topics* **1993**, *27*, 467.
- (67) Zhao, D. F.; Buchholz, A.; Kortner, B.; Schlag, P.; Rubach, F.; Kiendler-Scharr, A.; Tillmann, R.; Wahner, A.; Flores, J. M.; Rudich, Y.; Watne, Å. K.; Hallquist, M.; Wildt, J.; Mentel, T. F. *Geophysical Research Letters* **2015**, *42*, 10.
- (68) Chan, M. N.; Kreidenweis, S. M.; Chan, C. K. *Environ Sci Technol* **2008**, *42*, 3602.
- (69) Bateman, A. P.; Bertram, A. K.; Martin, S. T. *The Journal of Physical Chemistry A* **2015**, *119*, 4386.
- (70) Hodas, N.; Zuend, A.; Mui, W.; Flagan, R. C.; Seinfeld, J. H. *Atmos. Chem. Phys.* **2015**, *15*, 5027.

- (71) Titos, G.; Jefferson, A.; Sheridan, P. J.; Andrews, E.; Lyamani, H.; Alados-Arboledas, L.; Ogren, J. A. *Atmos. Chem. Phys.* **2014**, *14*, 7031.
- (72) Vu, T.; Delgado-Saborit, J.; Harrison, R. *Air Qual Atmos Health* **2015**, *1*.
- (73) Kidd, C.; Perraud, V.; Wingen, L. M.; Finlayson-Pitts, B. J. *P Natl Acad Sci USA* **2014**, *111*, 7552.

CHAPTER 6. SUBTLETIES IN MOLECULAR-LEVEL DYNAMICS; VOC STRUCTURE, OZONOLYSIS KINETICS AND SOA YIELD

The following is an expansion upon a manuscript that has been submitted and accepted for publication in Atmospheric Environment. The full reference follows and a reprint of the published manuscript can be found in the Appendix.

Harvey, R. M.; Petrucci, G. A., Control of ozonolysis kinetics and aerosol yield by nuances in the molecular structure of volatile organic compounds. *Atmos Environ* 2015, 122, 188-195.

6.1 Introduction

It has been well established that SOA plays integral roles in climate and human health, yet there remains a limited understanding of the mechanisms that lead to its formation and ultimate fate, as evidenced by a disparity between modelled atmospheric SOA loadings and field measurements. This disparity highlights the need for a more accurate representation of the molecular-level interactions between SOA sources and oxidative pathways. Due to the paucity of detailed chemical data for most SOA precursors of atmospheric relevance, models generally predict SOA loadings using structure activity relationships generalized to classes of SOA precursors. However, the kinetics and SOA-forming potential of molecules are nuanced by seemingly minor structural differences in parent molecules that are currently neglected in models.

In Chapter 5, I point to the role that environmental conditions (namely RH) on the chemical and optical properties of SOA, but the following experiments were designed to

increase our understanding of how nuances in the *molecular structure* of VOCs control ozonolysis kinetics and aerosol yield. This work was also driven by observations made during turfgrass ozonolysis experiments (Chapter 4, see Section 4.3.2), where VOCs with similar molecular structure gave significantly different (and unexpected) SOA yields. Ultimately, the goal of the work presented in this chapter is to stimulate conversation to establish which seemingly minor chemical nuances drive the chemistry of SOA formation and warrant inclusion in atmospheric models.

As reviewed in Chapter 2, organic aerosol (OA) is a ubiquitous component of atmospheric particulate matter that influences both human health and global climate. A large fraction of OA is secondary in nature (SOA), being produced by the oxidation of anthropogenic or biogenic VOCs (A/BVOCs). Despite the integral role of SOA in atmospheric processes, there remains a limited understanding of its formation and fate in the atmosphere. This challenge is rooted not only in identifying the sources of SOA but also in understanding the fundamental chemical processes that lead to SOA formation and transformation.

In spite of the breadth of atmospheric A/BVOCs, an extensive amount of work has focused primarily on biogenically emitted terpenes and monoterpenes.¹⁻³ Despite efforts to characterize the roles of these prevalent BVOCs, atmospheric models largely under-predict SOA mass as compared to field measurements,^{1,4-7} due in part to uncertainties in measured VOC emissions, omission of key VOCs, missing chemical and physical processes that contribute to SOA, errors associated with extrapolating laboratory-derived data to the atmosphere and uncertainties in ambient OA measurements.⁸ Herein, I propose

that another contributor to the disparity between field measurements and atmospheric models may lie in the coarse level of chemical assumptions and approximations that must be made by modelers due to a lack of chemical data for the majority of compounds of interest. I highlight this recognized need for a more complete understanding of VOC reactivity and SOA formation at the molecular level by examining the ozonolysis rates and SOA formation yields for a number of compound classes of atmospheric relevance, demonstrating the dramatic impact of small nuances in molecular structure on these chemical parameters.

Reaction rate constants and SOA yield data for input to atmospheric models have been measured experimentally for a number of key VOCs,⁹⁻¹⁸ yet the list of studied compounds is far from exhaustive. In order to circumvent the paucity of kinetic data, structure activity relationships (SARs) have been developed to estimate oxidation rate constants based on the molecular structure of parent compounds. In some cases, SARs have been shown to follow experimental data well,^{19,20} but there is still considerable error associated with data calculated using this approach.²¹⁻²³ In addition to SARs, which marry structure and (re)activity, several studies have demonstrated correlations between VOC structure and SOA mass yield, although this discussion has been predominantly limited to alkanes^{13,14,24-26} and alkyl-substituted alkenes.^{9,10,19} SARs and SOA yield correlations have, by necessity, been used in lieu of experimental data in atmospheric models to predict large scale air quality and climate trends. Inaccuracies or incompleteness in SARs/yield correlations will be reflected in model outputs.

The omission of many VOCs from atmospheric models may also prove to be an important source of error. Semi-volatile organic compounds (SVOCs) and other reactive VOCs (ORVOCs) have received growing attention as potential SOA precursors.⁵ In Chapter 4 and in its accompanying manuscript (Harvey et al., 2013) I demonstrated that lawn mowing results in the emission of ORVOCs (HXL, CHA, and PTL) that, upon ozonolysis, contribute to SOA formation at levels approaching those of predominant terpenes.²⁷ Interestingly, despite having similar molecular backbones consisting of 3-hexene, the SOA-forming potential of HXL was found to be much greater than CHA, even though HXL was emitted at a 5x lower rate. This disparity was attributed to the molecular structure of each ORVOC.^{27,28} Similarly, although PTL has a similar molecular structure to HXL (oxygenated internal alkene), it was found to have limited reactivity to ozone and a negligible SOA yield. These observations led us to posit that the chemical processes leading to SOA formation from the oxidation of VOCs are quite nuanced; that a seemingly small change in molecular structure can have a profound impact on the molecule's atmospheric behavior.

Several recent studies have expanded our understanding of SARs by describing mechanisms by which certain molecular features impact reaction kinetics and/or SOA forming potential.^{12,19,20,29-34} The discussion thus far has focused on unsaturated hydrocarbons, with little work reported with regard to oxygenated species, which contribute a significant fraction of atmospheric reactive VOCs. A more complete understanding of the chemical basis of SARs in oxygenated alkenes

may allow for the development of more accurate atmospheric models. In the present work, rate constants for the ozonolysis of a series of cyclic and linear C₅-C₇ unsaturated methyl esters and alcohols are measured and discussed with respect to molecular structure. This work adds to the discussion of SARs of VOCs by focusing on the effect of oxygenated substituents.

6.2 Experimental

All experiments were performed at ambient pressure and temperature (~23°C) in a 775-L Teflon chamber (Figure 3.1, Chapter 3). Between experiments, the chamber was passivated overnight with 1-2 ppm O₃ and flushed with zero air to attain background aerosol mass loadings < 0.1 μg m⁻³. VOCs were injected via a heated bulb under a steady flow of zero air and mixed by gentle rocking. Once VOC concentrations were stable (15 min), ozone was injected as a short burst and monitored along with particle mass distributions throughout experiments.

1-pentene, 1-pentene-3-ol (PTL), 2-pentene, 1-hexene, cis-3-hexenyl acetate (CHA), cis-3-hexenol (HXL), cyclohexene, 3-hexene-2,5-diol (HXNDL), 3-heptene (racemic), and cycloheptene were purchased from Sigma Aldrich. Cyclopentene and cis-3-hexene were purchased from Alfa Aesar. Reagents (all > 95%) were used without further purification. Dry, zero air was produced by passing compressed air sequentially through silica, activated carbon and HEPA filters. This zero air was also used to generate ozone using a commercial corona discharge ozone generator (OLSOA/DLS OzoneLab).

Thermal desorption gas chromatography mass spectrometry (TD-GC/MS) was used to monitor VOC consumption. Air samples were collected from the reaction chamber onto AirToxics glass sorption tubes (Perkin Elmer N9307008) that had been previously conditioned at 310°C for 20 min and stored with Swagelok caps. Air was drawn through the sorption tubes using a personal sampler pump (SKC Airchek Sampler, model 224-44XR) at a rate of approximately 100 mL min⁻¹ (actual flow rate monitored by a F&J Specialty Products mini calibrator, model MC-500cc) for a known duration of time, allowing the total volume of air sampled to be determined. Typical sample volumes ranged between 0.6 L and 3.6 L.

Air samples were transferred from the sorbent tubes by thermal two-step desorption (TurboMatrix TD 350, Perkin Elmer) to a gas chromatograph (Clarus 600, Perkin Elmer) equipped with a mass spectrometer (Clarus 600 T Perkin Elmer) detector. Prior to desorption, an internal standard of fluorobenzene (AirLiquide) was automatically injected by the Turbomatrix TD directly onto the sorption tubes. During the first step of desorption, the sorbent tubes were heated to 330 °C for 8 min to desorb and cryofocus VOCs onto an Air Monitoring trap held at -10°C. The trap was then heated at a rate of 40 °C s⁻¹ to a final temperature of 310 °C, where it was held for 8 min. The VOCs were transferred to a GC analytical column (Stabilwax 30 m, 0.32 mm i.d., Restek) via a heated transfer line (250 °C) and a split ratio of 1:48. The GC oven was programmed as follows: held at 35 °C for 4 min, increasing 10 °C min⁻¹ to a final temperature of 220 °C. The total run time per sample was 22.5 min. The helium carrier gas flow rate was 1.52 mL/min. Electron impact ionization

(70 eV) was used and masses were scanned from 15 to 300 m/z. Chromatographic peaks for VOC standards were confirmed by spectral matching with the NIST 2005 mass spectral library. Compounds were quantified on area basis using single ion monitoring.

Aerosol particle size distributions, as well as total aerosol mass loadings were measured continuously with a scanning mobility particle sizer (SMPS, model 3080, TSI Inc., Shoreview, MN). A sheath flow rate of 0.3 L min⁻¹ and sample flow of 3.0 L min⁻¹ were used. The vapor pressure of predicted ozonolysis products was estimated using structure based estimators courtesy of the US EPA Estimation Programs Interface Suite.³⁵

Reaction rate constants (k) for the ozonolysis of VOCs were determined using experimental protocol described by Grosjean et al.³⁶ (and references therein). Briefly, the rate of ozone decay was measured in the presence of at least a 10-fold initial molar excess of VOC (to ensure pseudo-first order conditions). VOCs were added to the chamber first followed by ozone, which was added as a quick burst (less than 45 seconds). Initial reaction conditions are summarized in Table 6.1. All experiments were performed at ambient pressure and temperature (~23°C) and at low relative humidity (< 10 %).

Ozone concentrations were monitored at 5-second intervals. A plot of $\ln([O_3]_0/[O_3]_t)$, where $[O_3]_0$ and $[O_3]_t$ are the ozone concentrations at time zero and t, respectively, versus time (t, seconds) yields a straight line with slope k' (sec⁻¹). From the rate expression of the reaction, $k = k'/[VOC]_0$, where $[VOC]_0$ is the VOC

concentration at time zero, we were able to determine k ($\text{cm}^3 \text{sec}^{-1} \text{molecule}^{-1}$). The loss of ozone, as well as the VOC, to chamber walls was measured and found to be negligible over the time scale of the kinetic experiments,²⁷ confirming that reaction with VOCs was the only significant removal process for ozone.

Separate experiments were used to calculate SOA yields, Y , according to Equation 3.4, as discussed in Chapter 3. Particle loss (to chamber walls, due to secondary reactions and/or phase transitions) was estimated by extrapolating decay trends in SOA mass loadings back to time zero of the reaction (i.e., at time of ozone injection), as discussed in Section 3.2 of Chapter 3. We report the average yield (\pm standard deviation) from at least three experiments for each VOC. Student's T-tests were used to determine if averages were statistically different for different VOCs, at given confidence intervals, which are indicated with alpha- (α) values as they are discussed.

	[ozone] _i (ppb)	[VOC] _i (ppb)	k (cm ³ sec ⁻¹ molecule ⁻¹)	Standard Error
1-pentene	195	2375	1.66 x 10 ⁻¹⁷	9.97 x 10 ⁻²⁰
1-pentene	320	3300	8.09 x 10 ⁻¹⁸	2.19 x 10 ⁻¹⁹
1-pentene	240	3100	1.16 x 10 ⁻¹⁷	1.27 x 10 ⁻¹⁹
2-pentene	120	2968	1.16 x 10 ⁻¹⁶	7.29 x 10 ⁻¹⁸
2-pentene	270	2140	7.92 x 10 ⁻¹⁷	9.86 x 10 ⁻¹⁹
2-pentene	10	3400	2.44 x 10 ⁻¹⁷	1.02 x 10 ⁻¹⁸
2-pentene	30	3000	1.11 x 10 ⁻¹⁷	1.21 x 10 ⁻¹⁹
cyclopentene	16	3540	1.99 x 10 ⁻¹⁷	7.52 x 10 ⁻¹⁹
cyclopentene	450	3540	3.23 x 10 ⁻¹⁶	6.31 x 10 ⁻¹⁷
cyclopentene	500	3540	1.63 x 10 ⁻¹⁶	2.52 x 10 ⁻¹⁷
PTL	145	3162	1.60 x 10 ⁻¹⁷	9.66 x 10 ⁻²⁰
PTL	130	3800	1.80 x 10 ⁻¹⁷	7.80 x 10 ⁻²⁰
PTL	130	3200	1.87 x 10 ⁻¹⁷	1.08 x 10 ⁻¹⁹
1-HXN	170	2600	1.19 x 10 ⁻¹⁷	5.82 x 10 ⁻²⁰
1-HXN	100	2600	1.75 x 10 ⁻¹⁷	7.21 x 10 ⁻²⁰
1-HXN	110	2600	1.30 x 10 ⁻¹⁷	4.95 x 10 ⁻²⁰
3-HXN	190	3100	9.95 x 10 ⁻¹⁷	3.90 x 10 ⁻¹⁸
3-HXN	110	2240	1.07 x 10 ⁻¹⁶	1.01 x 10 ⁻¹⁷
3-HXN	250	2600	1.19 x 10 ⁻¹⁷	2.54 x 10 ⁻²⁰
cyclohexene	100	3000	7.18 x 10 ⁻¹⁷	2.45 x 10 ⁻¹⁸
cyclohexene	80	2540	8.11 x 10 ⁻¹⁷	2.85 x 10 ⁻¹⁸
cyclohexene	80	3400	5.72 x 10 ⁻¹⁷	3.63 x 10 ⁻¹⁸
cyclohexene	200	2800	6.38 x 10 ⁻¹⁷	3.01 x 10 ⁻¹⁸
HXL	110	1010	5.79 x 10 ⁻¹⁷	6.02 x 10 ⁻¹⁹
HXL	150	1010	9.75 x 10 ⁻¹⁷	1.28 x 10 ⁻¹⁹
HXL	65	1170	9.25 x 10 ⁻¹⁷	8.20 x 10 ⁻¹⁹
HXL	85	2750	4.41 x 10 ⁻¹⁷	1.46 x 10 ⁻¹⁴
CHA	230	966	4.58 x 10 ⁻¹⁷	3.58 x 10 ⁻¹⁹
CHA	255	1071	2.79 x 10 ⁻¹⁷	2.23 x 10 ⁻¹⁹
CHA	145	2140	6.02 x 10 ⁻¹⁷	5.35 x 10 ⁻¹⁹
CHA	120	1270	6.89 x 10 ⁻¹⁷	3.86 x 10 ⁻¹⁹

Table 6.1 Initial experimental conditions. All experiments were performed at ambient pressure and temperature (~23°C) and at low relative humidity (< 10 %).

	[ozone] _i (ppb)	[VOC] _i (ppb)	k (cm ³ sec ⁻¹ molecule ⁻¹)	Standard Error
HXNDL	180	2760	1.83 x 10 ⁻¹⁷	3.05 x 10 ⁻¹⁹
HXNDL	235	2760	6.60 x 10 ⁻¹⁸	6.97 x 10 ⁻²⁰
HXNDL	215	2760	3.02 x 10 ⁻¹⁸	2.82 x 10 ⁻²⁰
3-heptene	130	2300	8.95 x 10 ⁻¹⁷	2.54 x 10 ⁻¹⁸
3-heptene	130	1590	1.00 x 10 ⁻¹⁶	3.33 x 10 ⁻¹⁸
3-heptene	23	2300	4.16 x 10 ⁻¹⁷	4.25 x 10 ⁻¹⁹
3-heptene	17	2300	3.31 x 10 ⁻¹⁷	2.73 x 10 ⁻¹⁹
cycloheptene	50	2300	1.23 x 10 ⁻¹⁶	1.18 x 10 ⁻¹⁷
cycloheptene	140	1880	1.53 x 10 ⁻¹⁶	1.23 x 10 ⁻¹⁷
cycloheptene	150	1400	1.45 x 10 ⁻¹⁶	1.27 x 10 ⁻¹⁸
cycloheptene	30	2600	5.13 x 10 ⁻¹⁷	7.78 x 10 ⁻¹⁹

Table 6.1 Continued

6.3 Results

6.3.1 SOA Yield of Cyclic vs. Linear Alkenes.

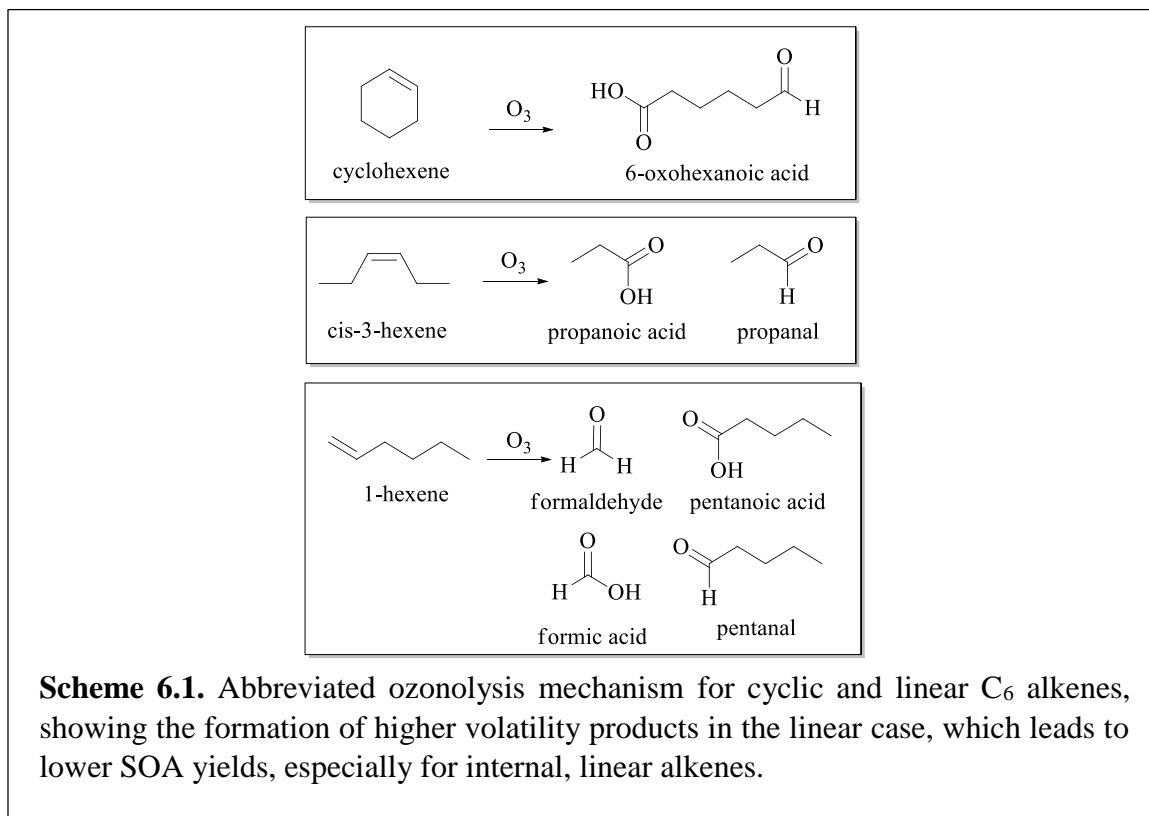
Relationships between VOC molecular structure and SOA yield have been reported for a number of chemical systems. Some studies identify surrogates for naturally occurring VOCs,^{10,38} some catalog the SOA yield of several compounds,^{9,13,37,39} while others identify key molecular structures that influence SOA yield.^{10,14,24-26,40} Most studies to date have focused on linear, branched and cyclic alkanes or cycloalkenes. In the case of alkanes, it has been shown that SOA yield increases with carbon number and, given two compounds with the same number of carbon atoms, follows the trend of cyclic alkanes > linear alkanes > branched alkanes and decreases further with degree of branching. SOA yield in alkanes also increases if the oxidation results in oligomerization.^{24,26}

SOA yield for linear alkenes is also expected to increase with carbon number.¹⁰ For the series of linear VOCs studied in this work, we generally observed SOA yields increasing in the order of pentene < hexene < heptene. The position of the double bond, however, also plays an important role in the SOA yield, with the 1-alkene generally producing a greater SOA yield than the internally bonded analog. For example, 1-pentene resulted in a SOA yield of 1.8 (\pm 0.2) %, which was greater ($\alpha = 0.05$) than that of 2-pentene (0.80 (\pm 0.6) %).

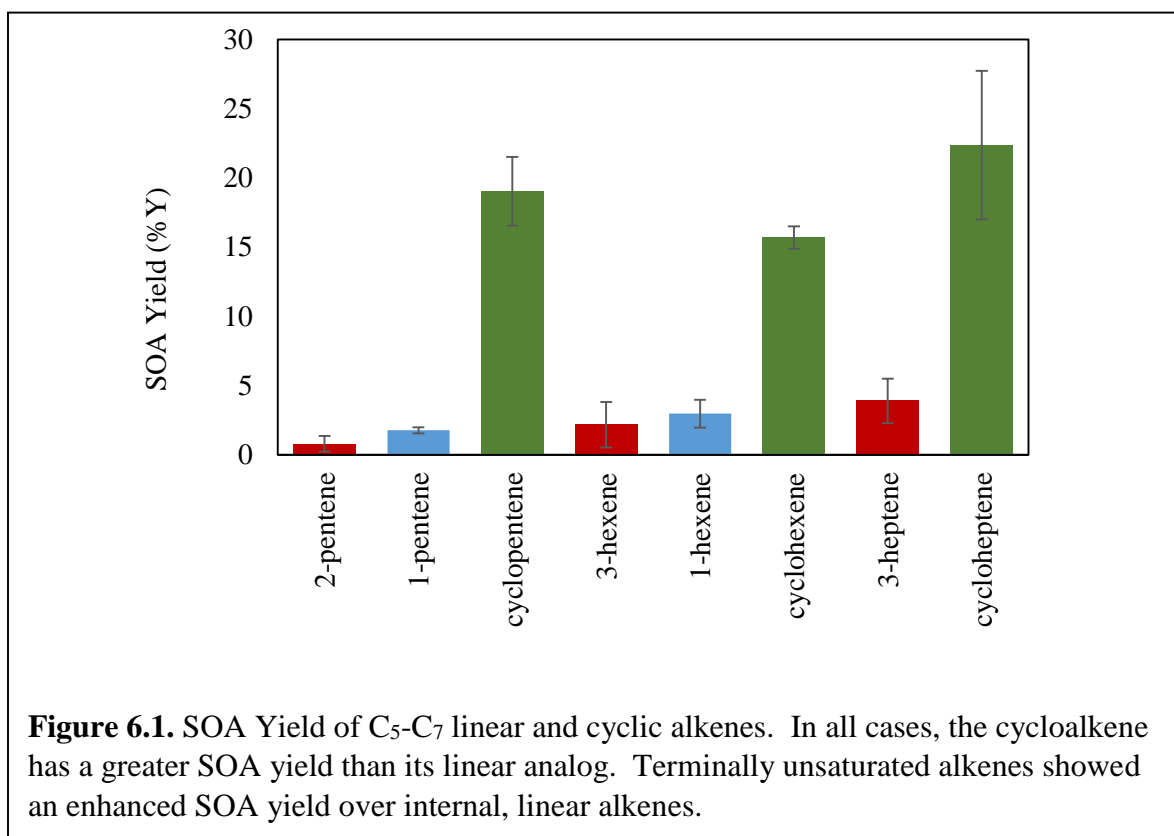
The mechanisms leading to SOA formation from the ozonolysis of alkenes has been reviewed extensively.^{1,8,41,42} Following the very simplified ozonolysis mechanism in Scheme 6.1, 1-pentene is expected to produce C₁ and C₄ carboxylic acids and aldehydes, while 2-pentene is expected to result in the production of C₂ and C₃ carboxylic acids and aldehydes. These species are relatively volatile, and will not nucleate to form SOA directly. Therefore, secondary oligomerization and/or condensation mechanisms are the likely route to SOA formation for these systems. In fact, secondary reactions of ozonolysis products, including oligomerization of stabilized Criegee Intermediates (CIs), are predominant drivers of SOA formation in the alkene-ozonolysis system.^{43 44} Oligomerization (and SOA yield) can be directly related to the fraction of CIs that exist in a peroxy-radical stabilized form, where a lower “stability fraction” results in lower SOA yields.⁴⁵⁻⁴⁷ It is possible that the enhanced stability of the C₁ and C₄ CIs in 1-pentene ozonolysis system allow it to undergo secondary oligomerization reactions more readily as

compared to the less stable C₂ and C₃ CIs found in 2-pentene system, resulting in an enhanced SOA yield for 1-pentene.⁴⁵⁻⁴⁷

Based on observations made for 1- and 2- pentene, we would anticipate 1-hexene to have a greater SOA yield than 3-hexene, yet both species gave the SOA yield, within experimental error (3.0 (± 1.0)% for 1-hexene and 2.2 (± 1.6)% for 3-hexene). Reaction kinetics will be discussed in depth in the following sections, but it is worth noting that in addition to having an enhanced SOA yield, 3-hexene also has a much greater rate constant (k) than 1-hexene. It is possible that the kinetics of the 3-hexene ozonolysis reaction favor a pathway that leads to a greater degree of oligomerization and/or lower volatility products, ultimately leading to a greater SOA yield.



In the case of cycloalkenes, it has been shown that SOA yield increases with carbon number, with the number of endocyclic double bonds and with the presence of alkyl substitution at the double bond.^{9,10} One important trend that has not been explicitly reported in the literature is that of increasing SOA yield for cyclic alkenes as compared to their linear analogues. As shown in the abbreviated Scheme 6.1, the oxidative cleavage of linear alkenes produces several low molecular weight species that are expected to be found in the gas phase. The ozonolysis of cyclic alkenes, on the other hand, produces molecules with greater molecular weight and lower vapour pressure, likely contributing to SOA more readily. Indeed, we observed an enhanced SOA yield for cyclopentene, cyclohexene and cycloheptene as compared to their linear analogs (Figure 6.1 and Table 6.2).



Chemical System	SOA % Yield (average \pm standard deviation)
1-pentene	1.77 \pm 0.22
2-pentene	0.79 \pm 0.57
PTL	3.28 \pm 0.7
cyclopentene	19 \pm 2.5
3-hexene	2.17 \pm 1.6
1-hexene	3.0 \pm 1.0
cyclohexene	15.7 \pm 0.8
CHA	3.9 \pm 2.4
HXL	6.5 \pm 2.6
HXNDL	9.3 \pm 0.4
3-heptene	3.9 \pm 1.6
cycloheptene	22.4 \pm 5.4

Table 6.2. SOA yield of linear, cyclic and oxygenated alkenes. Initial concentrations of the parent hydrocarbon and ozone in each experiment were 1000 ± 100 ppbv. N=3 for all reported values.

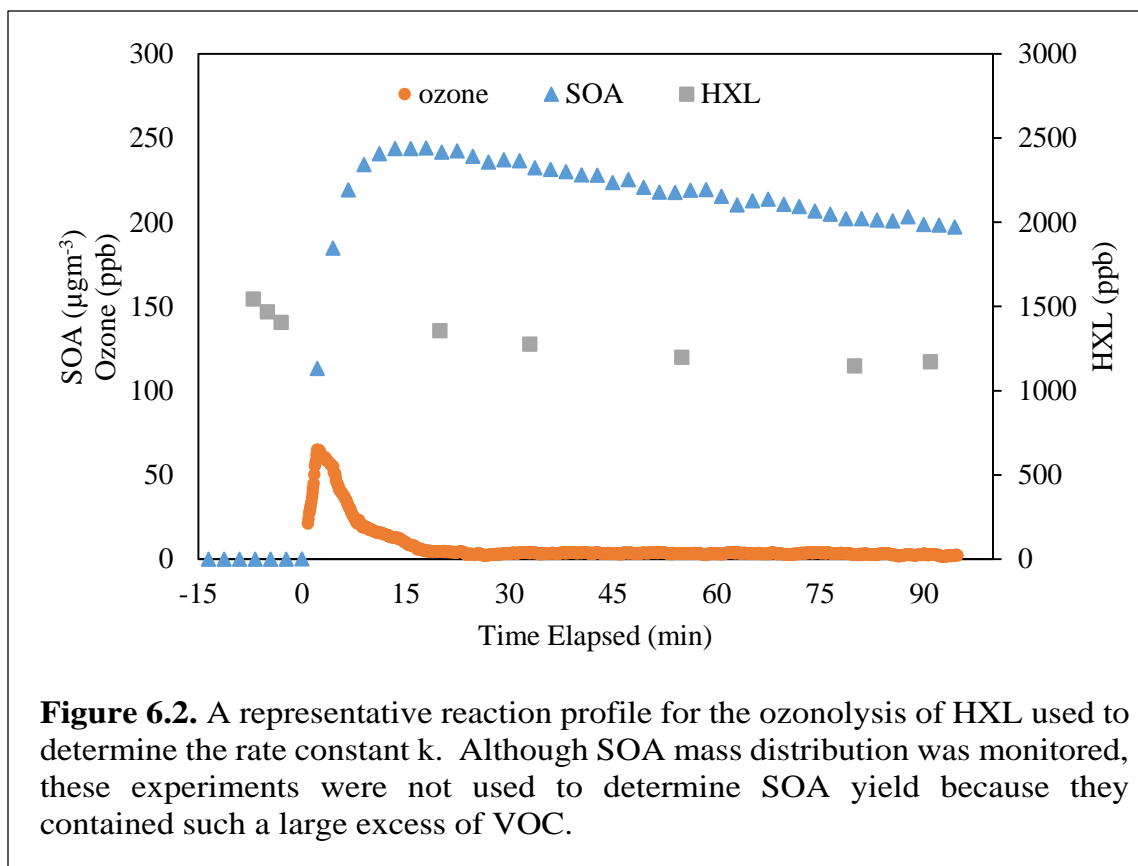
For unsubstituted C₅ – C₇ cyclic VOCs, we measured a SOA yield trend of cyclohexene < cyclopentene \leq cycloheptene in contrast to the results of Keywood et al.,¹⁰ who found that SOA yield increased with carbon number for C₅-C₈ cycloalkenes. Although Keywood et al.¹⁰ worked at lower VOC concentrations and used ammonium sulfate seed particles, our yields for cyclohexene and cycloheptene are in good agreement with theirs. Our cyclopentene yield (19 \pm 2.5%) however, was about twice that reported by Keywood et al.¹⁰ Again, it is worth noting that cyclopentene has the greatest rate constant (k) of these cyclic systems (See Table 6.3 and Section 6.3.2). It is possible that the enhanced k for cyclopentene contributes to its greater SOA yield. The reasons for the disparity between our measurements

and those of Keywood et al.¹⁰ and for our deviation from the trend of increasing SOA yield with increasing carbon number are unclear.

Autoxidation reactions may also result in enhanced SOA yield. Autoxidation involves the incorporation of molecular oxygen into product structure after the initial oxidation by ozone and results in highly oxidized multifunction molecules (HOM) that contribute to SOA.⁴⁸⁻⁵³ It has been shown that cyclic alkenes undergo autoxidation more readily than their linear analogs,⁵³ which may contribute to the enhanced SOA yield we observed for cyclic vs linear alkenes. Autoxidation processes require available hydrogen atoms for H-shift rearrangements and is thus limited to ozonolysis intermediates with three or more carbon atoms,⁵³ which may contribute to our observation of equivalent yields for 1-hexene and 3-hexene. The ozonolysis of 1-hexene yields only one product that could undergo autoxidation while 3-hexene yields two. Without molecular-level characterization of resultant SOA, however, we cannot comment on the amount of HOM formed or the role of autoxidation in the formation of SOA herein. This additional analysis would be a logical next step in this research.

6.3.2 Ozonolysis rate constants (k) for linear and cyclic alkenes

Rate constants (k) for the ozonolysis of VOCs have been a predominant focus in the recent literature, especially with regard to the impact of VOC molecular structure.^{12,19,20,22,23,54,55} It is important, however, to distinguish between SOA yield (% Y) and reactivity (k), which are not *necessarily* related. For example, a VOC may be highly reactive to atmospheric oxidants, yet contribute very little SOA or vice versa.



A representative reaction profile for experiments to determine k for the ozonolysis of HXL is given in Figure 6.2. As described above, VOCs were added to the chamber first followed by ozone, which was added as a quick burst (less than 45 seconds). Ozone decay was then measured at 5-second intervals and a plot of $\ln([O_3]_0/[O_3]_t)$, where $[O_3]_0$ and $[O_3]_t$ are the ozone concentrations at time zero and t , respectively, versus time (t , seconds) yields a straight line with slope k' (sec^{-1}). This plot is shown in Figure 6.3 for several of the VOCs studied, which all show good linearity with very little scatter, indicating that pseudo-first order reaction conditions were met. The rate constant k ($\text{cm}^3 \text{sec}^{-1} \text{molecule}^{-1}$) is then found from the rate expression of the reaction:

$$k = \frac{k'}{[\text{VOC}]_0} \quad (6.1)$$

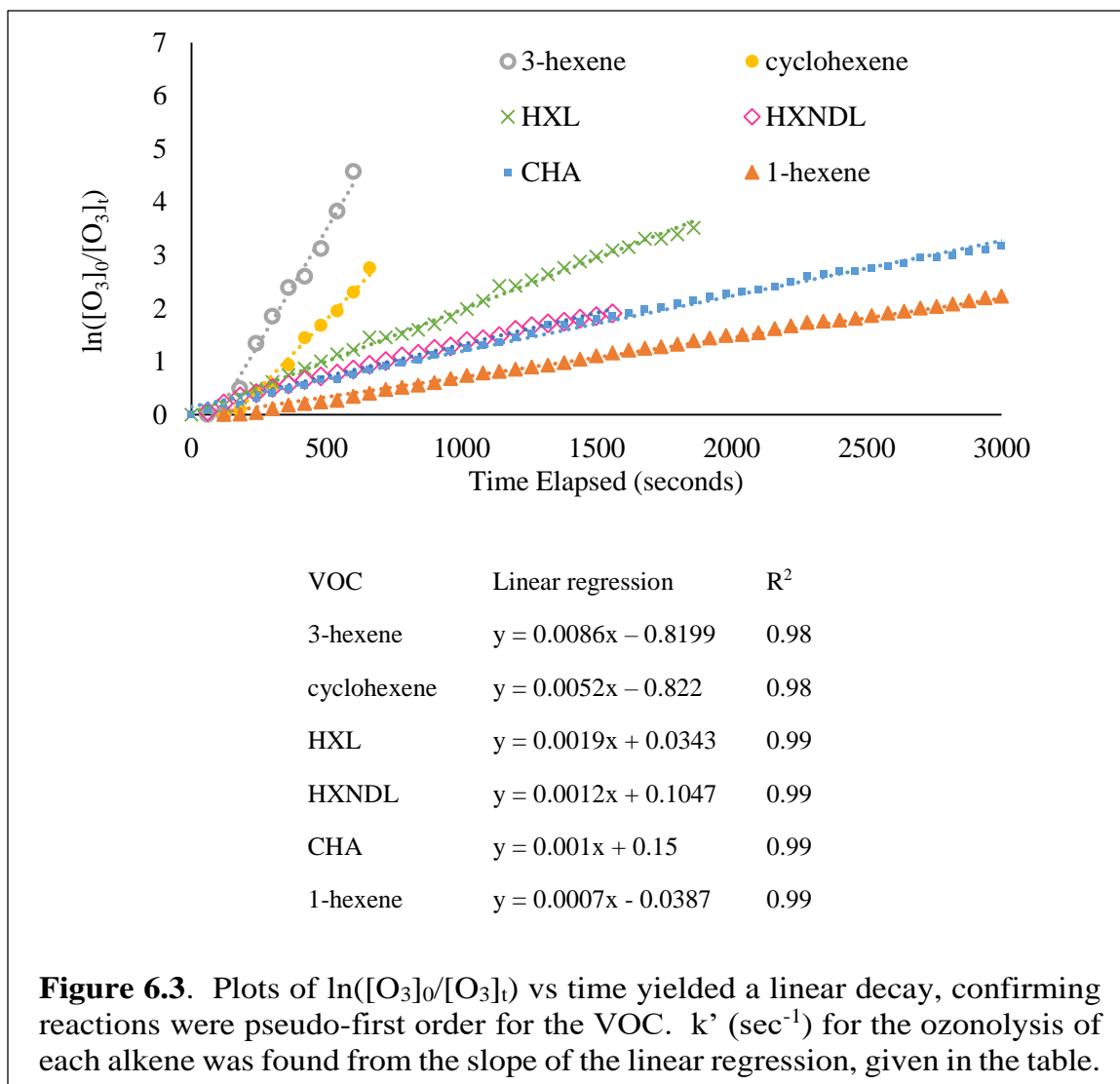
where $[\text{VOC}]_0$ is the initial VOC concentration (see Table 6.1).

For linear alkenes, our results (**Table 6.3**) support previous observations that terminal alkenes have a reduced k compared to internal alkenes.^{20,22,54} This trend may be explained by the inductive effect, wherein substituents near the double bond increase electron density at the reaction center, promoting electrophilic addition of ozone across the double bond. Terminal alkenes, which contain alkyl substituents on only one side of the double bond, experience a lower inductive effect and a correspondingly reduced k as compared to internal alkenes, which are substituted on both sides. Steric effects also impact the kinetics of the ozonolysis of internal vs terminal alkenes, whereby the approaching ozone molecule has easier access to the terminal species, which would enhance k over the internally double bonded analog. However, the marked increase in k that we observe for 3-hexene compared to 1-hexene indicates that, overall, the steric hindrance encountered in 3-hexene is outweighed by the enhancement of k due to the inductive effect (at least for these relatively small alkenes).

The interplay between the inductive effect and steric hindrance can be better appreciated with the Arrhenius equation,

$$k = Ae^{\frac{-Ea}{RT}} \quad (6.2)$$

The pre-exponential factor, A , is inversely related to steric effects and thus directly



proportional to k . Activation energy, E_a , is inversely related to both the inductive effect and to k .^{19,20,56-58} An increase in chain length from C_3 to C_6 results in a decrease in both E_a and A ⁵⁶ and ultimately results in an increase in k for ozonolysis. Lengthening the carbon backbone also increases steric hindrance, but not enough to overcome inductive effects or to limit k . McGillen et al.²⁰ experimentally confirmed that k increases with carbon number for 1-hexene and 1-pentene, yet their SAR-predicted rate constants were identical for 1-heptene, 1-hexene and 1-pentene.

VOC	k	Reference	VOC	k	Reference
1-pentene-3-ol (PTL)	1.7 ± 0.1	This work	3-hexene	5.9 ± 0.5	This work
	1.64	12		15.0	36
	1.79	36		14.4	20
1-pentene	1.2 ± 0.4	This work		12.2	20*
	0.92	56	cyclohexene	6.8 ± 0.1	This work
	0.99	58		7.00	62
	1.20	35		8.50	57
0.753	20*	7.90		41	
2-pentene	1.7 ± 0.9	This work	cis-3-hexenol (HXL)	5.8 ± 0.9	This work
cis-2-pentene	13.0	35		10.5	36
	20.9	20		6.14	15
trans-2-pentene	20.0	35	6.47	63	
	31.6	20	cis-3-hexenyl acetate (CHA)	5.8 ± 0.1	This work
cyclopentene	24 ± 11	This work		5.40	15
	20.0	35		5.90	62
	61.0	62	hex-3-ene-2,5-diol (HXNDL)	0.9 ± 0.8	This work
	67	41	3-heptene	6.6 ± 0.3	This work
1-hexene	1.4 ± 0.3	This work	cycloheptene	12.8 ± 4.6	This work
	1.42	58		22.6	62
	1.01	20		23.7	57

Table 6.3 Ozonolysis rate constants (k , $\times 10^{-17} \text{ cm}^3 \text{ sec}^{-1} \text{ molecule}^{-1}$) of alkenes are reported \pm the standard deviation of replicate experiments. Individual experimental conditions can be found in Table 6.1. * indicates a predicted/modelled value and $N = 3$ for all reported values.

Our measured rate constants for 1-hexene and 1-pentene were equal within error, confirming the modelled behaviour predicted by McGillen et al.,²⁰ but not experimental data as reported by their group or by others.⁵⁶ The reasons for the discrepancy are not clear, but the inconsistencies between modelled and measured k further support our supposition that additional, unknown nuances in molecular structure may exist that result in profound impacts on atmospheric SOA formation and reactivity. As shown in Table 6.3, we measured k values on the same order of magnitude as those reported by others, with the exception of 2-pentene, which was

approximately one order of magnitude smaller than that measured and predicted by McGillen et al.^{20,35} The methods they used to measure k were analogous to those used herein, so the reason for this disparity is not clear.

We found no correlation between k and ring size. However, our observed order of cyclohexene < cycloheptene < cyclopentene, was in accord with previously reported data.^{57,59} These variations in k -values for cycloalkenes could be related to differences in ring strain energies⁶⁰ wherein the oxidative cleavage of an endocyclic double bond relieves ring strain in cyclic molecules. In cyclopentene, the transition between cycloalkene to ozonide alleviates a considerable amount of ring strain, strongly favoring the reaction, whereas cyclohexene contains relatively little strain energy, resulting in a moderate k .⁶¹ Cycloheptene has been shown to experience a similar ring strain as cyclopentene,⁶¹ which could rationalize the enhanced k for cycloheptene over cyclohexene.

Both cyclopentene and cycloheptene had a greater k than their linear (internal/terminal) analogs, further supporting the theory that ring strain is a significant driver in these reactions. However, we measured the same k (within experimental error) for cyclohexene and 3-hexene. This observation suggests that ring strain in cyclohexene is not sufficient to enhance ozonolysis kinetics. Cyclohexene did, however, show a much greater k than 1-hexene, pointing back to the importance of the inductive effect; cyclohexene is more substituted at the double bond (two effective alkyl substituents) than 1-hexene (1 alkyl substituent), increasing the inductive effect and the overall k .

6.3.3 SOA Yield for Oxygenated Linear Alkenes

Despite extensive research to establish the SARs for ozonolysis of alkyl substituted linear alkenes, there has been a limited effort to understand the relationship between reactivity (k) or SOA yield and oxygenated substituents or their proximity to the double bond. To shed light on this knowledge gap, we measured the SOA yields and ozonolysis reaction rates of a series of C₅-C₇ linear, oxygenated alkenes (Table 6.2).

The SOA yield for 1-penten-3-ol (PTL) (3.3 ± 0.7 %) was greater than that measured for its non-oxygenated analog, 1-pentene (1.7 ± 0.2 %) ($\alpha = 0.05$). The ozonolysis of 1-pentene is expected to produce C₁ and C₄ products, which can undergo secondary oligomerization reactions (including hemi-acetal, aldol and ester condensation reactions) to form SOA. The ozonolysis of 1-PTL will produce the same C₁ products but its C₄ products will also contain an additional hydroxyl functionality, which (in addition to lowering the overall vapor pressure of the products) can undergo additional secondary reactions that are known to form SOA²⁸. Analogously, HXL (6.5 ± 2.6 %) and HXNDL (9.3 ± 0.4 %) have greater SOA yield than 3-hexene (2.2 ± 1.6 %). CHA was found to have the same SOA yield as HXL (3.9 ± 2.4 %) despite the fact that its methyl ester substituent shuts down the additional oligomerization pathway.²⁸ The reasons for this deviation from expected trends are unclear, but the large error associated with these measurements may be masking a general trend for HXL having a greater yield than CHA.

6.3.4 Ozonolysis Kinetics for Oxygenated Linear Alkenes

As stated above, electron donating substituents at the site of a double bond can promote the electrophilic addition of ozone, enhancing reactivity through the inductive effect.^{12,19,20,22,54} Hydroxyl groups are strongly electron donating and may therefore be predicted to enhance reactivity to an even greater degree than alkyl substituents. However, as we observed, HXNDL and HXL had *lower* reaction rates than their unsubstituted analogs. The hydroxyl substitution(s) at the beta (HXNDL) or gamma (HXL) position may be too distant from the double bond to enhance reactivity via the inductive effect, and actually seem to inhibit reactivity, likely due to steric interference. This interference is particularly strong for HXNDL, which has two hydroxyl groups in very close proximity to the double bond.

Analogous to the case of non-oxygenated alkenes, the reactivity of oxygenated molecules is a trade-off between both steric hindrance and inductive enhancement.^{19,20,22,54} Though it may seem intuitive, it has been well established that the steric effect diminishes with increasing distance from the reactive site.^{19,20,22,54,64} Aschmann and Atkinson²³ measured the steric effect for methyl-substituted alkenes and found no difference between that measured for 1-hexene and 5-methyl-1-hexene, yet as the methyl substituent moved closer to the double bond, steric effects increased, and the (NO₃) oxidation rate constant decreased, though the trend was not statistically significant. Since steric effects are expected to be more pronounced in ozone-alkene reactions than in corresponding NO₃-alkene reactions,²³ the trend in ozonolysis rate constant is expected to follow to a more significant degree. Based on these results, it appears that the steric hindrance

provided by the hydroxyl substituents in HXL and HXNDL out-competes any reactivity enhancement they may contribute via the inductive effect, resulting in a lower ozonolysis rate constant as compared to 3-hexene.

Alternatively, a slight enhancement was observed in the ozonolysis rate constant for PTL as compared to 1-pentene, echoing results from O'Dwyer et al.,¹² and suggesting that the terminal position of the double bond in PTL offers sufficient room for an approaching ozone molecule so the inductive effect associated with the hydroxyl substituent enhances reactivity overall. 3-methyl-1-pentene was found to have a diminished k compared to 1-pentene, suggesting that the methyl substituent provides significant steric hindrance to ozone to overcome any inductive enhancement it may also provide. 3-methyl-1-pentene has slightly less steric hindrance than PTL, suggesting that (if steric effects alone were considered) the methylated 1-pentene might have a greater k than PTL.^{19,20} However, a much greater k was measured for PTL than what has been reported for 3-methyl-1-pentene.^{19,20} Although steric hindrance due to the hydroxyl group is large for PTL, it enhances k overall as compared to the methylated analog due to the inductive effect.

Acetate esters are also electron donating, although not as strongly as hydroxyl groups, and would therefore be expected to enhance k . In fact, ester groups β to the alkene are predicted to enhance the inductive effect over unsubstituted alkenes by about 1.5 times.¹⁹ However, CHA has a slightly (albeit not significantly) *smaller* rate constant than the 3-hexene. I would also expect CHA to have a smaller

rate constant than HXL, since β -hydroxyl groups are estimated to increase the inductive effect over β -esters by a factor of about three,¹⁹ and that methyl esters would provide more steric hindrance than hydroxyl groups, which would also result in a smaller k . However, CHA had a slightly greater k than HXL. Transition state theory could be used to shed further light on the factors affecting these systems. Nonetheless, our data clearly demonstrate that the presence, position and identity of substituents are all key to predicting ozonolysis reaction kinetics.

6.4 Atmospheric Implications

The marked disparity between predicted SOA mass loadings and those measured in the field highlights the need for more accurate representation of the molecular level interactions between VOCs and oxidants. Some SARs have been shown to match chamber studies well,^{19,20,54} but chamber studies rarely match atmospheric conditions (with chamber studies working at unrealistically high VOC concentrations and mass loadings) and experimental results are often irreproducible between (and even within) laboratories.^{10,65} In Chapter 4, I reported the SOA yield of several green leaf volatiles using an experimental design analogous to that used by Hamilton et al.,⁶⁶ yet gave very different results (and also a high degree of uncertainty).²⁷ Keywood et al.¹⁰ also demonstrated the large degree of variability in making SOA yield measurements, reporting yields ranging from 0% to 19% for a single VOC in a single laboratory. Herein, I also report rather large ranges in SOA yield for replicate experiments (between 5% and 75% relative error). The reasons for the disparity in yield measurements made for the same chemical

systems under the same nominal conditions are unclear, but there is growing evidence to suggest that inconsistencies in the instrumental parameters used by different laboratories play a role.⁶⁷ For a laboratory where instrumental parameters are not variable, like ours for example, differences in SOA mass measurements may suggest a degree of chaos during the initial reaction steps that have yet to be understood, making them all but impossible to predict or model.

The mechanisms and product yields of VOC oxidation are impacted by subtleties in molecular structure. Due to computational costs and limited kinetic data available, these relationships are not always incorporated into atmospheric models. I have shown, however, that both the aerosol yield and the rate constant of structural isomers (cyclic vs linear, internally unsaturated vs terminally unsaturated and presence, type and position of substituents) vary significantly. It is in these seemingly minor (and rarely considered) molecular variations where error can be born, which can then be extrapolated in models and may result in the large disparities between modelled and measured atmospheric aerosol levels and properties. Ultimately, advances in computing power and our state of knowledge will permit models to evolve to incorporate much of this nuanced chemistry. Until such time, I offer this glimpse of the dramatic impact of seemingly small variations in molecular structure on reactivity and SOA formation. These initial steps will serve to further inform the atmospheric chemistry community on considerations that must be taken in order to harmonize laboratory findings with field studies and model outputs.

6.5 References

- (1) Hallquist, M.; Wenger, J. C.; Baltensperger, U.; Rudich, Y.; Simpson, D.; Claeys, M.; Dommen, J.; Donahue, N. M.; George, C.; Goldstein, A. H.; Hamilton, J. F.; Herrmann, H.; Hoffmann, T.; Iinuma, Y.; Jang, M.; Jenkin, M. E.; Jimenez, J. L.; Kiendler-Scharr, A.; Maenhaut, W.; McFiggans, G.; Mentel, T. F.; Monod, A.; Prévôt, A. S. H.; Seinfeld, J. H.; Surratt, J. D.; Szmigielski, R.; Wildt, J. *Atmos. Chem. Phys.* **2009**, *9*, 5155.
- (2) Ng, N. L.; Kroll, J. H.; Keywood, M. D.; Bahreini, R.; Varutbangkul, V.; Flagan, R. C.; Seinfeld, J. H.; Lee, A.; Goldstein, A. H. *Environ Sci Technol* **2006**, *40*, 2283.
- (3) Lee, J. D.; Lewis, A. C.; Monks, P. S.; Jacob, M.; Hamilton, J. F.; Hopkins, J. R.; Watson, N. M.; Saxton, J. E.; Ennis, C.; Carpenter, L. J.; Carslaw, N.; Fleming, Z.; Bandy, B. J.; Oram, D. E.; Penkett, S. A.; Slemr, J.; Norton, E.; Rickard, A. R.; Whalley, L. K.; Heard, D. E.; Bloss, W. J.; Gravesstock, T.; Smith, S. C.; Stanton, J.; Pilling, M. J.; Jenkin, M. E. *Atmos Environ* **2006**, *40*, 7598.
- (4) Heald, C. L.; Jacob, D. J.; Park, R. J.; Russell, L. M.; Huebert, B. J.; Seinfeld, J. H.; Liao, H.; Weber, R. J. *Geophysical Research Letters* **2005**, *32*, L18809.
- (5) Kanakidou, M.; Seinfeld, J. H.; Pandis, S. N.; Barnes, I.; Dentener, F. J.; Facchini, M. C.; Van Dingenen, R.; Ervens, B.; Nenes, A.; Nielsen, C. J.; Swietlicki, E.; Putaud, J. P.; Balkanski, Y.; Fuzzi, S.; Horth, J.; Moortgat, G. K.; Winterhalter, R.; Myhre, C. E. L.; Tsigaridis, K.; Vignati, E.; Stephanou, E. G.; Wilson, J. *Atmos. Chem. Phys.* **2005**, *5*, 1053.
- (6) Jo, D. S.; Park, R. J.; Kim, M. J.; Spracklen, D. V. *Atmos Environ* **2013**, *81*, 230.
- (7) Goldstein, A. H.; Galbally, I. E. *Environ Sci Technol* **2007**, *41*, 1514.
- (8) Carlton, A. G.; Wiedinmyer, C.; Kroll, J. H. *Atmos. Chem. Phys.* **2009**, *9*, 4987.
- (9) Lee, A.; Goldstein, A. H.; Keywood, M. D.; Gao, S.; Varutbangkul, V.; Bahreini, R.; Ng, N. L.; Flagan, R. C.; Seinfeld, J. H. *Journal of Geophysical Research: Atmospheres* **2006**, *111*, D07302.
- (10) Keywood, M. D.; Varutbangkul, V.; Bahreini, R.; Flagan, R. C.; Seinfeld, J. H. *Environ Sci Technol* **2004**, *38*, 4157.
- (11) Kroll, J. H.; Seinfeld, J. H. *Atmos Environ* **2008**, *42*, 3593.
- (12) O'Dwyer, M. A.; Carey, T. J.; Healy, R. M.; Wenger, J. C.; Picquet-Varrault, B.; Doussin, J. F. *Z Phys Chem* **2010**, *224*, 1059.
- (13) Loza, C. L.; Craven, J. S.; Yee, L. D.; Coggon, M. M.; Schwantes, R. H.; Shiraiwa, M.; Zhang, X.; Schilling, K. A.; Ng, N. L.; Canagaratna, M. R.; Ziemann, P. J.; Flagan, R. C.; Seinfeld, J. H. *Atmos. Chem. Phys.* **2014**, *14*, 1423.
- (14) Tkacik, D. S.; Presto, A. A.; Donahue, N. M.; Robinson, A. L. *Environ Sci Technol* **2012**, *46*, 8773.

- (15) Atkinson, R.; Arey, J.; Aschmann, S. M.; Corchnoy, S. B.; Shu, Y. *Int J Chem Kinet* **1995**, *27*, 941.
- (16) Khamaganov, V. G.; Hites, R. A. *The Journal of Physical Chemistry A* **2001**, *105*, 815.
- (17) Papagni, C.; Arey, J.; Atkinson, R. *Int J Chem Kinet* **2001**, *33*, 142.
- (18) Cusick, R. D.; Atkinson, R. *Int J Chem Kinet* **2005**, *37*, 183.
- (19) McGillen, M. R.; Archibald, A. T.; Carey, T.; Leather, K. E.; Shallcross, D. E.; Wenger, J. C.; Percival, C. J. *Phys Chem Chem Phys* **2011**, *13*, 2842.
- (20) McGillen, M. R.; Carey, T. J.; Archibald, A. T.; Wenger, J. C.; Shallcross, D. E.; Percival, C. J. *Phys Chem Chem Phys* **2008**, *10*, 1757.
- (21) Pfrang, C.; King, M. D.; Canosa-Mas, C. E.; Wayne, R. P. *Atmos Environ* **2006**, *40*, 1180.
- (22) McGillen, M. R.; Crosier, J.; Percival, C. J.; Sanchez-Reyna, G.; Shallcross, D. E. *Chemosphere* **2006**, *65*, 2035.
- (23) Aschmann, S. M.; Atkinson, R. *The Journal of Physical Chemistry A* **2011**, *115*, 1358.
- (24) Lim, Y. B.; Ziemann, P. J. *Environ Sci Technol* **2009**, *43*, 2328.
- (25) Aumont, B.; Camredon, M.; Mouchel-Vallon, C.; La, S.; Ouzebidour, F.; Valorso, R.; Lee-Taylor, J.; Madronich, S. *Faraday Discuss* **2013**, *165*, 105.
- (26) Yee, L. D.; Craven, J. S.; Loza, C. L.; Schilling, K. A.; Ng, N. L.; Canagaratna, M. R.; Ziemann, P. J.; Flagan, R. C.; Seinfeld, J. H. *Atmos. Chem. Phys. Discuss.* **2013**, *13*, 10859.
- (27) Harvey, R. M.; Zahardis, J.; Petrucci, G. A. *Atmos. Chem. Phys.* **2014**, *14*, 797.
- (28) Jain, S.; Zahardis, J.; Petrucci, G. A. *Environ Sci Technol* **2014**.
- (29) Boyd, A. A.; Villenave, E.; Lesclaux, R. *Atmos Environ* **2003**, *37*, 2751.
- (30) Peeters, J.; Boullart, W.; Pultau, V.; Vandenberk, S.; Vereecken, L. *J Phys Chem A* **2007**, *111*, 1618.
- (31) Peeters, J.; Boullart, W.; Pultau, V.; Vandenberk, S.; Vereecken, L. *The Journal of Physical Chemistry A* **2007**, *111*, 1618.
- (32) Al Mulla, I.; Viera, L.; Morris, R.; Sidebottom, H.; Treacy, J.; Mellouki, A. *Chemphyschem* **2010**, *11*, 4069.
- (33) Vereecken, L.; Francisco, J. S. *Chem Soc Rev* **2012**, *41*, 6259.
- (34) Stewart, D. J.; Almarok, S. H.; Lockhart, J. P.; Mohamed, O. M.; Nutt, D. R.; Pfrang, C.; Marston, G. *Atmos Environ* **2013**, *70*, 227.
- (35) Agency, U. S. E. P.; 4.11 ed. Washington DC, USA, 2014.

- (36) Grosjean, E.; Grosjean, D. *Int J Chem Kinet* **1994**, *26*, 1185.
- (37) Odum, J. R.; Hoffmann, T.; Bowman, F.; Collins, D.; Flagan, R. C.; Seinfeld, J. H. *Environ Sci Technol* **1996**, *30*, 2580.
- (38) Epstein, S. A.; Donahue, N. M. *The Journal of Physical Chemistry A* **2010**, *114*, 7509.
- (39) Gao, S.; Keywood, M.; Ng, N. L.; Surratt, J.; Varutbangkul, V.; Bahreini, R.; Flagan, R. C.; Seinfeld, J. H. *The Journal of Physical Chemistry A* **2004**, *108*, 10147.
- (40) Jathar, S. H.; Miracolo, M. A.; Tkacik, D. S.; Donahue, N. M.; Adams, P. J.; Robinson, A. L. *Environ Sci Technol* **2013**, *47*, 12886.
- (41) Atkinson, R.; Arey, J. *Chem Rev* **2003**, *103*, 4605.
- (42) Zahardis, J.; Petrucci, G. A. *Atmos. Chem. Phys.* **2007**, *7*, 1237.
- (43) Tolocka, M. P.; Jang, M.; Ginter, J. M.; Cox, F. J.; Kamens, R. M.; Johnston, M. V. *Environ Sci Technol* **2004**, *38*, 1428.
- (44) Sakamoto, Y.; Inomata, S.; Hirokawa, J. *The Journal of Physical Chemistry A* **2013**, *117*, 12912.
- (45) Sadezky, A.; Chaimbault, P.; Mellouki, A.; Römpp, A.; Winterhalter, R.; Le Bras, G.; Moortgat, G. K. *Atmos. Chem. Phys.* **2006**, *6*, 5009.
- (46) Sadezky, A.; Winterhalter, R.; Kanawati, B.; Römpp, A.; Spengler, B.; Mellouki, A.; Le Bras, G.; Chaimbault, P.; Moortgat, G. K. *Atmos. Chem. Phys.* **2008**, *8*, 2667.
- (47) Donahue, N. M.; Drozd, G. T.; Epstein, S. A.; Presto, A. A.; Kroll, J. H. *Phys Chem Chem Phys* **2011**, *13*, 10848.
- (48) Ehn, M.; Kleist, E.; Junninen, H.; Petäjä, T.; Lönn, G.; Schobesberger, S.; Dal Maso, M.; Trimborn, A.; Kulmala, M.; Worsnop, D. R.; Wahner, A.; Wildt, J.; Mentel, T. F. *Atmos. Chem. Phys.* **2012**, *12*, 5113.
- (49) Crounse, J. D.; Nielsen, L. B.; Jørgensen, S.; Kjaergaard, H. G.; Wennberg, P. O. *The Journal of Physical Chemistry Letters* **2013**, *4*, 3513.
- (50) Jokinen, T.; Sipilä, M.; Richters, S.; Kerminen, V.-M.; Paasonen, P.; Stratmann, F.; Worsnop, D.; Kulmala, M.; Ehn, M.; Herrmann, H.; Berndt, T. *Angewandte Chemie International Edition* **2014**, *53*, 14596.
- (51) Rissanen, M. P.; Kurtén, T.; Sipilä, M.; Thornton, J. A.; Kangasluoma, J.; Sarnela, N.; Junninen, H.; Jørgensen, S.; Schallhart, S.; Kajos, M. K.; Taipale, R.; Springer, M.; Mentel, T. F.; Ruuskanen, T.; Petäjä, T.; Worsnop, D. R.; Kjaergaard, H. G.; Ehn, M. *J Am Chem Soc* **2014**, *136*, 15596.
- (52) Ehn, M.; Thornton, J. A.; Kleist, E.; Sipilä, M.; Junninen, H.; Pullinen, I.; Springer, M.; Rubach, F.; Tillmann, R.; Lee, B.; Lopez-Hilfiker, F.; Andres, S.; Acir, I.-H.; Rissanen, M.; Jokinen, T.; Schobesberger, S.; Kangasluoma, J.; Kontkanen, J.; Nieminen, T.; Kurten, T.; Nielsen, L. B.; Jørgensen, S.; Kjaergaard, H. G.; Canagaratna, M.; Maso, M. D.; Berndt,

- T.; Petaja, T.; Wahner, A.; Kerminen, V.-M.; Kulmala, M.; Worsnop, D. R.; Wildt, J.; Mentel, T. F. *Nature* **2014**, *506*, 476.
- (53) Mentel, T. F.; Springer, M.; Ehn, M.; Kleist, E.; Pullinen, I.; Kurtén, T.; Rissanen, M.; Wahner, A.; Wildt, J. *Atmos. Chem. Phys.* **2015**, *15*, 6745.
- (54) McGillen, M. R.; Ghalaieny, M.; Percival, C. J. *Phys Chem Chem Phys* **2011**, *13*, 10965.
- (55) Johnson, D.; Rickard, A. R.; McGill, C. D.; Marston, G. *Phys Chem Chem Phys* **2000**, *2*, 323.
- (56) Treacy, J.; Elhag, M.; Ofarrell, D.; Sidebottom, H. *Ber Bunsen Phys Chem* **1992**, *96*, 422.
- (57) Treacy, J.; Curley, M.; Wenger, J.; Sidebottom, H. *Journal of the Chemical Society, Faraday Transactions* **1997**, *93*, 2877.
- (58) Leather, K. E.; McGillen, M. R.; Percival, C. J. *Phys Chem Chem Phys* **2010**, *12*, 2935.
- (59) Sidebottom, H.; Tracy, J. In *Chemical Processes in Atmospheric Oxidation*; Le Bras, G., Ed.; Springer Berlin Heidelberg: 1997; Vol. 3, p 218.
- (60) Atkinson, R.; Aschmann, S. M.; Carter, W. P. L.; Pitts, J. N. *Int J Chem Kinet* **1983**, *15*, 721.
- (61) Benson, S. W. *Thermochemical Kinetics*; Wiley: New York, 1966.
- (62) Greene, C. R.; Atkinson, R. *Int J Chem Kinet* **1992**, *24*, 803.
- (63) Kirstine, W. V.; Galbally, I. E. *J Air Waste Manage* **2004**, *54*, 1299.
- (64) Taft, R. *Steric Effects in Organic Chemistry*; John Wiley & Sons, Inc.: New York, 1356.
- (65) Bahreini, R.; Ervens, B.; Middlebrook, A. M.; Warneke, C.; de Gouw, J. A.; DeCarlo, P. F.; Jimenez, J. L.; Brock, C. A.; Neuman, J. A.; Ryerson, T. B.; Stark, H.; Atlas, E.; Brioude, J.; Fried, A.; Holloway, J. S.; Peischl, J.; Richter, D.; Walega, J.; Weibring, P.; Wollny, A. G.; Fehsenfeld, F. C. *J Geophys Res-Atmos* **2009**, *114*.
- (66) Hamilton, J. F.; Lewis, A. C.; Carey, T. J.; Wenger, J. C.; Borrás i Garcia, E.; Muñoz, A. *Atmos. Chem. Phys.* **2009**, *9*, 3815.
- (67) Wiedensohler, A.; Birmili, W.; Nowak, A.; Sonntag, A.; Weinhold, K.; Merkel, M.; Wehner, B.; Tuch, T.; Pfeifer, S.; Fiebig, M.; Fjåraa, A. M.; Asmi, E.; Sellegri, K.; Depuy, R.; Venzac, H.; Villani, P.; Laj, P.; Aalto, P.; Ogren, J. A.; Swietlicki, E.; Williams, P.; Roldin, P.; Quincey, P.; Hüglin, C.; Fierz-Schmidhauser, R.; Gysel, M.; Weingartner, E.; Riccobono, F.; Santos, S.; Grünig, C.; Faloon, K.; Beddows, D.; Harrison, R.; Monahan, C.; Jennings, S. G.; O'Dowd, C. D.; Marinoni, A.; Horn, H. G.; Keck, L.; Jiang, J.; Scheckman, J.; McMurry, P. H.; Deng, Z.; Zhao, C. S.; Moerman, M.; Henzing, B.; de Leeuw, G.; Lösschau, G.; Bastian, S. *Atmos. Meas. Tech.* **2012**, *5*, 657.

CHAPTER 7. SUBTLETIES IN MOLECULAR-LEVEL DYNAMICS: ORDER OF INTRODUCTION

As described in the preceding chapters, atmospheric models largely under-predict SOA mass as compared to field measurements¹⁻⁵ due in part to uncertainties in ambient OA and VOC measurements, omission of key VOCs, missing chemical and physical processes that contribute to SOA, and errors associated with extrapolating laboratory-derived data to the atmosphere.⁶ Much of the work reported in this dissertation has focused on identifying BVOCs and understanding their contribution to atmospheric SOA on a molecular level. In Chapter 6, I discussed how nuances in BVOC molecular structure influence their SOA-forming potential. However, I have also found that chamber studies themselves are quite nuanced. In this chapter, I will discuss chamber experiments that differ subtly in their procedure, yet yield very different results, suggesting very different chemistry. This work was used to develop the standard operation procedure for chamber studies used in the preceding chapters, yet also offers a unique opportunity to discuss one of the aforementioned challenges in atmospheric science: the errors associated with extrapolating laboratory-derived data to the atmosphere.⁶

7.0 Introduction

Environmental chambers have been used to study atmospheric chemistry for decades.⁷⁻¹⁰ While their design, material and advantages vary, the primary goal of chamber studies is to study relevant chemical systems that emulate atmospheric conditions. Unfortunately, as alluded to in Chapter 6, chamber studies rarely match atmospheric conditions (with chamber studies working at unrealistically high VOC concentrations and

mass loadings and also being conducted with a single VOC and single oxidant) and experimental results are often irreproducible between (and even within) laboratories.^{11, 12} For example, in Chapter 4 the SOA Yield of several GLVs was reported. The experimental design used for those experiments was analogous to that used by others,¹³ yet gave very different SOA Yield measurements (and also with a high degree of uncertainty).¹⁴ In Chapters 4 and 6, I report rather large ranges in SOA yield values for replicate experiments (between 5% and 75% relative error). Others have also demonstrated the large degree of variability in making SOA yield measurements, reporting values ranging from 0% to 19% for a single VOC in a single laboratory under nominally analogous conditions.¹¹ Various studies, have also shown that the chemical composition and properties of aerosols formed in chambers differ from those of real atmospheric particles. The reasons for the disparity in SOA measurements for the same chemical systems under the same conditions are unclear,¹⁵ but suggest that extrapolation of results derived from chamber-based studies may be inappropriate for modeling the atmospheric production of aerosols. There is growing evidence to suggest that disparities in intra-laboratory measurements may stem from inconsistencies in the instrumental parameters used by different laboratories.¹⁵ However, for a laboratory where instrumental parameters are not variable, like ours for example, differences in SOA mass measurements may suggest a degree of chaos during the initial reaction steps that have yet to be understood.

In this chapter, I will explore one particular operating procedure that may contribute to intra-laboratory disparities. What began as perhaps a naïve question led to anecdotal observations that continue to pose an interesting question with respect to the development

and implementation of chamber studies: “which goes first, the VOC or oxidant?” It turns out, that it makes a difference.

7.1 Experimental

In a series of experiments, limonene and ozone were added to a 775 L Teflon reaction chamber in alternating order. Initial reaction conditions are given in Table 7.1. In all experiments, 1 μL of limonene was injected, resulting in a concentration of 390 ppb. Ozone was injected as a brief burst at initial concentrations between 260-300 ppb, representing an approximately 1:1 ratio of VOC and oxidant. The consumption of limonene was monitored using TD-GC/MS while SOA mass was measured with an SMPS. The initial ozone concentration was measured using a commercial ozone monitor, but was taken offline after initial conditions were established to minimize sample consumption (the ozone monitor samples at 2 L min^{-1} , which would quickly deplete the 775-L reaction chamber).

Date	[Limonene] _i (ppb)	[Ozone] _i (ppb)	Added First
2/2/2012	390	300	limonene
2/9/2012	390	200	ozone
2/11/2012	390	260	limonene
2/16/2012 a	390	300	ozone
2/16/2012 b	390	300	ozone

Table 7.1 Initial conditions for introduction order experiments

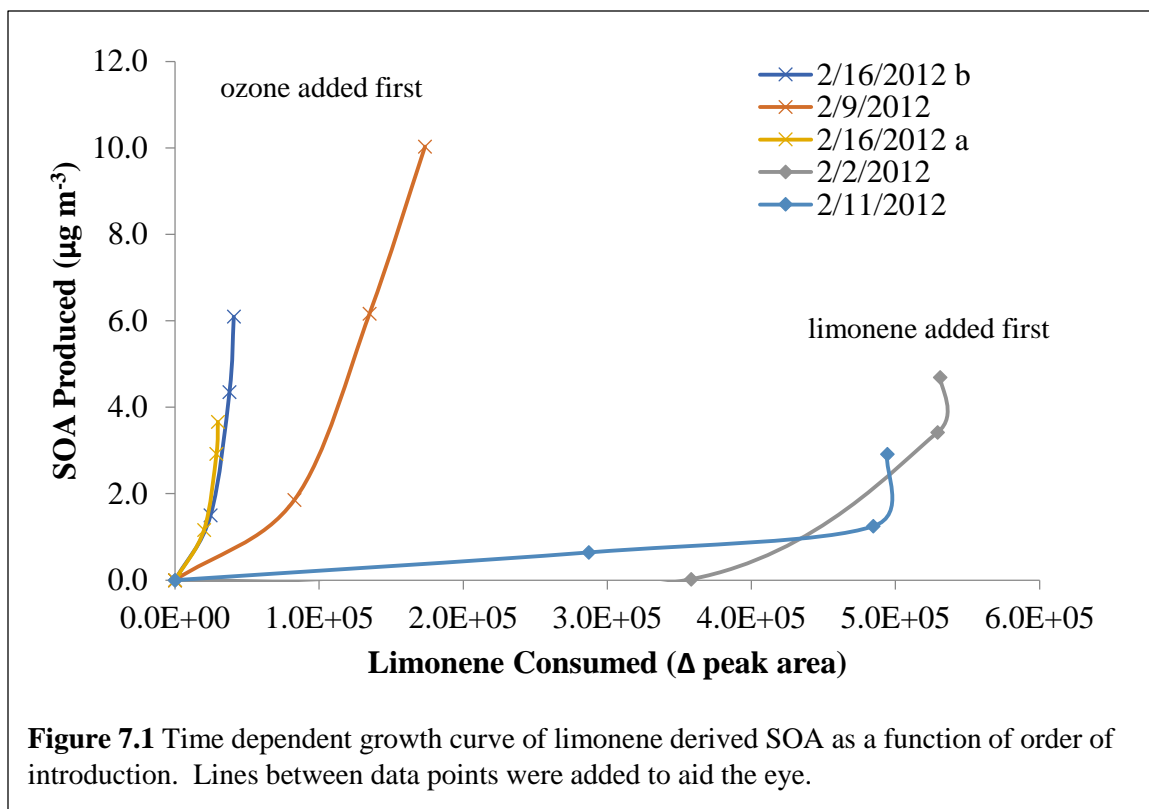
7.2 Data Treatment

The limonene signal was not mass-calibrated but, instead, is given as a normalized peak area from the GC/MS, where the peak area was normalized to the volume of the sample collected, which varied between 0.6 and 1.8 L.

The change in limonene peak area from time zero was used as a proxy for limonene consumption and was plotted against the total aerosol produced from time zero, where time zero was the time at which the second reagent was added to chamber. This plot yields the time dependent growth curve, which shows the mass of aerosol produced as a function of VOC consumed for a given experiment.^{16, 17}

7.3 Results and Discussion

As shown in Figure 7.1 (time dependent growth curves for limonene as a function of order of introduction) there is a clear distinction between the two groups of data based on the shapes of the growth curves. When limonene is added to the chamber first, there is a large amount of limonene consumed before SOA growth begins, resulting in a ‘hooked’ growth curve. Alternatively, when ozone is added to the chamber first, there is limited VOC consumption per unit SOA generated and no ‘hooked’ shape. Both conditions yield approximately the same total aerosol mass, between 4 and 6 $\mu\text{g m}^{-3}$ SOA, except for the 2/9/2012 experiment, which yielded $\sim 10 \mu\text{g m}^{-3}$ SOA.

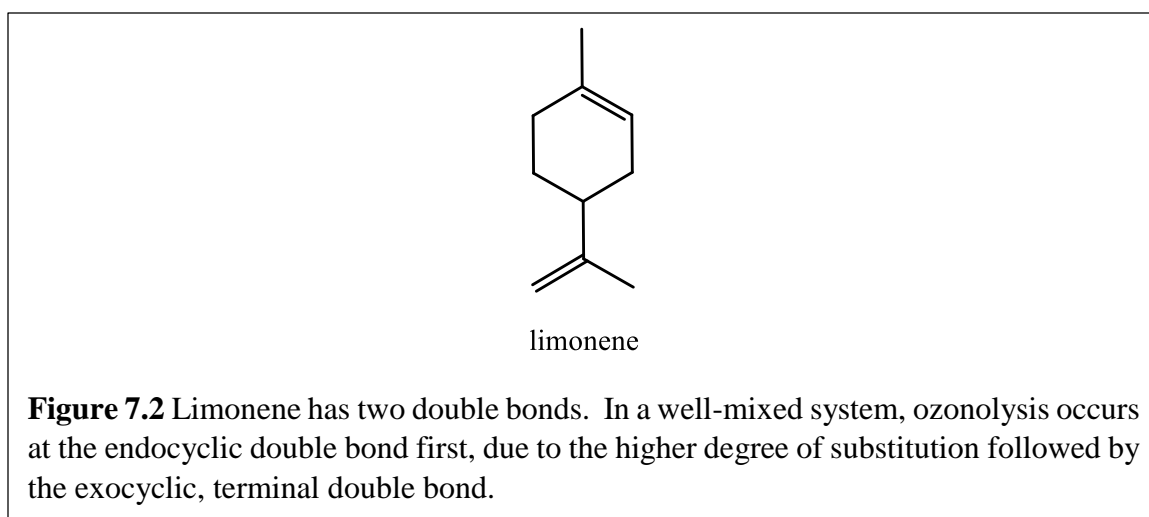


Ng et al. (2006)¹⁷ observed similar ‘hooked’ behavior in their time dependent growth curve for SOA generated by the ozonolysis of several different terpenes (myrcene, α -humulene, α -terpinene, terpinolene and β -caryophyllene). In their case, the terpene was always added to the chamber first, which agrees with our observations. A hooked growth curve ultimately stems from a delay in aerosol production, which could be due to either a very slow partitioning of condensable products into the aerosol phase or due to the formation of condensable products from the further oxidation of first-generation products, and that this second oxidation step determines the rate of SOA formation. Note that the terpenes studied by Ng et al. (2006) had more than one double bond, so the first generation ozonolysis products are still unsaturated and can react further (with ozone or OH) to yield more oxidized products that more readily condense to form particles. Limonene, too, has

multiple double bonds, which could explain why we observe the hooked behavior. If the hook is due to further oxidation of first-generation products, then the excess ozone in “limonene second” reactions must preferentially react with the second double bond in limonene ozonolysis products over any ‘unreacted’ limonene as it is injected.

Generally, ozone preferentially reacts with the endocyclic (endo) double bond of limonene (Figure 7.2) due to the fact that it is more substituted than the terminal exocyclic (exo) double bond.¹⁸ (Recall, that we observed this same trend in Chapter 6, where terminal alkenes had a reduced rate constant over internally bonded alkenes.) In fact, the endo double bond in limonene has a rate constant 50 times greater than the exo double bond.¹⁸¹⁹ So, in a well-mixed system the ozonolysis would first occur at the endo double bond of all limonene molecules present before proceeding to the second, forming first-generation products with sufficiently low vapor pressures to condense to the particle phase and may result in a hooked growth curve.

Consider the limonene first experiments, where this hooked behavior is observed. Because ozone is being added as a quick burst (< 10 sec) into a limonene-rich environment,



it has ample opportunity to react with unreacted limonene molecules before further oxidizing first generation products, stimulating the stepwise oxidation that results in a hooked growth curve. However, in the ozone-first scenario, limonene is injected via a heated bulb and takes ~ 10 min to fully transfer. So the ozone already in the batch reactor may react with **both** double bonds of a single limonene molecule before having the opportunity to react with new limonene molecules (because they're being injected relatively slowly).

7.4 Conclusions

The delayed onset of SOA as VOC is consumed (hooked growth curve) suggests that secondary oxidation reactions play a dominant role in new particle formation under these conditions. As is the trend in many of the chapters herein, it seems that minor subtleties (in this case: order of introduction) play a major role in the molecular level dynamics of SOA formation. Further work to elucidate the dynamics of these reactions should be done. This work could include incorporation of molecular-level analysis of the gas and particle phase products under the two conditions. TD-GC/MS has a temporal resolution of 5-10 minutes at these mixing ratios, and *could* be used for gas phase analysis, but since these reactions happen so quickly, real-time Proton Transfer Reaction MS (PTR-MS) would be better suited to monitor the gas phase dynamics of these reactions. NIR-LDI-AMS could provide molecular-level analysis of the particle phase but also requires several minutes of sampling before analysis (depending on mass loading). The Aerodyne aerosol mass spectrometer can offer real time analysis of particle chemistry, but at the cost of molecular-level analysis. Despite this limitation, the Aerodyne aerosol mass

spectrometer can provide bulk chemical properties (O:C, H:C) that could be used to compare degree of oxidation in these different systems.

In these ozonolysis reactions, the order of introduction of limonene versus ozone may seem to be an inconsequential subtlety in operating procedure. However, as we observed in the time dependent growth curve, the order of introduction impacts the onset of SOA, which may have implications on overall SOA lifetime and chemistry. The different orders of introduction also represent relevant environmental scenarios. Imagine for instance, the early morning commute at the interface rural/urban landscapes, where vehicle emissions result in an ozone-rich environment. As the sun rises, trees and plants emit terpenes into this ozone rich environment. Our ozone first reactions may more accurately represent this scenario than if the VOCs were injected into the chamber first. An alternative picture could be painted for the evening commute, where VOCs are already present and the evening rush hour results in the emission of ozone into VOC-rich air mass.

Despite remaining questions and a limited understanding of the molecular level dynamics contributing to these different time dependent growth curves, this work demonstrates the need for consistency in experimental design and also detailed reporting of procedures for inter- and intralaboratory comparisons.

7.5 References

(1) Hallquist, M.; Wenger, J. C.; Baltensperger, U.; Rudich, Y.; Simpson, D.; Claeys, M.; Dommen, J.; Donahue, N. M.; George, C.; Goldstein, A. H.; Hamilton, J. F.; Herrmann, H.; Hoffmann, T.; Iinuma, Y.; Jang, M.; Jenkin, M. E.; Jimenez, J. L.; Kiendler-Scharr, A.; Maenhaut, W.; McFiggans, G.; Mentel, T. F.; Monod, A.; Prévôt, A. S. H.; Seinfeld, J. H.; Surratt, J. D.; Szmigielski, R.; Wildt, J. *Atmos. Chem. Phys.* **2009**, *9*, 5155.

- (2) Heald, C. L.; Jacob, D. J.; Park, R. J.; Russell, L. M.; Huebert, B. J.; Seinfeld, J. H.; Liao, H.; Weber, R. J. *Geophysical Research Letters* **2005**, *32*, L18809.
- (3) Kanakidou, M.; Seinfeld, J. H.; Pandis, S. N.; Barnes, I.; Dentener, F. J.; Facchini, M. C.; Van Dingenen, R.; Ervens, B.; Nenes, A.; Nielsen, C. J.; Swietlicki, E.; Putaud, J. P.; Balkanski, Y.; Fuzzi, S.; Horth, J.; Moortgat, G. K.; Winterhalter, R.; Myhre, C. E. L.; Tsigaridis, K.; Vignati, E.; Stephanou, E. G.; Wilson, J. *Atmos. Chem. Phys.* **2005**, *5*, 1053.
- (4) Jo, D. S.; Park, R. J.; Kim, M. J.; Spracklen, D. V. *Atmos Environ* **2013**, *81*, 230.
- (5) Goldstein, A. H.; Galbally, I. E. *Environ Sci Technol* **2007**, *41*, 1514.
- (6) Carlton, A. G.; Wiedinmyer, C.; Kroll, J. H. *Atmos. Chem. Phys.* **2009**, *9*, 4987.
- (7) Wang, J.; Doussin, J. F.; Perrier, S.; Perraudin, E.; Katrib, Y.; Pangui, E.; Picquet-Varrault, B. *Atmos. Meas. Tech.* **2011**, *4*, 2465.
- (8) Rossignol, S.; Chiappini, L.; Perraudin, E.; Rio, C.; Fable, S.; Valorso, R.; Doussin, J. F. *Atmos. Meas. Tech.* **2012**, *5*, 1459.
- (9) Wang, X.; Liu, T.; Bernard, F.; Ding, X.; Wen, S.; Zhang, Y.; Zhang, Z.; He, Q.; Lü, S.; Chen, J.; Saunders, S.; Yu, J. *Atmos. Meas. Tech.* **2014**, *7*, 301.
- (10) Leskinen, A.; Yli-Pirilä, P.; Kuuspallo, K.; Sippula, O.; Jalava, P.; Hirvonen, M. R.; Jokiniemi, J.; Virtanen, A.; Komppula, M.; Lehtinen, K. E. J. *Atmos. Meas. Tech.* **2015**, *8*, 2267.
- (11) Keywood, M. D.; Varutbangkul, V.; Bahreini, R.; Flagan, R. C.; Seinfeld, J. H. *Environ Sci Technol* **2004**, *38*, 4157.
- (12) Bahreini, R.; Ervens, B.; Middlebrook, A. M.; Warneke, C.; de Gouw, J. A.; DeCarlo, P. F.; Jimenez, J. L.; Brock, C. A.; Neuman, J. A.; Ryerson, T. B.; Stark, H.; Atlas, E.; Brioude, J.; Fried, A.; Holloway, J. S.; Peischl, J.; Richter, D.; Walega, J.; Weibring, P.; Wollny, A. G.; Fehsenfeld, F. C. *J Geophys Res-Atmos* **2009**, *114*.
- (13) Hamilton, J. F.; Lewis, A. C.; Carey, T. J.; Wenger, J. C.; Borrás i Garcia, E.; Muñoz, A. *Atmos. Chem. Phys.* **2009**, *9*, 3815.
- (14) Harvey, R. M.; Zahardis, J.; Petrucci, G. A. *Atmos. Chem. Phys.* **2014**, *14*, 797.
- (15) Wiedensohler, A.; Birmili, W.; Nowak, A.; Sonntag, A.; Weinhold, K.; Merkel, M.; Wehner, B.; Tuch, T.; Pfeifer, S.; Fiebig, M.; Fjåraa, A. M.; Asmi, E.; Sellegri, K.; Depuy, R.; Venzac, H.; Villani, P.; Laj, P.; Aalto, P.; Ogren, J. A.; Swietlicki, E.; Williams, P.; Roldin, P.; Quincey, P.; Hüglin, C.; Fierz-Schmidhauser, R.; Gysel, M.; Weingartner, E.; Riccobono, F.; Santos, S.; Gruning, C.; Faloon, K.; Beddows, D.; Harrison, R.; Monahan, C.; Jennings, S. G.; O'Dowd, C. D.; Marinoni, A.; Horn, H. G.; Keck, L.; Jiang, J.; Scheckman, J.; McMurry, P. H.; Deng, Z.; Zhao, C. S.; Moerman, M.; Henzing, B.; de Leeuw, G.; Lösschau, G.; Bastian, S. *Atmos. Meas. Tech.* **2012**, *5*, 657.
- (16) Ng, N. L.; Kwan, A. J.; Surratt, J. D.; Chan, A. W. H.; Chhabra, P. S.; Sorooshian, A.; Pye, H. O. T.; Crounse, J. D.; Wennberg, P. O.; Flagan, R. C.; Seinfeld, J. H. *Atmos. Chem. Phys.* **2008**, *8*, 4117.

- (17) Ng, N. L.; Kroll, J. H.; Keywood, M. D.; Bahreini, R.; Varutbangkul, V.; Flagan, R. C.; Seinfeld, J. H.; Lee, A.; Goldstein, A. H. *Environ Sci Technol* **2006**, *40*, 2283.
- (18) Zhang, J.; Huff Hartz, K. E.; Pandis, S. N.; Donahue, N. M. *The Journal of Physical Chemistry A* **2006**, *110*, 11053.
- (19) Donahue, N. M.; Tischuk, J. E.; Marquis, B. J.; Huff Hartz, K. E. *Phys Chem Chem Phys* **2007**, *9*, 2991.

CHAPTER 8. DETERMINATION OF THE VOLATILE EMISSIONS OF SUGARCANE AND THEIR ROLE IN ATMOSPHERIC CHEMISTRY

8.1 Introduction

Among the greatest challenges in atmospheric chemistry is the identification of VOCs that contribute to SOA. Our approach to discovering new BVOCs has been to identify land uses that cover large areas, characterize VOC emissions from those areas and measure and characterize SOA formed from oxidation of these emissions. Using this approach, we recently found that, under certain scenarios, lawn mowing can contribute over 940 μg SOA per square meter of lawn mowed, analogous to accepted predominant SOA sources.^{1,2} This work demonstrated that GLVs have an important role in atmospheric chemistry. That being said, there is still little known about the sources and total contribution of GLVs to atmospheric aerosol. As a follow-up to this work with GLVs, we have recently completed an exploratory project designed to characterize the BVOC emissions of and to determine the potential SOA mass loading of sugarcane.

Interestingly, both grass and sugarcane are C_4 plants in the *poacea* family. Therefore, they are likely to have similar emission profiles, dominated by GLVs. Additionally, sugarcane covers a vast area of land (70 million acres globally and nearly 1 million acres in the US alone³) and yet the impacts of sugarcane-derived SOA are largely unknown. The large land area covered by sugarcane and the potential it has to emit reactive BVOCs, begs the question “do natural sugarcane emissions contribute to SOA and, if so, to what extent?”

It has been well established that the cultivation of sugarcane emits significant

amounts of primary OA (POA),⁴⁻⁸ but its potential contribution to SOA has not been evaluated. In 2005, Chang et al.⁹ characterized the emissions of sugarcane extract and found that the predominant emissions were isoprene and monoterpenes and that about 30% of the emissions were “other VOCs,” which have yet to be characterized and are likely to contain additional SOA precursors. Nonetheless, we still lack a baseline understanding of the emissions of the sugarcane plant itself and their potential contribution to SOA.

In light of this deficiency, we performed emissions and SOA yield experiments analogous to those described in Chapter 4 to identify and quantify sugarcane emissions and to quantify the SOA-forming potential (or aerosol yield) of identified compounds under atmospherically relevant conditions.

8.2 Experimental

Sugarcane samples were collected by collaborators at the University of Central Florida, Everglades Research and Education Center and stored in plastic oven bags. Samples were shipped to the University of Vermont overnight and analysis was performed within 24-36 hours of harvest. Between 100-150 g of sugarcane (wet weight) was freshly cut into 2-3 inch pieces and placed in a 775-L Teflon reaction chamber (Figure 8.1). Plant emissions were monitored using solid phase microextraction (SPME) before ozone was injected as a quick burst.

As described in Chapter 3, the SPME sampling device consists of a small polymer-coated fiber to which VOCs adsorb. After a suitable period of time, which was determined to be 40 min, as described in Section 3.1.2, the fiber is extracted from the sample gas and injected directly into the heated injection port (200 °C) of the gas chromatograph (GC,



Figure 8.1 Sugarcane in 775-L reaction chamber for emission and SOA yield experiments.

Clarus 600, Perkin Elmer) equipped with an analytical column (Stabilwax 30 m, 0.32 mm i.d., Restek) and a mass spectrometer (MS, Clarus 600 T Perkin Elmer) for analysis.¹⁰⁻¹² The GC oven was programmed as follows: held at 120°C for 4 min, increasing 10°C min⁻¹ to a final temperature of 220°C. The total run time per sample was 22 min. The head pressure of the helium carrier gas was 1.8 psi, which resulted in a flow rate of 1.52 ml/min. Electron impact ionization (70 eV) was used and masses were scanned from 15 to 300 m/z. Chromatographic peaks were identified by spectral matching with the NIST 2005 mass spectral library and confirmed by comparison of retention times to those of known standards, when available. Compounds were quantified on peak area basis using single ion monitoring.

VOC emissions were monitored for several hours before ozone was injected into the reaction chamber. Once ozone was injected, the consumption of VOC emissions was measured along with the evolution of gas phase products and SOA. A summary of initial conditions for all sugarcane experiments can be found in Table 8.1.

Table 8.1 Initial Experimental Conditions for sugarcane experiments

Date	Sugarcane Mass (g)	Ozone Injected (ppb)	Max SOA Mass ($\mu\text{g m}^{-3}$)	Comments
7/21/2015	~ 150	0	n/a	Pilot experiment, sugarcane mass not measured but estimated. No ozone injected, just characterized the gaseous emissions as proof of concept
11/04/2015	130	800	$1.6 \pm 0.2^*$	
11/06/2015	200	200	$3.8 \pm 0.4^*$	Sugarcane clippings were reused from 11/04/2016 experiment, so they have already been stressed due to ozonolysis. Sample was freshly wounded (cut into 1-2 inch pieces) before analysis.
12/16/2016	290	80	2.3 ± 0.59	

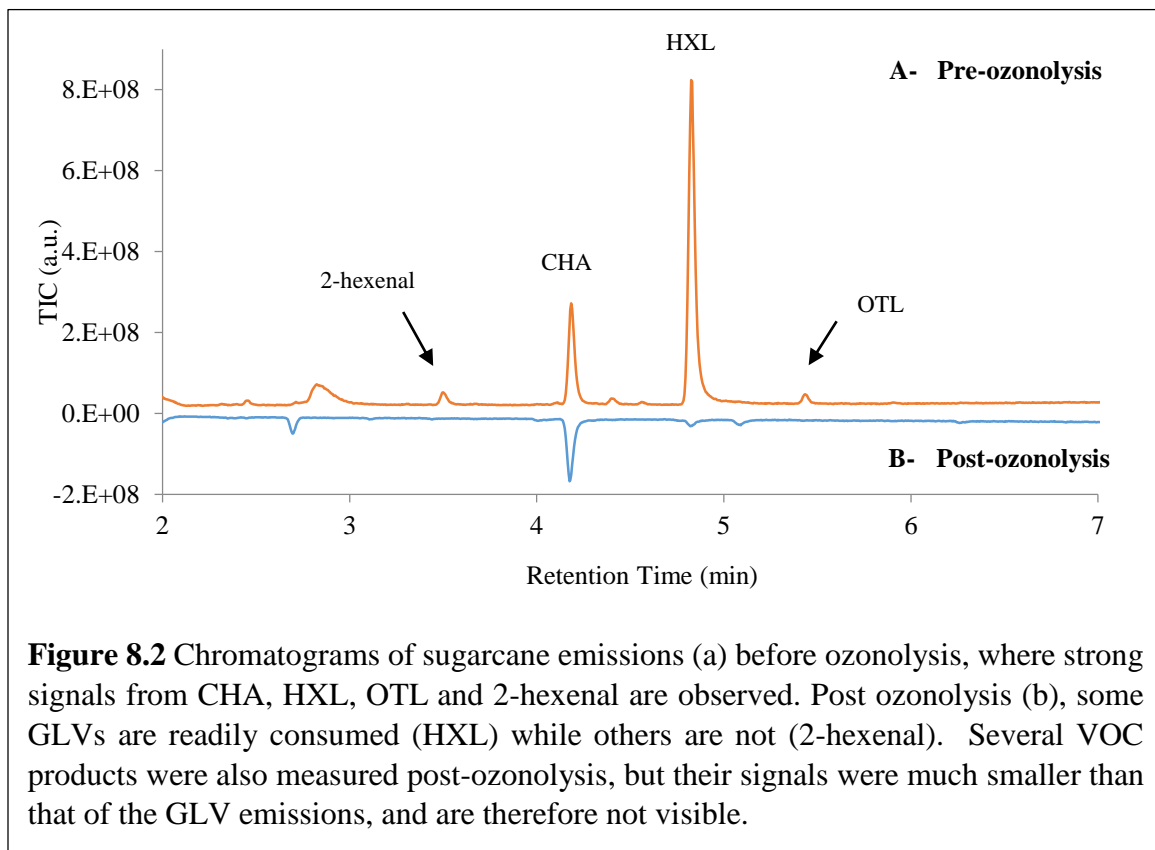
* Due to instrumental errors, the actual value for SOA mass was not directly measured. Instead, the reported values represent estimates and were determined according to methods described in Appendix 2.

8.3 Results

8.3.1 VOC Emissions

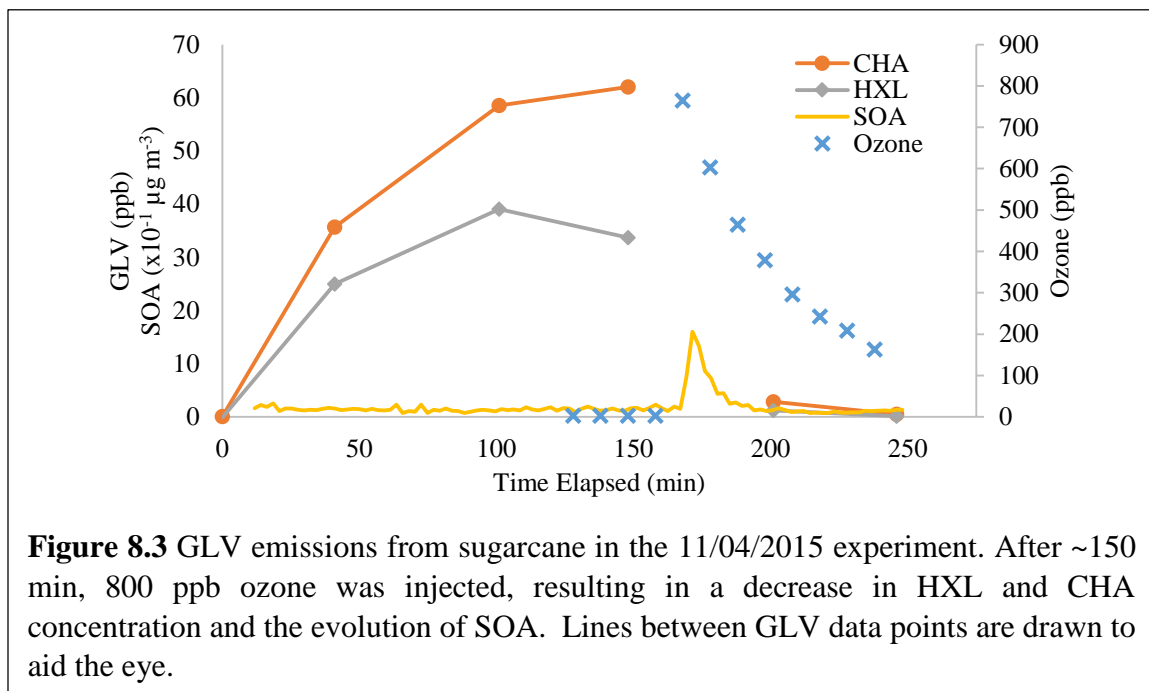
Figure 8.2 is a representative chromatogram of sugarcane emissions (a) before and after (b) the injection of ozone. Emissions were identified using the NIST Spectral Much like grass clippings, the dominant emissions include CHA and HXL, with lesser amounts

of 1-octene-3-ol (OTL), 2-hexenal, 3-hexenal, 1-heptanal and toluene. In fact, the signal from some of these compounds is so weak that their chromatographic peaks cannot be seen on the scale of Figure 8.2 but a summary of their retention times can be found in Table 8.2. CHA, HXL and OTL were confirmed with standards. The entire chromatographic run was 20 min, but no compounds were found at retention times greater than ~6.5 min, so this section is not shown.



Using the SPME *K* described and reported in Chapter 3, the concentrations of HXL and CHA were determined. Figure 8.3 is a plot of CHA and HXL concentration as a function of time for the 11/04/2015 experiment. The sugarcane sample emissions were measured for ~150 min before ozone was injected, after which CHA and HXL

concentrations decreased. In all three experiments, CHA concentrations were greater than HXL. The concentrations of each GLV just before ozone was injected are given in Table 8.3.



Also in Table 8.3 are the average emission rates of each GLV, which were given by the slope of a linear regression of the concentration as a function of time and normalized to the mass of sugarcane sample. In the 11/04 and 11/06 experiments, CHA was emitted at a greater rate than HXL. Recall that the 11/06 experiment used the same sugarcane sample as 11/04, which likely explains why the relative amounts of each GLV was the same. The 11/06 experiment had a much lower emission rate and final GLV concentration than the 11/04 experiment, however. The decrease in emissions is likely due to the fact that the sample used on 11/06 was aged and had been exposed to ozone in experiments two days prior. In the 12/16 experiment, CHA and GLV were emitted at the same rate as each other, resulting in nearly the same concentrations of each GLV (values within ~20%).

Although *K* values for 1-octen-3-ol (OTL) were determined and reported in Chapter 3, the signals measured here were smaller than we could quantitatively measure in the aqueous phase. Therefore, calibrations could not be completed and OTL emissions could not be quantified.

Table 8.2 VOC Emissions from Sugarcane and volatile ozonolysis products

Emission	Retention time (min)	Product	Retention Time (min)
Toluene *	2.3	methyl ester butanoic acid*	2.7
3-hexenal *	2.8	heptanal	3.1
2-hexenal	3.5	octanal *	4.0
CHA	4.2	nonanal	5.10
HXL	4.8	decanal	6.2
OTL	5.4		

* These compounds were tentatively identified by comparison to the NIST spectral library but were not confirmed using known standards.

A typical reaction profile for VOCs other than the GLVs is given in Figure 8.4. The raw peak areas for each compound scaled several orders of magnitude, so they were each normalized to their respective greatest peak area to allow for easier comparison. 3-hexenal, OTL, toluene and methyl ester hexanoic acid were initially emitted very quickly but then decreased in peak area even before ozone was injected. 2-hexenal was emitted and then appeared to plateau until ozone was injected.

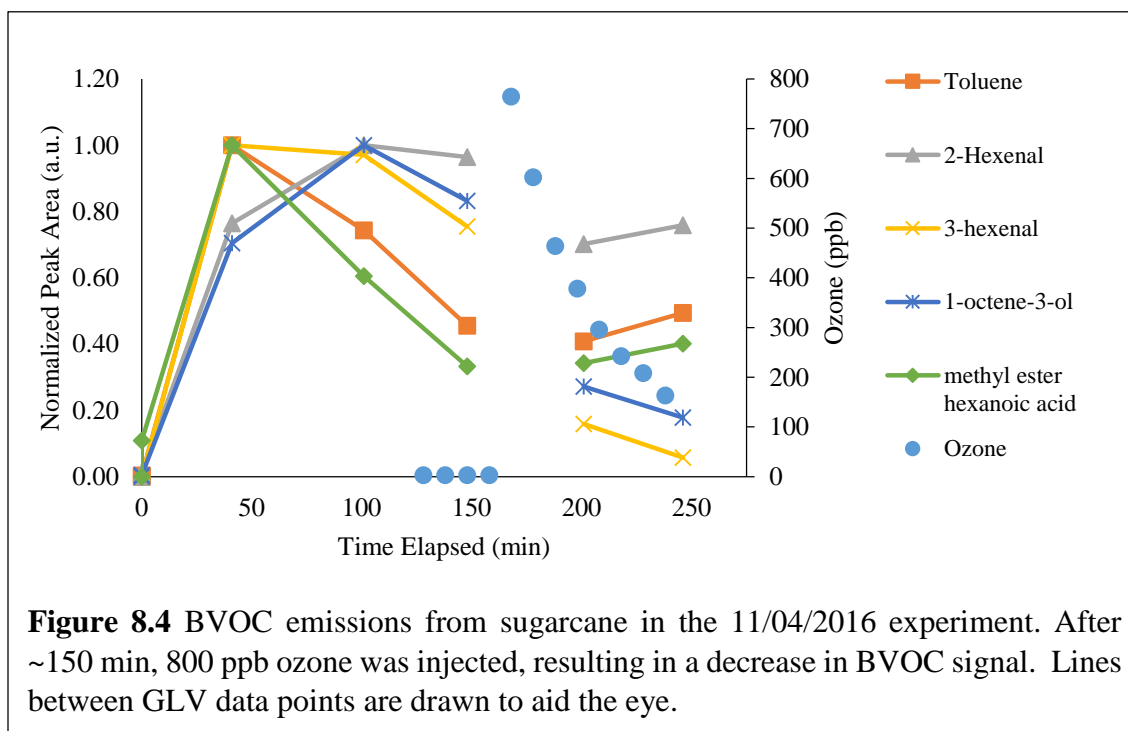


Table 8.3 Pre-ozonolysis concentration (“initial concentration”) and emission rate of CHA and HXL from sugarcane samples.

	Initial CHA Concentration (ppb)	CHA Emission Rate (ppb/hr/g sugarcane)	Initial HXL Concentration (ppb)	HXL Emission Rate (ppb/hr/g sugarcane)
11/04/2015	62	0.27 ± 0.04	40	0.18 ± 0.03
11/06/2015	7.0	0.009 ± 0.006	2.5	0.005 ± 0.002
12/16/2016	13.5	0.15 ± 0.05	17.0	0.16 ± 0.05

8.3.2 VOCs and SOA Post Ozonolysis

After emission rates were determined, ozone was injected into the reaction chamber. Ozone levels used are given in Table 8.1. Post ozonolysis, (Figure 8.3 and 8.4) there is a dramatic reduction in signal for HXL, CHA, 3-hexenal, 2-hexenal and OTL,

while the signal for toluene and methyl ester hexanoic acid did not decrease, and even seemed to increase slightly.

Ozone is expected to oxidatively cleave double bonds, resulting in the consumption of unsaturated parent compounds and evolution of oxygenated products. This reactivity likely explains the disappearance of HXL, CHA, 3-hexenal, 1-octene-3-ol. Toluene, however is expected to react with ozone,^{13,14} yet only 10% was consumed. Similarly, 2-hexenal also contains one double bond (in the second position) and is expected to react with ozone, yet only ~25% of this VOC was consumed post ozonolysis. The limited reactivity, then, may be a result of complex structure-activity relationships like those discussed in Chapter 6. We measured the ozonolysis rate constant (see method description in Chapter 3) of 2-hexenal to be $1.62 \pm 0.2 \times 10^{-18} \text{ cm}^3\text{sec}^{-1}\text{molecule}^{-1}$, which agrees well with reported values ($1.28 \pm 0.2 \times 10^{-18} \text{ cm}^3\text{sec}^{-1}\text{molecule}^{-1}$)¹⁵, but is an order of magnitude smaller than that measured for CHA, HXL (Table 6.3) and OTL (see discussion below), which is likely its signal did not decrease as dramatically as the other sugarcane emissions post ozonolysis. This reduced reactivity may be due to the fact that the aldehyde moiety in 2-hexenal is in close proximity to its double bond and may be effectively blocking ozone, limiting reactivity via steric effects. As discussed in Chapter 9, transition state theory could be used to shed further light on the factors affecting the kinetics of this system.

We also observed several volatile products from the ozonolysis of sugarcane emissions. These included methyl ester butanoic acid, heptanal, octanal, nonanal and decanal. The identification of heptanal, nonanal and decanal were confirmed by comparing retention times and mass spectra to those of known standards. Aldehydes and carboxylic

acids are among the compounds expected from the ozonolysis of alkenes. The general scheme shown in Scheme 2.1 does not lead directly to these particular molecules from the observed sugarcane emissions but a detailed mechanism warrants additional investigation.

The evolution of SOA was also observed post ozonolysis (Figure 8.3 and Table 8.1.) HXL and CHA are known to contribute to SOA^{1,16-18} and have aerosol yields of 6.5(±2.4)% and 3.9 (±2.6)%, respectively.¹⁸ Recall, however, that aerosol yield scales with VOC loading, where higher loadings result in greater yield. These aerosol yields were determined at VOC loadings of 1000 ppb, when GLV emissions from sugarcane were on the order of 10-50 ppb (Table 8.3). Based on these yields and the maximum CHA and HXL concentrations measured, the predicted GLV-derived SOA loadings grossly exceeded the actual, measured SOA loadings on both 11/04 and 12/16 (Table 8.4).

Table 8.4 Estimated Contribution of HXL and CHA to total sugarcane SOA loadings based on their emission rates and *reported* SOA Yields (for 1000 ppb GLV).

Experiment	HXL Derived SOA ($\mu\text{g m}^{-3}$)	CHA Derived SOA ($\mu\text{g m}^{-3}$)	Total GLV-Derived SOA ($\mu\text{g m}^{-3}$)	Max Measured SOA
11/04/2015	10 ± 4	14 ± 9	24 ± 10	1.6 ± 0.2
11/06/2015	0.9 ± 0.3	1.6 ± 1.0	2.5 ± 1.1	3.8 ± 0.4
12/16/2015	5 ± 2	3 ± 2	8 ± 3	2.3 ± 0.6

Using more appropriate, yet still high VOC loadings (500 ppb), aerosol yields of 0.3% and 0.7% were found for CHA and HXL, respectively. Using these aerosol yields, the predicted GLV-derived SOA concentrations were over-predicted on 11/4 but under predicted on both 11/6 and 12/16 (Table 8.5). As discussed in Section 3.3, partitioning to chamber walls is a significant loss mechanism for particles in chamber studies, and results

in an erroneously low SOA mass measurement. Therefore, an over-prediction in SOA loading, like on 11/04, may indicate that there is substantial particle loss to both chamber walls and/or to the sugarcane itself

Table 8.5 Estimated Contribution of HXL and CHA to total sugarcane SOA loadings based on their emission rates and measured SOA Yields (for 500 ppb GLV).

Experiment	HXL Derived SOA ($\mu\text{g m}^{-3}$)	CHA Derived SOA ($\mu\text{g m}^{-3}$)	Total GLV-Derived SOA ($\mu\text{g m}^{-3}$)	Max Measured SOA
11/04/2015	1.12	1.1	2.2	1.6 ± 0.2
11/06/2015	0.09	0.12	0.22	3.8 ± 0.4
12/16/2015	0.55	0.23	0.78	2.3 ± 0.6

An underestimation in SOA production may result from a still incomplete understanding of SOA forming mechanisms and/or the omission of significant SOA precursors. One such precursor may be 1-octene-3-ol (OTL). As shown in Figure 8.3, OTL signal decreased post ozonolysis, suggesting it is reactive with ozone. There is limited data on the role of OTL in atmospheric oxidation reactions^{19,20} and I am not aware of any studies of its reaction with ozone to produce SOA. However, as shown in Scheme 8.1, OTL has one terminal double bond, which likely reacts with ozone to form 2-hydroxyheptanoic acid, 2-hydroxyheptanal, formaldehyde and formic acid. Formaldehyde and formic acid are expected to be found in the vapor phase but were not observed as products. Given that SPME is efficient at sampling *semi*-VOCs, though, the high volatility of these compounds may have limited our ability to sample and therefore detect/measure them. 2-hydroxyheptanoic acid and 2-hydroxyheptanal, however, have sufficiently low vapor pressures (0.0349 Pa and 4.57 Pa, as calculated by the EPA EPI database), that they are

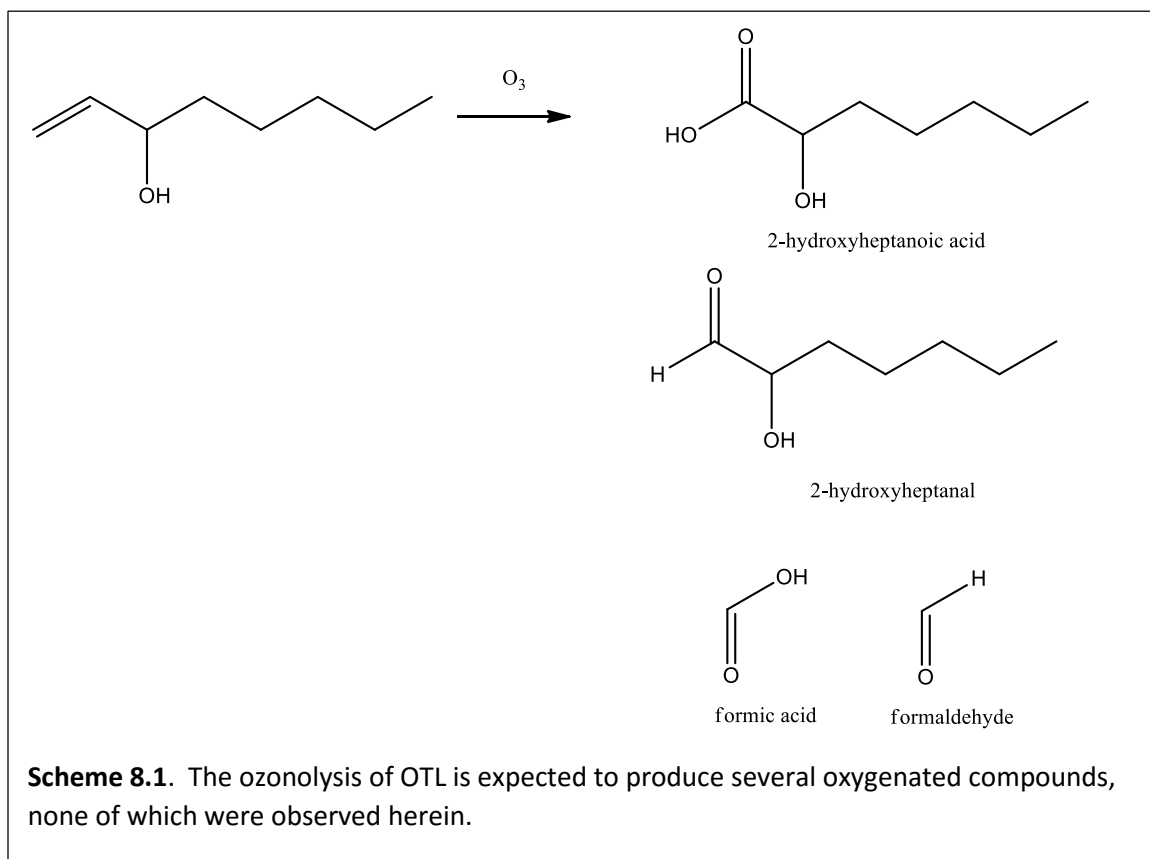
expected to contribute to SOA. Additionally, the hydroxyl group in OTL is expected to participate in secondary oligomerization reactions that would lead to additional SOA mass.²¹

To determine the reactivity of OTL with ozone, its ozonolysis rate constant (k) was measured as described in section 3.6^{22,23}. Briefly, pseudo-first-order reaction conditions were induced, whereby OTL was present in 10-fold excess of ozone (2125 ppb and 200 ppb, respectively). Ozone was injected as a brief burst which was monitored throughout the reaction. A plot of $\ln([\text{Ozone}]_{t0}/[\text{Ozone}]_t)$ vs time yields a straight line with slope k_{observed} . From the rate expression of the reaction, $k = k_{\text{observed}}/[\text{OTL}]_{t0}$. The rate constant of OTL was found to be $2.45 \pm 0.05 \times 10^{-17} \text{ cm}^3\text{sec}^{-1}\text{molecule}^{-1}$, which is slightly smaller but on the same order of magnitude as the ozonolysis rate constants measured for CHA and HXL (5.8 ± 0.9 and 5.8 ± 0.1 , respectively, Table 6.3).

To determine the SOA-forming potential of OTL, its aerosol yield (Y) was measured using pure standards of OTL in accordance to the method described in Chapters 3 and used in Chapter 4 and 6. The aerosol yield for OTL at 1000 ppb was found to be 2.5%, which is on the same order of magnitude as other GLVs (CHA and HXL).

During these yield experiments, the production of heptanal from the ozonolysis of pure OTL was also observed, suggesting that OTL may be the source of heptanal in sugarcane experiments. The ozonolysis of OTL also resulted in the production of a compound that was identified by the NIST database as 4-methyl pentanol and one that was identified as n-Caprioc acid vinyl ester or 6,7-dodecanedione. The exact mechanisms

leading to any of these compounds from the ozonolysis of OTL are not clear, but warrant additional attention.



8.4 Influence of Sugarcane on Global SOA and Further Conclusions

Recall that the SOA loadings reported for 11/04 and 11/06 experiments were estimates, so the SOA mass loading measured experimentally in the 12/16/2015 experiment was used to estimate the potential global impact of sugarcane on atmospheric aerosols. In the 12/16 experiment, a maximum SOA concentration of $2.3 \mu\text{g m}^{-3}$ was measured for 290 g of sugarcane, which corresponds to $0.26 \mu\text{g m}^{-3}$ per g of sugarcane. Accounting for the volume of the reaction chamber (775 L), this SOA concentration corresponds to an absolute mass of $6.15 \times 10^{-3} \mu\text{g}$ per gram of sugarcane. According to the

Food and Agriculture Organization, in 2014 there was a reported 30 million hectares of sugarcane worldwide²⁴ and on average each hectare of sugarcane can produce up to 40 tons of sugarcane annually.²⁵ Assuming a uniform SOA contribution, then, sugarcane harvesting worldwide has the potential to contribute 16 Mg SOA to the atmosphere. Recall that global estimates of SOA loading range from 12-70 Tg SOA.²⁶ Sugarcane, therefore, has the potential to contribute a minimal yet significant amount of atmospheric SOA.

Sugarcane emits some of the same GLVs as turf grass (CHA and HXL) but in much smaller amounts, resulting in a smaller SOA contribution. On average the CHA emission rate was 0.14 ± 0.02 ppb/hr/g sugarcane while that for HXL was 0.15 ± 0.02 ppb/hr/g sugarcane. In addition to CHA and HXL, however sugarcane also emits significant amounts of OTL, which was not observed in the emission profile of grass clippings. Either turf grass does not emit OTL or we were not able to measure OTL with the thermal desorption GC/MS method used in those experiments. OTL was also found to be reactive with ozone to yield SOA (2.5% Y) and some of the same gas phase products that were observed in the ozonolysis of sugarcane emissions.

In order to fully understand the role that a particular source of SOA can play on the Earth's radiative budget, we must also characterize the physical and optical properties of the resultant SOA. Considering a significant amount of sugarcane SOA is derived from CHA and HXL, it is likely that sugarcane SOA has similar physical and optical properties as SOA derived from these pure GLVs, which are discussed in Chapter 6. The properties of OTL-derived SOA, however have not yet been determined. Since OTL has the potential

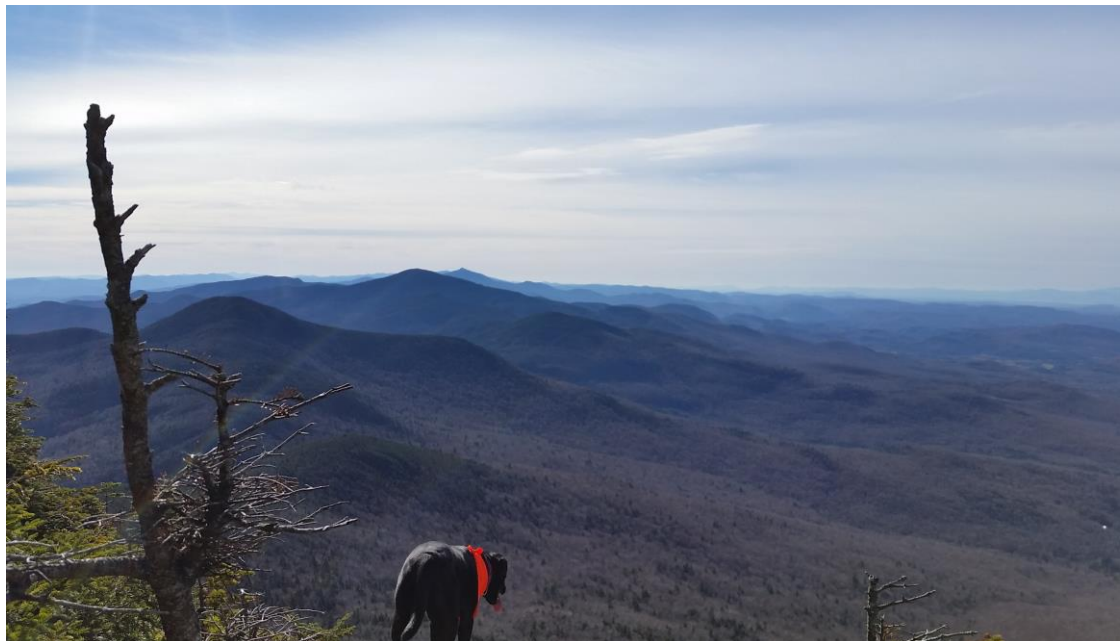
to contribute a significant fraction of sugarcane derived SOA, it is of interest to determine its physical properties and optical properties.

8.5 GLV SOA and Visibility

The absorbance and scatter of light by particles determines their direct effect on climate, but they both also contribute to the total light extinction by particles, which affects visibility. The impact of particulate matter on visibility is clearly evidenced by the presence of smog in urban regions or in rural regions by the changing opacity of close versus distant features (Figure 8.5). The term *visibility* is rather subjective and refers to the clarity with which a distant object can be seen, which as you can imagine relies on an individual's visual acuity and perception. A more useful and quantitative term is *visual range* (L_v), which gives the distance at which an object is barely discernable and is driven by the contrast between an object and its surroundings.²⁷

Visual range has been identified as a major concern by the US Environmental Protection Agency (EPA), and, despite the passage of the 1977 US Clean Air Act,²⁷ has decreased from ~ 145 km to less than 30 km in the Eastern US and from 240 km to less than 150 km in the Western US, about half of what it would be without anthropogenic influence.^{28,29}

Figure 8.5 The effect of particulate matter on visual range can be seen by my baby, Jade, from the summit of Mount Mansfield, VT. Mountains in the foreground are easily distinguished, but more distant mountains grow increasingly opaque in color and less clearly defined due in part to light extinction by atmospheric particles.



Visual range is governed primarily by the extinction of light due to particles, with extinction by gaseous air molecules having a minor effect, and is given by Equation 8.2 below:

$$L_v = \frac{3.9}{\sigma_{ext}} \quad (8.2)$$

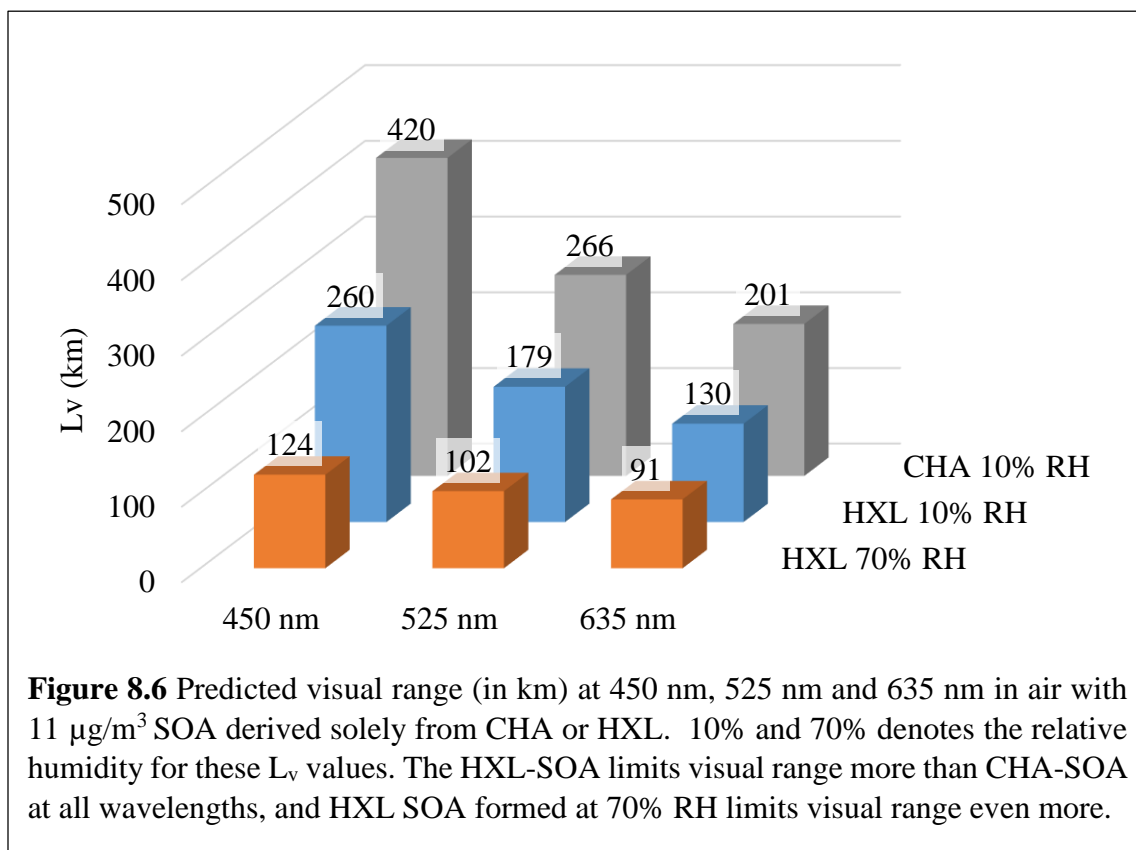
Where total extinction (σ_{ex}) is the sum of extinction due to scatter (σ_{scat}) and absorbance (σ_{abs}). In Chapter 5, we report the mass absorbance coefficient (MAC) and mass scatter coefficient (MSC) for CHA and HXL derived SOA (also given in Table 8.6), the sum of which is mass normalized extinction (MEC). Recall that the different HXL experiments correspond to experiments done under different relative humidity regimes.

Table 8.6 Mass extinction coefficients for SOA derived from CHA at 10% RH and HXL at 10% RH and 70% RH. These data were first presented in Chapter 5.

Experiment	HXL 1	HXL 2	CHA 1
Date	11/3/2015	11/4/2015	11/12/2015
RH %	10	70	10
SOA Mass Conc. ($\mu\text{g m}^{-3}$)	80	30	15
MEC (m^2g^{-1} , 450 nm)	0.45	0.57	3.9
MEC (m^2g^{-1} , 525 nm)	0.31	0.47	2.4
MEC (m^2g^{-1} , 635 nm)	0.22	0.42	1.8

Sugarcane-derived SOA may only contribute a small fraction of the *global* SOA mass, but individual sugarcane farms may have the potential to emit a concerted burst of SOA that impacts visual range. According to the US 2012 Agricultural Census, 50% of sugarcane fields in the US are 500 acres or larger (31% actually exceed 1,000 acres). A farm of 500 acres has the potential to emit an absolute mass of 1.12×10^4 Mg SOA. Assuming this SOA is emitted into the air 5 m above the sugarcane, this mass loading corresponds to a total concentration of about $11 \mu\text{g}/\text{m}^3$ SOA. By multiplying the MEC in Table 8.6 by this theoretical SOA concentration, we can estimate a theoretical σ_{ex} due to sugarcane harvesting in that air shed, permitting us to estimate L_v . Figure 8.6 gives the visual range at 450 nm, 525 nm, and 635 nm in air containing $11 \mu\text{g}/\text{m}^3$ SOA derived solely from CHA or HXL. HXL-SOA limits the visual range more than CHA-SOA, especially under humid conditions, where estimates predict a visual range of about 100 km. These visual ranges assume that CHA or HXL-SOA are the only SOA contributing to visual range, when in fact there are countless other sources of SOA that could contribute,

including OTL. These estimates, therefore represent an upper limit on visual range in air above or near sugarcane fields.



8.6 Conclusions

Upon wounding, sugarcane emits several GLVs that, upon ozonolysis, form SOA in significant amounts. This wounding could occur in a few different ways: during the harvesting of the plant or during sugarcane processing, which involves chopping the plant into small pieces before sugar is extracted. In both cases, there is opportunity for GLVs to be released and SOA to form. Globally, the harvesting of sugarcane has the potential to contribute 16 Mg of SOA to the atmosphere, which represents a small, yet significant fraction of global SOA loadings.

Sugarcane emits the same primary GLVs as turgrasses, likely because the two plants are in the same family. Sugarcane also emits significant amounts of OTL, which was not measured in the emission profile of turfgrasses (Chapter 4). In fact there is little known about the ozonolysis kinetics or SOA forming potential of OTL. We therefore report what we believe are the first measurements of SOA yield and volatile products of OTL ozonolysis.

Based on visual range estimates made herein, it is unlikely that the ozonolysis products from sugarcane emissions contribute to reduced visibility at the airshed level. The hand cultivation of sugarcane, however, requires a pre-harvest burn, during which a significant amount of primary OA (POA) is emitted.^{4,5,7,8,30} Interestingly, the combustion of sugarcane also emits significant amounts of VOCs that are known to form SOA.⁶ Sugarcane harvests, therefore represent a system that has the potential to contribute both POA and SOA, simultaneously. There is growing evidence to suggest that mixed systems like these form particulate matter with very unique properties that cannot yet be modelled; in some cases SOA yield is enhanced, while in others it is suppressed.³¹⁻³⁴ The sugarcane system, therefore, offers a prime system to also study the dynamics of a mixed system and warrants additional work.

8.7 References

- (1) Harvey, R. M.; Zahardis, J.; Petrucci, G. A. *Atmos. Chem. Phys.* **2014**, *14*, 797.
- (2) Jain, S.; Zahardis, J.; Petrucci, G. A. *Environ Sci Technol* **2014**.
- (3) Agriculture, U. D. o. *USDA 2012 Agriculture Report*, 2012.
- (4) Chow, J. C.; Watson, J. G.; Lu, Z.; Lowenthal, D. H.; Frazier, C. A.; Solomon, P. A.; Thuillier, R. H.; Magliano, K. *Atmos Environ* **1996**, *30*, 2079.
- (5) Godoi, R. H. M.; Godoi, A. F. L.; Worobiec, A.; Andrade, S. J.; de Hoog, J.; Santiago-Silva, M. R.; Van Grieken, R. *Microchim Acta* **2004**, *145*, 53.
- (6) Hall, D.; Wu, C.-Y.; Hsu, Y.-M.; Stormer, J.; Engling, G.; Capeto, K.; Wang, J.; Brown, S.; Li, H.-W.; Yu, K.-M. *Atmos Environ* **2012**, *55*, 164.
- (7) Lara, L. L.; Artaxo, P.; Martinelli, L. A.; Camargo, P. B.; Victoria, R. L.; Ferraz, E. S. B. *Atmos Environ* **2005**, *39*, 4627.
- (8) Yokelson, R. J.; Christian, T. J.; Karl, T. G.; Guenther, A. *Atmos. Chem. Phys.* **2008**, *8*, 3509.
- (9) Chang, K. H.; Chen, T. F.; Huang, H. C. *Sci Total Environ* **2005**, *346*, 184.
- (10) Baker, B.; Sinnott, M. *J Chromatogr A* **2009**, *1216*, 8442.
- (11) Cornu, A.; Carnat, A.-P.; Martin, B.; Coulon, J.-B.; Lamaison, J.-L.; Berdagué, J.-L. *J Agr Food Chem* **2001**, *49*, 203.
- (12) Bouvier-Brown, N. C.; Holzinger, R.; Palitzsch, K.; Goldstein, A. H. *J Chromatogr A* **2007**, *1161*, 113.
- (13) Baltaretu, C. O.; Lichtman, E. I.; Hadler, A. B.; Elrod, M. J. *The Journal of Physical Chemistry A* **2009**, *113*, 221.
- (14) Yakobi, V. A.; Galstyan, G. A.; Rister, I. A.; Galstyan, T. M.; Dvortsevoi, M. M. *Petroleum Chemistry U.S.S.R.* **1974**, *14*, 99.
- (15) Grosjean, E.; Grosjean, D.; Seinfeld, J. H. *Int J Chem Kinet* **1996**, *28*, 373.
- (16) Hamilton, J. F.; Lewis, A. C.; Carey, T. J.; Wenger, J. C. *Anal Chem* **2007**, *80*, 474.
- (17) Hamilton, J. F.; Lewis, A. C.; Carey, T. J.; Wenger, J. C.; Borrás i Garcia, E.; Muñoz, A. *Atmos. Chem. Phys.* **2009**, *9*, 3815.
- (18) Harvey, R. M.; Petrucci, G. A. *Atmos Environ* **2015**, *122*, 188.
- (19) Gibilisco, R. G.; Blanco, M. a. B.; Bejan, I.; Barnes, I.; Wiesen, P.; Teruel, M. A. *Environ Sci Technol* **2015**, *49*, 7717.
- (20) Joutsensaari, J.; Yli-Pirilä, P.; Korhonen, H.; Arola, A.; Blande, J. D.; Heijari, J.; Kivimäenpää, M.; Mikkonen, S.; Hao, L.; Miettinen, P.; Lyytikäinen-Saarenmaa, P.; Faiola, C. L.; Laaksonen, A.; Holopainen, J. K. *Atmos. Chem. Phys.* **2015**, *15*, 12139.
- (21) Jain, S.; Zahardis, J.; Petrucci, G. A. *Environ Sci Technol* **2014**, *48*, 4835.

- (22) Grosjean, D.; Grosjean, E.; Williams, E. L. *Int J Chem Kinet* **1993**, *25*, 783.
- (23) Grosjean, E.; Grosjean, D. *Int J Chem Kinet* **1994**, *26*, 1185.
- (24) NATIONS, F. A. A. O. O. T. U. <http://faostat3.fao.org/>, 2013.
- (25) Linderman, J. In *The Times - Piquane* Greater New Orleans, LA, 2012.
- (26) Kanakidou, M.; Seinfeld, J. H.; Pandis, S. N.; Barnes, I.; Dentener, F. J.; Facchini, M. C.; Van Dingenen, R.; Ervens, B.; Nenes, A.; Nielsen, C. J.; Swietlicki, E.; Putaud, J. P.; Balkanski, Y.; Fuzzi, S.; Horth, J.; Moortgat, G. K.; Winterhalter, R.; Myhre, C. E. L.; Tsigaridis, K.; Vignati, E.; Stephanou, E. G.; Wilson, J. *Atmos. Chem. Phys.* **2005**, *5*, 1053.
- (27) Hinds, W. *Aerosol Technology, Properties Behavior and Measurement of Airborne Particles*; John Wiley and Sons, 1982.
- (28) Agency, U. E. P. 2015.
- (29) Malm, W. C.; Cooperative Institute for Research in the Atmosphere (CIARA) NPS Visibility Program: Fort Collins, CO, 1999, p 70.
- (30) Tsao, C. C.; Campbell, J. E.; Mena-Carrasco, M.; Spak, S. N.; Carmichael, G. R.; Chen, Y. *Nat Clim Change* **2012**, *2*, 53.
- (31) Emanuelsson, E. U.; Hallquist, M.; Kristensen, K.; Glasius, M.; Bohn, B.; Fuchs, H.; Kammer, B.; Kiendler-Scharr, A.; Nehr, S.; Rubach, F.; Tillmann, R.; Wahner, A.; Wu, H. C.; Mentel, T. F. *Atmos. Chem. Phys.* **2013**, *13*, 2837.
- (32) Hildebrandt, L.; Henry, K. M.; Kroll, J. H.; Worsnop, D. R.; Pandis, S. N.; Donahue, N. M. *Environ Sci Technol* **2011**, *45*, 6329.
- (33) Hoyle, C. R.; Boy, M.; Donahue, N. M.; Fry, J. L.; Glasius, M.; Guenther, A.; Hallar, A. G.; Huff Hartz, K.; Petters, M. D.; Petäjä, T.; Rosenoern, T.; Sullivan, A. P. *Atmos. Chem. Phys.* **2011**, *11*, 321.
- (34) Shilling, J. E.; Zaveri, R. A.; Fast, J. D.; Kleinman, L.; Alexander, M. L.; Canagaratna, M. R.; Fortner, E.; Hubbe, J. M.; Jayne, J. T.; Sedlacek, A.; Setyan, A.; Springston, S.; Worsnop, D. R.; Zhang, Q. *Atmos. Chem. Phys.* **2013**, *13*, 2091.

CHAPTER 9. CONCLUSIONS AND FUTURE WORK

9.1 General Conclusions

Despite advances made to discern the role of aerosols in atmospheric processes, there remains significant uncertainty in our understanding of their broad environmental impact, owing to a still-limited knowledge of their sources, composition, properties, and the mechanisms that lead to their formation and ageing.¹⁻³ The work presented in the preceding chapters was designed to help fill some of these knowledge gaps. To the end of identifying novel SOA sources, I estimated the contribution of turfgrass mowing to the global aerosol budget (Chapter 1) and found that, as a concerted burst, the mowing of grass has the ability to contribute as much SOA as other, known predominant BVOC sources. In conjunction with this work, a sister report⁵ has been published that characterizes the chemical composition of the resultant grass-derived SOA and proposes relevant oxidation mechanisms that would lead to its formation. This work was limited however, in its consideration of **all** relevant atmospheric oxidants, as it omits oxidation by hydroxyl radicals, NO_x and photooxidation mechanisms. Incidentally this limitation provides an obvious next step for this work; the incorporation of other atmospherically relevant oxidants to further understand the molecular level dynamics leading to SOA. This will be discussed in detail below (Section 9.2)

Knowing the SOA mass loading attributed to lawn mowing, however, is not sufficient for us to estimate its impact on radiative forcing. Characterizing the optical properties of SOA (its ability to absorb and scatter light) is of prime importance to understanding its role in radiative forcing, which is the primary focus of Chapter 5. I found

that both HXL and CHA produced SOA that was weakly absorbing, yet CHA-SOA was a more efficient absorber than HXL-SOA. The scatter efficiency of SOA from both systems was wavelength-dependent, as shown by the angstrom scatter exponent (ASE) with the stronger dependence exhibited by HXL-SOA, likely due to differences in particle size. Interestingly, HXL-SOA formed under both dry (10% RH) and wet (70% RH) conditions had the same bulk chemical properties (O:C), yet significantly different optical properties, which can be attributed to subtle differences in molecular-level composition.

The importance of subtleties in the molecular-level dynamics of SOA formation was further demonstrated in Chapter 6. In this chapter, I reported the SOA yields and rate constants for the ozonolysis of several linear, cyclic and oxygenated C₅-C₇ alkenes whose molecular structure vary in the site of unsaturation and/or the presence/position of functional groups and that represent atmospherically relevant classes of molecules. Essentially, what we found was that not all alkenes are created equally, but that both the identity and position of oxygenated functional groups influenced SOA yield and kinetics through steric and electronic effects. This work demonstrates the nuanced behavior of ozonolysis reactions, which results from the relationships between parent VOC molecular structure and SOA yield and kinetics.

In Chapter 6, I described that both steric hindrance and electronic effects play important roles in determining ozonolysis rate constants, predicting that large bulky groups would general impede it, unless they were electron donating, promoting the addition of ozone to the alkene. I also indicate that transition state theory could be used to shed further light on the factors affecting these systems. This approach was not within the scope of

this work, but would offer a prime opportunity to use theoretical/computational chemistry to explore the mechanisms and kinetics of GLV ozonolysis reactions, on which I will elaborate in Section 9.3.

With the exception of the research presented herein, there has been a limited amount of work on the sources of GLVs and their impact on atmospheric chemistry. To further evaluate the large-scale contribution of GLVs, I identified another novel source, sugarcane, which is presented in Chapter 8. Sugarcane, being of the same family as many turfgrasses, was found to emit several GLVs upon wounding that that may contribute to atmospheric SOA. As reported in Chapter 5, GLV-derived SOA may also limit visual range. Interestingly, many space centers and airports, whose operations can be highly impacted by aspects of visibility, are located in close proximity to sugarcane fields. As I report in Chapter 8, the harvesting of sugarcane *may* ultimately impact aeronautic research.

9.2 Expanding Research to Include Other Relevant Oxidants

Oxidation by hydroxyl radicals (OH) has the potential to impact both mass yields and the chemical composition of GLV-derived SOA. Yet, compared to ozonolysis-driven SOA formation, new particle formation solely by the OH oxidation of VOCs has been investigated less frequently, due in part to the fact that ozone is formed as a byproduct during OH oxidation, making OH-driven chemistry difficult to isolate,⁶⁻⁹ but also because OH is difficult to *quantitatively* generate at atmospherically relevant concentrations (0.4-0.4 pptv or $\sim 2 \times 10^6$ radicals cm^{-3})^{4, 10, 11} in the laboratory, presenting experimental challenges. Those few studies that do report the impact of purely OH oxidation on new particle formation (NPF), however often use unrealistically high VOC loading and report

contradicting results. Not only is OH oxidation a much faster reaction than ozonolysis (greater rate constants),¹² but OH oxidation also follows unique reaction pathways resulting in smaller, yet more oxidized, products. It follows, then, that initial OH oxidation products would not condense and contribute to SOA formation directly, but that more oxidized, later generation products might. In fact this was recently found to be the case for the OH oxidation of several terpenes under atmospherically relevant conditions; that multigenerational OH oxidation products played an important role in new particle formation.⁶ I believe a similar trend would be observed for OH-driven oxidation of GLVs. Although the kinetics (rate constants) for the OH-oxidation of some GLVs have been reported,¹³⁻¹⁷ to my knowledge there has not yet been a study of the SOA-forming potential of these reactions or chemical characterization of the resultant SOA. Additionally, the instrumental infrastructure at UVM (namely the GC/MS and NIR-LDI-AMS) affords the Petrucci Group the unique ability to elucidate the chemical mechanisms leading to SOA by OH oxidation. This integrative approach would allow for the identification of key multigenerational products that stimulate NPF, which is of prime importance if we're to understand the molecular-level dynamics of particle genesis.

NO_x also plays an important role in the overall SOA forming potential of alkenes, especially during night-time chemistry. The presence of high levels of NO_x has been shown to both decrease and increase SOA yield, as a result of competing reaction pathways that lead to either high or low volatility products.⁸ Generally, the deciding factor contributing to whether high NO_x conditions will increase or decrease SOA yield comes down to the size of the parent hydrocarbon.⁸ Isoprene¹⁸ and α -pinene¹⁹⁻²¹ experience a

decreased SOA yield under high NO_x conditions, while longifolene and aromadendrene see an enhanced SOA yield under high NO_x conditions.⁸ It follows, then that GLVs, which are relatively small C₆ alkenes, would have a reduced SOA yield under high NO_x conditions. Again, confirming this trend at the Petrucci Lab, with the use of our unique instrumental infrastructure, would also allow for the characterization of gas and particle phase compounds and elucidation of different chemical pathways under varying NO_x conditions.

9.3 Mie Theory to Further Characterize Optical Properties

The scatter of light by particles falls into different regimes based on the size of the particles relative to the wavelength of light. Mie Theory describes the scattering of light by particles on the same order as or larger than the wavelength of light. Since actinic light at the Earth's surface is between ~300-750 nm, Mie Scattering best describes particles of the size studied herein (D_p ~ 200-300 nm). With the help of efficient algorithms and powerful computers, Mie Theory has been used to predict the light scattering by numerous different atmospheric aerosols, which can then be used to determine its index of refraction.²²⁻²⁵ ²⁶ The complex index of refraction (m) describes the relative contribution of light scatter and absorption of a material. It takes the form:

$$m = n + ik$$

where n is the real part of the refractive index, which is closely tied to the light scattering efficiency of the material and k is the imaginary part, closely tied to light absorption. It follows, then that a purely scattering material would have a negligibly small k -term, as shown in Table 9.1.

Table 9.1 The complex index of refraction of several atmospheric materials. Recreated from Ref 4

Material	Index of Refraction (m)
Air	$1.00029 - 0i$
Water Vapor	$1.00025 - 0i$
α -pinene	$1.465 - 0i$
Oleic Acid	$1.46 - 0i$
Carbon	$1.59 - 0.66i$
Iron	$1.51 - 1.63i$

The complex index of refraction can then be used to describe the total light attenuation by a particle, which is a model input to predict the overall contribution of a particle (or type of particle) to the Earth's radiative budget. It is, therefore, a very important and powerful tool and warrants additional work in the future.

9.4 Theoretical Study of Mechanisms and Kinetics of GLV Ozonolysis

The ozonolysis mechanisms that are proposed in this work and in complimentary work done in the Petrucci Group during my tenure at UVM are based off known reaction pathways that have been confirmed experimentally. For a detailed description, see Jain et al. (2014)⁵ and references therein, but briefly, product molecules were found with a given mass and then reasonable reaction schemes were proposed that lead to products with those masses. Since many of the proposed product molecules are not readily available as standards, their identity could not be confirmed. A *theoretical* study of the products and kinetics of GLV ozonolysis, however may provide additional support for the proposed mechanisms. Li et al. (2014)²⁷ has recently performed such a study on the ozonolysis of CHA. Using density function theory, they were able to confirm key mechanistic steps in

the reaction between CHA and ozone that also agree with reported kinetics.²⁷ Although it was outside the scope of this work (and the expertise of this group) a thorough theoretical study of the ozonolysis mechanisms for GLVs may prove impactful to support the work done in both Chapter 6 (structure activity relationships) and Chapter 5 (the impact of molecular water on reaction mechanisms), and would also provide an opportunity for diversification through meaningful collaborations.

9.5 Instrument Development

In Chapter 5, the absorbance of light by particles was measured using an integrating sphere coupled to a UV/Vis spectrometer, which allowed for the determination of the mass absorption coefficient between 200-900 nm. The light scattering efficiency was measured using a nephelometer, which measures scatter at only three discrete wavelengths (450 nm, 525 nm and 635 nm) while the angstrom scatter exponent (ASE) is used to interpolate scatter data for other wavelengths.²⁸ In fact, several different methods used to measure the scatter of light by particles are limited to certain wavelengths of light.^{25,28,29} Together, these absorbance and scatter data are used to estimate the total light extinction by particles, which is then in turn used to estimate the material's radiative forcing. So as you may intuit, this interpolation may introduce significant error. Instead, a method that directly measures light scatter across a continuum of wavelengths may provide more accurate data. I suggest that IS-UV/Vis could be used to measure light scatter continuously between 200-900 nm.

For absorbance measurements, SOA was collected on quartz fibers and analyzed as shown in Figure 9.1a, where the filter was placed at the front of IS and the percent

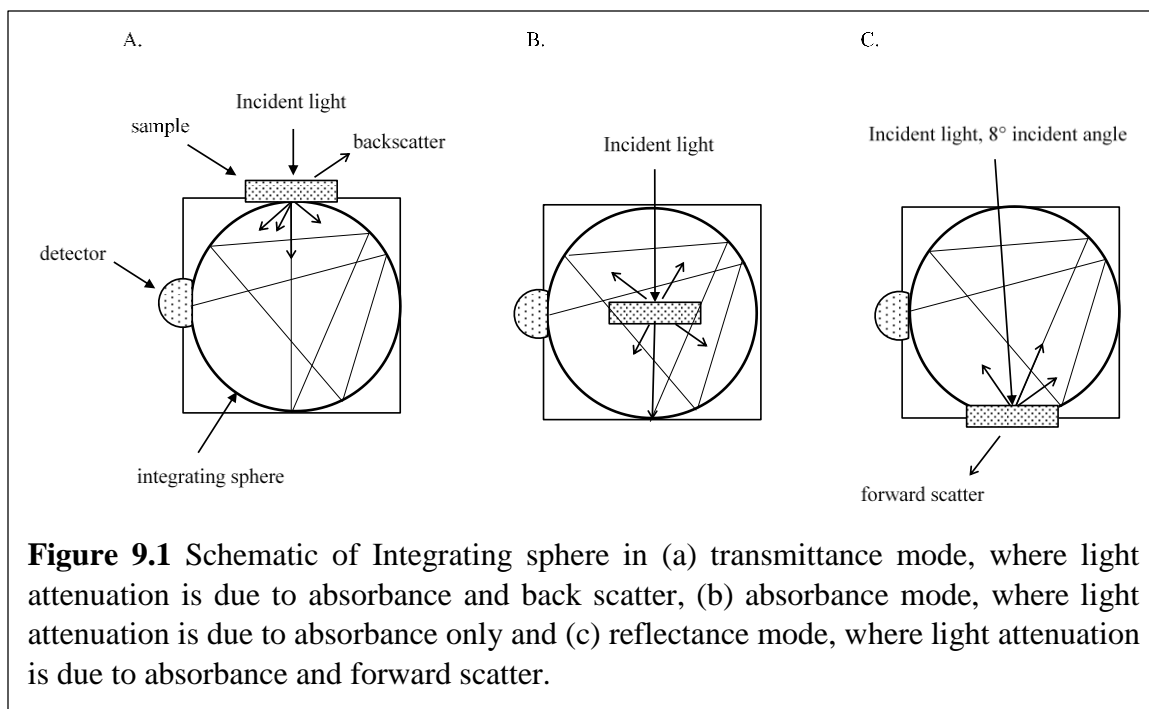


Figure 9.1 Schematic of Integrating sphere in (a) transmittance mode, where light attenuation is due to absorbance and back scatter, (b) absorbance mode, where light attenuation is due to absorbance only and (c) reflectance mode, where light attenuation is due to absorbance and forward scatter.

transmitted light was measured by the detector in the IS. The absorbance that is then calculated, however, is an overestimation, since light attenuation is also due to back scatter by particles doped on the filter. To limit this error, a center-mounted IS/UV-Vis, as shown in Figure 9.1 b, should be used. In this setup, light attenuation is due only to absorbance by the sample. These center mount IS-UV/Vis instruments are commercially available, but to the best of my knowledge, they have neither been used in this field, nor with samples collected on filters (as opposed to extracted in solvent). When analysis is done in both transmittance and absorbance modes, one can also determine the ratio of backscattered light. Additionally, when absorbance-mode measurements are compared to those made in reflectance mode (Figure 9.1c), the forward scattered light can also be determined. Not only does this one instrument have the potential to measure absorbance *and* scatter, it

would also make these measurements across a continuum of wavelengths, limiting potential errors due to interpolating ASE data.

9.6 Factors Affecting New Particle Formation- Unanswered Questions Without Projected Answers (AKA future members' PhDs)

Aerosol yields were a key measurement used to answer several questions about GLVs in the atmosphere and are reported in both Chapter 4 and Chapter 6. Despite using the same instrumental parameters, the aerosols reported have a high degree of uncertainty with relative standard deviations ranging from 5-75%. We are not alone in these high RSDs, though. In fact it is not uncommon to see aerosol yields for the same system, under the same initial conditions in the same laboratory ranging from 0-100%.^{7, 30-32} This marked disparity in SOA yields (within and between laboratories) highlights the need for more accurate representation of the molecular level interactions between VOCs and oxidants or may suggest a degree of chaos during the initial reaction steps that has yet to be understood, making predicting or modelling difficult, if even possible. Don't let me convince you that 'it can't be done,' though. Anecdotal evidence points to seemingly minor differences in environmental conditions leading to significantly different SOA mass loading and SOA properties.

As shown in Chapter 7, the order of introduction of VOC and oxidant plays an important role in the aerosol yield, where SOA yields seem to be inhibited when VOCs are introduced to an oxidant-rich environment. Intuitively, this makes sense, where the high oxidant concentration may effectively chew up product molecules, preventing nucleation and particle formation. Alternatively, second generation chemistry may become increasingly important for new particle formation when oxidants are introduced into a

VOC-rich chamber. The molecular-level dynamics of these interactions have yet to be investigated but represent an interesting and relevant scenario for future work and may shed light on the reasons for such disparate aerosol yield measurements.

In Chapter 5, we saw the impact of water on particle genesis; we observed a reduced SOA mass loading and much smaller sized particles in the presence of water, which may be counterintuitive. We also observed unique chemical and physical properties for SOA formed under the two conditions and we were not able to generate ANY SOA at intermediate RH conditions (50% RH). The reasons for these observations are not immediately clear but it seems that the presence of water at particle genesis plays an important role in NPF.

9.7 Final Thoughts

The work presented in the preceding chapters has added significantly to our understanding of the role of GLVs in atmospheric chemistry. But, in the true nature of research, it has resulted in additional questions that open doors to new and exciting research, some of which are outlined above. GLVs are emitted by plants in response to environmental stressors, so it's only natural to suspect that the role of GLVs in atmospheric chemistry will continue to evolve as our plant ecosystems respond to different stress conditions. These considerations should be taken into account for the future climate change scenarios.

9.8 References

- (1) Carlton, A. G.; Wiedinmyer, C.; Kroll, J. H. *Atmos. Chem. Phys.* **2009**, *9*, 4987.
- (2) Hamilton, J. F.; Lewis, A. C.; Carey, T. J.; Wenger, J. C.; Borrás i Garcia, E.; Muñoz, A. *Atmos. Chem. Phys.* **2009**, *9*, 3815.
- (3) Shilling, J. E.; Zaveri, R. A.; Fast, J. D.; Kleinman, L.; Alexander, M. L.; Canagaratna, M. R.; Fortner, E.; Hubbe, J. M.; Jayne, J. T.; Sedlacek, A.; Setyan, A.; Springston, S.; Worsnop, D. R.; Zhang, Q. *Atmos. Chem. Phys.* **2013**, *13*, 2091.
- (4) Finnlaysen-Pitts, B. J. a. J. N. P. J. *Chemistry of the Upper and Lower Atmosphere*; Academic Press: San Diego, CA, 2000.
- (5) Jain, S.; Zahardis, J.; Petrucci, G. A. *Environ Sci Technol* **2014**, *48*, 4835.
- (6) Zhao, D. F.; Kaminski, M.; Schlag, P.; Fuchs, H.; Acir, I. H.; Bohn, B.; Häsel, R.; Kiendler-Scharr, A.; Rohrer, F.; Tillmann, R.; Wang, M. J.; Wegener, R.; Wildt, J.; Wahner, A.; Mentel, T. F. *Atmos. Chem. Phys.* **2015**, *15*, 991.
- (7) Lee, A.; Goldstein, A. H.; Keywood, M. D.; Gao, S.; Varutbangkul, V.; Bahreini, R.; Ng, N. L.; Flagan, R. C.; Seinfeld, J. H. *Journal of Geophysical Research: Atmospheres* **2006**, *111*, D07302.
- (8) Ng, N. L.; Chhabra, P. S.; Chan, A. W. H.; Surratt, J. D.; Kroll, J. H.; Kwan, A. J.; McCabe, D. C.; Wennberg, P. O.; Sorooshian, A.; Murphy, S. M.; Dalleska, N. F.; Flagan, R. C.; Seinfeld, J. H. *Atmos. Chem. Phys.* **2007**, *7*, 5159.
- (9) Eddingsaas, N. C.; Loza, C. L.; Yee, L. D.; Chan, M.; Schilling, K. A.; Chhabra, P. S.; Seinfeld, J. H.; Wennberg, P. O. *Atmos Chem Phys* **2012**, *12*, 7413.
- (10) Seinfeld, J. H. a. S. N. P. *Atmospheric Chemistry and Physics: From Air Pollution to Climate Change*; 2 ed.; John Wiley and Sons, INC: Hoboken, N.J., 2006.
- (11) Jacob, D. J. *Introduction to Atmospheric Chemistry*; Princeton University Press: Princeton University, NJ, Chichester, West Sussex, United Kingdom, 1999.
- (12) Atkinson, R.; Arey, J. *Chem Rev* **2003**, *103*, 4605.
- (13) Hansel, A. K.; Ehrenhauser, F. S.; Richards-Henderson, N. K.; Anastasio, C.; Valsaraj, K. T. *Atmos Environ* **2015**, *102*, 43.
- (14) Peirone, S. A.; Barrera, J. A.; Taccone, R. A.; Cometto, P. M.; Lane, S. I. *Atmos Environ* **2014**, *85*, 92.
- (15) Aschmann, S. M.; Shu, Y.; Arey, J.; Atkinson, R. *Atmos Environ* **1997**, *31*, 3551.
- (16) Davis, M. E.; Burkholder, J. B. *Atmos. Chem. Phys.* **2011**, *11*, 3347.
- (17) Gibilisco, R. G.; Santiago, A. N.; Teruel, M. A. *Atmos Environ* **2013**, *77*, 358.
- (18) Kroll, J. H.; Ng, N. L.; Murphy, S. M.; Flagan, R. C.; Seinfeld, J. H. *Environ Sci Technol* **2006**, *40*, 1869.

- (19) Ng, N. L.; Chhabra, P. S.; Chan, A. W. H.; Surratt, J. D.; Kroll, J. H.; Kwan, A. J.; McCabe, D. C.; Wennberg, P. O.; Sorooshian, A.; Murphy, S. M.; Dalleska, N. F.; Flagan, R. C.; Seinfeld, J. H. *Atmos Chem Phys* **2007**, *7*, 5159.
- (20) Presto, A. A.; Hartz, K. E. H.; Donahue, N. M. *Environ Sci Technol* **2005**, *39*, 7036.
- (21) Ng, N. L.; Kroll, J. H.; Chan, A. W. H.; Chhabra, P. S.; Flagan, R. C.; Seinfeld, J. H. *Atmos Chem Phys* **2007**, *7*, 3909.
- (22) Kim, H.; Barkey, B.; Paulson, S. E. *J Phys Chem A* **2012**, *116*, 6059.
- (23) Hand, J. L.; Kreidenweis, S. M.; Kreisberg, N.; Hering, S.; Stolzenburg, M.; Dick, W.; McMurry, P. H. *Atmos Environ* **2002**, *36*, 1853.
- (24) Moosmüller, H.; Chakrabarty, R. K.; Arnott, W. P. *Journal of Quantitative Spectroscopy and Radiative Transfer* **2009**, *110*, 844.
- (25) Toole, J. R.; Renbaum-Wolff, L.; Smith, G. D. *Aerosol Sci Tech* **2013**, *47*, 955.
- (26) Lang-Yona, M.; Rudich, Y.; Segre, E.; Dinar, E.; Abo-Riziq, A. *Anal Chem* **2009**, *81*, 1762.
- (27) Li, J.; Sun, Y.; Cao, H.; Han, D.; He, M. *Struct Chem* **2014**, *25*, 71.
- (28) Wagner, F.; Silva, A. M. *Atmos. Chem. Phys.* **2008**, *8*, 481.
- (29) Reid, J. S.; Eck, T. F.; Christopher, S. A.; Hobbs, P. V.; Holben, B. *J Geophys Res-Atmos* **1999**, *104*, 27473.
- (30) Keywood, M. D.; Varutbangkul, V.; Bahreini, R.; Flagan, R. C.; Seinfeld, J. H. *Environ Sci Technol* **2004**, *38*, 4157.
- (31) Donahue, N. M.; Hartz, K. E. H.; Chuong, B.; Presto, A. A.; Stanier, C. O.; Rosenhorn, T.; Robinson, A. L.; Pandis, S. N. *Faraday Discuss* **2005**, *130*, 295.
- (32) Loza, C. L.; Craven, J. S.; Yee, L. D.; Coggon, M. M.; Schwantes, R. H.; Shiraiwa, M.; Zhang, X.; Schilling, K. A.; Ng, N. L.; Canagaratna, M. R.; Ziemann, P. J.; Flagan, R. C.; Seinfeld, J. H. *Atmos. Chem. Phys.* **2014**, *14*, 1423.

BIBLIOGRAPHY

- Aimanant, S.; Ziemann, P. J., Development of Spectrophotometric Methods for the Analysis of Functional Groups in Oxidized Organic Aerosol. *Aerosol Sci Tech* **2013**, *47*, (6), 581-591.
- Al Mulla, I.; Viera, L.; Morris, R.; Sidebottom, H.; Treacy, J.; Mellouki, A., Kinetics and Mechanisms for the Reactions of Ozone with Unsaturated Oxygenated Compounds. *Chemphyschem* **2010**, *11*, (18), 4069-4078.
- Andreae, M. O.; Crutzen, P. J., Atmospheric aerosols: Biogeochemical sources and role in atmospheric chemistry. *Science* **1997**, *276*, (5315), 1052-1058.
- Ariya, P. A.; Sun, J.; Eltouny, N. A.; Hudson, E. D.; Hayes, C. T.; Kos, G., Physical and chemical characterization of bioaerosols – Implications for nucleation processes. *International Reviews in Physical Chemistry* **2009**, *28*, (1), 1-32.
- Arnott, W. P.; Moosmüller, H.; Sheridan, P. J.; Ogren, J. A.; Raspet, R.; Slaton, W. V.; Hand, J. L.; Kreidenweis, S. M.; Collett, J. L., Photoacoustic and filter-based ambient aerosol light absorption measurements: Instrument comparisons and the role of relative humidity. *Journal of Geophysical Research: Atmospheres* **2003**, *108*, (D1), 4034.
- Aschmann, S. M.; Atkinson, R., Effect of Structure on the Rate Constants for Reaction of NO₃ Radicals with a Series of Linear and Branched C₅–C₇ 1-Alkenes at 296 ± 2 K. *The Journal of Physical Chemistry A* **2011**, *115*, (8), 1358-1363.
- Aschmann, S. M.; Shu, Y.; Arey, J.; Atkinson, R., Products of the gas-phase reactions of cis-3-hexen-1-ol with OH radicals and O₃. *Atmos Environ* **1997**, *31*, (21), 3551-3560.
- Atkinson, R.; Arey, J., Atmospheric degradation of volatile organic compounds. *Chem Rev* **2003**, *103*, (12), 4605-4638.
- Atkinson, R.; Arey, J.; Aschmann, S. M.; Corchnoy, S. B.; Shu, Y., Rate constants for the gas-phase reactions of cis-3-Hexen-1-ol, cis-3-Hexenylacetate, trans-2-Hexenal, and Linalool with OH and NO₃ radicals and O₃ at 296 ± 2 K, and OH radical formation yields from the O₃ reactions. *Int J Chem Kinet* **1995**, *27*, (10), 941-955.
- Atkinson, R.; Aschmann, S. M.; Carter, W. P. L.; Pitts, J. N., Effects of ring strain on gas-phase rate constants. I. Ozone reactions with cycloalkenes. *Int J Chem Kinet* **1983**, *15*, (8), 721-731.
- Aumont, B.; Camredon, M.; Mouchel-Vallon, C.; La, S.; Ouzebidou, F.; Valorso, R.; Lee-Taylor, J.; Madronich, S., Modeling the influence of alkane molecular structure on secondary organic aerosol formation. *Faraday Discuss* **2013**, *165*, (0), 105-122.
- Bahreini, R.; Ervens, B.; Middlebrook, A. M.; Warneke, C.; de Gouw, J. A.; DeCarlo, P. F.; Jimenez, J. L.; Brock, C. A.; Neuman, J. A.; Ryerson, T. B.; Stark, H.; Atlas, E.; Brioude, J.; Fried, A.; Holloway, J. S.; Peischl, J.; Richter, D.; Walega, J.; Weibring, P.; Wollny, A. G.; Fehsenfeld, F. C., Organic aerosol formation in urban and industrial plumes near Houston and Dallas, Texas. *J Geophys Res-Atmos* **2009**, *114*.

- Baker, B.; Sinnott, M., Analysis of sesquiterpene emissions by plants using solid phase microextraction. *J Chromatogr A* **2009**, *1216*, (48), 8442-8451.
- Baltaretu, C. O.; Lichtman, E. I.; Hadler, A. B.; Elrod, M. J., Primary Atmospheric Oxidation Mechanism for Toluene. *The Journal of Physical Chemistry A* **2009**, *113*, (1), 221-230.
- Bateman, A. P.; Bertram, A. K.; Martin, S. T., Hygroscopic Influence on the Semisolid-to-Liquid Transition of Secondary Organic Materials. *The Journal of Physical Chemistry A* **2015**, *119*, (19), 4386-4395.
- Benson, S. W., *Thermochemical Kinetics*. Wiley: New York, 1966.
- Bond, T. C.; Bergstrom, R. W., Light absorption by carbonaceous particles: An investigative review. *Aerosol Sci Tech* **2006**, *40*, (1), 27-67.
- Bones, D. L.; Henricksen, D. K.; Mang, S. A.; Gonsior, M.; Bateman, A. P.; Nguyen, T. B.; Cooper, W. J.; Nizkorodov, S. A., Appearance of strong absorbers and fluorophores in limonene-O₃ secondary organic aerosol due to NH₄⁺-mediated chemical aging over long time scales. *Journal of Geophysical Research: Atmospheres* **2010**, *115*, (D5), D05203.
- Boucher, O.; Randall, D.; rtaxo, P.; Bretherton, C.; Feingold, G.; Forster, P.; Kerminen, V.-M.; Kondo, Y.; Liao, H.; Lohmann, U.; Rasch, P.; Satheesh, S. K.; Stevens, B.; Zhang, X. Y. *The Physical Science Basis. Contribution of Working Group I to the Fifth Assessment Report of the Intergovernmental Panel on Climate Change*; Cambridge, United Kingdom and New York, NY, USA, 2013.
- Bouvier-Brown, N. C.; Holzinger, R.; Palitzsch, K.; Goldstein, A. H., Quantifying sesquiterpene and oxygenated terpene emissions from live vegetation using solid-phase microextraction fibers. *J Chromatogr A* **2007**, *1161*, (1-2), 113-120.
- Boyd, A. A.; Villenave, E.; Lesclaux, R., Self- and cross-reactions of β -hydroxyperoxy radicals of relevance to tropospheric monoterpene oxidation: structure–activity relationships for rate coefficients. *Atmos Environ* **2003**, *37*, (20), 2751-2760.
- Brilli, F.; Hörtnagl, L.; Bamberger, I.; Schnitzhofer, R.; Ruuskanen, T. M.; Hansel, A.; Loreto, F.; Wohlfahrt, G., Qualitative and Quantitative Characterization of Volatile Organic Compound Emissions from Cut Grass. *Environ Sci Technol* **2012**, *46*, (7), 3859-3865.
- Brilli, F.; Ruuskanen, T. M.; Schnitzhofer, R.; Müller, M.; Breitenlechner, M.; Bittner, V.; Wohlfahrt, G.; Loreto, F.; Hansel, A., Detection of Plant Volatiles after Leaf Wounding and Darkening by Proton Transfer Reaction “Time-of-Flight” Mass Spectrometry (PTR-TOF). *Plos One* **2011**, *6*, (5), e20419.
- Calvert, J. G.; Atkinson, R.; Kerr, J. A.; Madronich, S.; Moortgat, G.; Wallington, T. J.; Yarwood, G., *The Mechanisms of Atmospheric Oxidation of the Alkenes*. Oxford University Press: New York, Oxford, 2000.

- Cappa, C. D.; Che, D. L.; Kessler, S. H.; Kroll, J. H.; Wilson, K. R., Variations in organic aerosol optical and hygroscopic properties upon heterogeneous OH oxidation. *Journal of Geophysical Research: Atmospheres* **2011**, *116*, (D15), D15204.
- Carlton, A. G.; Wiedinmyer, C.; Kroll, J. H., A review of Secondary Organic Aerosol (SOA) formation from isoprene. *Atmos. Chem. Phys.* **2009**, *9*, (14), 4987-5005.
- Chan, M. N.; Kreidenweis, S. M.; Chan, C. K., Measurements of the Hygroscopic and Deliquescence Properties of Organic Compounds of Different Solubilities in Water and Their Relationship with Cloud Condensation Nuclei Activities. *Environ Sci Technol* **2008**, *42*, (10), 3602-3608.
- Chang, K. H.; Chen, T. F.; Huang, H. C., Estimation of biogenic volatile organic compounds emissions in subtropical island - Taiwan. *Sci Total Environ* **2005**, *346*, (1-3), 184-199.
- Chen, J.; Zhao, C. S.; Ma, N.; Yan, P., Aerosol hygroscopicity parameter derived from the light scattering enhancement factor measurements in the North China Plain. *Atmos. Chem. Phys.* **2014**, *14*, (15), 8105-8118.
- Chen, Q.; Liu, Y. J.; Donahue, N. M.; Shilling, J. E.; Martin, S. T., Particle-Phase Chemistry of Secondary Organic Material: Modeled Compared to Measured O:C and H:C Elemental Ratios Provide Constraints. *Environ Sci Technol* **2011**, *45*, (11), 4763-4770.
- Chen, Z. M.; Wang, H. L.; Zhu, L. H.; Wang, C. X.; Jie, C. Y.; Hua, W., Aqueous-phase ozonolysis of methacrolein and methyl vinyl ketone: a potentially important source of atmospheric aqueous oxidants. *Atmos. Chem. Phys.* **2008**, *8*, (8), 2255-2265.
- Chow, J. C.; Watson, J. G.; Lu, Z.; Lowenthal, D. H.; Frazier, C. A.; Solomon, P. A.; Thuillier, R. H.; Magliano, K., Descriptive analysis of PM_{2.5} and PM₁₀ at regionally representative locations during SJVAQS/AUSPEX. *Atmos Environ* **1996**, *30*, (12), 2079-2112.
- Clarke, A. D.; Noone, K. J.; Heintzenberg, J.; Warren, S. G.; Covert, D. S., Aerosol Light-Absorption Measurement Techniques - Analysis and Intercomparisons. *Atmos Environ* **1987**, *21*, (6), 1455-1465.
- Cocker, D. R.; Flagan, R. C.; Seinfeld, J. H., State-of-the-Art Chamber Facility for Studying Atmospheric Aerosol Chemistry. *Environ Sci Technol* **2001**, *35*, (12), 2594-2601.
- Cooper, O. R.; Parrish, D. D.; Ziemke, J.; Balashov, N. V.; Cuperio, M.; Galbally, I. E.; Gilge, S.; Horowitz, L.; Jensen, N. R.; Lamarque, J. F.; Naik, V.; Oltmans, S. J.; Schwab, J.; Shindell, D.; Thompson, A. M.; Thouret, V.; Wang, Y.; Zbinden, R. M., Global distribution and trends of tropospheric ozone: An observation-based review. *Elementa Science of the Anthropocene* **July 10, 2014**, *2*, (000029).
- Cornu, A.; Carnat, A.-P.; Martin, B.; Coulon, J.-B.; Lamaison, J.-L.; Berdagué, J.-L., Solid-Phase Microextraction of Volatile Components from Natural Grassland Plants. *J Agr Food Chem* **2001**, *49*, (1), 203-209.

- Covert, D. S.; Charlson, R. J.; Ahlquist, N. C., A Study of the Relationship of Chemical Composition and Humidity to Light Scattering by Aerosols. *Journal of Applied Meteorology* **1972**, *11*, (6), 968-976.
- Crouse, J. D.; Nielsen, L. B.; Jørgensen, S.; Kjaergaard, H. G.; Wennberg, P. O., Autoxidation of Organic Compounds in the Atmosphere. *The Journal of Physical Chemistry Letters* **2013**, *4*, (20), 3513-3520.
- Cusick, R. D.; Atkinson, R., Rate constants for the gas-phase reactions of O₃ with a series of cycloalkenes at 296 ± 2 K. *Int J Chem Kinet* **2005**, *37*, (3), 183-190.
- Davis, M. E.; Burkholder, J. B., Rate coefficients for the gas-phase reaction of OH with (Z)-3-hexen-1-ol, 1-penten-3-ol, (E)-2-penten-1-ol, and (E)-2-hexen-1-ol between 243 and 404 K. *Atmos. Chem. Phys.* **2011**, *11*, (7), 3347-3358.
- de Gouw, J. A.; Howard, C. J.; Custer, T. G.; Fall, R., Emissions of volatile organic compounds from cut grass and clover are enhanced during the drying process. *Geophysical Research Letters* **1999**, *26*, (7), 811-814.
- DeCarlo, P. F.; Slowik, J. G.; Worsnop, D. R.; Davidovits, P.; Jimenez, J. L., Particle Morphology and Density Characterization by Combined Mobility and Aerodynamic Diameter Measurements. Part 1: Theory. *Aerosol Sci Tech* **2004**, *38*, (12), 1185-1205.
- Denjean, C.; Formenti, P.; Picquet-Varrault, B.; Pangui, E.; Zapf, P.; Katrib, Y.; Giorio, C.; Tapparo, A.; Monod, A.; Temime-Roussel, B.; Decorse, P.; Mangeney, C.; Doussin, J. F., Relating hygroscopicity and optical properties to chemical composition and structure of secondary organic aerosol particles generated from the ozonolysis of α -pinene. *Atmos. Chem. Phys. Discuss.* **2014**, *14*, (7), 10543-10596.
- Diaz, E. A.; Lemos, M.; Coull, B.; Long, M. S.; Rohr, A. C.; Ruiz, P.; Gupta, T.; Kang, C. M.; Godleski, J. J., Toxicological Evaluation of Realistic Emission Source Aerosols (TERESA)-Power plant studies: assessment of breathing pattern. *Inhal Toxicol* **2011**, *23*, 42-59.
- Donahue, N. M.; Drozd, G. T.; Epstein, S. A.; Presto, A. A.; Kroll, J. H., Adventures in ozoneland: down the rabbit-hole. *Phys Chem Chem Phys* **2011**, *13*, (23), 10848-10857.
- Donahue, N. M.; Hartz, K. E. H.; Chuong, B.; Presto, A. A.; Stanier, C. O.; Rosenhorn, T.; Robinson, A. L.; Pandis, S. N., Critical factors determining the variation in SOA yields from terpene ozonolysis: A combined experimental and computational study. *Faraday Discuss* **2005**, *130*, 295-309.
- Donahue, N. M.; Tischuk, J. E.; Marquis, B. J.; Huff Hartz, K. E., Secondary organic aerosol from limona ketone: insights into terpene ozonolysis via synthesis of key intermediates. *Phys Chem Chem Phys* **2007**, *9*, (23), 2991-2998.
- Eddingsaas, N. C.; Loza, C. L.; Yee, L. D.; Chan, M.; Schilling, K. A.; Chhabra, P. S.; Seinfeld, J. H.; Wennberg, P. O., α -pinene photooxidation under controlled chemical conditions - Part 2: SOA yield and composition in low- and high-NO_x environments. *Atmos Chem Phys* **2012**, *12*, (16), 7413-7427.

- Ehn, M.; Kleist, E.; Junninen, H.; Petäjä, T.; Lönn, G.; Schobesberger, S.; Dal Maso, M.; Trimborn, A.; Kulmala, M.; Worsnop, D. R.; Wahner, A.; Wildt, J.; Mentel, T. F., Gas phase formation of extremely oxidized pinene reaction products in chamber and ambient air. *Atmos. Chem. Phys.* **2012**, *12*, (11), 5113-5127.
- Ehn, M.; Thornton, J. A.; Kleist, E.; Sipila, M.; Junninen, H.; Pullinen, I.; Springer, M.; Rubach, F.; Tillmann, R.; Lee, B.; Lopez-Hilfiker, F.; Andres, S.; Acir, I.-H.; Rissanen, M.; Jokinen, T.; Schobesberger, S.; Kangasluoma, J.; Kontkanen, J.; Nieminen, T.; Kurten, T.; Nielsen, L. B.; Jorgensen, S.; Kjaergaard, H. G.; Canagaratna, M.; Maso, M. D.; Berndt, T.; Petaja, T.; Wahner, A.; Kerminen, V.-M.; Kulmala, M.; Worsnop, D. R.; Wildt, J.; Mentel, T. F., A large source of low-volatility secondary organic aerosol. *Nature* **2014**, *506*, (7489), 476-479.
- Emanuelsson, E. U.; Hallquist, M.; Kristensen, K.; Glasius, M.; Bohn, B.; Fuchs, H.; Kammer, B.; Kiendler-Scharr, A.; Nehr, S.; Rubach, F.; Tillmann, R.; Wahner, A.; Wu, H. C.; Mentel, T. F., Formation of anthropogenic secondary organic aerosol (SOA) and its influence on biogenic SOA properties. *Atmos. Chem. Phys.* **2013**, *13*, (5), 2837-2855.
- Epstein, S. A.; Donahue, N. M., Ozonolysis of Cyclic Alkenes as Surrogates for Biogenic Terpenes: Primary Ozonide Formation and Decomposition. *The Journal of Physical Chemistry A* **2010**, *114*, (28), 7509-7515.
- Ervens, B.; Cubison, M.; Andrews, E.; Feingold, G.; Ogren, J. A.; Jimenez, J. L.; DeCarlo, P.; Nenes, A., Prediction of cloud condensation nucleus number concentration using measurements of aerosol size distributions and composition and light scattering enhancement due to humidity. *Journal of Geophysical Research: Atmospheres* **2007**, *112*, (D10), D10S32.
- Esteban, J. L.; MartinezCastro, I.; Morales, R.; Fabrellas, B.; Sanz, J., Rapid identification of volatile compounds in aromatic plants by automatic thermal desorption-GC-MS. *Chromatographia* **1996**, *43*, (1-2), 63-72.
- Fierz-Schmidhauser, R.; Zieger, P.; Wehrle, G.; Jefferson, A.; Ogren, J. A.; Baltensperger, U.; Weingartner, E., Measurement of relative humidity dependent light scattering of aerosols. *Atmos. Meas. Tech.* **2010**, *3*, (1), 39-50.
- Finnlayson-Pitts, B. J. a. J. N. P. J., *Chemistry of the Upper and Lower Atmosphere*. Academic Press: San Diego, CA, 2000.
- Flores, J. M.; Washenfelder, R. A.; Adler, G.; Lee, H. J.; Segev, L.; Laskin, J.; Laskin, A.; Nizkorodov, S. A.; Brown, S. S.; Rudich, Y., Complex refractive indices in the near-ultraviolet spectral region of biogenic secondary organic aerosol aged with ammonia. *Phys Chem Chem Phys* **2014**, *16*, (22), 10629-10642.
- Flores, J. M.; Zhao, D. F.; Segev, L.; Schlag, P.; Kiendler-Scharr, A.; Fuchs, H.; Watne, Å. K.; Bluvshstein, N.; Mentel, T. F.; Hallquist, M.; Rudich, Y., Evolution of the complex refractive index in the UV spectral region in ageing secondary organic aerosol. *Atmos. Chem. Phys.* **2014**, *14*, (11), 5793-5806.

- Gäb, S.; Turner, W. V.; Wolff, S.; Becker, K. H.; Ruppert, L.; Brockmann, K. J., Formation of alkyl and hydroxyalkyl hydroperoxides on ozonolysis in water and in air. *Atmos Environ* **1995**, *29*, (18), 2401-2407.
- Gao, S.; Keywood, M.; Ng, N. L.; Surratt, J.; Varutbangkul, V.; Bahreini, R.; Flagan, R. C.; Seinfeld, J. H., Low-Molecular-Weight and Oligomeric Components in Secondary Organic Aerosol from the Ozonolysis of Cycloalkenes and α -Pinene. *The Journal of Physical Chemistry A* **2004**, *108*, (46), 10147-10164.
- Geddes, S.; Nichols, B.; Flemer, S.; Eisenhauer, J.; Zahardis, J.; Petrucci, G. A., Near-Infrared Laser Desorption/Ionization Aerosol Mass Spectrometry for Investigating Primary and Secondary Organic Aerosols under Low Loading Conditions. *Anal Chem* **2010**, *82*, (19), 7915-7923.
- Gettelman, A.; Liu, X.; Barahona, D.; Lohmann, U.; Chen, C., Climate impacts of ice nucleation. *Journal of Geophysical Research: Atmospheres* **2012**, *117*, (D20), n/a-n/a.
- Ghorai, S.; Laskin, A.; Tivanski, A. V., Spectroscopic Evidence of Keto–Enol Tautomerism in Deliquesced Malonic Acid Particles. *The Journal of Physical Chemistry A* **2011**, *115*, (17), 4373-4380.
- Gibilisco, R. G.; Blanco, M. a. B.; Bejan, I.; Barnes, I.; Wiesen, P.; Teruel, M. A., Atmospheric Sink of (E)-3-Hexen-1-ol, (Z)-3-Hepten-1-ol, and (Z)-3-Octen-1-ol: Rate Coefficients and Mechanisms of the OH-Radical Initiated Degradation. *Environ Sci Technol* **2015**, *49*, (13), 7717-7725.
- Gibilisco, R. G.; Santiago, A. N.; Teruel, M. A., OH-initiated degradation of a series of hexenols in the troposphere. Rate coefficients at 298 K and 1 atm. *Atmos Environ* **2013**, *77*, 358-364.
- Godoi, R. H. M.; Godoi, A. F. L.; Worobiec, A.; Andrade, S. J.; de Hoog, J.; Santiago-Silva, M. R.; Van Grieken, R., Characterisation of sugar cane combustion particles in the Araraquara region, Southeast Brazil. *Microchim Acta* **2004**, *145*, (1-4), 53-56.
- Goldstein, A. H.; Galbally, I. E., Known and unexplored organic constituents in the earth's atmosphere. *Environ Sci Technol* **2007**, *41*, (5), 1514-1521.
- Greene, C. R.; Atkinson, R., Rate Constants for the Gas-Phase Reactions of O₃ with a Series of Alkenes at 296-K \pm 2-K. *Int J Chem Kinet* **1992**, *24*, (9), 803-811.
- Grosjean, E.; Grosjean, D., Rate constants for the gas-phase reactions of Ozone with unsaturated Aliphatic Alcohols. *Int J Chem Kinet* **1994**, *26*, (12), 1185-1191.
- Grosjean, E.; Grosjean, D., The gas phase reaction of unsaturated oxygenates with ozone: Carbonyl products and comparison with the alkene-ozone reaction. *J Atmos Chem* **1997**, *27*, (3), 271-289.
- Grosjean, E.; Grosjean, D., Rate constants for the gas-phase reaction of ozone with unsaturated oxygenates. *Int J Chem Kinet* **1998**, *30*, (1), 21-29.

- Grosjean, E.; Grosjean, D.; Seinfeld, J. H., Gas-phase reaction of ozone with trans-2-hexenal, trans-2-hexenyl acetate, ethylvinyl ketone, and 6-methyl-5-hepten-2-one. *Int J Chem Kinet* **1996**, *28*, (5), 373-382.
- Guenther, A.; Geron, C.; Pierce, T.; Lamb, B.; Harley, P.; Fall, R., Natural emissions of non-methane volatile organic compounds, carbon monoxide, and oxides of nitrogen from North America. *Atmos Environ* **2000**, *34*, (12-14), 2205-2230.
- Guenther, A.; Hewitt, C. N.; Erickson, D.; Fall, R.; Geron, C.; Graedel, T.; Harley, P.; Klinger, L.; Lerdau, M.; McKay, W. A.; Pierce, T.; Scholes, B.; Steinbrecher, R.; Tallamraju, R.; Taylor, J.; Zimmerman, P., A global model of natural volatile organic compound emissions. *Journal of Geophysical Research: Atmospheres* **1995**, *100*, (D5), 8873-8892.
- Guenther, A.; Karl, T.; Harley, P.; Wiedinmyer, C.; Palmer, P. I.; Geron, C., Estimates of global terrestrial isoprene emissions using MEGAN (Model of Emissions of Gases and Aerosols from Nature). *Atmos. Chem. Phys.* **2006**, *6*, (11), 3181-3210.
- Guenther, A. B.; Jiang, X.; Heald, C. L.; Sakulyanontvittaya, T.; Duhl, T.; Emmons, L. K.; Wang, X., The Model of Emissions of Gases and Aerosols from Nature version 2.1 (MEGAN2.1): an extended and updated framework for modeling biogenic emissions. *Geosci. Model Dev.* **2012**, *5*, (6), 1471-1492.
- Hall, D.; Wu, C.-Y.; Hsu, Y.-M.; Stormer, J.; Engling, G.; Capeto, K.; Wang, J.; Brown, S.; Li, H.-W.; Yu, K.-M., PAHs, carbonyls, VOCs and PM_{2.5} emission factors for pre-harvest burning of Florida sugarcane. *Atmos Environ* **2012**, *55*, (0), 164-172.
- Hallquist, M.; Wenger, J. C.; Baltensperger, U.; Rudich, Y.; Simpson, D.; Claeys, M.; Dommen, J.; Donahue, N. M.; George, C.; Goldstein, A. H.; Hamilton, J. F.; Herrmann, H.; Hoffmann, T.; Iinuma, Y.; Jang, M.; Jenkin, M. E.; Jimenez, J. L.; Kiendler-Scharr, A.; Maenhaut, W.; McFiggans, G.; Mentel, T. F.; Monod, A.; Prévôt, A. S. H.; Seinfeld, J. H.; Surratt, J. D.; Szmigielski, R.; Wildt, J., The formation, properties and impact of secondary organic aerosol: current and emerging issues. *Atmos. Chem. Phys.* **2009**, *9*, (14), 5155-5236.
- Hamilton, J. F.; Lewis, A. C.; Carey, T. J.; Wenger, J. C., Characterization of Polar Compounds and Oligomers in Secondary Organic Aerosol Using Liquid Chromatography Coupled to Mass Spectrometry. *Anal Chem* **2007**, *80*, (2), 474-480.
- Hamilton, J. F.; Lewis, A. C.; Carey, T. J.; Wenger, J. C.; Borrás i Garcia, E.; Muñoz, A., Reactive oxidation products promote secondary organic aerosol formation from green leaf volatiles. *Atmos. Chem. Phys.* **2009**, *9*, (11), 3815-3823.
- Hand, J. L.; Kreidenweis, S. M.; Kreisberg, N.; Hering, S.; Stolzenburg, M.; Dick, W.; McMurry, P. H., Comparisons of aerosol properties measured by impactors and light scattering from individual particles: refractive index, number and volume concentrations, and size distributions. *Atmos Environ* **2002**, *36*, (11), 1853-1861.
- Hansel, A. K.; Ehrenhauser, F. S.; Richards-Henderson, N. K.; Anastasio, C.; Valsaraj, K. T., Aqueous-phase oxidation of green leaf volatiles by hydroxyl radical as a source of

- SOA: Product identification from methyl jasmonate and methyl salicylate oxidation. *Atmos Environ* **2015**, *102*, (0), 43-51.
- Hartikainen, K.; Riikonen, J.; Nerg, A.-M.; Kivimäenpää, M.; Ahonen, V.; Tervahauta, A.; Kärenlampi, S.; Mäenpää, M.; Rousi, M.; Kontunen-Soppela, S.; Oksanen, E.; Holopainen, T., Impact of elevated temperature and ozone on the emission of volatile organic compounds and gas exchange of silver birch (*Betula pendula* Roth). *Environ Exp Bot* **2012**, *84*, 33-43.
- Harvey, R. M.; Petrucci, G. A., Control of ozonolysis kinetics and aerosol yield by nuances in the molecular structure of volatile organic compounds. *Atmos Environ* **2015**, *122*, 188-195.
- Harvey, R. M.; Zahardis, J.; Petrucci, G. A., Establishing the contribution of lawn mowing to atmospheric aerosol levels in American suburbs. *Atmos. Chem. Phys.* **2014**, *14*, (2), 797-812.
- Hatanaka, A., The Biogenesis of Green Odor by Green Leaves. *Phytochemistry* **1993**, *34*, (5), 1201-1218.
- Haywood, J.; Boucher, O., Estimates of the direct and indirect radiative forcing due to tropospheric aerosols: A review. *Rev Geophys* **2000**, *38*, (4), 513-543.
- Heald, C. L.; Jacob, D. J.; Park, R. J.; Russell, L. M.; Huebert, B. J.; Seinfeld, J. H.; Liao, H.; Weber, R. J., A large organic aerosol source in the free troposphere missing from current models. *Geophysical Research Letters* **2005**, *32*, (18), L18809.
- Hecobian, A.; Zhang, X.; Zheng, M.; Frank, N.; Edgerton, E. S.; Weber, R. J., Water-Soluble Organic Aerosol material and the light-absorption characteristics of aqueous extracts measured over the Southeastern United States. *Atmos. Chem. Phys.* **2010**, *10*, (13), 5965-5977.
- Heintzenberg, J.; Charlson, R. J., Design and Applications of the Integrating Nephelometer: A Review. *J Atmos Ocean Tech* **1996**, *13*, (5), 987-1000.
- Hildebrandt, L.; Henry, K. M.; Kroll, J. H.; Worsnop, D. R.; Pandis, S. N.; Donahue, N. M., Evaluating the Mixing of Organic Aerosol Components Using High-Resolution Aerosol Mass Spectrometry. *Environ Sci Technol* **2011**, *45*, (15), 6329-6335.
- Hinds, W., *Aerosol Technology, Properties Behavior and Measurement of Airborne Particles*. John Wiley and Sons: 1982.
- Hodas, N.; Zuend, A.; Mui, W.; Flagan, R. C.; Seinfeld, J. H., Influence of particle-phase state on the hygroscopic behavior of mixed organic-inorganic aerosols. *Atmos. Chem. Phys.* **2015**, *15*, (9), 5027-5045.
- Hoffer, A.; Gelencsér, A.; Guyon, P.; Kiss, G.; Schmid, O.; Frank, G. P.; Artaxo, P.; Andreae, M. O., Optical properties of humic-like substances (HULIS) in biomass-burning aerosols. *Atmos. Chem. Phys.* **2006**, *6*, (11), 3563-3570.
- Hoyle, C. R.; Boy, M.; Donahue, N. M.; Fry, J. L.; Glasius, M.; Guenther, A.; Hallar, A. G.; Huff Hartz, K.; Petters, M. D.; Petäjä, T.; Rosenoern, T.; Sullivan, A. P., A review

- of the anthropogenic influence on biogenic secondary organic aerosol. *Atmos. Chem. Phys.* **2011**, *11*, (1), 321-343.
- Jacob, D. J., *Introduction to Atmospheric Chemistry*. Princeton University Press: Princeton University, NJ, Chichester, West Sussex, United Kingdom, 1999.
- Jain, S.; Petrucci, G. A., A New Method to Measure Aerosol Particle Bounce Using a Cascade Electrical Low Pressure Impactor. *Aerosol Sci Tech* **2015**, *49*, (6), 390-399.
- Jain, S.; Zahardis, J.; Petrucci, G. A., Soft Ionization Chemical Analysis of Secondary Organic Aerosol from Green Leaf Volatiles Emitted by Turf Grass. *Environ Sci Technol* **2014**.
- Jardine, K.; Barron-Gafford, G. A.; Norman, J. P.; Abrell, L.; Monson, R. K.; Meyers, K. T.; Pavao-Zuckerman, M.; Dontsova, K.; Kleist, E.; Werner, C.; Huxman, T. E., Green leaf volatiles and oxygenated metabolite emission bursts from mesquite branches following light–dark transitions. *Photosynth Res* **2012**, *113*, (1-3), 321-333.
- Jathar, S. H.; Miracolo, M. A.; Tkacik, D. S.; Donahue, N. M.; Adams, P. J.; Robinson, A. L., Secondary Organic Aerosol Formation from Photo-Oxidation of Unburned Fuel: Experimental Results and Implications for Aerosol Formation from Combustion Emissions. *Environ Sci Technol* **2013**, *47*, (22), 12886-12893.
- Jayne, J. T.; Leard, D. C.; Zhang, X.; Davidovits, P.; Smith, K. A.; Kolb, C. E.; Worsnop, D. R., Development of an Aerosol Mass Spectrometer for Size and Composition Analysis of Submicron Particles. *Aerosol Sci Tech* **2000**, *33*, (1-2), 49-70.
- Jo, D. S.; Park, R. J.; Kim, M. J.; Spracklen, D. V., Effects of chemical aging on global secondary organic aerosol using the volatility basis set approach. *Atmos Environ* **2013**, *81*, 230-244.
- Johnson, D.; Rickard, A. R.; McGill, C. D.; Marston, G., The influence of orbital asymmetry on the kinetics of the gas-phase reactions of ozone with unsaturated compounds. *Phys Chem Chem Phys* **2000**, *2*, (3), 323-328.
- Jokinen, T.; Sipilä, M.; Richters, S.; Kerminen, V.-M.; Paasonen, P.; Stratmann, F.; Worsnop, D.; Kulmala, M.; Ehn, M.; Herrmann, H.; Berndt, T., Rapid Autoxidation Forms Highly Oxidized RO₂ Radicals in the Atmosphere. *Angewandte Chemie International Edition* **2014**, *53*, (52), 14596-14600.
- Joutsensaari, J.; Yli-Pirilä, P.; Korhonen, H.; Arola, A.; Blande, J. D.; Heijari, J.; Kivimäenpää, M.; Mikkonen, S.; Hao, L.; Miettinen, P.; Lyytikäinen-Saarenmaa, P.; Faiola, C. L.; Laaksonen, A.; Holopainen, J. K., Biotic stress accelerates formation of climate-relevant aerosols in boreal forests. *Atmos. Chem. Phys.* **2015**, *15*, (21), 12139-12157.
- Kallenbach, M.; Oh, Y.; Eilers, E. J.; Veit, D.; Baldwin, I. T.; Schuman, M. C., A robust, simple, high-throughput technique for time-resolved plant volatile analysis in field experiments. *Plant J* **2014**, *78*, (6), 1060-1072.

- Kanakidou, M.; Seinfeld, J. H.; Pandis, S. N.; Barnes, I.; Dentener, F. J.; Facchini, M. C.; Van Dingenen, R.; Ervens, B.; Nenes, A.; Nielsen, C. J.; Swietlicki, E.; Putaud, J. P.; Balkanski, Y.; Fuzzi, S.; Horth, J.; Moortgat, G. K.; Winterhalter, R.; Myhre, C. E. L.; Tsigaridis, K.; Vignati, E.; Stephanou, E. G.; Wilson, J., Organic aerosol and global climate modelling: a review. *Atmos. Chem. Phys.* **2005**, *5*, (4), 1053-1123.
- Karl, T.; Harren, F.; Warneke, C.; de Gouw, J.; Grayless, C.; Fall, R., Senescing grass crops as regional sources of reactive volatile organic compounds. *J Geophys Res-Atmos* **2005**, *110*, (D15).
- Kaufman, Y. J., Satellite observations of natural and anthropogenic aerosol effects on clouds and climate. *Space Sci Rev* **2006**, *125*, (1-4), 139-147.
- Keyword, M. D.; Varutbangkul, V.; Bahreini, R.; Flagan, R. C.; Seinfeld, J. H., Secondary Organic Aerosol Formation from the Ozonolysis of Cycloalkenes and Related Compounds. *Environ Sci Technol* **2004**, *38*, (15), 4157-4164.
- Khamaganov, V. G.; Hites, R. A., Rate Constants for the Gas-Phase Reactions of Ozone with Isoprene, α - and β -Pinene, and Limonene as a Function of Temperature. *The Journal of Physical Chemistry A* **2001**, *105*, (5), 815-822.
- Kidd, C.; Perraud, V.; Wingen, L. M.; Finlayson-Pitts, B. J., Integrating phase and composition of secondary organic aerosol from the ozonolysis of alpha-pinene. *P Natl Acad Sci USA* **2014**, *111*, (21), 7552-7557.
- Kim, H.; Barkey, B.; Paulson, S. E., Real Refractive Indices and Formation Yields of Secondary Organic Aerosol Generated from Photooxidation of Limonene and alpha-Pinene: The Effect of the HC/NO_x Ratio. *J Phys Chem A* **2012**, *116*, (24), 6059-6067.
- Kim, H.; Liu, S.; Russell, L. M.; Paulson, S. E., Dependence of Real Refractive Indices on O:C, H:C and Mass Fragments of Secondary Organic Aerosol Generated from Ozonolysis and Photooxidation of Limonene and α -Pinene. *Aerosol Sci Tech* **2014**, *48*, (5), 498-507.
- Kim, H.; Paulson, S. E., Real refractive indices and volatility of secondary organic aerosol generated from photooxidation and ozonolysis of limonene, α -pinene and toluene. *Atmos. Chem. Phys.* **2013**, *13*, (15), 7711-7723.
- Kirstine, W.; Galbally, I.; Ye, Y.; Hooper, M., Emissions of volatile organic compounds (primarily oxygenated species) from pasture. *Journal of Geophysical Research: Atmospheres* **1998**, *103*, (D9), 10605-10619.
- Kirstine, W. V.; Galbally, I. E., A Simple Model for Estimating Emissions of Volatile Organic Compounds from Grass and Cut Grass in Urban Airsheds and Its Application to Two Australian Cities. *J Air Waste Manage* **2004**, *54*, (10), 1299-1311.
- Koziel, J. A.; Pawliszyn, J., Air Sampling and Analysis of Volatile Organic Compounds with Solid Phase Microextraction. *J Air Waste Manage* **2001**, *51*, (2), 173-184.

- Kroll, J. H.; Ng, N. L.; Murphy, S. M.; Flagan, R. C.; Seinfeld, J. H., Secondary organic aerosol formation from isoprene photooxidation. *Environ Sci Technol* **2006**, *40*, (6), 1869-1877.
- Kroll, J. H.; Seinfeld, J. H., Chemistry of secondary organic aerosol: Formation and evolution of low-volatility organics in the atmosphere. *Atmos Environ* **2008**, *42*, (16), 3593-3624.
- Laden, F.; Neas, L. M.; Dockery, D. W.; Schwartz, J., Association of fine particulate matter from different sources with daily mortality in six US cities. *Environ Health Persp* **2000**, *108*, (10), 941-947.
- Lambe, A. T.; Cappa, C. D.; Massoli, P.; Onasch, T. B.; Forestieri, S. D.; Martin, A. T.; Cummings, M. J.; Croasdale, D. R.; Brune, W. H.; Worsnop, D. R.; Davidovits, P., Relationship between Oxidation Level and Optical Properties of Secondary Organic Aerosol. *Environ Sci Technol* **2013**, *47*, (12), 6349-6357.
- Lang-Yona, M.; Rudich, Y.; Segre, E.; Dinar, E.; Abo-Riziq, A., Complex Refractive Indices of Aerosols Retrieved by Continuous Wave-Cavity Ring Down Aerosol Spectrometer. *Anal Chem* **2009**, *81*, (5), 1762-1769.
- Lara, L. L.; Artaxo, P.; Martinelli, L. A.; Camargo, P. B.; Victoria, R. L.; Ferraz, E. S. B., Properties of aerosols from sugar-cane burning emissions in Southeastern Brazil. *Atmos Environ* **2005**, *39*, (26), 4627-4637.
- Laskin, J.; Laskin, A.; Roach, P. J.; Slysz, G. W.; Anderson, G. A.; Nizkorodov, S. A.; Bones, D. L.; Nguyen, L. Q., High-Resolution Desorption Electrospray Ionization Mass Spectrometry for Chemical Characterization of Organic Aerosols. *Anal Chem* **2010**, *82*, (5), 2048-2058.
- Leather, K. E.; McGillen, M. R.; Percival, C. J., Temperature-dependent ozonolysis kinetics of selected alkenes in the gas phase: an experimental and structure-activity relationship (SAR) study. *Phys Chem Chem Phys* **2010**, *12*, (12), 2935-2943.
- Lee, A.; Goldstein, A. H.; Keywood, M. D.; Gao, S.; Varutbangkul, V.; Bahreini, R.; Ng, N. L.; Flagan, R. C.; Seinfeld, J. H., Gas-phase products and secondary aerosol yields from the ozonolysis of ten different terpenes. *Journal of Geophysical Research: Atmospheres* **2006**, *111*, (D7), D07302.
- Lee, J. D.; Lewis, A. C.; Monks, P. S.; Jacob, M.; Hamilton, J. F.; Hopkins, J. R.; Watson, N. M.; Saxton, J. E.; Ennis, C.; Carpenter, L. J.; Carslaw, N.; Fleming, Z.; Bandy, B. J.; Oram, D. E.; Penkett, S. A.; Slemr, J.; Norton, E.; Rickard, A. R.; Whalley, L. K.; Heard, D. E.; Bloss, W. J.; Gravestock, T.; Smith, S. C.; Stanton, J.; Pilling, M. J.; Jenkin, M. E., Ozone photochemistry and elevated isoprene during the UK heatwave of August 2003. *Atmos Environ* **2006**, *40*, (39), 7598-7613.
- Leskinen, A.; Yli-Pirilä, P.; Kuusalo, K.; Sippula, O.; Jalava, P.; Hirvonen, M. R.; Jokiniemi, J.; Virtanen, A.; Komppula, M.; Lehtinen, K. E. J., Characterization and testing of a new environmental chamber. *Atmos. Meas. Tech.* **2015**, *8*, (6), 2267-2278.

- Li, J.; Sun, Y.; Cao, H.; Han, D.; He, M., Mechanisms and kinetics of the ozonolysis reaction of cis-3-hexenyl acetate and trans-2-hexenyl acetate in atmosphere: a theoretical study. *Struct Chem* **2014**, *25*, (1), 71-83.
- Li, K.; Wang, W.; Ge, M.; Li, J.; Wang, D., Optical properties of secondary organic aerosols generated by photooxidation of aromatic hydrocarbons. *Sci. Rep.* **2014**, *4*.
- Lim, Y. B.; Ziemann, P. J., Effects of Molecular Structure on Aerosol Yields from OH Radical-Initiated Reactions of Linear, Branched, and Cyclic Alkanes in the Presence of NOx. *Environ Sci Technol* **2009**, *43*, (7), 2328-2334.
- Lin, Y.-H.; Budisulistiorini, S. H.; Chu, K.; Siejack, R. A.; Zhang, H.; Riva, M.; Zhang, Z.; Gold, A.; Kautzman, K. E.; Surratt, J. D., Light-Absorbing Oligomer Formation in Secondary Organic Aerosol from Reactive Uptake of Isoprene Epoxydiols. *Environ Sci Technol* **2014**, *48*, (20), 12012-12021.
- Linderman, J., High yields, low prices: Robust sugar cane harvest driving down sugar value. *The Times - Piquane* December 24, 2012, 2012.
- Liu, P.; Zhang, Y.; Martin, S. T., Complex Refractive Indices of Thin Films of Secondary Organic Materials by Spectroscopic Ellipsometry from 220 to 1200 nm. *Environ Sci Technol* **2013**, *47*, (23), 13594-13601.
- Loza, C. L.; Chan, A. W. H.; Galloway, M. M.; Keutsch, F. N.; Flagan, R. C.; Seinfeld, J. H., Characterization of Vapor Wall Loss in Laboratory Chambers. *Environ Sci Technol* **2010**, *44*, (13), 5074-5078.
- Loza, C. L.; Craven, J. S.; Yee, L. D.; Coggon, M. M.; Schwantes, R. H.; Shiraiwa, M.; Zhang, X.; Schilling, K. A.; Ng, N. L.; Canagaratna, M. R.; Ziemann, P. J.; Flagan, R. C.; Seinfeld, J. H., Secondary organic aerosol yields of 12-carbon alkanes. *Atmos. Chem. Phys.* **2014**, *14*, (3), 1423-1439.
- Malm, W. C., INTRODUCTION TO VISIBILITY. In Cooperative Institute for Research in the Atmosphere (CIRA) NPS Visibility Program: Fort Collins, CO, 1999; p 70.
- Martins, J. V.; Artaxo, P.; Kaufman, Y. J.; Castanho, A. D.; Remer, L. A., Spectral absorption properties of aerosol particles from 350–2500nm. *Geophysical Research Letters* **2009**, *36*, (13), L13810.
- McGillen, M. R.; Archibald, A. T.; Carey, T.; Leather, K. E.; Shallcross, D. E.; Wenger, J. C.; Percival, C. J., Structure-activity relationship (SAR) for the prediction of gas-phase ozonolysis rate coefficients: an extension towards heteroatomic unsaturated species. *Phys Chem Chem Phys* **2011**, *13*, (7), 2842-2849.
- McGillen, M. R.; Carey, T. J.; Archibald, A. T.; Wenger, J. C.; Shallcross, D. E.; Percival, C. J., Structure-activity relationship (SAR) for the gas-phase ozonolysis of aliphatic alkenes and dialkenes. *Phys Chem Chem Phys* **2008**, *10*, (13), 1757-1768.
- McGillen, M. R.; Crosier, J.; Percival, C. J.; Sanchez-Reyna, G.; Shallcross, D. E., Can topological indices be used to predict gas-phase rate coefficients of importance to

- tropospheric chemistry? Reactions of alkenes with OH, NO₃ and O₃. *Chemosphere* **2006**, *65*, (11), 2035-2044.
- McGillen, M. R.; Ghalaieny, M.; Percival, C. J., Determination of gas-phase ozonolysis rate coefficients of C₈-14 terminal alkenes at elevated temperatures using the relative rate method. *Phys Chem Chem Phys* **2011**, *13*, (23), 10965-10969.
- Mentel, T. F.; Springer, M.; Ehn, M.; Kleist, E.; Pullinen, I.; Kurtén, T.; Rissanen, M.; Wahner, A.; Wildt, J., Formation of highly oxidized multifunctional compounds: autoxidation of peroxy radicals formed in the ozonolysis of alkenes – deduced from structure–product relationships. *Atmos. Chem. Phys.* **2015**, *15*, (12), 6745-6765.
- Monks, P. S., Gas-phase radical chemistry in the troposphere. *Chem Soc Rev* **2005**, *34*, (5), 376-395.
- Monks, P. S.; Granier, C.; Fuzzi, S.; Stohl, A.; Williams, M. L.; Akimoto, H.; Amann, M.; Baklanov, A.; Baltensperger, U.; Bey, I.; Blake, N.; Blake, R. S.; Carslaw, K.; Cooper, O. R.; Dentener, F.; Fowler, D.; Fragkou, E.; Frost, G. J.; Generoso, S.; Ginoux, P.; Grewe, V.; Guenther, A.; Hansson, H. C.; Henne, S.; Hjorth, J.; Hofzumahaus, A.; Huntrieser, H.; Isaksen, I. S. A.; Jenkin, M. E.; Kaiser, J.; Kanakidou, M.; Klimont, Z.; Kulmala, M.; Laj, P.; Lawrence, M. G.; Lee, J. D.; Liousse, C.; Maione, M.; McFiggans, G.; Metzger, A.; Mieville, A.; Moussiopoulos, N.; Orlando, J. J.; O'Dowd, C. D.; Palmer, P. I.; Parrish, D. D.; Petzold, A.; Platt, U.; Pöschl, U.; Prévôt, A. S. H.; Reeves, C. E.; Reimann, S.; Rudich, Y.; Sellegri, K.; Steinbrecher, R.; Simpson, D.; ten Brink, H.; Theloke, J.; van der Werf, G. R.; Vautard, R.; Vestreng, V.; Vlachokostas, C.; von Glasow, R., Atmospheric composition change – global and regional air quality. *Atmos Environ* **2009**, *43*, (33), 5268-5350.
- Moosmüller, H.; Arnott, W. P., Angular truncation errors in integrating nephelometry. *Review of Scientific Instruments* **2003**, *74*, (7), 3492-3501.
- Moosmüller, H.; Chakrabarty, R. K.; Arnott, W. P., Aerosol light absorption and its measurement: A review. *Journal of Quantitative Spectroscopy and Radiative Transfer* **2009**, *110*, (11), 844-878.
- Müller, T.; Laborde, M.; Kassell, G.; Wiedensohler, A., Design and performance of a three-wavelength LED-based total scatter and backscatter integrating nephelometer. *Atmos. Meas. Tech.* **2011**, *4*, (6), 1291-1303.
- Nakayama, T.; Matsumi, Y.; Sato, K.; Imamura, T.; Yamazaki, A.; Uchiyama, A., Laboratory studies on optical properties of secondary organic aerosols generated during the photooxidation of toluene and the ozonolysis of α -pinene. *Journal of Geophysical Research: Atmospheres* **2010**, *115*, (D24), D24204.
- Nakayama, T.; Sato, K.; Matsumi, Y.; Imamura, T.; Yamazaki, A.; Uchiyama, A., Wavelength Dependence of Refractive Index of Secondary Organic Aerosols Generated during the Ozonolysis and Photooxidation of α -Pinene. *SOLA* **2012**, *8*, 119-123.

- Nakayama, T.; Sato, K.; Matsumi, Y.; Imamura, T.; Yamazaki, A.; Uchiyama, A., Wavelength and NO_x dependent complex refractive index of SOAs generated from the photooxidation of toluene. *Atmos. Chem. Phys.* **2013**, *13*, (2), 531-545.
- NATIONS, F. A. A. O. O. T. U., FAOSTAT. In <http://faostat3.fao.org/>, 2013.
- Nemitz, E.; Dorsey, J. R.; Flynn, M. J.; Gallagher, M. W.; Hensen, A.; Erisman, J. W.; Owen, S. M.; Dämmgen, U.; Sutton, M. A., Aerosol fluxes and particle growth above managed grassland. *Biogeosciences* **2009**, *6*, (8), 1627-1645.
- Ng, N. L.; Chhabra, P. S.; Chan, A. W. H.; Surratt, J. D.; Kroll, J. H.; Kwan, A. J.; McCabe, D. C.; Wennberg, P. O.; Sorooshian, A.; Murphy, S. M.; Dalleska, N. F.; Flagan, R. C.; Seinfeld, J. H., Effect of NO_x level on secondary organic aerosol (SOA) formation from the photooxidation of terpenes. *Atmos. Chem. Phys.* **2007**, *7*, (19), 5159-5174.
- Ng, N. L.; Kroll, J. H.; Chan, A. W. H.; Chhabra, P. S.; Flagan, R. C.; Seinfeld, J. H., Secondary organic aerosol formation from m-xylene, toluene, and benzene. *Atmos Chem Phys* **2007**, *7*, (14), 3909-3922.
- Ng, N. L.; Kroll, J. H.; Keywood, M. D.; Bahreini, R.; Varutbangkul, V.; Flagan, R. C.; Seinfeld, J. H.; Lee, A.; Goldstein, A. H., Contribution of first- versus second-generation products to secondary organic aerosols formed in the oxidation of biogenic hydrocarbons. *Environ Sci Technol* **2006**, *40*, (7), 2283-2297.
- Ng, N. L.; Kwan, A. J.; Surratt, J. D.; Chan, A. W. H.; Chhabra, P. S.; Sorooshian, A.; Pye, H. O. T.; Crouse, J. D.; Wennberg, P. O.; Flagan, R. C.; Seinfeld, J. H., Secondary organic aerosol (SOA) formation from reaction of isoprene with nitrate radicals (NO₃). *Atmos. Chem. Phys.* **2008**, *8*, (14), 4117-4140.
- Nguyen, T. B.; Lee, P. B.; Updyke, K. M.; Bones, D. L.; Laskin, J.; Laskin, A.; Nizkorodov, S. A., Formation of nitrogen- and sulfur-containing light-absorbing compounds accelerated by evaporation of water from secondary organic aerosols. *Journal of Geophysical Research: Atmospheres* **2012**, *117*, (D1), D01207.
- Nguyen, T. B.; Roach, P. J.; Laskin, J.; Laskin, A.; Nizkorodov, S. A., Effect of humidity on the composition of isoprene photooxidation secondary organic aerosol. *Atmos. Chem. Phys.* **2011**, *11*, (14), 6931-6944.
- O'Dwyer, M. A.; Carey, T. J.; Healy, R. M.; Wenger, J. C.; Picquet-Varrault, B.; Doussin, J. F., The Gas-phase Ozonolysis of 1-Penten-3-ol, (Z)-2-Penten-1-ol and 1-Penten-3-one: Kinetics, Products and Secondary Organic Aerosol Formation. *Z Phys Chem* **2010**, *224*, (7-8), 1059-1080.
- Odum, J. R.; Hoffmann, T.; Bowman, F.; Collins, D.; Flagan, R. C.; Seinfeld, J. H., Gas/particle partitioning and secondary organic aerosol yields. *Environ Sci Technol* **1996**, *30*, (8), 2580-2585.
- Ofner, J.; Krüger, H. U.; Grothe, H.; Schmitt-Kopplin, P.; Whitmore, K.; Zetzsch, C., Physico-chemical characterization of SOA derived from catechol and guaiacol – a model substance for the aromatic fraction of atmospheric HULIS. *Atmos. Chem. Phys.* **2011**, *11*, (1), 1-15.

- Ormeño, E.; Gentner, D. R.; Fares, S.; Karlik, J.; Park, J. H.; Goldstein, A. H., Sesquiterpenoid Emissions from Agricultural Crops: Correlations to Monoterpenoid Emissions and Leaf Terpene Content. *Environ Sci Technol* **2010**, *44*, (10), 3758-3764.
- Papagni, C.; Arey, J.; Atkinson, R., Rate constants for the gas-phase reactions of OH radicals with a series of unsaturated alcohols. *Int J Chem Kinet* **2001**, *33*, (2), 142-147.
- Peeters, J.; Boullart, W.; Pultau, V.; Vandenberg, S.; Vereecken, L., Structure–Activity Relationship for the Addition of OH to (Poly)alkenes: Site-Specific and Total Rate Constants. *The Journal of Physical Chemistry A* **2007**, *111*, (9), 1618-1631.
- Peirone, S. A.; Barrera, J. A.; Taccone, R. A.; Cometto, P. M.; Lane, S. I., Relative rate coefficient measurements of OH radical reactions with (Z)-2-hexen-1-ol and (E)-3-hexen-1-ol under simulated atmospheric conditions. *Atmos Environ* **2014**, *85*, 92-98.
- Pfrang, C.; King, M. D.; Canosa-Mas, C. E.; Wayne, R. P., Structure-activity relations (SARs) for gas-phase reactions of NO₃, OH and O₃ with alkenes: An update. *Atmos Environ* **2006**, *40*, (6), 1180-1186.
- Pinto, D. M.; Nerg, A. M.; Holopainen, J. K., The role of ozone-reactive compounds, terpenes, and green leaf volatiles (GLVs), in the orientation of *Cotesia plutellae*. *J Chem Ecol* **2007**, *33*, (12), 2218-2228.
- Presto, A. A.; Hartz, K. E. H.; Donahue, N. M., Secondary organic aerosol production from terpene ozonolysis. 1. Effect of UV radiation. *Environ Sci Technol* **2005**, *39*, (18), 7036-7045.
- Presto, A. A.; Huff Hartz, K. E.; Donahue, N. M., Secondary Organic Aerosol Production from Terpene Ozonolysis. 2. Effect of NO_x Concentration. *Environ Sci Technol* **2005**, *39*, (18), 7046-7054.
- Reid, J. S.; Eck, T. F.; Christopher, S. A.; Hobbs, P. V.; Holben, B., Use of the Angstrom exponent to estimate the variability of optical and physical properties of aging smoke particles in Brazil. *J Geophys Res-Atmos* **1999**, *104*, (D22), 27473-27489.
- Reisen, F.; Aschmann, S. M.; Atkinson, R.; Arey, J., Hydroxyaldehyde products from hydroxyl radical reactions of Z-3-hexen-1-ol and 2-methyl-3-buten-2-ol quantified by SPME and API-MS. *Environ Sci Technol* **2003**, *37*, (20), 4664-4671.
- Rissanen, M. P.; Kurtén, T.; Sipilä, M.; Thornton, J. A.; Kangasluoma, J.; Sarnela, N.; Junninen, H.; Jørgensen, S.; Schallhart, S.; Kajos, M. K.; Taipale, R.; Springer, M.; Mentel, T. F.; Ruuskanen, T.; Petäjä, T.; Worsnop, D. R.; Kjaergaard, H. G.; Ehn, M., The Formation of Highly Oxidized Multifunctional Products in the Ozonolysis of Cyclohexene. *J Am Chem Soc* **2014**, *136*, (44), 15596-15606.
- Risticvic, S.; Lord, H.; Gorecki, T.; Arthur, C. L.; Pawliszyn, J., Protocol for solid-phase microextraction method development. *Nat. Protocols* **2010**, *5*, (1), 122-139.
- Rohr, A. C., The health significance of gas- and particle-phase terpene oxidation products: A review. *Environ Int* **2013**, *60*, 145-162.

- Rollins, A. W.; Browne, E. C.; Min, K. E.; Pusede, S. E.; Wooldridge, P. J.; Gentner, D. R.; Goldstein, A. H.; Liu, S.; Day, D. A.; Russell, L. M.; Cohen, R. C., Evidence for NO_x Control over Nighttime SOA Formation. *Science* **2012**, *337*, (6099), 1210-1212.
- Rossignol, S.; Chiappini, L.; Perraudin, E.; Rio, C.; Fable, S.; Valorso, R.; Doussin, J. F., Development of a parallel sampling and analysis method for the elucidation of gas/particle partitioning of oxygenated semi-volatile organics: a limonene ozonolysis study. *Atmos. Meas. Tech.* **2012**, *5*, (6), 1459-1489.
- Sadezky, A.; Chaimbault, P.; Mellouki, A.; Römpp, A.; Winterhalter, R.; Le Bras, G.; Moortgat, G. K., Formation of secondary organic aerosol and oligomers from the ozonolysis of enol ethers. *Atmos. Chem. Phys.* **2006**, *6*, (12), 5009-5024.
- Sadezky, A.; Winterhalter, R.; Kanawati, B.; Römpp, A.; Spengler, B.; Mellouki, A.; Le Bras, G.; Chaimbault, P.; Moortgat, G. K., Oligomer formation during gas-phase ozonolysis of small alkenes and enol ethers: new evidence for the central role of the Criegee Intermediate as oligomer chain unit. *Atmos. Chem. Phys.* **2008**, *8*, (10), 2667-2699.
- Sakamoto, Y.; Inomata, S.; Hirokawa, J., Oligomerization Reaction of the Criegee Intermediate Leads to Secondary Organic Aerosol Formation in Ethylene Ozonolysis. *The Journal of Physical Chemistry A* **2013**, *117*, (48), 12912-12921.
- Sauer, F.; Schäfer, C.; Neeb, P.; Horie, O.; Moortgat, G. K., Formation of hydrogen peroxide in the ozonolysis of isoprene and simple alkenes under humid conditions. *Atmos Environ* **1999**, *33*, (2), 229-241.
- Scala, A.; Allmann, S.; Mirabella, R.; Haring, M. A.; Schuurink, R. C., Green Leaf Volatiles: A Plant's Multifunctional Weapon against Herbivores and Pathogens. *Int J Mol Sci* **2013**, *14*, (9), 17781-17811.
- Scott, C. E.; Rap, A.; Spracklen, D. V.; Forster, P. M.; Carslaw, K. S.; Mann, G. W.; Pringle, K. J.; Kivekäs, N.; Kulmala, M.; Lihavainen, H.; Tunved, P., The direct and indirect radiative effects of biogenic secondary organic aerosol. *Atmos. Chem. Phys. Discuss.* **2013**, *13*, (6), 16961-17019.
- Seinfeld, J. H.; Kleindienst, T. E.; Edney, E. O.; Cohen, J. B., Aerosol Growth in a Steady-State, Continuous Flow Chamber: Application to Studies of Secondary Aerosol Formation. *Aerosol Sci Tech* **2003**, *37*, (9), 728-734.
- Seinfeld, J. H. a. S. N. P., *Atmospheric Chemistry and Physics: From Air Pollution to Climate Change*. 2 ed.; John Wiley and Sons, INC: Hoboken, N.J., 2006; p 1203.
- Shilling, J. E.; Chen, Q.; King, S. M.; Rosenoern, T.; Kroll, J. H.; Worsnop, D. R.; McKinney, K. A.; Martin, S. T., Particle mass yield in secondary organic aerosol formed by the dark ozonolysis of α -pinene. *Atmos. Chem. Phys.* **2008**, *8*, (7), 2073-2088.
- Shilling, J. E.; Zaveri, R. A.; Fast, J. D.; Kleinman, L.; Alexander, M. L.; Canagaratna, M. R.; Fortner, E.; Hubbe, J. M.; Jayne, J. T.; Sedlacek, A.; Setyan, A.; Springston, S.; Worsnop, D. R.; Zhang, Q., Enhanced SOA formation from mixed anthropogenic and

- biogenic emissions during the CARES campaign. *Atmos. Chem. Phys.* **2013**, *13*, (4), 2091-2113.
- Sidebottom, H.; Tracy, J., Kinetics and Mechanism for the Reaction of Ozone with Cycloalkenes. In *Chemical Processes in Atmospheric Oxidation*, Le Bras, G., Ed. Springer Berlin Heidelberg: 1997; Vol. 3, pp 218-224.
- Song, C.; Gyawali, M.; Zaveri, R. A.; Shilling, J. E.; Arnott, W. P., Light absorption by secondary organic aerosol from α -pinene: Effects of oxidants, seed aerosol acidity, and relative humidity. *Journal of Geophysical Research: Atmospheres* **2013**, *118*, (20), 11,741-11,749.
- Steinbrecher, R.; Klauer, M.; Hauff, K.; R. Stockwell, W.; Jaeschke, W.; Dietrich, T.; Herbert, F., Biogenic and anthropogenic fluxes of non-methane hydrocarbons over an urban-impacted forest, Frankfurter Stadtwald, Germany. *Atmos Environ* **2000**, *34*, (22), 3779-3788.
- Stewart, D. J.; Altabrok, S. H.; Lockhart, J. P.; Mohamed, O. M.; Nutt, D. R.; Pfrang, C.; Marston, G., The kinetics of the gas-phase reactions of selected monoterpenes and cyclo-alkenes with ozone and the NO₃ radical. *Atmos Environ* **2013**, *70*, (0), 227-235.
- Taft, R., *Steric Effects in Organic Chemistry*. John Wiley & Sons, Inc.: New York, 1356.
- Tang, I. N.; Munkelwitz, H. R., Composition and temperature dependence of the deliquescence properties of hygroscopic aerosols. *Atmospheric Environment. Part A. General Topics* **1993**, *27*, (4), 467-473.
- Tijjani, B. I.; Aliyu, A.; Shuaibu, F., The Effect of Hygroscopic Growth on Continental Aerosols. *Open Journal of Applied Sciences* **2013**, *Vol.03No.06*, 12.
- Titos, G.; Jefferson, A.; Sheridan, P. J.; Andrews, E.; Lyamani, H.; Alados-Arboledas, L.; Ogren, J. A., Aerosol light-scattering enhancement due to water uptake during the TCAP campaign. *Atmos. Chem. Phys.* **2014**, *14*, (13), 7031-7043.
- Titos, G.; Lyamani, H.; Cazorla, A.; Sorribas, M.; Foyo-Moreno, I.; Wiedensohler, A.; Alados-Arboledas, L., Study of the relative humidity dependence of aerosol light-scattering in southern Spain. *2014* **2014**.
- Tkacik, D. S.; Presto, A. A.; Donahue, N. M.; Robinson, A. L., Secondary Organic Aerosol Formation from Intermediate-Volatility Organic Compounds: Cyclic, Linear, and Branched Alkanes. *Environ Sci Technol* **2012**, *46*, (16), 8773-8781.
- Tolocka, M. P.; Jang, M.; Ginter, J. M.; Cox, F. J.; Kamens, R. M.; Johnston, M. V., Formation of Oligomers in Secondary Organic Aerosol. *Environ Sci Technol* **2004**, *38*, (5), 1428-1434.
- Toole, J. R.; Renbaum-Wolff, L.; Smith, G. D., A Calibration Technique for Improving Refractive Index Retrieval from Aerosol Cavity Ring-Down Spectroscopy. *Aerosol Sci Tech* **2013**, *47*, (9), 955-965.

- Treacy, J.; Curley, M.; Wenger, J.; Sidebottom, H., Determination of Arrhenius parameters for the reactions of ozone with cycloalkenes. *Journal of the Chemical Society, Faraday Transactions* **1997**, *93*, (16), 2877-2881.
- Treacy, J.; Elhag, M.; Ofarrell, D.; Sidebottom, H., Reactions of Ozone with Unsaturated Organic-Compounds. *Ber Bunsen Phys Chem* **1992**, *96*, (3), 422-427.
- Tsao, C. C.; Campbell, J. E.; Mena-Carrasco, M.; Spak, S. N.; Carmichael, G. R.; Chen, Y., Increased estimates of air-pollution emissions from Brazilian sugar-cane ethanol. *Nat Clim Change* **2012**, *2*, (1), 53-57.
- Uchida, R.; Sato, K.; Imamura, T., Gas Phase Ozone Reactions with Z-3-Hexenal and Z-3-Hexen-1-ol: Formation Yields of OH radical, Propanal, and Ethane. *Chemistry Letters* **2015**, *advpub*.
- Updyke, K. M.; Nguyen, T. B.; Nizkorodov, S. A., Formation of brown carbon via reactions of ammonia with secondary organic aerosols from biogenic and anthropogenic precursors. *Atmos Environ* **2012**, *63*, (0), 22-31.
- Utry, N.; Ajtai, T.; Filep, Á.; Dániel Pintér, M.; Hoffer, A.; Bozoki, Z.; Szabó, G., Mass specific optical absorption coefficient of HULIS aerosol measured by a four-wavelength photoacoustic spectrometer at NIR, VIS and UV wavelengths. *Atmos Environ* **2013**, *69*, (0), 321-324.
- Vallat, A.; Gu, H. N.; Dorn, S., How rainfall, relative humidity and temperature influence volatile emissions from apple trees in situ. *Phytochemistry* **2005**, *66*, (13), 1540-1550.
- Vereecken, L.; Francisco, J. S., Theoretical studies of atmospheric reaction mechanisms in the troposphere. *Chem Soc Rev* **2012**, *41*, (19), 6259-6293.
- Vu, T.; Delgado-Saborit, J.; Harrison, R., A review of hygroscopic growth factors of submicron aerosols from different sources and its implication for calculation of lung deposition efficiency of ambient aerosols. *Air Qual Atmos Health* **2015**, 1-12.
- Wagner, F.; Silva, A. M., Some considerations about Ångström exponent distributions. *Atmos. Chem. Phys.* **2008**, *8*, (3), 481-489.
- Wang, H. L.; Huang, D.; Zhang, X.; Zhao, Y.; Chen, Z. M., Understanding the aqueous phase ozonolysis of isoprene: distinct product distribution and mechanism from the gas phase reaction. *Atmos. Chem. Phys.* **2012**, *12*, (15), 7187-7198.
- Wang, J.; Doussin, J. F.; Perrier, S.; Perraudin, E.; Katrib, Y.; Pangui, E.; Picquet-Varrault, B., Design of a new multi-phase experimental simulation chamber for atmospheric photochemistry, aerosol and cloud chemistry research. *Atmos. Meas. Tech.* **2011**, *4*, (11), 2465-2494.
- Wang, X.; Liu, T.; Bernard, F.; Ding, X.; Wen, S.; Zhang, Y.; Zhang, Z.; He, Q.; Lü, S.; Chen, J.; Saunders, S.; Yu, J., Design and characterization of a smog chamber for studying gas-phase chemical mechanisms and aerosol formation. *Atmos. Meas. Tech.* **2014**, *7*, (1), 301-313.

- Wiedensohler, A.; Birmili, W.; Nowak, A.; Sonntag, A.; Weinhold, K.; Merkel, M.; Wehner, B.; Tuch, T.; Pfeifer, S.; Fiebig, M.; Fjåraa, A. M.; Asmi, E.; Sellegri, K.; Depuy, R.; Venzac, H.; Villani, P.; Laj, P.; Aalto, P.; Ogren, J. A.; Swietlicki, E.; Williams, P.; Roldin, P.; Quincey, P.; Hüglin, C.; Fierz-Schmidhauser, R.; Gysel, M.; Weingartner, E.; Riccobono, F.; Santos, S.; Gruning, C.; Faloon, K.; Beddows, D.; Harrison, R.; Monahan, C.; Jennings, S. G.; O'Dowd, C. D.; Marinoni, A.; Horn, H. G.; Keck, L.; Jiang, J.; Scheckman, J.; McMurry, P. H.; Deng, Z.; Zhao, C. S.; Moerman, M.; Henzing, B.; de Leeuw, G.; Löschau, G.; Bastian, S., Mobility particle size spectrometers: harmonization of technical standards and data structure to facilitate high quality long-term observations of atmospheric particle number size distributions. *Atmos. Meas. Tech.* **2012**, *5*, (3), 657-685.
- Wiedinmyer, C.; Guenther, A.; Harley, P.; Hewitt, N.; Geron, C.; Artaxo, P.; Steinbrecher, R.; Rasmussen, R., Global Organic Emissions from Vegetation. In *Emissions of Atmospheric Trace Compounds*, Granier, C.; Artaxo, P.; Reeves, C., Eds. Kluwer Academic Publishers: Dordrecht, The Netherlands, 2004; pp 115-170.
- Wu, S.; Lu, Z. F.; Hao, J. M.; Zhao, Z.; Li, J. H.; Hideto, T.; Hiroaki, M.; Akio, Y., Construction and characterization of an atmospheric simulation smog chamber. *Adv Atmos Sci* **2007**, *24*, (2), 250-258.
- Xu, L.; Kollman, M. S.; Song, C.; Shilling, J. E.; Ng, N. L., Effects of NO_x on the Volatility of Secondary Organic Aerosol from Isoprene Photooxidation. *Environ Sci Technol* **2014**, *48*, (4), 2253-2262.
- Yakobi, V. A.; Galstyan, G. A.; Rister, I. A.; Galstyan, T. M.; Dvortsevoi, M. M., Vapour phase oxidation of toluene by ozone. *Petroleum Chemistry U.S.S.R.* **1974**, *14*, (2), 99-104.
- Yee, L. D.; Craven, J. S.; Loza, C. L.; Schilling, K. A.; Ng, N. L.; Canagaratna, M. R.; Ziemann, P. J.; Flagan, R. C.; Seinfeld, J. H., Effect of chemical structure on secondary organic aerosol formation from C₁₂ alkanes. *Atmos. Chem. Phys. Discuss.* **2013**, *13*, (4), 10859-10903.
- Yee, L. D.; Kautzman, K. E.; Loza, C. L.; Schilling, K. A.; Coggon, M. M.; Chhabra, P. S.; Chan, M. N.; Chan, A. W. H.; Hersey, S. P.; Crouse, J. D.; Wennberg, P. O.; Flagan, R. C.; Seinfeld, J. H., Secondary organic aerosol formation from biomass burning intermediates: phenol and methoxyphenols. *Atmos. Chem. Phys.* **2013**, *13*, (16), 8019-8043.
- Yokelson, R. J.; Christian, T. J.; Karl, T. G.; Guenther, A., The tropical forest and fire emissions experiment: laboratory fire measurements and synthesis of campaign data. *Atmos. Chem. Phys.* **2008**, *8*, (13), 3509-3527.
- Yu, J.; Cocker, D. R.; Griffin, R. J.; Flagan, R. C.; Seinfeld, J. H., Gas-Phase Ozone Oxidation of Monoterpenes: Gaseous and Particulate Products. *J Atmos Chem* **34**, (2), 207-258.

- Zahardis, J.; Petrucci, G. A., The oleic acid-ozone heterogeneous reaction system: products, kinetics, secondary chemistry, and atmospheric implications of a model system – a review. *Atmos. Chem. Phys.* **2007**, *7*, (5), 1237-1274.
- Zhang, J.; Huff Hartz, K. E.; Pandis, S. N.; Donahue, N. M., Secondary Organic Aerosol Formation from Limonene Ozonolysis: Homogeneous and Heterogeneous Influences as a Function of NO_x. *The Journal of Physical Chemistry A* **2006**, *110*, (38), 11053-11063.
- Zhang, X.; Chen, Z.; Wang, H.; He, S.; Huang, D., An important pathway for ozonolysis of alpha-pinene and beta-pinene in aqueous phase and its atmospheric implications. *Atmos Environ* **2009**, *43*, (29), 4465-4471.
- Zhao, D. F.; Buchholz, A.; Kortner, B.; Schlag, P.; Rubach, F.; Kiendler-Scharr, A.; Tillmann, R.; Wahner, A.; Flores, J. M.; Rudich, Y.; Watne, Å. K.; Hallquist, M.; Wildt, J.; Mentel, T. F., Size-dependent hygroscopicity parameter (κ) and chemical composition of secondary organic cloud condensation nuclei. *Geophysical Research Letters* **2015**, *42*, (24), 10,920-10,928.
- Zhao, D. F.; Kaminski, M.; Schlag, P.; Fuchs, H.; Acir, I. H.; Bohn, B.; Häsel, R.; Kiendler-Scharr, A.; Rohrer, F.; Tillmann, R.; Wang, M. J.; Wegener, R.; Wildt, J.; Wahner, A.; Mentel, T. F., Secondary organic aerosol formation from hydroxyl radical oxidation and ozonolysis of monoterpenes. *Atmos. Chem. Phys.* **2015**, *15*, (2), 991-1012.
- Zhong, M.; Jang, M., Light absorption coefficient measurement of SOA using a UV–Visible spectrometer connected with an integrating sphere. *Atmos Environ* **2011**, *45*, (25), 4263-4271.
- Zieger, P.; Fierz-Schmidhauser, R.; Weingartner, E.; Baltensperger, U., Effects of relative humidity on aerosol light scattering: results from different European sites. *Atmos Chem Phys* **2013**, *13*, (21), 10609-10631.
- Zieger, P.; Weingartner, E.; Henzing, J.; Moerman, M.; de Leeuw, G.; Mikkilä, J.; Ehn, M.; Petäjä, T.; Clémer, K.; van Roozendaal, M.; Yilmaz, S.; Frieß, U.; Irie, H.; Wagner, T.; Shaiganfar, R.; Beirle, S.; Apituley, A.; Wilson, K.; Baltensperger, U., Comparison of ambient aerosol extinction coefficients obtained from in-situ, MAX-DOAS and LIDAR measurements at Cabauw. *Atmos. Chem. Phys.* **2011**, *11*, (6), 2603-2624.

APPENDIX I: PREPARATION OF HONO/ HIGH NO_x EXPERIMENTS

AI.1 Atmospheric NO_x and its Roles in SOA Formation

NO_x is a common anthropogenic oxidant emitted by automobiles, trucks and various non-road vehicles (e.g., construction equipment, boats, etc.) as well as industrial sources such as power plants, industrial boilers, cement kilns, and turbines. It is a strong oxidizing agent and plays a major role in the atmospheric reactions with volatile organic compounds (VOC). Ambient NO_x concentrations are lesser for remote regions (~ 25 ppt in Alaska, ~ 40 ppb NO₂ in Rutland, VT) than for urban regions (~ 70 ppb NO₂ in NYC) and are usually greater mid-day (vs nighttime). In 2010, the EPA established primary standards for NO₂ at 100 ppb (1 hour average).

Oxidation reactions are sensitive to the presence of NO_x, primarily because under high NO_x conditions, NO and NO₂ react with organo-peroxy radicals (RO₂) that would otherwise react with other peroxy-radicals (other RO₂ species and HO₂). Therefore, the presence of NO_x introduces additional reaction pathways to the oxidation of organic compounds that are expected to alter SOA yield (both decreasing and increasing SOA yield, depending on mixing ratios and the VOC being studied) and composition (new products include organic nitrates (RONO₂)). The new pathways can also shift existing reaction branching ratios, altering the distribution of common products. See Figure A1.1, which was adapted from Presto et al. (2005).¹

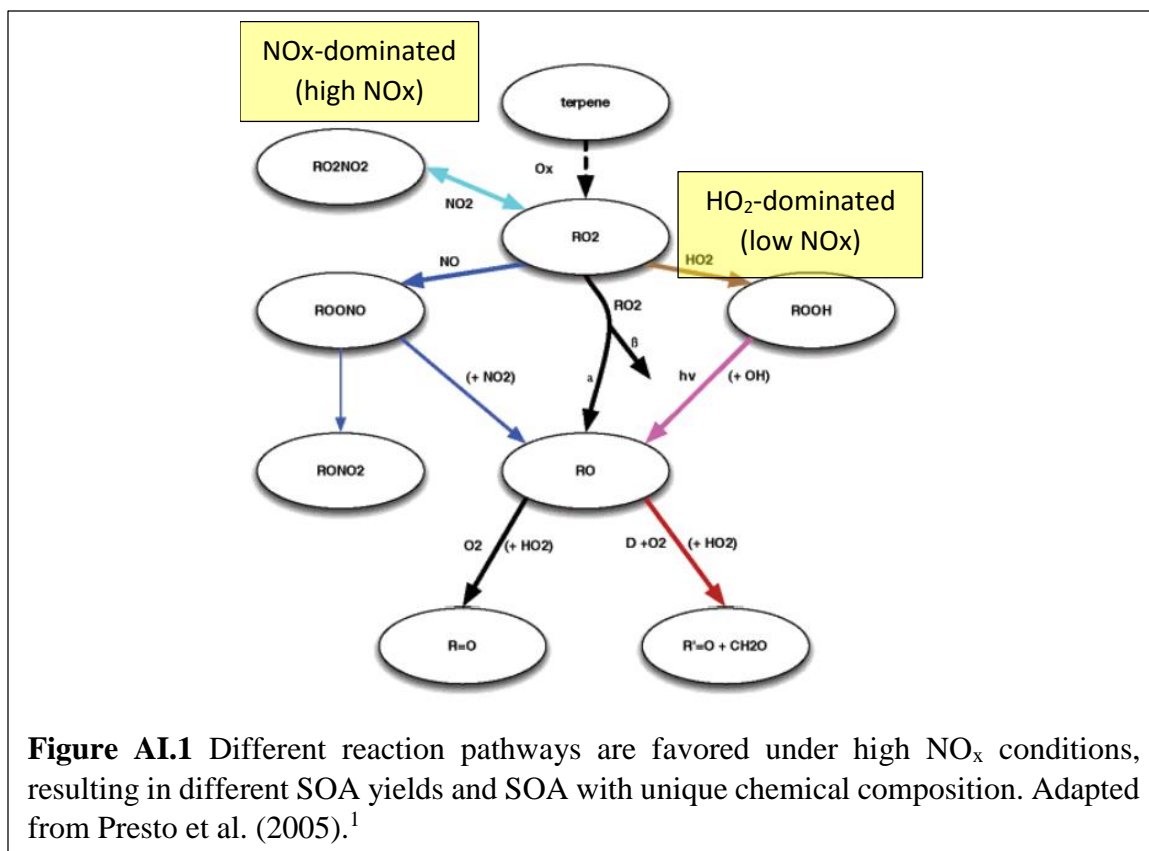


Figure AI.1 Different reaction pathways are favored under high NO_x conditions, resulting in different SOA yields and SOA with unique chemical composition. Adapted from Presto et al. (2005).¹

AI.2 Generation of NO_x

HONO was prepared by dropwise addition of 1% NaNO₂ into 10% H₂SO₄ in a glass bulb. The bulb is attached to the chamber and a stream of zero air is passed through the bulb into the chamber, carrying HONO with it. NO and NO₂, formed as side products in the preparation of HONO, are also introduced into the chamber, and are measured by a commercial NO_x monitor (American Ecotech EC9841).



The concentrations and volumes NaNO₂ and H₂SO₄ used herein and the resulting in NO_x and NO concentrations in the UVMEC and in the 775 L reaction chamber are summarized in Table AI.1.

HONO is also a source of hydroxyl radical (OH) and Ozone (O₃)

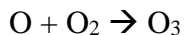
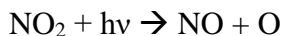
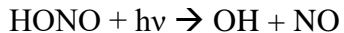


Table AI.1 NO_x and NO concentrations from HONO

Volume of 1% NaNO ₂ (mL)	15	15
Volume of 10% H ₂ SO ₄ (mL)	30	30
Chamber (Volume, L)	Pillow Bag (775)	UVMEC (8000)
Injection time	10 min	10 min
NO _x (ppm)	25	~1
NO (ppm)	10	~0.5

This method to generate NO_x for chamber experiments was developed for the Petrucci Group, but was not used in any oxidation reactions, due in part to instrumental difficulties and then a shift in project scopes. The method is reported herein, however so that others' might use it in future works (i.e. addressing item 9.2 in Future Research Ideas).

AI.3 References

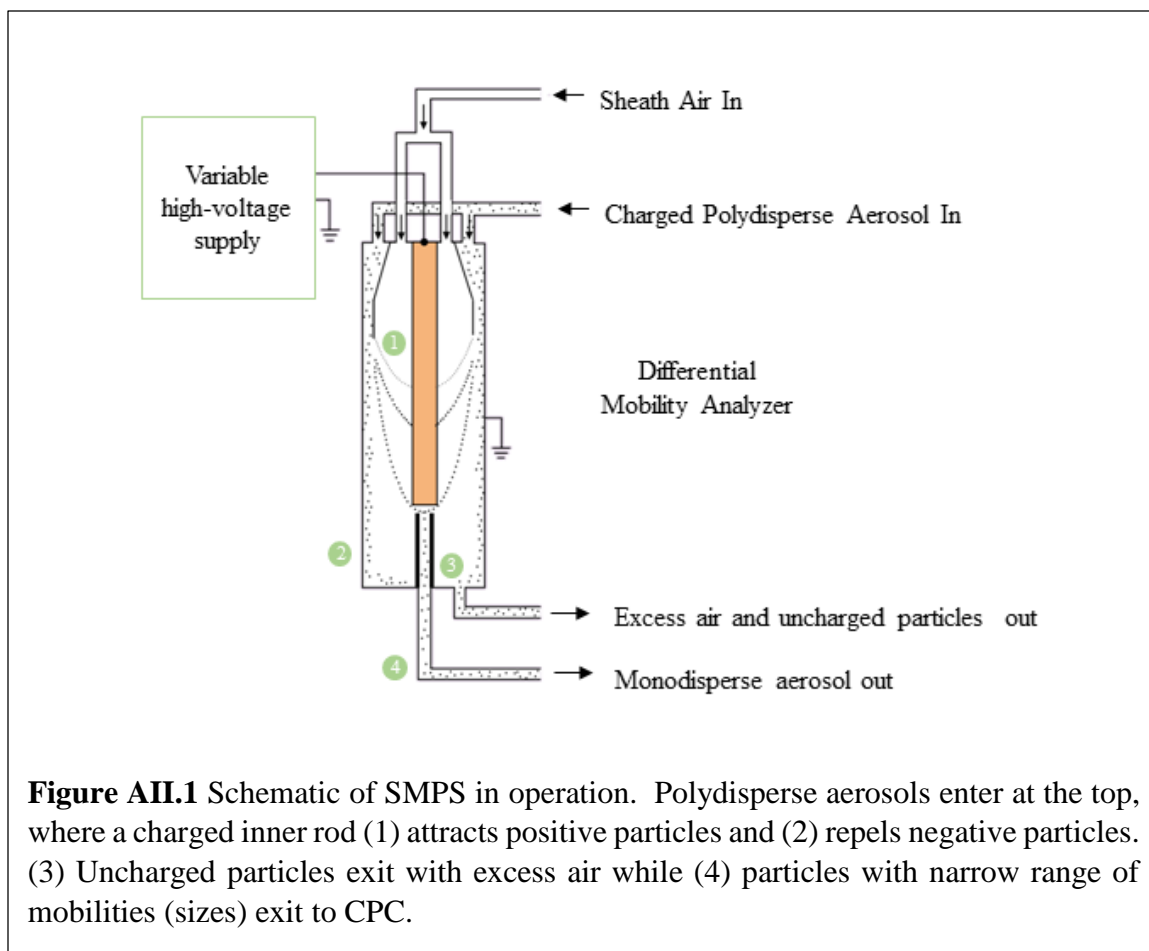
- (1) Presto, A. A.; Huff Hartz, K. E.; Donahue, N. M. *Environ Sci Technol* **2005**, *39*, 7046.

APPENDIX II: CORRECTIONS FOR ERRONEOUS SMPS MEASUREMENTS

During the 11/4 and 11/6 sugarcane ozonolysis experiments, incorrect flow settings were used in the software of the SMPS. The SMPS is a high resolution nanoparticle sizer and is considered standard instrumentation for SOA size characterization.

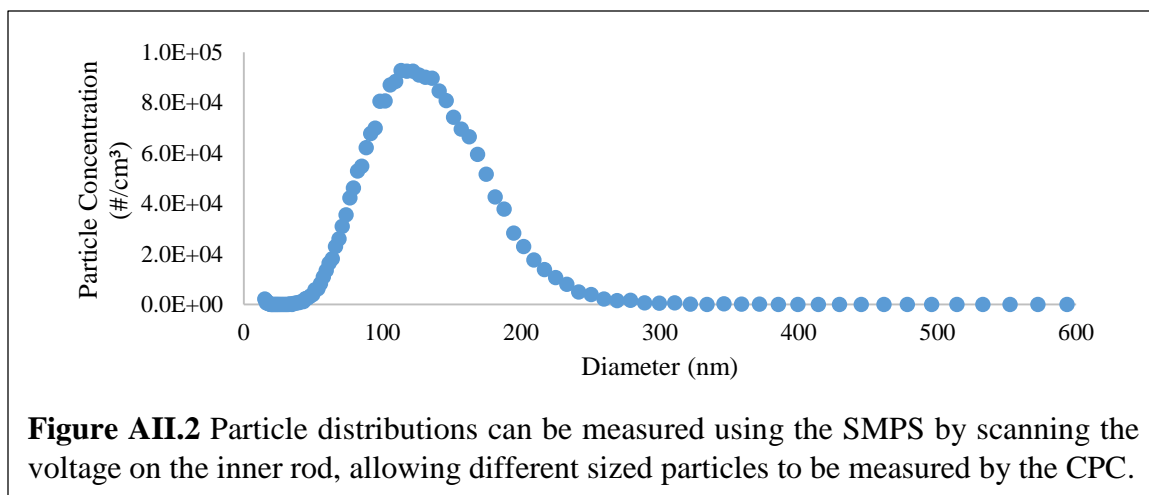
A schematic of the SMPS is given in Figure AII.1. In operation, polydisperse, submicrometer aerosols are sampled and passed through a radioactive bipolar charger. Nearly all particles with diameters of 2 to 300 nm receive a single positive or negative charge, though few receive no charge or a double charge. The particles enter (at a known flow rate: the aerosol flow rate) a differential mobility analyzer (DMA) that separates particles according to their electrical mobility, which is inversely related to particle size.

The DMA contains an inner cylinder connected to a negative power supply (0 to 10,000 VDC) that creates an electric field that, with the help of a flow of sheath air, influence the flow trajectory of the charged particles. Particles with a negative charge repelled from the inner rod and deposit on the outer wall. Particles with a positive charge move rapidly towards the negatively charged inner rod. Only particles within a narrow range of electrical mobility (size range) have the correct trajectory to pass through an open slit near the DMA exit. The process is akin to the Goldilocks scenario; at a given voltage, particles that are too large or too small will deposit onto the inner rod or the inside walls of the DMA. Only particles of just the right mobility (size) are allowed to exit the DMA. These particles are then counted by a condensation particle counter (CPC). By adjusting the voltage on the inner rod, the user can isolate a single size regime of particles. By



ramping the voltage, the particle size distribution can be measured. A typical particle distribution can be seen in Figure AII.2. Assuming a spherical particle and constant density, the number density given in Figure AII.2 can be converted to a mass concentration.

In order to measure the particle size regime we're interested in, the aerosol flow rate is set to 3.0 liters per min (LPM) and the sheath flow rate is set to 0.3 LPM to ensure a 10 to 1 ratio of flows, as defined by the manufacturer. These flow rates are manually set in the SMPS and then entered into the instrument software to allow for calculation between electrical mobility and size. During the 11/4 and 11/6 experiments, the flow rates were set correctly (aerosol flow rate and sheath flow rate were 3.0 LPM and 0.3 LPM, respectively)



but the settings in the software were erroneously set to 3.0 LPM and 1.0 LPM, respectively.

In order to determine how this incorrect setting would affect the resultant SOA mass measurements, standards of 1-octene-3-ol (OTL) were oxidized in the 775 L Teflon chamber to form SOA, which was measured alternately with the “correct” vs “incorrect” SMPS settings. Figure AII.3 below is the SOA mass evolution as a function of reaction time for the ozonolysis of OTL (Exp Date 02/20/2016). Initial reaction conditions are in Table AII.1.

Experiment Date	Initial OTL (ppb)	Initial Ozone (ppb)	SOA Correction Factor
02/20/2016	215	150	9.3 ± 11%
02/22/2016	1000	800	9.5 ± 6%

Table AII.1 Initial reaction conditions for correction factor experiments.

As shown in Figure AII.3, the incorrect settings yielded SOA concentrations significantly less than the correct settings. Interpolating between the two sets of correct settings gives an estimate to what the correct settings would have measured between

80 min and 125 min (when the incorrect settings were used). By comparing the interpolated true SOA concentration to the incorrect SOA concentration (correct SOA/incorrect SOA), we see that the incorrect settings yield SOA mass concentrations erroneously low, by a factor of 9.3 ($\pm 11\%$). Therefore, multiplying the SOA mass concentrations measured using the incorrect settings, by 9.3 we can estimate the true SOA mass concentration within 11%. This experiment was repeated at high mass loading (02/22/2016) and yielded the same correction factor.

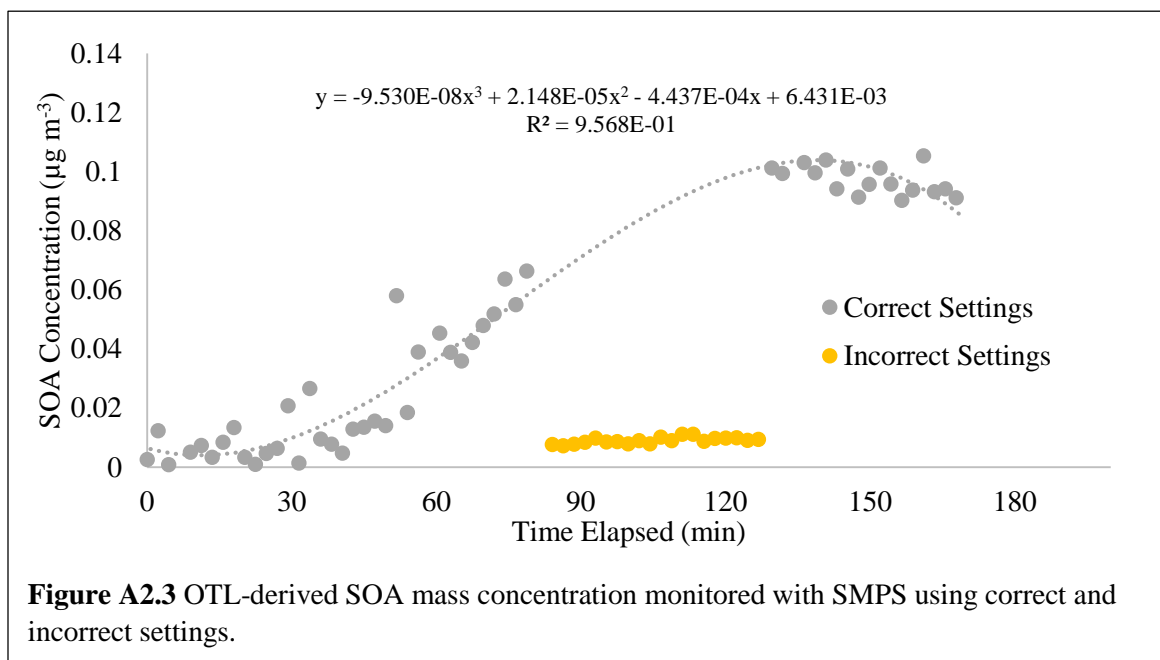


Figure A2.3 OTL-derived SOA mass concentration monitored with SMPS using correct and incorrect settings.

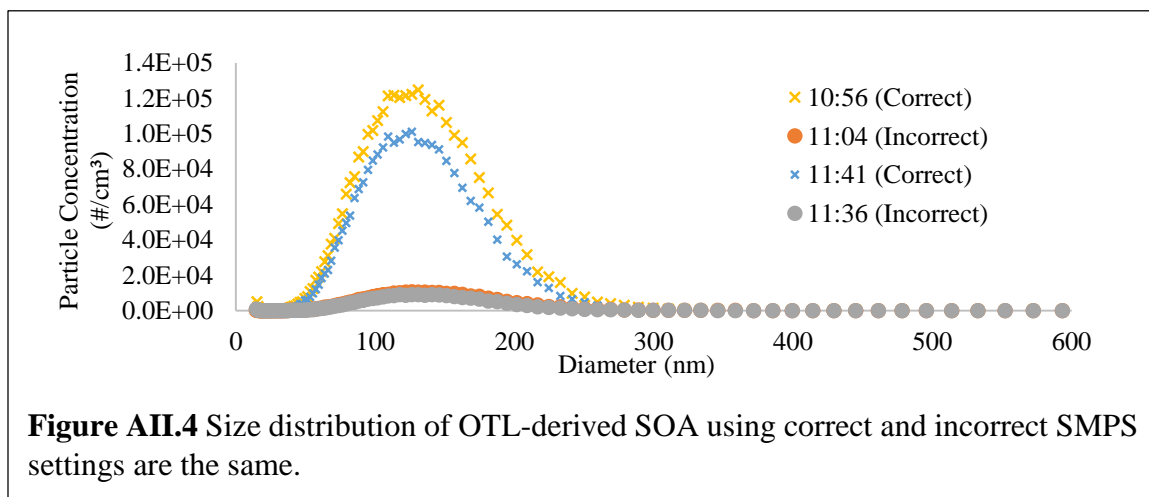
This correction factor collected on 02/20/2016 was applied to SOA mass concentrations collected from the ozonolysis of sugarcane on 11/4 and 11/6 to yield estimated SOA mass concentrations (Table AII.2). This correction factor (rather than an average) was used because the experimental conditions used to obtain it were in better agreement with those used in sugarcane experiments (low mass loading). This correction assumes that SOA formed in sugarcane ozonolysis experiments is well represented by

OTL, which we believe is a safe assumption considering OTL was emitted by sugarcane and likely contributes to its SOA profile. Additional experiments should be done to measure correction factors associated with CHA- and HXL- derived SOA, which are also sources of SOA in sugarcane to establish whether this assumption is correct.

Table AII.2 Raw and corrected SOA mass concentrations in sugarcane experiments.

Date	Measured SOA Concentration (incorrect settings) ($\mu\text{g m}^{-3}$)	Estimated SOA Concentration (with correction) ($\mu\text{g m}^{-3}$)
11/4/2015	0.171	1.6 ± 0.2
11/6/2016	0.412	3.8 ± 0.4

The SMPS software accounts for the different charging efficiencies of particles, which is size dependent, so another assumption of this correction is that the size distributions with both correct and incorrect settings is the same. Figure AII.4 shows the size distribution of SOA measured using correct and incorrect settings for the same parcel of SOA (experiment 2/22/2016). The distributions for correct vs incorrect are paired where each distribution was taken within 10 min of its partner. Although all raw number counts



with each setting are different, the distribution is centered on the same diameter regardless of the SMPS settings. This observation confirms that the SMPS measures the same distribution regardless of the flow settings and that the correction can be applied to estimate SOA mass concentration.

APPENDIX III: REPRINT OF “Establishing the Contribution of Lawn Mowing to Atmospheric Aerosol Levels in American Suburbs”

Full Citation:

Harvey, R. M.; Zahardis, J.; Petrucci, G. A.. Establishing the contribution of lawn mowing to atmospheric aerosol levels in American suburbs. *Atmos. Chem. Phys.* **2014**, *14* (2), 797-812.



Establishing the contribution of lawn mowing to atmospheric aerosol levels in American suburbs

R. M. Harvey, J. Zahardis, and G. A. Petrucci

Department of Chemistry, University of Vermont, 82 University Place, Burlington, VT, USA

Correspondence to: G. A. Petrucci (giuseppe.petrucci@uvm.edu)

Received: 20 August 2013 – Published in Atmos. Chem. Phys. Discuss.: 16 September 2013

Revised: 2 December 2013 – Accepted: 6 December 2013 – Published: 23 January 2014

Abstract. Green leaf volatiles (GLVs) are a class of wound-induced volatile organic compounds emitted by several plant species. Turf grasses emit a complex profile of GLVs upon mowing, as evidenced by the “freshly cut grass” smell, some of which are readily oxidized in the atmosphere to contribute to secondary organic aerosol (SOA). The contribution of lawn-mowing-induced SOA production may be especially impactful at the urban–suburban interface, where urban hubs provide a source of anthropogenic oxidants and SOA while suburban neighborhoods have the potential to emit large quantities of reactive, mow-induced GLVs. This interface provides a unique opportunity to study aerosol formation in a multicomponent system and at a regionally relevant scale. Freshly cut grass was collected from a study site in Essex Junction, Vermont, and was placed inside a 775 L Teflon experimental chamber. Thermal desorption gas chromatography–mass spectrometry (TD-GC/MS) was used to characterize the emitted GLV profile. Ozone was introduced to the experimental chamber and TD-GC/MS was used to monitor the consumption of these GLVs and the subsequent evolution of gas-phase products, while a scanning mobility particle sizer was used to continuously measure aerosol size distributions and mass loadings as a result of grass clipping ozonolysis.

Freshly cut grass was found to emit a complex mixture of GLVs, dominated by *cis*-3-hexenyl acetate (CHA) and *cis*-3-hexenol (HXL), which were released at an initial rate of $1.8 (\pm 0.5) \mu\text{g}$ and $0.07 (\pm 0.03) \mu\text{g}$ per square meter of lawn mowed with each mowing. Chamber studies using pure standards of CHA and HXL were found to have aerosol yields of $1.2 (\pm 1.1)\%$ and $3.3 (\pm 3.1)\%$, respectively. Using these aerosol yields and the emission rate of CHA and HXL by grass, SOA evolution by ozonolysis of grass clip-

pings was predicted. However, the measured SOA mass produced from the ozonolysis of grass clippings exceeded the predicted amount, by upwards of $\sim 150\%$. The ozonolysis of a mixture of CHA and HXL representative of environmental mixing ratios also failed to accurately model the SOA mass produced by grass clippings. The disparity between measured SOA mass and the predicted SOA mass suggests that grass clippings contain other SOA precursors in addition to CHA and HXL.

Aerial photographs and geospatial analysis were used to determine the area of turfgrass coverage in a suburban neighborhood, which was then used along with measured SOA production as a function of grass mowed to determine that lawn mowing has the potential to contribute $47 \mu\text{g}$ SOA per m^{-2} of lawn to the atmosphere per mowing event by ozonolysis, which cannot be modeled solely by the ozonolysis of CHA, HXL or a representative mixture of the two.

1 Introduction

Volatile organic compounds (VOCs) are emitted by both biogenic (BVOCs) and anthropogenic (AVOCs) sources and play an important role in the chemistry of the atmosphere. The photooxidation of VOCs can lead to the formation of ozone, with which other VOCs can react (along with other atmospheric oxidants) to produce secondary organic aerosol (SOA) (Hallquist et al., 2009; Kroll and Seinfeld, 2008). Organic aerosols, including SOA, are a major component of fine aerosols and influence climate through direct and indirect effects, although there is an expressed high degree of uncertainty about the magnitude of these effects (Kanakidou et al., 2005; Solomon et al., 2007). SOA also impacts local

therefore provide an opportunity for concerted bursts of SOA into an airshed. The interface between urban and suburban landscapes provides the opportunity to study SOA formation in a multi-component system at a small spatial and temporal scale, where ASOA can exceed BSOA and where processes leading to SOA formation could be different from those in largely forested regions (Emanuelsson et al., 2013; Fushimi et al., 2011; Steinbrecher et al., 2000; Starn et al., 1998; Aiken et al., 2009).

Although the GLV emission profile of several grass and clover species has been characterized (Watkins et al., 2006; Olofsson et al., 2003; Kirstine et al., 1998; Karl et al., 2001; de Gouw et al., 1999; Brill et al., 2011, 2012; Kirstine and Galbally, 2004; Kirstine, 2002) and the SOA yields of several individual GLVs have been estimated (Hamilton et al., 2009; Aschmann et al., 1997; O'Dwyer et al., 2010; Joutsensaari et al., 2005), to the best of our knowledge there is no reported work on GLV mixtures with respect to their aerosol yields. In this work, a holistic approach to understanding GLV oxidation and SOA evolution has been used to characterize the contribution of lawn mowing to local SOA levels. Thermal desorption gas chromatography–mass spectrometry (TD-GC/MS) was used to characterize the VOC profile of mowed grass. TD-GC/MS was also used to monitor the consumption of GLVs upon ozonolysis and the subsequent evolution of gas-phase products, while aerosol size distributions and mass loadings were continuously measured using a scanning mobility particle sizer.

We show that the mow-induced GLV emission profile from turfgrass in a suburban neighborhood in Vermont, USA, is dominated by CHA and HXL, which readily undergo oxidation by ozone to form SOA. Aerosol yields were determined for standards of CHA and HXL individually and used to predict SOA evolution for simple, atmospherically relevant mixtures of the two GLVs and for grass clippings collected from the field. An apparent disparity between predicted and measured SOA production, along with the volatile product profile of each chemical system, are discussed herein, highlighting the need to understand more fully the dynamic chemical interactions posed at the urban–suburban interface.

2 Experimental

Cis-3-hexenyl acetate (>98 %) and *cis*-3-hexenol (99 %) were purchased from Sigma Aldrich and were used without further purification. Dry, zero air was produced by passing compressed air sequentially through silica, activated carbon and high-efficiency particulate absorption (HEPA) filters. This zero air was also used to generate ozone using a commercially available corona discharge ozone generator (OLSOA/DLS OzoneLab). Ozone concentrations were monitored with an American Ecotech Serinus O₃ Monitor (model E020010).

All experiments were performed in a Teflon chamber with a volume of 775 L at ambient temperature (~23 °C) and atmospheric pressure. Between experiments, the chamber was passivated with O₃ (1–2 ppm) and flushed with zero air to attain background aerosol mass loadings below 0.1 μg m⁻³.

Air samples were collected from the reaction chamber onto Air Toxics glass sorption tubes (Perkin Elmer N9307008) that had been previously conditioned at 310 °C for 20 min and stored with Swagelok caps. Air was drawn through the sorption tubes using a personal sampler pump (SKC Airchek Sampler, model 224-44XR) at a constant rate of approximately 100 ml min⁻¹ (actual flow rate monitored by a F&J Specialty Products mini calibrator, model MC-500cc) for a known duration of time, allowing the total volume of air sampled to be determined. Typical sample volumes ranged between 0.6 L and 3.6 L. Rather than diluting with clean air to account for volume loss during sampling, the chamber was allowed to collapse slightly throughout an experiment. Particle filters and ozone scrubbers were not used because some have been shown to retain ozonolysis products (Uchiyama et al., 2012; Helmig, 1997).

Air samples were then transferred from the sorbent tubes by thermal two-step desorption (TurboMatrix TD 350, Perkin Elmer) to a gas chromatograph (Clarus 600, Perkin Elmer) equipped with a mass spectrometer (Clarus 600 T, Perkin Elmer) detector. Prior to desorption, an internal standard of fluorobenzene (AirLiquide) was injected by the TurboMatrix TD directly onto the sorption tubes. During the first step of desorption, the sorbent tubes were heated to 330 °C for 8 min to desorb and cryo-focus GLVs onto an Air Monitoring trap (Perkin Elmer, P/N M041-3628) trap held at -10 °C. The trap was then heated at a rate of 40 °C s⁻¹ to a final temperature of 310 °C, where it was held for 8 min. The GLVs were transferred to a GC analytical column (Stabilwax 30 m, 0.32 mm i.d., Restek) via a heated transfer line (250 °C). The GC oven was programmed as follows: held at 35 °C for 4 min, increasing 10 °C min⁻¹ to a final temperature of 220 °C. The total run time per sample was 22.5 min. The head pressure of the helium carrier gas was 1.8 psi, which resulted in a flow rate of 1.52 ml min⁻¹. Electron impact ionization (70 eV) was used and masses were scanned from 15 to 300 *m/z*. Chromatographic peaks were identified by comparison of retention times to those of known standards and by spectral matching with the NIST 2005 mass spectral library. Compounds were quantified on area basis using single ion monitoring. Detection limits were found by $LOD = s_y \cdot t_{crit} m^{-1}$, where s_y and m are the error in the y intercept and slope of the calibration curve, respectively, and t_{crit} was taken at 95 % confidence level. The detection limits for CHA, HXL and propanal were 0.096 μg, 0.058 μg and 0.052 μg, respectively. Depending on the volume of air sampled, these masses correspond to ppb-level concentrations.

Aerosol particle number and mass size distributions, as well as total aerosol mass loadings (assuming an average particle density of 1.2 g cm⁻³), were measured continuously

with a scanning mobility particle sizer (SMPS, model SMPS 3080, TSI Inc., Shoreview, MN).

The vapor pressure of several organic ozonolysis products was estimated using structure-based estimators courtesy of the Dortmund Data Bank found in the online database by Clegg et al. (2008). Estimates were made at 298 K and are reported as an average of three estimates determined using methods described by Moller et al. (2008), Myrdal and Yalkowsky (1997), Nannoolal et al. (2008), Nannoolal et al. (2004) and Stein and Brown (1994).

2.1 Grass experiments

The grass collection site chosen was located in a residential neighborhood in Essex Junction, VT (44.487653, -73.09365), approximately 10 miles east of Burlington, VT (Fig. 1). A geospatial analysis of the study site was performed using ArcGIS 9.0 software. Aerial photographs taken in 2004 were obtained from the Vermont Center for Geographic Information. The resolution of these photos was sufficient to visually identify residential turfgrass; ArcGIS software was used to quantify the area of turfgrass (36 acres) along with the total site area (131 acres).

A section of representative turfgrass comprised predominantly of genera *Festuca*, *Lolium* and *Poa* was mowed using a commercially available, residential lawn mower. Clippings were collected and transported in sealed paper bags to the University of Vermont, Burlington, VT, for analysis. Total time elapsed between mowing and sampling in Teflon chamber was between 60 and 90 min. Samples were collected from nine mowing events between September and November of 2012 and one event in May of 2013.

In grass “clipping” experiments, approximately 0.5 kg of grass clippings (wet weight) were placed directly inside the experimental chamber, which was then filled with zero air. Approximately 800 ppb ozone was injected directly into the chamber over the course of ~60 s. Grass clipping experiments were designed to represent environmentally relevant conditions, where ozone was allowed to interact with volatile species in the gas phase along with any reactive species contained within or on the blades of grass themselves. In “headspace” experiments, approximately 150 grams of grass clippings (wet weight) were placed in a 0.4 L conical flask. Zero air was flushed through the conical flask for ~20 min into the reaction chamber, carrying the GLVs with it. Ozone was injected in the same manner as above. Headspace experiments represented a simplified version of the chemical system of interest, where only the volatile species emitted by cut grass were oxidized by ozone. In general, initial CHA and HXL concentrations were greater in headspace experiments than in clipping experiments. This difference is likely due to experimental design; grass clippings were allowed to equilibrate in the experimental chamber for 20–30 min before ozone was injected while grass headspace was allowed to build up in the paper sampling bag for up to 60 min be-

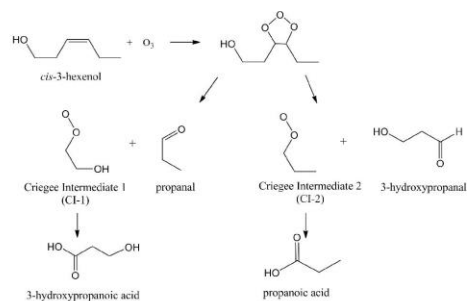


Fig. 1. Turfgrass (light green) in a suburban neighborhood in Essex, VT, comprises 28 % of the total land cover (131 acres), the mowing of which releases a complex profile of unsaturated GLVs, which upon ozonolysis have the potential to contribute to atmospheric SOA. The study site (44.487653, -73.09365) denoted by yellow circle.

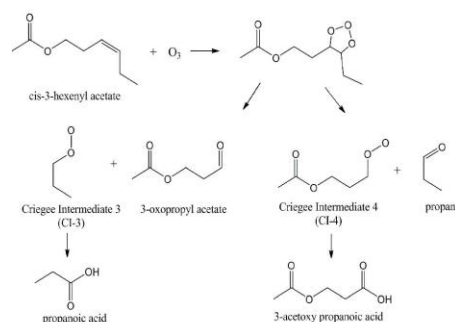
fore being flushed into the chamber. Grass clippings, however, continuously emitted GLVs (Fig. S1).

2.2 GLV standard experiments

GLV standard experiments were designed to further simplify headspace experiments and were used to determine whether SOA produced as the result of grass ozonolysis could be modeled by a single GLV or a two-component mixture of GLVs. Standards of CHA or HXL were introduced to the experimental chamber by evaporation via injection into a 3-neck flask over a warm water bath. After injection, zero air was flushed through the flask and into the reaction chamber for at least 15 min to ensure complete standard transfer. Gaseous wall loss of GLV standards was determined by monitoring GLV concentration within the reaction chamber for six hours. GLV concentration did not decrease over the course of this experiment, however, and gaseous wall loss was found to be insignificant (Fig. S2). Since the bag volume was known, GLV calibration was completed by collecting a known volume and thereby known mass of GLV standards from the experimental chamber onto TD tubes. Ozone was then injected as a brief burst and sampling continued. Standard experiments were carried out at a 1 : 1 and 1 : 2 GLV-to-O₃ molar ratio to determine aerosol yields and measure reaction products. High GLV mass loadings were used to ensure



Scheme 1a. The ozonolysis of HXL is predicted to produce 3-hydroxypropanal and propanal along with the stabilized Criegee intermediates CI-1 and CI-2, which produce 3-hydroxypropanoic acid and propanoic acid, respectively, upon isomerization and hydration.



Scheme 1b. The ozonolysis of CHA is predicted to produce 3-oxopropyl acetate and propanal, along with two stabilized Criegee intermediates (CI-3 and CI-4) that produce propanoic acid and 3-acetoxypropanoic acid, respectively.

sufficient SOA mass and volatile product evolution for analysis.

Reaction rate constants (k) for the ozonolysis of CHA and HXL were determined using experimental protocol described elsewhere (Grosjean et al., 1993; Grosjean and Grosjean, 1994). Briefly, pseudo-first-order reaction conditions were induced, whereby the GLV was present in excess of ozone, which was monitored throughout the reaction. A plot of $\ln([Ozone]_t/[Ozone]_0)$ vs. time yields a straight line with slope $k_{observed}$. From the rate expression of the reaction, $k = k_{observed}/[GLV]_{t=0}$ (Fig. S6).

3 Results

3.1 GLV standard chamber experiments

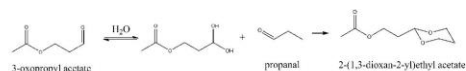
3.1.1 Single GLV system

In order to characterize the emission profile of cut grass, a preliminary grass clipping ozonolysis experiment was performed. As shown in the total ion chromatogram (TIC) of GLVs emitted by cut grass (Fig. 2a), grass clippings emit a relatively complex mixture of volatile organics, dominated by CHA, 1-penten-3-ol and 2-pentanone (peaks 5, 4 and 3, respectively). Also present is a significant amount of HXL (peak 6), which, along with CHA, is a SOA precursor when subjected to ozone (Scheme 1a and b). This reactivity is clearly demonstrated by the TIC of the GLV mixture post-ozonolysis (Fig. 2b). 2-pentanone contains no chemical unsaturations and is therefore nonreactive with ozone, while 1-penten-3-ol, despite its unsaturations, does not appear to be highly reactive with ozone either, although chamber experiments with 1-penten-3-ol standards (Fig. S3) along with work done by Orlando et al. (2001) did indicate minimal re-

activity with ozone. Both headspace and grass clipping experiments had the same VOC emission profile, though the amount of each GLV differed between experiments, as shown in Table 2. Because of their relatively high emissions and their reactivity with ozone, we chose to “model” grass GLVs with CHA and HXL. Standards of each GLV were used to estimate their contribution to mow-induced SOA evolution, as described below.

A simplified scheme representing the ozonolysis of CHA is given in Scheme 1b. The ozonolysis of CHA is expected to form 3-oxopropyl acetate and propanal, along with two stabilized Criegee intermediates (CI-3 and CI-4) that produce propanoic acid and 3-acetoxypropanoic acid, respectively, upon isomerization and hydration (Hamilton et al., 2008; Grosjean and Grosjean, 1997). Upon ozonolysis of CHA (Fig. 3a), we observed the evolution of propanal and propanoic acid, but not 3-oxopropyl acetate or 3-acetoxypropanoic acid. The vapor pressure of 3-oxopropyl acetate (5×10^{-3} atm) is on the same order of magnitude as that of propanal and propanoic acid (0.4 atm and 4×10^{-3} atm, respectively), suggesting that it should be measured in the gas phase. However, it was not observed in this work and experimental identification of 3-oxopropyl acetate by others has been tentative at best (Grosjean and Grosjean, 1999; Li et al., 2013; Hamilton et al., 2008). The estimated vapor pressure of 3-acetoxypropanoic acid (4×10^{-5} atm) is relatively low, suggesting that it may partition to the particle phase and/or that the GC-based method used herein was insufficient to quantify this species.

According to Scheme 1a, propanal, propanoic acid, 3-hydroxypropanal and 3-hydroxypropanoic acid are expected products of the ozonolysis of HXL, of which we observed the evolution of both propanal and propanoic acid in the gas phase (Fig. 3b). In accord with the estimated vapor



Scheme 2. Upon hydration, aldehyde functionality of 3-oxopropyl acetate could react with propanal, both predicted products of CHA ozonolysis (Scheme 1b), to produce 2-(1,3-dioxan-2-yl) ethyl acetate ($VP\ 5 \times 10^{-7}$ atm).

oligomer formation proposed by Hamilton et al. (2009), hydrated 3-oxopropyl acetate (CHA ozonolysis system) could react with propanal to produce 2-(1,3-dioxan-2-yl)ethyl acetate (Scheme 2). Based on this oligomer's estimated vapor pressure (5×10^{-7} atm), it would likely partition between both the particle and gaseous phase; however we did not observe this species using our GC-based methods (Reisen et al., 2003). This secondary reaction may also explain why 3-oxopropyl acetate was not observed in CHA ozonolysis experiments.

In the general mechanism shown in Scheme 1b, propanoic acid is produced by ozonolysis of CHA. According to Li et al. (2013), the evolution of propanoic acid is a result of the α -addition of water to CI-3 to form 1-hydroperoxypropan-1-ol, which further decomposes to produce propanoic acid. Li et al. (2013) performed a kinetic investigation of the mechanism for CHA ozonolysis that confirmed that formation of 1-hydroperoxypropan-1-ol is the favored reaction pathway for CI-3. However, they found that the subsequent decomposition of 1-hydroperoxypropan-1-ol to propanoic acid and water has an energy barrier of $45.57\text{ kcal mol}^{-1}$ and is therefore not likely. Nevertheless, we observed propanoic acid as a product of CHA ozonolysis (Fig. 3a), and this is the only pathway proposed by Li et al. (2013) that leads to its formation. The highly oxidizing environment in which these reactions were performed could lead to further oxidation of propanal to produce propanoic acid, which may explain both the valley/peak behavior in the propanal signal and our observation of propanoic acid. However, we saw no evidence of the consumption of propanal coinciding with the production of propanoic acid in the reaction profile of CHA or HXL. Additionally, separate experiments showed that the ozonolysis of propanal alone did not oxidize to form propanoic acid when injected into the experimental chamber in the presence of high ozone (Fig. S4). The decomposition pathway leading to the formation of propanoic acid, (as proposed by Li et al. (2013), therefore, appears relevant, despite being energetically disfavored.

In the ozonolysis of each GLV, SOA evolution began immediately upon introduction of ozone into the reaction chamber and reached a maximum concentration in ~ 60 – 90 min before decreasing slowly, likely due in part to particle loss to the chamber walls. Aerosol yields, Y , for CHA and HXL were calculated according to Eq. (1), where $\Delta[\text{SOA}]$ is the

maximum SOA concentration ($\mu\text{g m}^{-3}$, assuming a particle density of 1.2 g cm^{-3}) and $\Delta[\text{GLV}]$ is the total amount of GLV consumed ($\mu\text{g m}^{-3}$) at that SOA maximum (Odum et al., 1996).

$$Y = \frac{\Delta[\text{SOA}]}{\Delta[\text{GLV}]} \times 100\% \quad (1)$$

Ozonolysis of CHA and HXL individually resulted in a measured aerosol yield of $0.24 (\pm 0.08)\%$ and $0.26 (\pm 0.1)\%$, respectively (Table 1). Particle loss to chamber walls was estimated according to Presto et al. (2005) and proved to be significant (Fig. S5), with an average wall deposition rate of $5.76 \times 10^{-4}\ \mu\text{g m}^{-3}\text{ s}^{-1}$, which is greater than experimental chambers used by others (2.5×10^{-5} and $1.0 \times 10^{-4}\ \mu\text{g m}^{-3}\text{ s}^{-1}$) (Presto et al., 2005; Cocker et al., 2001; Carter et al., 2005; Wu et al., 2007). Given the large surface-to-volume ratio of our chamber, however (5.3 m^{-1}), compared to that of others (2.12 m^{-1} to 2.8 m^{-1}), a greater deposition rate is expected (Presto et al., 2005; Wu and Bauer, 2012). Unless otherwise noted, all subsequent reports of “measured” or “observed” SOA concentrations account for these wall losses.

Our wall loss coefficient was used to correct aerosol yield from GLV standard experiments. The corrected aerosol yields from ozonolysis of CHA and HXL were $1.2 (\pm 1.1)\%$ and $3.3 (\pm 3.1)\%$, respectively (Table 1). The error associated with these yields is due to the variability in the amount of SOA formed in experiments. Our aerosol yield values are lower than the wall-loss-corrected aerosol yields reported by Hamilton et al. (2008, 2009), which were on the order of magnitude of prevalent monoterpenes: 9.5 – 24% for CHA and 8.6% for HXL. The chamber studies by Hamilton et al. (2009, 2009) were carried out at 1.6 ppm GLV and 1.6 ppm ozone, while our yield experiments were carried out at 1.0 ppm GLV and 0.8 ppm ozone. In both studies, the absolute amount of SOA produced was limited by the GLV species. The aerosol yield, however, is representative of the total amount of GLV consumed as a function of total amount of SOA produced, so it should be independent of starting conditions. The disparity between literature aerosol yields for these GLVs (Hamilton et al., 2008, 2009) and those reported herein is not readily explained; nonetheless, contrary to cyclic monoterpenes, we believe that linear alkene systems (such as GLVs) will produce lower SOA yields due to fragmentation of the precursors upon ozonolysis to produce higher-volatility products that will not enter the particle phase.

3.1.2 Two GLV component mixtures

As stated above, we measured several different, potentially reactive compounds in the complex mixture of GLVs emitted by grass clippings. Recent work by Shilling et al. (2013) in the CARES campaign indicates that VOC mixtures have a significant impact on SOA formation. With the goal of better

Table 1. Experimental conditions and SOA yields for several GLV standard ozonolysis experiments, used to determine average aerosol yield for GLVs. Corrected SOA accounts for aerosol wall loss (Eq. S1 and Fig. S5 in the Supplement) and was used to determine the average corrected SOA yield for CHA and HXL, 1.2 (± 1.1) % and 3.3 (± 3.1) % respectively, as indicated by the bolded text below.

Date	CHA consumed ($\times 10^3 \mu\text{g m}^{-3}$)	HXL consumed ($\times 10^3 \mu\text{g m}^{-3}$)	Ozone injected (ppb)	Measured SOA ($\mu\text{g m}^{-3}$)	Corrected SOA ($\mu\text{g m}^{-3}$)	Measured aerosol yield	Corrected aerosol yield
HXL							
10/01/2013		2.08	800	6.3	60.1	0.30 %	2.88 %
18/02/2013		5.47	1000	11.8	22.8	0.22 %	0.42 %
23/04/2013		2.72	950	27.5	178.0	1.01 %	6.54 %
average						0.26 %	3.28 %
standard deviation						0.1 %	3.1 %
CHA							
10/04/2013	5.61		500	7.1	25.4	0.13 %	0.45 %
10/04/2013	5.86		3400	15.3	33.4	0.26 %	0.57 %
12/04/2013	5.76		950	18.7	67.2	0.32 %	1.17 %
18/04/2013	2.97		1500	7.4	21.0	0.25 %	0.70 %
26/04/2013	2.86		1100	17.8	91.1	0.62 %	3.19 %
average						0.24 %	1.22 %
standard deviation						0.08 %	1.1 %

Table 2. Experimental conditions, SOA and GLV results for several grass clipping and headspace experiments. Ozone concentration was ~ 800 ppb for each experiment. Predicted SOA concentration was determined using initial GLV emissions and wall-loss-corrected aerosol yields. RSD is the relative standard error in the value to the left. RSD of predicted SOA is driven by the high uncertainty in the aerosol yield calculation (Table 1). RSD in HXL and CHA concentrations and masses determined using each GLV calibration.

Date	SOA ($\mu\text{g m}^{-3}$)	SOA ($\mu\text{g m}^{-3}$)	Wall Loss Corrected SOA ($\mu\text{g m}^{-3}$)	Predicted SOA ($\mu\text{g m}^{-3}$)	RSD	HXL ($\mu\text{g m}^{-3}$)	RSD	HXL per m^2 lawn ($\mu\text{g m}^{-2}$)	RSD	CHA ($\mu\text{g m}^{-3}$)	RSD	CHA per m^2 lawn ($\mu\text{g m}^{-2}$)	RSD	
Clippings	23/10/2012	11 835	39	55	9.55	2.51	137	0.09	0.14	0.04	2100	0.04	2.29	0.04
	27/10/2012	6077	16	27	1.21	1.12	31.4	0.49	0.022	0.19	75.7	0.87	0.05	0.87
	06/11/2012	46 102	82	113	10.05	4.12	39.2	0.39	0.033	0.18	3650	0.04	3.10	0.04
	28/05/2013	73 630	120	153	3.74	2.41	56.6	0.30	0.0079	0.03	785	0.04	0.11	0.04
Headspace	23/10/2012	1190	5.9	8.8	43.56	1.58	885	0.03	1.7	0.02	6060	0.04	11.36	0.42
	27/10/2012	348	2.9	3.8	13.34	3.34	120	0.13	0.19	0.12	3920	0.04	6.35	0.49
	06/11/2012	1422	5.2	16	9.66	1.44	205	0.22	0.089	0.16	1220	0.04	0.53	0.39
	08/05/2013	793	6.8	12	5.59	1.60	113	0.11	0.23	0.11	788	0.03	1.60	0.35

understanding SOA formation and yield under environmentally relevant conditions (where VOCs exist as a mixture), we performed two-component ozonolysis experiments with CHA and HXL. In one experiment, ozone was introduced to a GLV mixture containing a 1 : 1 mole ratio mix of the two components, while a second experiment used a 1 : 5 mole ratio of HXL to CHA, analogous to that measured from real grass clippings.

The reaction profile for the ozonolysis of the 1 : 1 GLV mixture (Fig. 4) shows that the majority of both CHA and HXL is consumed within the first five min of the reaction. SOA and volatile product evolution occurred immediately, reaching maxima less than 20 min into the reaction. SOA and volatile product concentrations remained relatively constant post-maxima, and propanal did not exhibit the peak/valley trend observed in the CHA-only ozonolysis experiments. Qualitatively, the 1 : 1 GLV mix reaction profile bares a

strong semblance to that of the HXL-only ozonolysis profile (Fig. 3b), suggesting that, in an equimolar concentration, HXL is more reactive to ozonolysis than CHA. The reaction rate constants we calculated also indicate that HXL ($k = 6.7 \times 10^{-17} \text{ cm}^3 \text{ s}^{-1} \text{ molecule}^{-1}$) is more reactive to ozone than CHA ($3.6 \times 10^{-17} \text{ cm}^3 \text{ s}^{-1} \text{ molecule}^{-1}$) (Fig. S6). These reaction rates agree well with those found by Kirstine and Galbally (2004) ($5.4 \times 10^{-17} \text{ cm}^3 \text{ s}^{-1} \text{ molecule}^{-1}$ for CHA and $6.4 \times 10^{-17} \text{ cm}^3 \text{ s}^{-1} \text{ molecule}^{-1}$ for HXL), who used the relative reaction rate method and also found that HXL was more reactive to ozonolysis. Using the wall-loss-corrected aerosol yields measured in this work and the initial mass of GLVs injected into the chamber, total SOA production for the 1 : 1 mix was expected to reach 125 (± 85) $\mu\text{g m}^{-3}$. However, the maximum wall-loss-corrected SOA concentration measured was 9.8 $\mu\text{g m}^{-3}$.

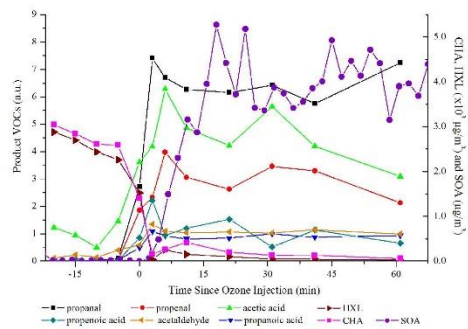


Fig. 4. Reaction profile of the ozonolysis of a 1 : 1 mix of CHA and HXL (initial concentration $2.8 (\pm 0.2) \times 10^3 \mu\text{g m}^{-3}$ each). 900 ppb ozone was injected at time zero, after which SOA and volatile products (propanal, propenal, propanoic acid, acetic acid, propanoic acid, acetaldehyde) increased in signal. Lines between data points drawn to aid the eye.

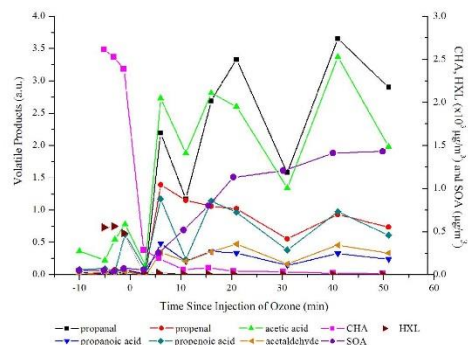


Fig. 5. Reaction profile of the ozonolysis of a 5:1 mix of CHA and HXL (initial concentration $2.5 (\pm 0.1) \times 10^3 \mu\text{g m}^{-3}$ and $0.5 (\pm 0.04) \times 10^3 \mu\text{g m}^{-3}$, respectively). 800 ppb ozone was injected at time zero, after which SOA and volatile products (propanal, propenal, propanoic acid, acetic acid, propanoic acid, acetaldehyde) increased in signal. Lines between data points drawn to aid the eye.

The ozonolysis of 1 HXL : 5 CHA mix also resulted in the rapid consumption of GLVs and the immediate evolution of SOA and volatile products (Fig. 5). This reaction profile more closely approximates the CHA-only reaction profile (Fig. 3b), with both propanal and acetic acid exhibiting the valley/peak trend. This suggests the occurrence of the same secondary reactions observed in the CHA-only system. Wall-loss-corrected aerosol yields predicted the formation of $50 (\pm 17) \mu\text{g m}^{-3}$ of SOA, much more than the maximum wall-loss-corrected SOA concentration observed: $5.3 \mu\text{g m}^{-3}$. The

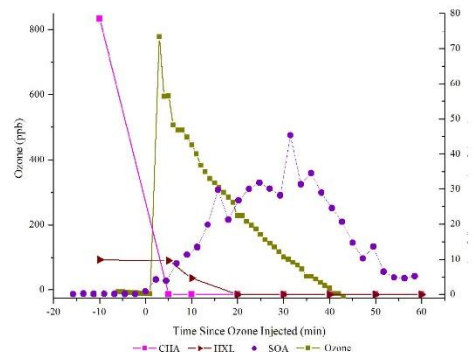


Fig. 6a. Approximately 0.5 kg of grass clippings were placed in the experimental chamber, which was then filled with zero air. Initial concentrations of CHA and HXL were $8.0 (\pm 2) \times 10^2 \mu\text{g m}^{-3}$ and $1.0 (\pm 0.8) \times 10^2 \mu\text{g m}^{-3}$, respectively. At time zero ~ 800 ppb ozone was injected and both CHA and HXL concentrations dropped below the instrument detection limit within the first five min of the reaction, while SOA concentration increased for about 30 min before reaching a maximum of $\sim 91 \mu\text{g m}^{-3}$ (wall-loss-corrected). Lines between data points drawn to aid the eye.

disparity between the measured and predicted SOA concentrations in mixture experiments could suggest the presence of secondary chemistry that resulted in the consumption of GLVs without the production of SOA.

3.2 Grass ozonolysis reaction profile

As stated above, although grass clippings emitted several volatile species, the GLV profile was dominated by CHA, HXL and 1-penten-3-ol (Fig. 2a), all of which are unsaturated and thereby have the potential to undergo oxidation by ozone. Despite its unsaturation, however, 1-penten-3-ol showed limited reactivity with ozone (Fig. S3). Initial CHA, HXL, and ozone concentrations for several experiments are listed in Table 2 and are on the same order of magnitude and mole ratio as the “1 : 5 GLV standard mixture” experiment above. In the ozonolysis of both grass headspace and grass clippings, these three GLVs decreased in signal (albeit to a much smaller extent for 1-penten-3-ol), while that of their corresponding gas-phase oxidation products, propanal, propanoic acid, and acetic acid, increased. As in the GLV standard reactions, we also observed the evolution of propenal, propanoic acid, acetic acid and acetaldehyde, which have not previously been observed as products of grass ozonolysis.

A typical reaction profile for the ozonolysis of grass clippings is shown in Fig. 6a and b. The injection of 800 ppb ozone (at time 0) resulted in an initial burst of SOA. High ozone loadings were used to ensure a complete oxidation of

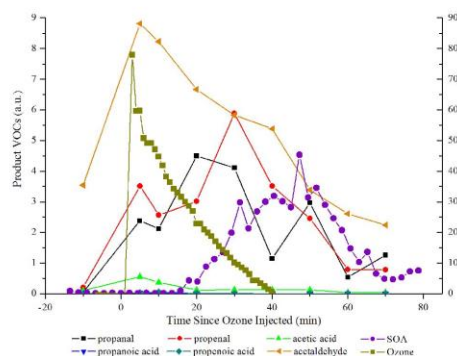


Fig. 6b. In addition to the evolution of SOA, the ozonolysis of grass clippings also resulted in the evolution of several volatile products, including propanal, propenal, acetaldehyde and acetic acid. Trace amounts of propanoic acid, and propanoic acid, were measured. Several of these volatile products have not previously been reported as products of CHA or HXL ozonolysis. Lines between data points drawn to aid the eye.

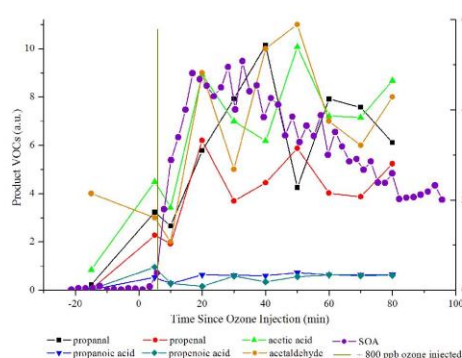


Fig. 7b. In addition to the evolution of SOA, the ozonolysis of grass headspace resulted in the evolution of several volatile products, including propanal, propenal, propanoic acid, acetic acid, propanoic acid, acetaldehyde, several of which have not previously been reported as products of CHA or HXL ozonolysis. Lines between data points drawn to aid the eye.

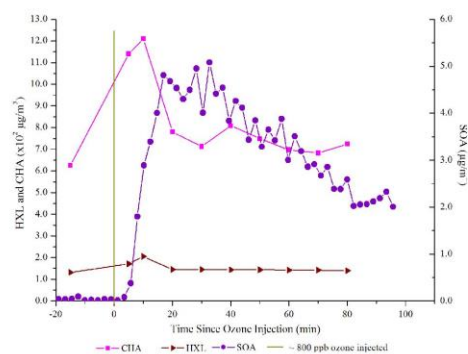


Fig. 7a. Zero air was flushed through grass clippings and into the experimental chamber, carrying with it GVLs contained in the grass headspace. Maximum concentrations of CHA and HXL ($12 (\pm 1) \times 10^2 \mu\text{g m}^{-3}$ and $2.05 (\pm 0.01) \times 10^2 \mu\text{g m}^{-3}$, respectively) were measured post-ozonolysis, which we believe was due to incomplete mixing within the experimental chamber before ozone injection. Ozone data were not available, but at time zero ~ 800 ppb ozone was injected (indicated by vertical line) and within 20 min HXL concentration dropped below the instrument detection limit while SOA reached its maximum wall-loss-corrected concentration ($15.7 \mu\text{g m}^{-3}$). CHA remained relatively constant after the first 20 min of the reaction ($0.74 (\pm 0.05) \times 10^3 \mu\text{g m}^{-3}$) and was never completely consumed. Lines between data points drawn to aid the eye.

all GLVs and to model GLV standard ozonolysis experiments (Table 1), but do not represent atmospherically relevant conditions, as discussed below. In several headspace and grass clipping experiments, the resultant SOA concentration increased to its maximum (up to $\sim 50 \mu\text{g m}^{-3}$ and $\sim 215 \mu\text{g m}^{-3}$ in headspace and clipping experiments, respectively) approximately 20–30 min post-ozonolysis before decreasing rapidly to background levels. As described above, in clipping experiments, the grass was placed inside the reaction chamber, providing a very large surface area for enhanced SOA loss. If SOA “grass loss” were significant, one might expect SOA levels in grass clipping experiments to decrease more quickly than in grass headspace experiments. However, the SOA loss in both headspace and clipping experiments occurred at similar rates, suggesting that the rapid decrease in SOA concentration in clipping experiments is not due to sorption to the grass clippings and cannot be explained entirely by wall loss mechanisms. The mechanism for SOA loss in grass clipping and headspace experiments is not understood but may involve secondary reactions that increase the volatility of SOA as it ages. Understanding SOA reactivity and loss warrants additional work.

In both headspace (reaction profile in Fig. 7a and b) and clipping experiments, volatile products increased as a concerted burst within the first 10 min of ozone injection. In the first 40 min of headspace experiments, 50 % of CHA, HXL and 1-penten-ol was consumed, while more than 90 % of the ozone was consumed. CHA concentration decreased then remained constant once ozone had been depleted. Propenal and acetaldehyde increased steadily post-ozonolysis. Propanal increased, but exhibited a peak-valley behavior similar to that

in GLV standards experiments. All other VOC products decreased post-ozonolysis.

In grass clipping experiments, CHA and HXL were completely consumed within the first ~20 min of the reaction, while ozone concentration fell to background levels ~45 min post-ozonolysis. GLV concentrations were lower in grass clipping experiments than in headspace experiments, but this may have been a result of experimental design, as grass clippings were not allowed to equilibrate in the reaction chamber for more than a few minutes before ozone was injected. Acetic acid, propanoic acid and propenoic acid signal fell after an initial burst, while propanal remained steady after its post-ozonolysis increase (similar to HXL standard experiments).

Applying the wall-loss-corrected aerosol yields above (Eq. 1) to the measured GLV emission rates in both headspace and clipping experiments, theoretical SOA production could be estimated (Table 2). The observed, wall-loss-corrected SOA concentration in grass headspace experiments was less than predicted by aerosol yields with a -120% difference. This difference was similar to the degree of disparity in predicted vs. measured predicted vs. measured SOA mass in the 1:1 the 1:1 mix ozonolysis experiment (-115% difference), suggesting the 1:1 mix may model SOA production from grass headspace to some degree.

The observed, wall-loss-corrected SOA production in grass clipping experiments was much greater than aerosol yields predicted (+170%). The ozonolysis of neither the 1:1 mix nor the 1:5 mix resulted in the overproduction of SOA, suggesting that neither mix accurately models grass clippings. Based on the corrected SOA yields, when summed, HXL and CHA account for only a small fraction of observed SOA (15 (± 13) %). Because GLVs are continuously emitted by grass clippings, they likely represent a continuous source of SOA, rather than a one-time burst, which may contribute to the observed disparity between predicted and measured SOA. This disparity may also suggest that other, potentially important processes are contributing to SOA evolution by the mowing and subsequent oxidation of grass, as will be discussed below.

The disparity in SOA yield between grass clippings and grass headspace ozonolysis experiments could be due to either the enhancement of SOA growth in clippings (i.e., chemical wounding by ozone, as discussed below) or the suppression of SOA growth in headspace and mixed GLV standard experiments. The presence of some volatile species (i.e., isoprene) has been shown to inhibit new particle formation (Kiendler-Scharr et al., 2009). Recently, Mentel et al. (2013) found that HXL suppressed SOA formation from the ozonolysis of α -pinene as a result of competing reactions with OH. In a mixture of reactive VOCs, we might expect the VOC with the greatest reaction rate for a given oxidant to consume that oxidant preferentially and contribute most to the resultant product profile. For example, in the case of α -pinene and HXL provided by Mentel et al.,

(2013), both the O₃ and the OH rate constant for α -pinene (0.28–3.3 × 10⁻¹⁶ and (5–6) × 10⁻¹¹ cm³ molecule⁻¹ s⁻¹, respectively) are less than that for HXL (7 ± 3 × 10⁻¹⁷ and 1.1 × 10⁻¹⁰ cm³ molecule⁻¹ s⁻¹, respectively), suggesting that both O₃ and OH would preferentially oxidize HXL over α -pinene. (Dash et al., 2013; Kirstine and Galbally, 2004). Since HXL has a smaller aerosol yield than α -pinene, this preferential reactivity would suppress total SOA growth. Similarly, SOA growth in the grass headspace experiments could have been suppressed by the preferential oxidation of some low-aerosol-yield volatile species that were not detectable using our methods. This rationalization, however, does not explain the low aerosol yields observed in the ozonolysis experiments using mixtures of GLV standards.

As demonstrated by the disparity between predicted and actual SOA production, the ozonolysis of HXL or CHA alone does not accurately represent SOA from the ozonolysis of grass clippings or grass headspace. Mixtures of the two dominant reactive GLVs are more representative of the grass headspace system than the grass clippings, and produce similar trends in SOA growth and volatile product evolution. Therefore, predictions of atmospheric SOA mass loading using even these two predominant GLVs underestimate actual SOA loading resulting from lawn mowing.

4 Contribution of lawn mowing to atmospheric SOA

The site area chosen for this study was a residential, suburban neighborhood in close proximity to an industrial, urban landscape. A geospatial analysis of the 131-acre area around the study site showed that lawns and turfgrass comprise 27.5% of the total land cover in this suburban neighborhood (36 acres). Remaining land cover was comprised of wooded lots, scrub brush and impervious surfaces such as roads, driveways and rooftops. Lawn mowing has been estimated to produce ~1.3 × 10⁵ gdw m⁻² yr⁻¹ of clippings (where gdw is grams dry weight) (Fig. S7). Stevenson (2010) estimated that New England homeowners mow their lawn 20 times annually, so we predict that approximately 66 gdw m⁻² mowing⁻¹ of grass clippings are produced by New England lawns. Using the measured GLV emissions normalized to the mass of grass (gdw) collected in each experiment, we estimate that lawns in this typical suburban neighborhood have the capacity to emit 8.66 (± 0.08) µg m⁻² of CHA and 1.21 (± 0.06) µg m⁻² of HXL as a concerted burst upon mowing. Based on our wall-loss-corrected aerosol yields, these GLVs have the capacity, therefore, to contribute 177 mg SOA to the neighborhood airshed, annually.

However, as shown above, the actual SOA mass measured due to the ozonolysis of grass clippings is much greater than predicted by our yields, so the 177 mg yr⁻¹ estimate is not truly representative of the potential contribution of lawn mowing to airshed SOA levels. Using the measured SOA as a function of grass mass (gdw) in a “top-down” approach

to this estimate, we predict that $0.9 \mu\text{g gdw}^{-1}$ SOA could be produced upon mowing, where $\mu\text{g gdw}^{-1}$ represents the mass of SOA produced (μg) as a function of grass dry weight in grams (gdw). For our study site, this SOA production rate corresponds to $47 \mu\text{g SOA per square meter mowed}$, or $940 \mu\text{g m}^{-2}$, annually (Fig. S7). Based on reported emissions from forested landscapes and the fraction of forested landscape in the region of the study area, isoprene and monoterpenes are estimated to contribute 2500 and $2000 \mu\text{g m}^{-2}$ SOA annually, respectively (Guenther et al., 1994; Zheng et al., 2013). Lawn mowing, therefore, has the potential to emit a significant amount of SOA, comparable to the two predominant SOA sources, as a concerted burst to the local airshed.

As stated above, ozone was introduced to the experimental chamber as a one-time burst that resulted in concentrations of about 800 ppb, which is much greater than average ozone levels in Chittenden County, VT (~ 60 ppb) (US Environmental Protection Agency, 2013). Eight hundred (800) ppb ozone was used in preliminary grass clipping experiments to ensure a sufficient concentration to result in SOA growth and was used in subsequent GLV standard and grass experiments for the sake of consistency. Though ambient ozone concentrations are lower than the experimental ones used herein, they are expected to be elevated on warm, sunny days, the same time lawn mowing is expected to occur. Additionally, ozone plumes can be transported several hundred kilometers from industrial or urban sources to rural sites where they can interact with BVOCs (Mao et al., 2006; Bertschi and Jaffe, 2005; Wang et al., 2006). For example, plumes originating in New York City, NY, can extend 600 km and contain up to 160 ppb ozone (Lee et al., 2011). The prevailing winds in Essex Junction, VT, are from the west, putting the study site five miles downwind from the City of Burlington, VT, and many industrial areas, which may introduce an additional source of ozone. Therefore, it is possible that local ozone levels in rural landscapes could be elevated during mowing events. Additionally, in the field any consumed ozone is expected to be replenished by other sources that are prevalent in the atmosphere, whereas in our experiments ozone was injected as a single burst (Steinbrecher et al., 2000). Exposure to a concerted burst of 800 ppb ozone is admittedly different than an exposure to 100 ppb over the course of 8 hours, which would be a more representative exposure scenario, but such exposures will require use of a continuous flow reaction chamber. Exposure to ozone itself has also been shown to cause VOC emission in several plant species (Heiden et al., 2003; Woodbury et al., 1994; Kivimäenpää et al., 2013; Miresmailli et al., 2013). Depending on the reactivity of these VOCs, they may also undergo ozonolysis and contribute to additional SOA mass and could help explain the disparity between SOA yields in headspace vs. clipping experiments. We did not detect the emission of VOCs by grass clippings as a result of ozonolysis; however they may have been immediately consumed by yet more ozone in the reaction chamber. Additional

work is necessary to understand ozone-induced VOC emission by grasses and their subsequent reactivity with ozone.

Despite our efforts to model real-world conditions in our experiments, the atmosphere offers complexities that may lead to additional SOA evolution as a result of lawn mowing. Work done by Kirstine et al. (2004), Orlando et al. (2001), and Papagani et al. (2001) has shown that grass GLVs have considerable reactivity with nitrate and hydroxyl radicals. Hamilton et al. (2009) predicted a 3.1% and 0.9% aerosol yield from the photooxidation of HXL and CHA, respectively. Given the established reactivity of GLVs with other atmospheric oxidants, additional work should be done to characterize the volatile products and SOA produced from the photooxidation of GLVs.

This work focused on the interaction of two predominant GLVs and their roles in SOA formation; however there is also growing evidence to indicate that the presence of ASOA and AVOC in conjunction with BVOC synergistically enhances the production of SOA (Shilling et al., 2013; Emanuelsson et al., 2013; Hildebrandt et al., 2011). The relatively large ratio of land cover encompassed by lawns in suburban neighborhoods represent a source of BVOCs, which by definition are in close proximity to urban and industrial sources of BVOCs and BSOA, as well as elevated concentrations of oxidants. There are several sources of A/BVOCs and A/BSOA at the urban–suburban interface that provide ample opportunity for interaction. For example, the emissions of lawn mowers themselves have been found to contribute $4 \mu\text{g m}^{-3}$ of aerosol during a mowing event, likely from unspent fuel emissions and agitated plant debris and soil (Drewnick et al., 2008). Additional work is needed to determine whether an anthropogenic enhancement effect drives additional SOA production from the ozonolysis of grass clippings, not seen in headspace or GLV standard experiments. These experiments should include the ozonolysis of GLVs in the presence of seed aerosols, which would serve as a proxy to ambient atmospheric particulate matter or primary organic aerosols and should also involve GLV oxidation in the presence of AVOCs and oxidants.

5 Conclusions

Though many volatile species are emitted by grass clippings, the profile is dominated by CHA and HXL, which are easily oxidized by ozone to produce significant amounts of SOA, in addition to a suite of oxygenated volatile products. Herein we report the first known observation of propenal and propenoic acid as ozonolysis products of both CHA and HXL, as well as support other products previously reported in the literature (Hamilton et al., 2009; Li et al., 2013; Reisen et al., 2003; O'Dwyer et al., 2010; Aschmann et al., 1997). We found that the mowing of lawns has the potential to contribute up to $47 \mu\text{g}$ of SOA to the atmosphere per m^2 of lawn, which cannot be modeled solely by the ozonolysis of CHA

and/or HXL. While these two GLVs were found to produce SOA upon ozonolysis, they each largely underpredict SOA mass loading from ozonolysis of grass clippings. The disparity between measured and predicted SOA mass loading may be rectified by incorporating additional oxidation sources, BVOCs, AVOCs and ASOA, which may contribute to an anthropogenic enhancement effect in grass clipping oxidation.

The ozonolysis of two-component mixtures of CHA and HXL confirms that the chemical processes leading to SOA formation could be better modeled by mixtures than by single-component systems. However, the chemical processes involved are not well understood and warrant additional work (Carlton et al., 2010; de Gouw et al., 2005; Shilling et al., 2013; Spracklen et al., 2011).

Supplementary material related to this article is available online at <http://www.atmos-chem-phys.net/14/797/2014/acp-14-797-2014-supplement.pdf>.

Acknowledgements. This material is based upon work supported by the National Science Foundation under grant no. CHE-1213632.

Edited by: S. A. Nizkorodov

References

- Aiken, A. C., Salcedo, D., Cubison, M. J., Huffman, J. A., DeCarlo, P. F., Ulbrich, I. M., Docherty, K. S., Sueper, D., Kimmel, J. R., Worsnop, D. R., Trimborn, A., Northway, M., Stone, E. A., Schauer, J. J., Volkamer, R. M., Fortner, E., de Foy, B., Wang, J., Laskin, A., Shuthanandan, V., Zheng, J., Zhang, R., Gaffney, J., Marley, N. A., Paredes-Miranda, G., Arnott, W. P., Molina, L. T., Sosa, G., and Jimenez, J. L.: Mexico City aerosol analysis during MILAGRO using high resolution aerosol mass spectrometry at the urban supersite (T0) – Part I: Fine particle composition and organic source apportionment, *Atmos. Chem. Phys.*, 9, 6633–6653, doi:10.5194/acp-9-6633-2009, 2009.
- Aschmann, S. M., Shu, Y. H., Arey, J., and Atkinson, R.: Products of the gas-phase reactions of cis-3-hexen-1-ol with OH radicals and O₃, *Atmos. Environ.*, 31, 3551–3560, doi:10.1016/S1352-2310(97)00205-7, 1997.
- Bahreini, R., Keywood, M. D., Ng, N. L., Varutbangkul, V., Gao, S., Flagan, R. C., Seinfeld, J. H., Worsnop, D. R., and Jimenez, J. L.: Measurements of secondary organic aerosol from oxidation of cycloalkenes, terpenes, and m-xylene using an Aerodyne aerosol mass spectrometer, *Environ. Sci. Technol.*, 39, 5674–5688, doi:10.1021/Es048061a, 2005.
- Bertschi, I. T. and Jaffe, D. A.: Long-range transport of ozone, carbon monoxide, and aerosols to the NE Pacific troposphere during the summer of 2003: Observations of smoke plumes from Asian boreal fires, *J. Geophys. Res.-Atmos.*, 110, D05303 doi:10.1029/2004jd005135, 2005.
- Brilli, F., Ruuskanen, T. M., Schnitzhofer, R., Muller, M., Breitenlechner, M., Bittner, V., Wohlfahrt, G., Loreto, F., and Hansel, A.: Detection of Plant Volatiles after Leaf Wounding and Darkening by Proton Transfer Reaction “Time-of-Flight” Mass Spectrometry (PTR-TOF), *PLOS One*, 6, E20419, doi:10.1371/journal.pone.0020419, 2011.
- Brilli, F., Hortnagl, L., Bamberger, I., Schnitzhofer, R., Ruuskanen, T. M., Hansel, A., Loreto, F., and Wohlfahrt, G.: Qualitative and Quantitative Characterization of Volatile Organic Compound Emissions from Cut Grass, *Environ. Sci. Technol.*, 46, 3859–3865, doi:10.1021/Es204025y, 2012.
- Cahill, T. M., Seaman, V. Y., Charles, M. J., Holzinger, R., and Goldstein, A. H.: Secondary organic aerosols formed from oxidation of biogenic volatile organic compounds in the Sierra Nevada Mountains of California, *J. Geophys. Res.-Atmos.*, 111, D16312, doi:10.1029/2006jd007178, 2006.
- Carlton, A. G., Wiedinmyer, C., and Kroll, J. H.: A review of Secondary Organic Aerosol (SOA) formation from isoprene, *Atmos. Chem. Phys.*, 9, 4987–5005, doi:10.5194/acp-9-4987-2009, 2009.
- Carlton, A. G., Pinder, R. W., Bhavsar, P. V., and Pouliot, G. A.: To What Extent Can Biogenic SOA be Controlled?, *Environ. Sci. Technol.*, 44, 3376–3380, doi:10.1021/es903506b, 2010.
- Carter, W. P. L., Cocker III, D. R., Fitz, D. R., Malkina, I. L., Bumiller, K., Sauer, C. G., Pisano, J. T., Bufalino, C., and Song, C.: A new environmental chamber for evaluation of gas-phase chemical mechanisms and secondary aerosol formation, *Atmos. Environ.*, 39, 7768–7788, doi:10.1016/j.atmosenv.2005.08.040, 2005.
- Clegg, S. L., Kleeman, M. J., Griffin, R. J., and Seinfeld, J. H.: Effects of uncertainties in the thermodynamic properties of aerosol components in an air quality model – Part 2: Predictions of the vapour pressures of organic compounds, *Atmos. Chem. Phys.*, 8, 1087–1103, doi:10.5194/acp-8-1087-2008, 2008.
- Cocker, D. R., Flagan, R. C., and Seinfeld, J. H.: State-of-the-Art Chamber Facility for Studying Atmospheric Aerosol Chemistry, *Environ. Sci. Technol.*, 35, 2594–2601, doi:10.1021/es0019169, 2001.
- Dash, M. R., Balaganesh, M., and Rajakumar, B.: Rate coefficients for the gas-phase reaction of OH radical with α -pinene: an experimental and computational study, *Molec. Phys.*, 1-17, doi:10.1080/00268976.2013.840395, 2013.
- de Gouw, J. A., Howard, C. J., Custer, T. G., and Fall, R.: Emissions of volatile organic compounds from cut grass and clover are enhanced during the drying process, *Geophys. Res. Lett.*, 26, 811–814, 1999.
- de Gouw, J. A., Middlebrook, A. M., Warneke, C., Goldan, P. D., Kuster, W. C., Roberts, J. M., Fehsenfeld, F. C., Worsnop, D. R., Canagaratna, M. R., Pszenny, A. A. P., Keene, W. C., Marchewka, M., Bertman, S. B., and Bates, T. S.: Budget of organic carbon in a polluted atmosphere: Results from the New England Air Quality Study in 2002, *J. Geophys. Res. Atmos.*, 110, D16305, doi:10.1029/2004JD005623, 2005.
- Diaz, E. A., Lemos, M., Coull, B., Long, M. S., Rohr, A. C., Ruiz, P., Gupta, T., Kang, C. M., and Godleski, J. J.: Toxicological Evaluation of Realistic Emission Source Aerosols (TERESA)-Power plant studies: assessment of breathing pattern, *Inhal. Toxicol.*, 23, 42–59, doi:10.3109/08958378.2010.578169, 2011.
- Drewnick, F., Dall’Osto, M., and Harrison, R. M.: Characterization of aerosol particles from grass mowing by joint deployment of ToF-AMS and ATOFMS instruments, *Atmos. Environ.*, 42, 3006–3017, doi:10.1016/j.atmosenv.2007.12.047, 2008.
- Emanuelsson, E. U., Hallquist, M., Kristensen, K., Glasius, M., Bohn, B., Fuchs, H., Kammer, B., Kiendler-Scharr, A., Nehr, S.,

- Rubach, F., Tillmann, R., Wahner, A., Wu, H. C., and Mentel, T. F.: Formation of anthropogenic secondary organic aerosol (SOA) and its influence on biogenic SOA properties, *Atmos. Chem. Phys.*, 13, 2837–2855, doi:10.5194/acp-13-2837-2013, 2013.
- Fushimi, A., Wagai, R., Uchida, M., Hasegawa, S., Takahashi, K., Kondo, M., Hirabayashi, M., Morino, Y., Shibata, Y., Ohara, T., Kobayashi, S., and Tanabe, K.: Radiocarbon (C-14) Diurnal Variations in Fine Particles at Sites Downwind from Tokyo, Japan in Summer, *Environ. Sci. Technol.*, 45, 6784–6792, doi:10.1021/Es201400p, 2011.
- Glasius, M., la Cour, A., and Lohse, C.: Fossil and nonfossil carbon in fine particulate matter: A study of five European cities, *J. Geophys. Res.-Atmos.*, 116, D11302, doi:10.1029/2011jd015646, 2011.
- Grosjean, D., Grosjean, E., and Williams, E. L.: Rate Constants for the Gas-Phase Reactions of Ozone with Unsaturated Alcohols, Esters, and Carbonyls, *Int. J. Chem. Kinet.*, 25, 783–794, doi:10.1002/kin.550250909, 1993.
- Grosjean, E. and Grosjean, D.: Rate Constants for the Gas-Phase Reactions of Ozone with Unsaturated Aliphatic-Alcohols, *Int. J. Chem. Kinet.*, 26, 1185–1191, doi:10.1002/kin.550261206, 1994.
- Grosjean, E. and Grosjean, D.: The gas phase reaction of unsaturated oxygenates with ozone: Carbonyl products and comparison with the alkene-ozone reaction, *J. Atmos. Chem.*, 27, 271–289, doi:10.1023/A:1005868119515, 1997.
- Grosjean, E. and Grosjean, D.: The reaction of unsaturated aliphatic oxygenates with ozone, *J. Atmos. Chem.*, 32, 205–232, doi:10.1023/A:1006122000643, 1999.
- Guenther, A., Zimmerman, P., and Wildermuth, M.: Natural volatile organic compound emission rate estimates for U.S. woodland landscapes, *Atmos. Environ.*, 28, 1197–1210, doi:10.1016/1352-2310(94)90297-6, 1994.
- Guenther, A., Geron, C., Pierce, T., Lamb, B., Harley, P., and Fall, R.: Natural emissions of non-methane volatile organic compounds, carbon monoxide, and oxides of nitrogen from North America, *Atmos. Environ.*, 34, 2205–2230, doi:10.1016/S1352-2310(99)00465-3, 2000.
- Guenther, A. B., Jiang, X., Heald, C. L., Sakulyanontvittaya, T., Duhl, T., Emmons, L. K., and Wang, X.: The Model of Emissions of Gases and Aerosols from Nature version 2.1 (MEGAN2.1): an extended and updated framework for modeling biogenic emissions, *Geosci. Model. Dev.*, 5, 1471–1492, doi:10.5194/gmd-5-1471-2012, 2012.
- Gulden, L. E., Yang, Z. L., and Niu, G. Y.: Interannual variation in biogenic emissions on a regional scale, *J. Geophys. Res.-Atmos.*, 112, D14103, doi:10.1029/2006jd008231, 2007.
- Hallquist, M., Wenger, J. C., Baltensperger, U., Rudich, Y., Simpson, D., Claeys, M., Dommen, J., Donahue, N. M., George, C., Goldstein, A. H., Hamilton, J. F., Herrmann, H., Hoffmann, T., Iinuma, Y., Jang, M., Jenkin, M. E., Jimenez, J. L., Kiendler-Scharr, A., Maenhaut, W., McFiggans, G., Mentel, T. F., Monod, A., Prevo, A. S. H., Seinfeld, J. H., Surratt, J. D., Szmigielski, R., and Wildt, J.: The formation, properties and impact of secondary organic aerosol: current and emerging issues, *Atmos. Chem. Phys.*, 9, 5155–5236, doi:10.5194/acp-9-5155-2009, 2009.
- Hamilton, J. F., Lewis, A. C., Carey, T. J., and Wenger, J. C.: Characterization of polar compounds and oligomers in secondary organic aerosol using liquid chromatography coupled to mass spectrometry, *Anal. Chem.*, 80, 474–480, doi:10.1021/Ac701852t, 2008.
- Hamilton, J. F., Lewis, A. C., Carey, T. J., Wenger, J. C., Garcia, E. B. I., and Munoz, A.: Reactive oxidation products promote secondary organic aerosol formation from green leaf volatiles, *Atmos. Chem. Phys.*, 9, 3815–3823, doi:10.5194/acp-9-3815-2009, 2009.
- Hartikainen, K., Riikonen, J., Nerg, A. M., Kivimäenpää, M., Ahonen, V., Tervahauta, A., Karenlampi, S., Maenpää, M., Rousi, M., Kontunen-Soppela, S., Oksanen, E., and Holopainen, T.: Impact of elevated temperature and ozone on the emission of volatile organic compounds and gas exchange of silver birch (*Betula pendula* Roth), *Environ. Exp. Bot.*, 84, 33–43, doi:10.1016/j.envexpbot.2012.04.014, 2012.
- Hatanaka, A.: The Biogenesis of Green Odor by Green Leaves, *Phytochemistry*, 34, 1201–1218, doi:10.1016/0031-9422(91)80003-J, 1993.
- Heiden, A. C., Kobel, K., Langebartels, C., Schuh-Thomas, G., and Wildt, J.: Emissions of oxygenated volatile organic compounds from plants – part I: Emissions from lipoxigenase activity, *J. Atmos. Chem.*, 45, 143–172, doi:10.1023/A:1024069605420, 2003.
- Helmig, D.: Ozone removal techniques in the sampling of atmospheric volatile organic trace gases, *Atmos. Environ.*, 31, 3635–3651, 1997.
- Hildebrandt, L., Henry, K. M., Kroll, J. H., Worsnop, D. R., Pandis, S. N., and Donahue, N. M.: Evaluating the Mixing of Organic Aerosol Components Using High-Resolution Aerosol Mass Spectrometry, *Environ. Sci. Technol.*, 45, 6329–6335, doi:10.1021/Es200825g, 2011.
- Hoyle, C. R., Boy, M., Donahue, N. M., Fry, J. L., Glasius, M., Guenther, A., Hallar, A. G., Hartz, K. H., Petters, M. D., Petaja, T., Rosenoern, T., and Sullivan, A. P.: A review of the anthropogenic influence on biogenic secondary organic aerosol, *Atmos. Chem. Phys.*, 11, 321–343, doi:10.5194/acp-11-321-2011, 2011.
- Keyword, M. D., Varutbangkul, V., Bahreini, R., Flagan, R. C., and Seinfeld, J. H.: Secondary organic aerosol formation from the ozonolysis of cycloalkenes and related compounds, *Environ. Sci. Technol.*, 38, 4157–4164, doi:10.1021/Es.035363o, 2004.
- Jardine, K., Barron-Gafford, G. A., Norman, J. P., Abrell, L., Monson, R. K., Meyers, K. T., Pavao-Zuckerman, M., Dontsova, K., Kleist, E., Werner, C., and Huxman, T. E.: Green leaf volatiles and oxygenated metabolite emission bursts from mesquite branches following light-dark transitions, *Photosynth. Res.*, 113, 321–333, doi:10.1007/s11120-012-9746-5, 2012.
- Joutsensaari, J., Loivamäki, M., Vuorinen, T., Miettinen, P., Nerg, A. M., Holopainen, J. K., and Laaksonen, A.: Nanoparticle formation by ozonolysis of inducible plant volatiles, *Atmos. Chem. Phys.*, 5, 1489–1495, 2005, <http://www.atmos-chem-phys.net/5/1489/2005/>.
- Kanakidou, M., Seinfeld, J. H., Pandis, S. N., Dentener, F. J., Facchini, M. C., Van Dingenen, R., Ervens, B., Nenes, A., Nielsen, C. J., Swietlicki, E., Putaud, J. P., Balkanski, Y., Fuzzi, S., Horth, J., Moortgat, G. K., Winterhalter, R., Myhre, C. E. L., Tsigaridis, K., Vignati, E., Stephanou, E. G., and Wilson, J.: Organic aerosol and global climate modelling: a review, *Atmos. Chem. Phys.*, 5, 1053–1123, doi:10.5194/acp-5-1053-2005, 2005.

- Karl, T., Fall, R., Jordan, A., and Lindinger, W.: On-line analysis of reactive VOCs from urban lawn mowing, *Environ. Sci. Technol.*, 35, 2926–2931, doi:10.1021/Es010637y, 2001.
- Karl, T., Harren, F., Warneke, C., de Gouw, J., Grayless, C., and Fall, R.: Senescing grass crops as regional sources of reactive volatile organic compounds, *J. Geophys. Res.-Atmos.*, 110, D15302, doi:10.1029/2005jd005777, 2005.
- Kiendler-Scharr, A., Wildt, J., Maso, M. D., Hohaus, T., Kleist, E., Mentel, T. F., Tillmann, R., Uerlings, R., Schurr, U., and Wahner, A.: New particle formation in forests inhibited by isoprene emissions, *Nature*, 461, 381–384, 2009.
- Kirstine, W., Galbally, I., Ye, Y. R., and Hooper, M.: Emissions of volatile organic compounds (primarily oxygenated species) from pasture, *J. Geophys. Res.-Atmos.*, 103, 10605–10619, doi:10.1029/97JD03753, 1998.
- Kirstine, W., Galbally, I., Hooper, M.: Air Pollution and the Smell of Cut Grass, 16th International Clean Air Conference, Christchurch, New Zealand, 2002.
- Kirstine, W. V. and Galbally, I. E.: A simple model for estimating emissions of volatile organic compounds from grass and cut grass in urban airsheds and its application to two Australian cities, *J. Air Waste Manage.*, 54, 1299–1311, 2004.
- Kivimäenpää, M., Riikonen, J., Ahonen, V., Tervahauta, A., and Holopainen, T.: Sensitivity of Norway spruce physiology and terpene emission dynamics to elevated ozone and elevated temperature under open-field exposure, *Environ. Exp. Bot.*, 90, 32–42, doi:10.1016/j.enxpb.2012.11.004, 2013.
- Kroll, J. H. and Seinfeld, J. H.: Chemistry of secondary organic aerosol: Formation and evolution of low-volatility organics in the atmosphere, *Atmos. Environ.*, 42, 3593–3624, doi:10.1016/j.atmosenv.2008.01.003, 2008.
- Lee, S. H., Kim, S. W., Trainer, M., Frost, G. J., McKeen, S. A., Cooper, O. R., Flocke, F., Holloway, J. S., Neuman, J. A., Ryerson, T., Senff, C. J., Swanson, A. L., and Thompson, A. M.: Modeling ozone plumes observed downwind of New York City over the North Atlantic Ocean during the ICARTT field campaign, *Atmos. Chem. Phys.*, 11, 7375–7397, doi:10.5194/acp-11-7375-2011, 2011.
- Lefohn, A. S., Shadwick, D., and Oltmans, S. J.: Characterizing changes in surface ozone levels in metropolitan and rural areas in the United States for 1980–2008 and 1994–2008, *Atmos. Environ.*, 44, 5199–5210, doi:10.1016/j.atmosenv.2010.08.049, 2010.
- Li, J., Sun, Y., Cao, H., Han, D., and He, M.: Mechanisms and kinetics of the ozonolysis reaction of cis-3-hexenyl acetate and trans-2-hexenyl acetate in atmosphere: a theoretical study, *Struct. Chem.*, 1–13, doi:10.1007/s11224-013-0226-0, 2013.
- Mao, H. T., Talbot, R., Troop, D., Johnson, R., Businger, S., and Thompson, A. M.: Smart balloon observations over the North Atlantic: O-3 data analysis and modeling, *J. Geophys. Res.-Atmos.*, 111, D23S56 doi:10.1029/2005JD006507, 2006.
- Mentel, T. F., Kleist, E., Andres, S., Maso, M. D., Hohaus, T., Kiendler-Scharr, A., Y. Rudich, M. S., R. Tillmann, R. U., Wahner, A., and Wildt, J.: Secondary aerosol formation from stress-induced biogenic emissions and possible climate feedbacks, *Atmos. Chem. Phys.*, 13, 8755–8770, doi:10.5194/acp-13-8755-2013, 2013.
- Miller-Schulze, J. P., Shafer, M. M., Schauer, J. J., Solomon, P. A., Lantz, J., Artamonova, M., Chen, B., Imashev, S., Sverdlik, L., Carmichael, G. R., and Deminter, J. T.: Characteristics of fine particle carbonaceous aerosol at two remote sites in Central Asia, *Atmos. Environ.*, 45, 6955–6964, doi:10.1016/j.atmosenv.2011.09.026, 2011.
- Miresmailli, S., Zeri, M., Zangerl, A. R., Bernacchi, C. J., Berenbaum, M. R., and DeLucia, E. H.: Impacts of herbaceous bioenergy crops on atmospheric volatile organic composition and potential consequences for global climate change, *Gcb Bioenergy*, 5, 375–383, doi:10.1111/j.1757-1707.2012.01189.x, 2013.
- Moller, B., Rarey, J., and Ramjugernath, D.: Estimation of the vapour pressure of non-electrolyte organic compounds via group contributions and group interactions, *J. Mol. Liq.*, 143, 52–63, doi:10.1016/j.molliq.2008.04.020, 2008.
- Myrdal, P. B. and Yalkowsky, S. H.: Estimating pure component vapor pressures of complex organic molecules, *Ind. Eng. Chem. Res.*, 36, 2494–2499, doi:10.1021/le950242l, 1997.
- Nannoolal, Y., Rarey, J., Ramjugernath, D., and Cordes, W.: Estimation of pure component properties Part 1. Estimation of the normal boiling point of non-electrolyte organic compounds via group contributions and group interactions, *Fluid Phase Equilib.*, 226, 45–63, doi:10.1016/j.fluid.2004.09.001, 2004.
- Nannoolal, Y., Rarey, J., and Ramjugernath, D.: Estimation of pure component properties - Part 3. Estimation of the vapor pressure of non-electrolyte organic compounds via group contributions and group interactions, *Fluid Phase Equilib.*, 269, 117–133, doi:10.1016/j.fluid.2008.04.020, 2008.
- Nemitz, E., Dorsey, J. R., Flynn, M. J., Gallagher, M. W., Hensen, A., Erisman, J. W., Owen, S. M., Damme, U., and Sutton, M. A.: Aerosol fluxes and particle growth above managed grassland, *Biogeosciences*, 6, 1627–1645, doi:10.5194/bg-6-1627-2009, 2009.
- O'Dwyer, M. A., Carey, T. J., Healy, R. M., Wenger, J. C., Picquet-Varrault, B., and Doussin, J. F.: The Gas-phase Ozonolysis of 1-Penten-3-ol, (Z)-2-Penten-1-ol and 1-Penten-3-one: Kinetics, Products and Secondary Organic Aerosol Formation, *Z. Phys. Chem.*, 224, 1059–1080, doi:10.1524/zpch.2010.6141, 2010.
- Odum, J. R., Hoffmann, T., Bowman, F., Collins, D., Flagan, R. C., and Seinfeld, J. H.: Gas/Particle partitioning and secondary organic aerosol yields, *Environ. Sci. Technol.*, 30, 2580–2585, 1996.
- Olofsson, M., Ek-Olausson, B., Ljungstrom, E., and Langer, S.: Flux of organic compounds from grass measured by relaxed eddy accumulation technique, *J. Environ. Monitor.*, 5, 963–970, doi:10.1039/B303329e, 2003.
- Orlando, J. J., Tyndall, G. S., and Ceazan, N.: Rate coefficients and product yields from reaction of OH with 1-penten-3-ol, (Z)-2-penten-1-ol, and allyl alcohol (2-propen-1-ol), *Journal of Physical Chemistry A*, 105, 3564–3569, doi:10.1021/jp0041712, 2001.
- Ormeno, E., Gentner, D. R., Fares, S., Karlik, J., Park, J. H., and Goldstein, A. H.: Sesquiterpenoid Emissions from Agricultural Crops: Correlations to Monoterpenoid Emissions and Leaf Terpene Content, *Environ. Sci. Technol.*, 44, 3758–3764, doi:10.1021/Es903674m, 2010.
- Papagni, C., Arey, J., and Atkinson, R.: Rate constants for the gas-phase reactions of OH radicals with a series of unsaturated alcohols, *Int. J. Chem. Kinet.*, 33, 142–147, doi:10.1002/1097-4601(200102)33:2<142::Aid-Kin1007>3.0.Co; 2-F, 2001.
- Pinto, D. M., Nerg, A. M., and Holopainen, J. K.: The role of ozone-reactive compounds, terpenes, and green leaf volatiles (GLVs),

- in the orientation of *Cotesia plutellae*, *J. Chem. Ecol.*, 33, 2218–2228, doi:10.1007/s10886-007-9376-0, 2007.
- Presto, A. A., Huff Hartz, K. E., and Donahue, N. M.: Secondary Organic Aerosol Production from Terpene Ozonolysis. 1. Effect of UV Radiation, *Environ. Sci. Technol.*, 39, 7036–7045, doi:10.1021/es050174m, 2005.
- Reisen, F., Aschmann, S. M., Atkinson, R., and Arey, J.: Hydroxyaldehyde products from hydroxyl radical reactions of Z-3-hexen-1-ol and 2-methyl-3-buten-2-ol quantified by SPME and API-MS, *Environ. Sci. Technol.*, 37, 4664–4671, doi:10.1021/Es034142f, 2003.
- Robbins, P. and Birkenholtz, T.: Turfgrass revolution: measuring the expansion of the American lawn, *Land Use Policy*, 20, 181–194, doi:10.1016/S0264-8377(03)00006-1, 2003.
- Shilling, J. E., Zaveri, R. A., Fast, J. D., Kleinman, L., Alexander, M. L., Canagaratna, M. R., Fortner, E., Hubbe, J. M., Jayne, J. T., Sedlacek, A., Setyan, A., Springston, S., Worsnop, D. R., and Zhang, Q.: Enhanced SOA formation from mixed anthropogenic and biogenic emissions during the CARES campaign, *Atmos. Chem. Phys.*, 13, 2091–2113, doi:10.5194/acp-13-2091-2013, 2013.
- Solomon, S. D., Qin, M. M., Chen, Z., Marquis, M., Averyt, K. B., Tignor, M., and Miller, H. L. e.: Contribution of Working Group I to the Fourth Assessment Report of the Intergovernmental Panel on Climate Change, 2007, Cambridge University Press, Cambridge, UK and New York, NY, USA, 2007.
- Spracklen, D. V., Jimenez, J. L., Carslaw, K. S., Worsnop, D. R., Evans, M. J., Mann, G. W., Zhang, Q., Canagaratna, M. R., Allan, J., Coe, H., McFiggans, G., Rap, A., and Forster, P.: Aerosol mass spectrometer constraint on the global secondary organic aerosol budget, *Atmos. Chem. Phys.*, 11, 12109–12136, doi:10.5194/acp-11-12109-2011, 2011.
- Starn, T. K., Shepson, P. B., Bertman, S. B., Riemer, D. D., Zika, R. G., and Olszyna, K.: Nighttime isoprene chemistry at an urban-impacted forest site, *J. Geophys. Res. Atmos.*, 103, 22437–22447, doi:10.1029/98jd01201, 1998.
- Stein, S. E. and Brown, R. L.: Estimation of Normal Boiling Points from Group Contributions, *J. Chem. Inf. Comp. Sci.*, 34, 581–587, doi:10.1021/Ci00019a016, 1994.
- Steinbrecher, R., Klauer, M., Hauff, K., Stockwell, W. R., Jaeschke, W., Dietrich, T., and Herbert, F.: Biogenic and anthropogenic fluxes of non-methane hydrocarbons over an urban-impacted forest, Frankfurter Stadtwald, Germany, *Atmos. Environ.*, 34, 3779–3788, doi:10.1016/S1352-2310(99)00518-X, 2000.
- Stevenson, N.: Encouraging Environmentally Responsible Lawn Care Behavior in New England: Utilizing Social Science to Develop Successful Outreach and Education, M. S., Environmental Science and Policy, Plymouth State University, 172 pp., 2010.
- Uchiyama, S., Inaba, Y., and Kunugita, N.: Ozone removal in the collection of carbonyl compounds in air, *Journal of chromatography. A*, 1229, 293–297, doi:10.1016/j.chroma.2012.01.062, 2012.
- US Environmental Protection Agency, Trends in Ozone Adjusted for Weather Conditions: <http://www.epa.gov/airtrends/weather.html> (last access: 13 May 2013), 2013.
- Wang, T., Ding, A. J., Gao, J., and Wu, W. S.: Strong ozone production in urban plumes from Beijing, China, *Geophys. Res. Lett.*, 33, L21806, doi:10.1029/2006gl027689, 2006.
- Watkins, E., Gianfagna, T. J., Sun, R. Q., and Meyer, W. A.: Volatile compounds of tufted hairgrass, *Crop. Sci.*, 46, 2575–2580, doi:10.2135/cropsci2006.02.0094, 2006.
- Woodbury, P. B., Laurence, J. A., and Hudler, G. W.: Chronic Ozone Exposure Increases the Susceptibility of Hybrid Populus to Disease Caused by *Septoria-Musiva*, *Environ. Pollut.*, 86, 109–114, doi:10.1016/0269-7491(94)90012-4, 1994.
- Wu, J. D. and Bauer, M. E.: Estimating Net Primary Production of Turfgrass in an Urban-Suburban Landscape with QuickBird Imagery, *Remote Sens.-Basel*, 4, 849–866, doi:10.3390/Rs4040849, 2012.
- Wu, S., Lu, Z. F., Hao, J. M., Zhao, Z., Li, J. H., Hideto, T., Hiroaki, M., and Akio, Y.: Construction and characterization of an atmospheric simulation smog chamber, *Adv. Atmos. Sci.*, 24, 250–258, doi:10.1007/s00376-007-0250-3, 2007.
- Zheng, D. L., Ducey, M. J., and Heath, L. S.: Assessing net carbon sequestration on urban and community forests of northern New England, USA, *Urban for Urban Greece*, 12, 61–68, doi:10.1016/j.ufug.2012.10.003, 2013.
- Yee, L. D., Craven, J. S., Loza, C. L., Schilling, K. A., Ng, N. L., Canagaratna, M. R., Ziemann, P. J., Flagan, R. C., and Seinfeld, J. H.: Effect of chemical structure on secondary organic aerosol formation from C12 alkanes, *Atmos. Chem. Phys.*, 13, 11121–11140, doi:10.5194/acp-13-11121-2013, 2013.

APPENDIX IV: REPRINT OF: “Control of ozonolysis kinetics and aerosol yield by nuances in the molecular structure of volatile organic compounds”

Full Citation:

Harvey, R. M.; Petrucci, G. A.. Control of ozonolysis kinetics and aerosol yield by nuances in the molecular structure of volatile organic compounds. *Atmos Environ* **2015**, *122*, 188-195.



Contents lists available at ScienceDirect

Atmospheric Environment

journal homepage: www.elsevier.com/locate/atmosenv

Control of ozonolysis kinetics and aerosol yield by nuances in the molecular structure of volatile organic compounds



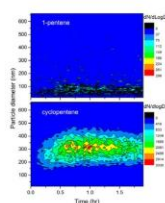
Rebecca M. Harvey, Giuseppe A. Petrucci*

University of Vermont, Cook Physical Sciences, Burlington VT, USA

HIGHLIGHTS

- We measure SOA yield and ozonolysis rate constants for a series of C₅–C₇ alkenes.
- SOA yields were greater for cyclic alkenes as compared to their linear analogs.
- Functional groups influence kinetics through both steric and electronic effects.
- We discuss relationships between VOC molecular structure and SOA yield/kinetics.

GRAPHICAL ABSTRACT



ARTICLE INFO

Article history:

Received 13 May 2015
 Received in revised form
 11 September 2015
 Accepted 14 September 2015
 Available online 24 September 2015

Keywords:

Structure activity relationships (SARs)
 SOA yield
 Ozonolysis
 Alkene
 Oxygenated alkene
 Green leaf volatile

ABSTRACT

Secondary organic aerosol (SOA) plays integral roles in climate and human health, yet there remains a limited understanding of the mechanisms that lead to its formation and ultimate fate, as evidenced by a disparity between modeled atmospheric SOA loadings and field measurements. This disparity highlights the need for a more accurate representation of the molecular-level interactions between SOA sources and oxidative pathways. Due to the paucity of detailed chemical data for most SOA precursors of atmospheric relevance, models generally predict SOA loadings using structure activity relationships generalized to classes of SOA precursors. However, the kinetics and SOA forming potential of molecules are nuanced by seemingly minor structural differences in parent molecules that may be neglected in models. Laboratory chamber studies were used to measure SOA yields and rate constants for the ozonolysis of several linear, cyclic and oxygenated C₅–C₇ alkenes whose molecular structure vary in the site of unsaturation and/or the presence/position of functional groups and that represent atmospherically relevant classes of molecules. For the alkenes studied in this work, we found greater SOA yields for cyclic compounds compared to their linear analogs. For 1-alkenes, SOA yield increased with carbon number but was also dependent on the position of the double bond (internal vs terminal). Both the identity and position of oxygenated functional groups influenced SOA yield and kinetics through steric and electronic effects. Additionally, terminal alkenes generally resulted in a greater SOA yield than analogous internal alkenes, indicating that the position of the double bond in alkenes plays an important role in its atmospheric fate. Herein, we demonstrate the nuanced behavior of these ozonolysis reactions and discuss relationships between parent compound molecular structure and SOA yield and kinetics.

© 2015 Elsevier Ltd. All rights reserved.

1. Introduction

Organic aerosol (OA) is a ubiquitous component of atmospheric

* Corresponding author.

E-mail address: giuseppe.petrucci@uvm.edu (G.A. Petrucci).

particulate matter that influences both human health and global climate. A large fraction of OA is secondary in nature (SOA), being produced by the oxidation of volatile organic compounds (VOCs) emitted by anthropogenic (AVOCs) and biogenic sources (BVOCs). Despite the integral role of SOA in atmospheric processes, there remains a limited understanding of its formation and fate in the atmosphere. This challenge is rooted not only in identifying the sources of SOA but also in understanding the fundamental chemical processes that lead to SOA formation and transformation.

In spite of the breadth of atmospheric A/BVOCs, an extensive amount of work has focused primarily on biogenically emitted terpenes and monoterpenes (Hallquist et al., 2009; Ng et al., 2006; Lee et al., 2006a). Despite efforts to characterize the roles of these prevalent BVOCs, atmospheric models largely under-predict SOA mass as compared to field measurements (Hallquist et al., 2009; Heald et al., 2005; Kanakidou et al., 2005; Jo et al., 2013; Goldstein and Galbally, 2007), due in part to uncertainties in measured VOC emissions, omission of key VOCs, missing chemical and physical processes that contribute to SOA, errors associated with extrapolating laboratory-derived data to the atmosphere and uncertainties in ambient OA measurements (Carlton et al., 2009). Herein, we propose that another contributor to the disparity between field measurements and atmospheric models may lie in the coarse level of chemical assumptions and approximations that must be made by modelers due to a lack of chemical data for the majority of compounds of interest. We highlight this recognized need for a more complete understanding of VOC reactivity and SOA formation at the molecular level by examining the ozonolysis rates and SOA formation yields for a number of compound classes of atmospheric relevance, demonstrating the dramatic impact of small nuances in molecular structure on these chemical parameters.

Reaction rate constants and SOA yield data for input to atmospheric models have been measured experimentally for a number of key VOCs (Lee et al., 2006b; Keywood et al., 2004; Kroll and Seinfeld, 2008; O'Dwyer et al., 2010; Loza et al., 2014; Tkacik et al., 2012; Atkinson et al., 1995; Khamaganov and Hites, 2001; Papagni et al., 2001; Cusick and Atkinson, 2005), yet the list of studied compounds is far from exhaustive. In order to circumvent the paucity of kinetic data, structure activity relationships (SARs) have been developed to estimate oxidation rate constants based on molecular structure of parent compounds. In some cases, SARs have been shown to follow experimental data well (McGillen et al., 2011a, 2008), but there is still considerable error associated with data calculated using this approach (Pfrang et al., 2006; McGillen et al., 2006; Aschmann and Atkinson, 2011). In addition to SARs, which marry structure and (re)activity, several studies have demonstrated correlations between VOC structure and SOA mass yield, although this discussion has been predominantly limited to alkanes (Loza et al., 2014; Tkacik et al., 2012; Lim and Ziemann, 2009; Aumont et al., 2013; Yee et al., 2013) and alkyl-substituted alkenes (Lee et al., 2006b; Keywood et al., 2004; McGillen et al., 2011a). SARs and SOA yield correlations have, by necessity, been used in lieu of experimental data in atmospheric models to predict large scale air quality and climate trends. Inaccuracies or incompleteness in SARs/yield correlations will be reflected in model outputs.

The omission of many VOCs from atmospheric models may also prove to be an important source of error. Semi-volatile organic compounds (SVOCs) and other reactive VOCs (ORVOCs) have received growing attention as potential SOA precursors (Kanakidou et al., 2005). We recently demonstrated that lawn mowing results in the emission of ORVOCs (cis-3-hexenol, HXL, cis-3-hexenyl acetate, CHA and 1-penten-3-ol, PTL) that, upon ozonolysis, contribute to SOA formation at levels approaching those of

predominant terpenes (Harvey et al., 2014). Interestingly, despite having similar molecular backbones consisting of 3-hexene, the SOA forming potential of HXL was found to be much greater than CHA, despite HXL being emitted at a 5x lower rate. This disparity was attributed to the molecular structure of each ORVOC (Harvey et al., 2014; Jain et al., 2014). Similarly, although PTL has a similar molecular structure to HXL (oxygenated internal alkene), it was found to have limited reactivity to ozone and a negligible SOA yield. These observations led us to posit that the chemical processes leading to SOA formation from the oxidation of VOCs are quite nuanced; that a seemingly small change in molecular structure has a profound impact on the molecule's atmospheric behavior.

Several recent studies have expanded our understanding of SARs by describing mechanisms by which certain molecular features impact reaction kinetics and/or SOA forming potential (O'Dwyer et al., 2010; McGillen et al., 2011a, 2008; Boyd et al., 2003; Peeters et al., 2007a, 2007b; Mulla et al., 2010; Vereecken and Francisco, 2012; Stewart et al., 2013). The discussion thus far has focused on unsaturated hydrocarbons, with little work reported with regard to oxygenated species, which contribute a significant fraction of atmospheric reactive VOCs. A more complete understanding of the chemical basis of SARs in oxygenated alkenes may allow for the development of more accurate atmospheric models. In the present work, rate constants for the ozonolysis of a series of cyclic and linear C₅–C₇ unsaturated methyl esters and alcohols are measured and discussed with respect to molecular structure. We add to the discussion of SARs of VOCs by focusing on the effect of oxygenated substituents.

2. Experimental

All experiments were performed at ambient pressure and temperature (~23 °C) in a 775 L Teflon chamber (Fig. 1). Between experiments, the chamber was passivated overnight with 1–2 ppm O₃ and flushed with zero air to attain background aerosol mass loadings <0.1 μg m⁻³.

1-pentene, 1-pentene-3-ol (PTL), 2-pentene, 1-hexene, cis-3-hexenyl acetate (CHA), cis-3-hexenol (HXL), cyclohexene, 3-hexene-2,5-diol (HXNDL), 3-heptene (racemic), and cycloheptene were purchased from Sigma Aldrich. Cyclopentene and cis-3-hexene were purchased from Alfa Aesar. Reagents (all > 95%) were used without further purification. Dry, zero air was produced by passing compressed air sequentially through silica, activated carbon and HEPA filters. This zero air was also used to generate ozone using a commercial corona discharge ozone generator (OLSOA/DLS OzoneLab).

Thermal desorption gas chromatography mass spectrometry (TD-GC/MS) was used to monitor VOC consumption. A detailed description of the TD-GC/MS used can be found in S1 of the

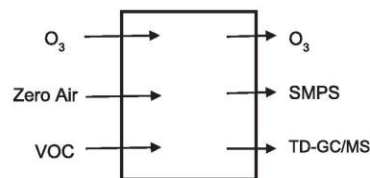


Fig. 1. All experiments were carried out in a 775 L Teflon pillow-style reaction chamber. VOCs were injected via a heated bulb under a steady flow of zero air and mixed by gentle rocking. Once VOC concentrations were stable (15 min), ozone was injected as a short burst and monitored along with particle mass distributions throughout experiments.

supplemental material. Aerosol particle size distributions, as well as total aerosol mass loadings were measured continuously with a scanning mobility particle sizer (SMPS, model 3080, TSI Inc., Shoreview, MN). The vapor pressure of predicted ozonolysis products was estimated using structure based estimators courtesy of the US EPA Estimation Programs Interface Suite (US Environmental Protection Agency, 2014).

Reaction rate constants (k) for the ozonolysis of VOCs were determined using experimental protocol described by Grosjean and Grosjean 1994 (and references therein). Briefly, the rate of ozone decay was measured in the presence of at least a 10-fold initial molar excess of VOC (to ensure pseudo-first order conditions). VOCs were added to the chamber first followed by ozone, which was added as a quick burst (less than 45 s). Initial reaction conditions are summarized in S1 of the Supplemental material. Ozone concentrations were monitored at 5 s intervals with an American Ecotech Serinus O₃ Monitor (model E020010). A plot of $\ln([O_3]_0/[O_3]_t)$, where $[O_3]_0$ and $[O_3]_t$ are the ozone concentrations at time zero and t , respectively, versus time (t , seconds) yields a straight line with slope k' (sec^{-1}). From the rate expression of the reaction, $k = k'/[VOC]_0$, where $[VOC]_0$ is the VOC concentration at time zero, we were able to determine k ($\text{cm}^3 \text{sec}^{-1} \text{molecule}^{-1}$). The loss of ozone, as well as the VOC, to chamber walls was measured and found to be negligible over the time scale of the kinetic experiments (Harvey et al., 2014), confirming that reaction with VOCs was the only significant removal process for ozone.

Separate experiments were used to calculate SOA yields, Y , according to Equation (1) (Odum et al., 1996) where $\Delta[\text{SOA}]$ is the maximum, particle-loss corrected SOA concentration ($\mu\text{g m}^{-3}$) and $\Delta[\text{VOC}]$ is the total amount of VOC consumed ($\mu\text{g m}^{-3}$) at that SOA maximum:

$$Y = \frac{\Delta[\text{SOA}]}{\Delta[\text{VOC}]} * 100\% \quad (1)$$

Particle loss (to chamber walls, due to secondary reactions and/or phase transitions) was estimated by extrapolating decay trends in SOA mass loadings back to time zero of the reaction (i.e., at time of ozone injection). A representative reaction profile can be found in S2 of the Supplemental material. We report the average yield (\pm standard deviation) from at least three experiments for each VOC. Student's T-tests were used to determine if averages were statistically different for different VOCs, at given confidence intervals, which are indicated with alpha- (α) values as they are discussed.

2.1. SOA yield of cyclic vs. linear alkenes

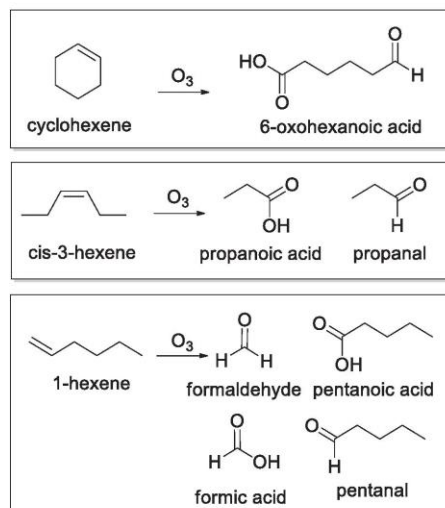
Relationships between VOC molecular structure and SOA yield have been reported for a number of chemical systems. Some studies identify surrogates for naturally occurring VOCs (Keywood et al., 2004; Epstein and Donahue, 2010), some catalog the SOA yield of several compounds (Lee et al., 2006b; Loza et al., 2014; Odum et al., 1996; Gao et al., 2004), while others identify key molecular structures that influence SOA yield (Keywood et al., 2004; Tkacik et al., 2012; Lim and Ziemann, 2009; Aumont et al., 2013; Yee et al., 2013; Jathar et al., 2013). Most studies to date have focused on linear, branched and cyclic alkanes or cycloalkenes. In the case of alkanes, it has been shown that SOA yield increases with carbon number and, given two compounds with the same number of carbon atoms, follows the trend of cyclic alkanes > linear alkanes > branched alkanes and decreases further with degree of branching. SOA yield in alkanes also increases if the oxidation results in oligomerization (Lim and Ziemann, 2009; Yee et al., 2013).

SOA yield for linear alkenes is also expected to increase with

carbon number (Keywood et al., 2004). For the series of linear VOCs studied in this work, we generally observed SOA yields increasing in the order of pentene < hexene < heptene. The position of the double bond, however, also plays an important role in the SOA yield, with the 1-alkene generally producing a greater SOA yield than the internally bonded analog. For example, 1-pentene resulted in a SOA yield of 1.8 (± 0.2)%, which was greater ($\alpha = 0.05$) than that of 2-pentene (0.80 (± 0.6)%).

The mechanisms leading to SOA formation from the ozonolysis of alkenes has been reviewed extensively (Hallquist et al., 2009; Carlton et al., 2009; Atkinson and Arey, 2003; Zahardis and Petrucci, 2007). Following the very simplified ozonolysis mechanism in Scheme 1, 1-pentene is expected to produce C₁ and C₄ carboxylic acids and aldehydes, while 2-pentene is expected to result in the production of C₂ and C₃ carboxylic acids and aldehydes. These species are relatively volatile, and will not nucleate to form SOA directly. Therefore, secondary oligomerization and/or condensation mechanisms are the likely route to SOA formation for these systems. In fact, secondary reactions of ozonolysis products, including oligomerization of stabilized Criegee Intermediates (CIs), are predominant drivers of SOA formation in the alkene-ozonolysis system (Tolocka et al., 2004; Sakamoto et al., 2013). Oligomerization (and SOA yield) can be directly related to the fraction of CIs that exist in a peroxy-radical stabilized form, where a lower "stability fraction" results in lower SOA yields (Sadezky et al., 2006, 2008; Donahue et al., 2011). It is possible that the enhanced stability of the C₁ and C₄ CIs in 1-pentene ozonolysis system allow it to undergo secondary oligomerization reactions more readily as compared to the less stable C₂ and C₃ CIs found in 2-pentene system, resulting in an enhanced SOA yield for 1-pentene (Sadezky et al., 2006, 2008; Donahue et al., 2011).

Based on observations made for 1- and 2-pentene, we would anticipate 1-hexene to have a greater SOA yield than 3-hexene, yet both species gave the same SOA yield, within experimental error



Scheme 1. Abbreviated ozonolysis schemes for cyclic and linear C₆ alkenes, showing the formation of higher volatility products in the linear case, which leads to lower SOA yields, especially for internal, linear alkenes.

(3.0 (± 1.0)% for 1-hexene and 2.2 (± 1.6)% for 3-hexene). Reaction kinetics will be discussed in depth in the following sections, but it is worth noting that in addition to having an enhanced SOA yield, 3-hexene also has a much greater rate constant (k) than 1-hexene. It is possible that the kinetics of the 3-hexene ozonolysis reaction favor a pathway that leads to a greater degree of oligomerization and/or lower volatility products, ultimately leading to a greater SOA yield.

In the case of cycloalkenes, it has been shown that SOA yield increases with carbon number, with the number of endocyclic double bonds and with the presence of alkyl substitution at the double bond (Lee et al., 2006b; Keywood et al., 2004). One important trend that has not been explicitly reported in the literature is that of increasing SOA yield for cyclic alkenes as compared to their linear analogues. As shown in the abbreviated Scheme 1, the oxidative cleavage of linear alkenes produces several low molecular weight species that are expected to be found in the gas phase. The ozonolysis of cyclic alkenes, on the other hand, produces molecules with greater molecular weight and lower vapour pressure, likely contributing to SOA more readily. Indeed, we observed an enhanced SOA yield for cyclopentene, cyclohexene and cycloheptene as compared to their linear analogs (Fig. 2 and Table 1).

For unsubstituted C₅–C₇ cyclic VOCs, we measured a SOA yield trend of cyclohexene < cyclopentene \leq cycloheptene in contrast to the results of Keywood et al. 2004 who found that SOA yield increased with carbon number for C₅–C₈ cycloalkenes. Although Keywood et al. 2004 worked at lower VOC concentrations and used ammonium sulfate seed particles, our yields for cyclohexene and cycloheptene are in good agreement with theirs. Our cyclopentene yield (19 \pm 2.5%) however, was about twice that reported by Keywood et al. 2004. It is worth noting that cyclopentene has the greatest rate constant (k) of these cyclic systems (See Table 2 and Section 3.2). It is possible that the enhanced k for cyclopentene contributes to its greater SOA yield. The reasons for the disparity between our measurements and those of Keywood et al. 2004 and for our deviation from the trend of increasing SOA yield with increasing carbon number are unclear.

Autoxidation reactions may also result in enhanced SOA yield. Autoxidation involves the incorporation of molecular oxygen into product structure after the initial oxidation by ozone and results in highly oxidized multifunction molecules (HOM) that contribute to

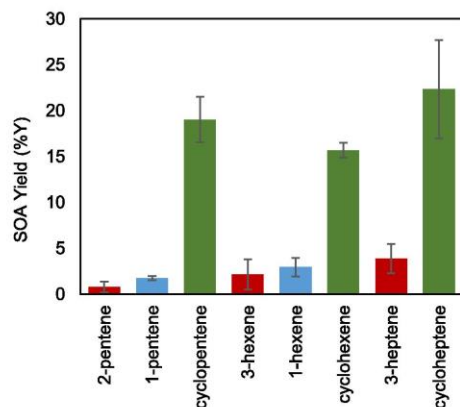


Fig. 2. SOA Yield of C₅–C₇ linear and cycloalkenes. In all cases, the cycloalkene has a greater SOA yield than its linear analog. Terminally unsaturated alkenes showed an enhanced SOA yield over internal, linear alkenes.

Table 1

SOA yield of linear, cyclic and oxygenated alkenes. Initial concentrations of the parent hydrocarbon and ozone in each experiment were 1000 \pm 100 ppbv. N = 3 for all reported values.

Chemical system	SOA % Yield (average \pm standard deviation)
1-pentene	1.77 \pm 0.22
2-pentene	0.79 \pm 0.57
PTL	3.28 \pm 0.7
Cyclopentene	19 \pm 2.5
3-hexene	2.17 \pm 1.6
1-hexene	3.0 \pm 1.0
Cyclohexene	15.7 \pm 0.8
CHA	3.9 \pm 2.4
HXL	6.5 \pm 2.6
HXNDL	9.3 \pm 0.4
3-heptene	3.9 \pm 1.6
Cycloheptene	22.4 \pm 5.4

SOA (Ehn et al., 2012; Crouse et al., 2013; Jokinen et al., 2014; Rissanen et al., 2014; Ehn et al., 2014; Mentel et al., 2015). It has been shown that cyclic alkenes undergo autoxidation more readily than their linear analogs (Mentel et al., 2015), which may contribute to the enhanced SOA yield we observed for cyclic vs linear alkenes. Autoxidation processes require available hydrogen atoms for H-shift rearrangements and is thus limited to ozonolysis intermediates with three or more carbon atoms (Mentel et al., 2015), which may contribute to our observation of equivalent yields for 1-hexene and 3-hexene. The ozonolysis of 1-hexene yields only one product that could undergo autoxidation while 3-hexene yields two. Without molecular-level characterization of resultant SOA, however, we cannot comment on the amount of HOM formed or the role of autoxidation in the formation of SOA herein. This additional analysis would be a logical next step in this research.

2.2. Ozonolysis rate constants (k) for linear and cyclic alkenes

Rate constants (k) for the ozonolysis of VOCs have been a predominant focus in the recent literature, especially with regard to the impact of VOC molecular structure (O'Dwyer et al., 2010; McGillen et al., 2011a, 2008, 2006; Aschmann and Atkinson, 2011; McGillen et al., 2011b; Johnson et al., 2000). It is important, however, to distinguish between SOA yield (%Y) and reactivity (k), which are not necessarily related. As we show, a VOC may be highly reactive to atmospheric oxidants, yet contribute very little SOA or vice versa.

We also measured and compared the ozonolysis rate constants (k) of the alkenes in this study. A representative reaction profile for the ozonolysis of HXL is given in Fig. 3. For linear alkenes, our results (Fig. 4, Table 2) support previous observations that terminal alkenes have a reduced k compared to internal alkenes (McGillen et al., 2008, 2006, 2011b). This trend may be explained by the inductive effect, wherein substituents near the double bond increase electron density at the reaction center, promoting electrophilic addition of ozone across the double bond. Terminal alkenes, which contain alkyl substituents on only one side of the double bond, experience a lower inductive effect and a correspondingly reduced k as compared to internal alkenes, which are substituted on both sides. Steric effects also impact the kinetics of the ozonolysis of internal vs terminal alkenes, whereby the approaching ozone molecule has easier access to the terminal species, which would enhance k over the internally double bonded analog. However, the marked increase in k that we observe for 3-hexene compared to 1-hexene indicates that, overall, the steric hindrance encountered in 3-hexene is outweighed by

clear.

We found no correlation between k and ring size. However our observed order of cyclohexene < cycloheptene < cyclopentene, was in accord with previously reported data (Treacy et al., 1997; Sidebottom et al., 1997). These variations in k -values for cycloalkenes could be related to differences in ring strain energies (Atkinson et al., 1983) wherein the oxidative cleavage of an endocyclic double bond relieves ring strain in cyclic molecules. In cyclopentene, the transition between cycloalkene to ozonide alleviates a considerable amount of ring strain, strongly favoring the reaction, whereas cyclohexene contains relatively little strain energy, resulting in a moderate k (Benson, 1966). Cycloheptene has been shown to experience a similar ring strain as cyclopentene (Benson, 1966), which could rationalize the enhanced k for cycloheptene over cyclohexene.

Both cyclopentene and cycloheptene had a greater k than their linear (internal/terminal) analogs, further supporting the theory ring strain is a significant driver in these reactions. However, we measured the same k (within experimental error) for cyclohexene and 3-hexene. This observation suggests that ring strain in cyclohexene is not sufficient to enhance ozonolysis kinetics. Cyclohexene did, however, show a much greater k than 1-hexene, pointing back to the importance of the inductive effect; cyclohexene is more substituted at the double bond (two effective alkyl substituents) than 1-hexene (1 alkyl substituent), increasing the inductive effect and the overall k .

2.3. SOA yield for oxygenated linear alkenes

Despite extensive research to establish the SARs for ozonolysis of alkyl substituted linear alkenes, there has been a limited effort to understand the relationship between reactivity (k) or SOA yield and oxygenated substituents or their proximity to the double bond. To shed light on this knowledge gap, we measured the SOA yields and ozonolysis reaction rates of a series of C₅–C₇ linear, oxygenated alkenes (Table 1).

The SOA yield for 1-penten-3-ol (PTL) ($3.3 \pm 0.7\%$) was greater than that measured for its non-oxygenated analog, 1-pentene ($1.7 \pm 0.2\%$) ($\alpha = 0.05$). The ozonolysis of 1-pentene is expected to produce C₁ and C₄ products, which can undergo secondary oligomerization reactions (including hemi-acetal, aldol and ester condensation reactions) to form SOA. The ozonolysis of 1-PTL will produce the same C₁ products but its C₄ products will also contain an additional hydroxyl functionality, which (in addition to lowering the overall vapour pressure of the products) can undergo additional secondary reactions that are known to form SOA (Jain et al., 2014). Analogously, HXL ($6.5 \pm 2.6\%$) and HXNDL ($9.3 \pm 0.4\%$) have greater SOA yield than 3-hexene ($2.2 \pm 1.6\%$). CHA was found to have the same SOA yield as HXL ($3.9 \pm 2.4\%$) despite the fact that its methyl ester substituent shuts down the additional oligomerization pathway (Jain et al., 2014). The reasons for this deviation from expected trends are unclear, but the large error associated with these measurements may be masking a general trend for HXL having a greater yield than CHA.

2.4. Ozonolysis kinetics for oxygenated linear alkenes

As stated above, electron donating substituents at the site of a double bond can promote the electrophilic addition of ozone, enhancing reactivity through the inductive effect (O'Dwyer et al., 2010; McGillen et al., 2011a, 2008, 2006, 2011b). Hydroxyl groups are strongly electron donating and may therefore be predicted to enhance reactivity to an even greater degree than alkyl substituents. However, as we observed, HXNDL and HXL had lower reaction rates than their unsubstituted analogs. The hydroxyl

substitution(s) at the beta (HXNDL) or gamma (HXL) position may be too distant from the double bond to enhance reactivity via the inductive effect, and actually seem to inhibit reactivity, likely due to steric interference. This interference is particularly strong for HXNDL, which has two hydroxyl groups in very close proximity to the double bond.

Analogous to the case of non-oxygenated alkenes, the reactivity of oxygenated molecules is a trade-off between both steric hindrance and inductive enhancement (McGillen et al., 2011a, 2008, 2006, 2011b). Though it may seem intuitive, it has been well established that the steric effect diminishes with increasing distance from the reactive site (McGillen et al., 2011a, 2008, 2006, 2011b; Taft, 1956). Aschmann and Atkinson (Aschmann and Atkinson, 2011) measured the steric effect for methyl-substituted alkenes and found no difference between that measured for 1-hexene and 5-methyl-1-hexene, yet as the methyl substituent moved closer to the double bond, steric effects increased, and the (NO₃) oxidation rate constant decreased, though the trend was not statistically significant. Since steric effects are expected to be more pronounced in ozone-alkene reactions than in corresponding NO₃-alkene reactions (Aschmann and Atkinson, 2011), the trend in ozonolysis rate constant is expected to follow to a more significant degree. Based on our results, it appears that the steric hindrance provided by the hydroxyl substituents in HXL and HXNDL out-competes any reactivity enhancement they may contribute via the inductive effect, resulting in a lower ozonolysis rate constant as compared to 3-hexene.

Alternatively, we observed a slight enhancement in the ozonolysis rate constant for PTL as compared to 1-pentene, echoing results from O'Dwyer et al. 2010 and suggesting that the terminal position of the double bond in PTL offers sufficient room for an approaching ozone molecule so the inductive effect associated with the hydroxyl substituent enhances reactivity overall. Using 3-methyl-1-pentene, we found a diminished k as compared to 1-pentene, suggesting that the methyl substituent provides significant steric hindrance to ozone to overcome any inductive enhancement it may also provide. 3-methyl-1-pentene has slightly less steric hindrance than PTL, suggesting that (if steric effects alone were considered) the methylated 1-pentene might have a greater k than PTL (McGillen et al., 2011a, 2008). However, we measure a much greater k for PTL than what has been reported for 3-methyl-1-pentene (McGillen et al., 2011a, 2008). Although steric hindrance due to the hydroxyl group is large for PTL, it enhances k overall as compared to the methylated analog due to the inductive effect.

Acetate esters are also electron donating, although not as strongly as hydroxyl groups, and would therefore be expected to enhance k . In fact, ester groups β to the alkene are predicted to enhance the inductive effect over unsubstituted alkenes by about 1.5 times (McGillen et al., 2011a). However, we found that CHA has a slightly (albeit not significantly) smaller rate constant than the 3-hexene. We would also expect CHA to have a smaller rate constant than HXL, since β -hydroxyl groups are estimated to increase the inductive effect over β -esters by a factor of about three (McGillen et al., 2011a). We also predict methyl esters in CHA to provide more steric hindrance than the hydroxyl groups in HXL, which would also result in a smaller k . However, we observed a slightly greater k for CHA compared to HXL. Transition state theory could be used to shed further light on the factors affecting these systems. Nonetheless, our data clearly demonstrate that the presence, position and identity of substituents are all key to predict ozonolysis reaction kinetics.

3. Atmospheric implications

The marked disparity between predicted SOA mass loadings and

Table 2

Ozonolysis rate constants (k , $\times 10^{-17}$ $\text{cm}^3 \text{sec}^{-1} \text{molecule}^{-1}$) of alkenes are reported \pm the standard deviation of replicate experiments. Individual experimental conditions can be found in Table S2 of the Supplemental Material (* indicates a predicted/modelled value). $N = 3$ for all reported values.

VOC	k	Reference	VOC	k	Reference
1-pentene-3-ol (PTL)	1.7 ± 0.1	This work	3-hexene	5.9 ± 0.5	This work
	1.64	12		15.0	36
	1.79	36		14.4	20
1-pentene	1.2 ± 0.4	This work	Cyclohexene	12.2	20*
	0.92	56		6.8 ± 0.1	This work
	0.99	58		7.00	62
	1.20	35		8.50	57
	0.753	20*		7.90	41
2-pentene	1.7 ± 0.9	This work	cis-3-hexenol (HXL)	5.8 ± 0.9	This work
cis-2-pentene	13.0	35		10.5	36
trans-2-pentene	20.9	20	6.14	15	
	20.0	35	6.47	63	
	31.6	20	5.8 ± 0.1	This work	
Cyclopentene	24 ± 11	This work	cis-3-hexenyl acetate (CHA)	5.40	15
	20.0	35		5.90	62
	61.0	62	hex-3-ene-2,5-diol (HXNDL)	0.9 ± 0.8	This work
	67	41		6.6 ± 0.3	This work
1-hexene	1.4 ± 0.3	This work	3-heptene	12.8 ± 4.6	This work
	1.42	58		22.6	62
	1.01	20	Cycloheptene	23.7	57

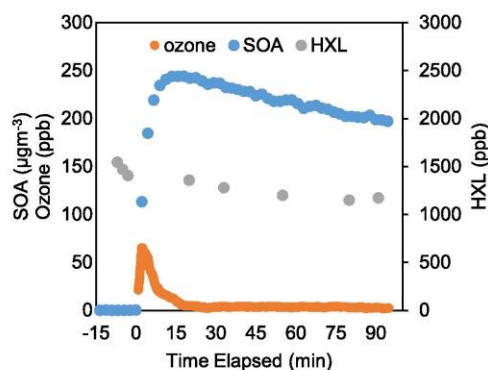


Fig. 3. A representative reaction profile for the ozonolysis of HXL used to determine the rate constant k . In all rate experiments, ozone decay was measured in the presence of at least a 10-fold excess of VOC (to ensure pseudo-first order conditions). Although SOA mass distribution was monitored, these experiments were not used to determine SOA yield because they contained such a large excess of VOC.

the enhancement of k due to the inductive effect (at least for these relatively small alkenes).

The interplay between the inductive effect and steric hindrance can be better appreciated with the Arrhenius equation,

$$k = Ae^{-\frac{E_a}{RT}} \quad (2)$$

The pre-exponential factor, A , is inversely related to steric effects and thus directly proportional to k . Activation energy, E_a , is inversely related to both the inductive effect and to k (McGillen et al., 2011a, 2008; Treacy et al., 1992; Treacy et al., 1997; Leather et al., 2010). An increase in chain length from C_3 to C_6 results in a decrease in both E_a and A (Treacy et al., 1992) and ultimately results in an increase in k for ozonolysis. Lengthening the carbon backbone also increases steric hindrance, but not enough to overcome inductive effects or to limit k . McGillen et al. 2008 experimentally confirmed that k increases with carbon number for 1-hexene and 1-pentene, yet their SAR-predicted rate constants were identical for

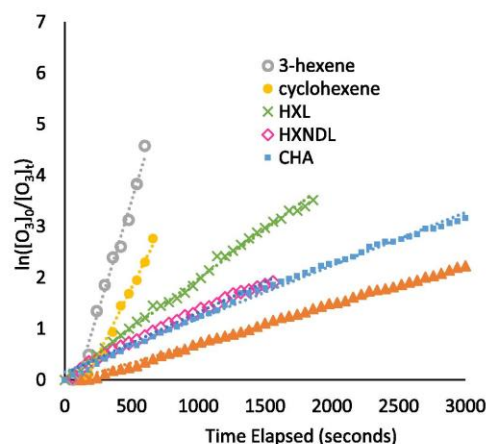


Fig. 4. Plots of $\ln([O_3]_0/[O_3]_t)$ vs time yielded a linear decay, confirming reactions were pseudo-first order for the VOC. k' (sec^{-1}) for the ozonolysis of each alkene was found from the slope of the linear regression, which is given in Supplemental Material S3.

1-heptene, 1-hexene and 1-pentene. Our measured rate constants for 1-hexene and 1-pentene were equal within error, confirming the modeled behavior predicted by McGillen et al. 2008 but not experimental data as reported by their group or by others (Treacy et al., 1992). The reasons for the discrepancy are not clear, but the inconsistencies between modeled and measured k further support our supposition that additional, unknown nuances in molecular structure may exist that result in profound impacts on atmospheric SOA formation and reactivity. As shown in Table 2, we measured k values on the same order of magnitude as those reported by others, with the exception of 2-pentene, which was approximately one order of magnitude smaller than that measured and predicted by McGillen et al. (McGillen et al., 2008; US Environmental Protection Agency, 2014). The methods they used to measure k were analogous to those used herein, so the reason for this disparity is not

those measured in the field highlights the need for more accurate representation of the molecular level interactions between VOCs and oxidants. Some SARs have been shown to match chamber studies well (McGillen et al., 2011a, 2008, 2011b), but chamber studies rarely match atmospheric conditions (with chamber studies working at unrealistically high VOC concentrations and mass loadings) and experimental results are often irreproducible between (and even within) laboratories (Keywood et al., 2004; Bahreini et al., 2009). We recently reported the SOA yield of several green leaf volatiles using an experimental design analogous to that used by Hamilton et al. 2009 yet measured very different SOA yields with a high degree of uncertainty (Harvey et al., 2014). Keywood et al. 2004 also demonstrated the large degree of variability in making SOA yield measurements, reporting yields ranging from 0% to 19% for a single VOC in a single laboratory. Herein, we also report rather large ranges in SOA yield for replicate experiments (between 5% and 75% relative error). The reasons for the disparity in yield measurements made for the same chemical systems under the same nominal conditions are unclear, but there is growing evidence to suggest that inconsistencies in the instrumental parameters used by different laboratories play a role (Wiedensohler et al., 2012). For a laboratory where instrumental parameters are not a variable, like ours for example, differences in SOA mass measurements may suggest a degree of chaos during the initial reaction steps that have yet to be understood, making them all but impossible to predict or model.

We have shown that the mechanisms and product yields of VOC oxidation are impacted by subtleties in molecular structure. Due to computational costs and limited kinetic data available, these relationships are not always incorporated into atmospheric models. We have shown that both the aerosol yield and the rate constant of structural isomers (cyclic vs linear, internally unsaturated vs terminally unsaturated and presence, type and position of substituents) vary significantly. It is in these seemingly minor (and rarely considered) molecular variations where error can be born, which can then be extrapolated in models and may result in the large disparities between modeled and measured atmospheric aerosol levels and properties. Ultimately, advances in computing power and our state of knowledge will permit models to evolve to incorporate much of this nuanced chemistry. Until such time, we offer this glimpse of the dramatic impact of seemingly small variations in molecular structure on reactivity and SOA formation. These initial steps will serve to further inform the atmospheric chemistry community on considerations that must be taken in order to harmonize laboratory findings with field studies and model outputs.

Acknowledgments

This material is based upon work supported by the National Science Foundation under Grant No. CHE-1213632.

Appendix A. Supplementary data

Supplementary data related to this article can be found at <http://dx.doi.org/10.1016/j.atmosenv.2015.09.038>.

References

Aschmann, S.M., Atkinson, R., 2011. *J. Phys. Chem. A* 115, 1358.
 Atkinson, R., Arey, J., 2003. *Chem. Rev.* 103, 4605.
 Atkinson, R., Aschmann, S.M., Carter, W.P.L., Pitts, J.N., 1983. *Int. J. Chem. Kinet.* 15, 721.
 Atkinson, R., Arey, J., Aschmann, S.M., Corchnoy, S.B., Shu, Y., 1995. *Int. J. Chem. Kinet.* 27, 941.
 Aumont, B., Camredon, M., Mouchel-Vallon, C., La, S., Ouzebidour, F., Valorso, R.,

Lee-Taylor, J., Madronich, S., 2013. *Faraday Discuss.* 165, 105.
 Bahreini, R., Ervens, B., Middlebrook, A.M., Warneke, C., de Gouw, J.A., DeCarlo, P.F., Jimenez, J.L., Brock, C.A., Neuman, J.A., Ryerson, T.B., Stark, H., Atlas, E., Brioude, J., Fried, A., Holloway, J.S., Peischl, J., Richter, D., Walega, J., Weibring, P., Wollny, A.G., Fehsenfeld, F.C., 2009. *J. Geophys. Res. Atmos.* 114.
 Benson, S.W., 1966. *Thermochemical Kinetics*. Wiley, New York.
 Boyd, A.A., Villenave, E., Lesclaux, R., 2003. *Atmos. Environ.* 37, 2751.
 Carlton, A.G., Wiedinmyer, C., Kroll, J.H., 2009. *Atmos. Chem. Phys.* 9, 4987.
 Crouse, J.D., Nielsen, L.B., Jørgensen, S., Kjaergaard, H.G., Wennberg, P.O., 2013. *J. Phys. Chem. Lett.* 4, 3513.
 Cusick, R.D., Atkinson, R., 2005. *Int. J. Chem. Kinet.* 37, 183.
 Donahue, N.M., Drozd, G.T., Epstein, S.A., Presto, A.A., Kroll, J.H., 2011. *Phys. Chem. Chem. Phys.* 13, 10848.
 Ehn, M., Kleist, E., Junninen, H., Petäjä, T., Lönn, G., Schobesberger, S., Dal Maso, M., Trimborn, A., Kulmala, M., Worsnop, D.R., Wahner, A., Wildt, J., Mentel, T.F., 2012. *Atmos. Chem. Phys.* 12, 5113.
 Ehn, M., Thornton, J.A., Kleist, E., Sipila, M., Junninen, H., Pullinen, I., Springer, M., Rubach, F., Tillmann, R., Lee, B., Lopez-Hilfiker, F., Andres, S., Acir, I.-H., Rissanen, M., Jokinen, T., Schobesberger, S., Kangasluoma, J., Kontkanen, J., Nieminen, T., Kurten, T., Nielsen, L.B., Jørgensen, S., Kjaergaard, H.G., Canagaratna, M., Maso, M.D., Berndt, T., Petaja, T., Wahner, A., Kerminen, V.-M., Kulmala, M., Worsnop, D.R., Wildt, J., Mentel, T.F., 2014. *Nature* 506, 476.
 Epstein, S.A., Donahue, N.M., 2010. *J. Phys. Chem. A* 114, 7509.
 Gao, S., Keywood, M., Ng, N.L., Surratt, J., Varutbangkul, V., Bahreini, R., Flagan, R.C., Seinfeld, J.H., 2004. *J. Phys. Chem. A* 108, 10147.
 Goldstein, A.H., Galbally, I.E., 2007. *Environ. Sci. Technol.* 41, 1514.
 Grosjean, E., Grosjean, D., 1994. *Int. J. Chem. Kinet.* 26, 1185.
 Hallquist, M., Wenger, J.C., Baltensperger, U., Rudich, Y., Simpson, D., Claeys, M., Dommen, J., Donahue, N.M., George, C., Goldstein, A.H., Hamilton, J.F., Herrmann, H., Hoffmann, T., Iinuma, Y., Jang, M., Jenkin, M.E., Jimenez, J.L., Kiendler-Scharr, A., Maenhaut, W., McFiggans, G., Mentel, T.F., Monod, A., Prevot, A.S.H., Seinfeld, J.H., Surratt, J.D., Szmigielski, R., Wildt, J., 2009. *Atmos. Chem. Phys.* 9, 5155.
 Hamilton, J.F., Lewis, A.C., Carey, T.J., Wenger, J.C., Borrás i Garcia, E., Muñoz, A., 2009. *Atmos. Chem. Phys.* 9, 3815.
 Harvey, R.M., Zahardis, J., Petrucci, G.A., 2014. *Atmos. Chem. Phys.* 14, 797.
 Heald, C.L., Jacob, D.J., Park, R.J., Russell, L.M., Huebert, B.J., Seinfeld, J.H., Liao, H., Weber, R.J., 2005. *Geophys. Res. Lett.* 32, L18809.
 Jain, S., Zahardis, J., Petrucci, G.A., 2014. Soft ionization chemical analysis of secondary organic aerosol from green leaf volatiles emitted by turf grass. *Environ. Sci. Technol.* 48 (9), 4835–4843.
 Jathar, S.H., Miracolo, M.A., Tkacik, D.S., Donahue, N.M., Adams, P.J., Robinson, A.L., 2013. *Environ. Sci. Technol.* 47, 12886.
 Jo, D.S., Park, R.J., Kim, M.J., Spracklen, D.V., 2013. *Atmos. Environ.* 81, 230.
 Johnson, D., Rickard, A.R., McGill, C.D., Marston, G., 2000. *Phys. Chem. Chem. Phys.* 2, 323.
 Jokinen, T., Sipilä, M., Richters, S., Kerminen, V.-M., Paasonen, P., Stratmann, F., Worsnop, D., Kulmala, M., Ehn, M., Herrmann, H., Berndt, T., 2014. *Angew. Chem. Int. Ed.* 53, 14596.
 Kanakidou, M., Seinfeld, J.H., Pandis, S.N., Barnes, I., Dentener, F.J., Facchini, M.C., Van Dingenen, R., Ervens, B., Nenes, A., Nielsen, C.J., Swietlicki, E., Putaud, J.P., Balkanski, Y., Fuzzi, S., Horth, J., Moortgat, G.K., Winterhalter, R., Myhre, C.E.L., Tsigaridis, K., Vignati, E., Stephanou, E.G., Wilson, J., 2005. *Atmos. Chem. Phys.* 5, 1053.
 Keywood, M.D., Varutbangkul, V., Bahreini, R., Flagan, R.C., Seinfeld, J.H., 2004. *Environ. Sci. Technol.* 38, 4157.
 Khamaganov, V.G., Hites, R.A., 2001. *J. Phys. Chem. A* 105, 815.
 Kroll, J.H., Seinfeld, J.H., 2008. *Atmos. Environ.* 42, 3593.
 Leather, K.E., McGillen, M.R., Percival, C.J., 2010. *Phys. Chem. Chem. Phys.* 12, 2935.
 Lee, J.D., Lewis, A.C., Monks, P.S., Jacob, M., Hamilton, J.F., Hopkins, J.R., Watson, N.M., Saxton, J.E., Ennis, C., Carpenter, L.J., Carslaw, N., Fleming, Z., Bandy, B.J., Oram, D.E., Penkett, S.A., Slemr, J., Norton, E., Rickard, A.R., Whalley, L.K., Heard, D.E., Bloss, W.J., Gravesock, T., Smith, S.C., Stanton, J., Pilling, M.J., Jenkin, M.E., 2006. *Atmos. Environ.* 40, 7598.
 Lee, A., Goldstein, A.H., Keywood, M.D., Gao, S., Varutbangkul, V., Bahreini, R., Ng, N.L., Flagan, R.C., Seinfeld, J.H., 2006. *J. Geophys. Res. Atmos.* 111, D07302.
 Lim, Y.B., Ziemann, P.J., 2009. *Environ. Sci. Technol.* 43, 2328.
 Loza, C.L., Craven, J.S., Yee, L.D., Coggon, M.M., Schwantes, R.H., Shiraiwa, M., Zhang, X., Schilling, K.A., Ng, N.L., Canagaratna, M.R., Ziemann, P.J., Flagan, R.C., Seinfeld, J.H., 2014. *Atmos. Chem. Phys.* 14, 1423.
 McGillen, M.R., Crosier, J., Percival, C.J., Sanchez-Reyna, G., Shallcross, D.E., 2006. *Chemosphere* 65, 2035.
 McGillen, M.R., Carey, T.J., Archibald, A.T., Wenger, J.C., Shallcross, D.E., Percival, C.J., 2008. *Phys. Chem. Chem. Phys.* 10, 1757.
 McGillen, M.R., Archibald, A.T., Carey, T., Leather, K.E., Shallcross, D.E., Wenger, J.C., Percival, C.J., 2011. *Phys. Chem. Chem. Phys.* 13, 2842.
 McGillen, M.R., Ghalaieny, M., Percival, C.J., 2011. *Phys. Chem. Chem. Phys.* 13, 10965.
 Mentel, T.F., Springer, M., Ehn, M., Kleist, E., Pullinen, I., Kurtén, T., Rissanen, M., Wahner, A., Wildt, J., 2015. *Atmos. Chem. Phys.* 15, 6745.
 Al Mulla, I., Viera, L., Morris, R., Sidebottom, H., Treacy, J., Mellouki, A., 2010. *Chemphyschem* 11, 4069.
 Ng, N.L., Kroll, J.H., Keywood, M.D., Bahreini, R., Varutbangkul, V., Flagan, R.C., Seinfeld, J.H., Lee, A., Goldstein, A.H., 2006. *Environ. Sci. Technol.* 40, 2283.
 O'Dwyer, M.A., Carey, T.J., Healy, R.M., Wenger, J.C., Picquet-Varrault, B., Doussin, J.F., 2010. *Z. Phys. Chem.* 224, 1059.

- Odum, J.R., Hoffmann, T., Bowman, F., Collins, D., Flagan, R.C., Seinfeld, J.H., 1996. *Environ. Sci. Technol.* 30, 2580.
- Papagni, C., Arey, J., Atkinson, R., 2001. *Int. J. Chem. Kinet.* 33, 142.
- Peeters, J., Boullart, W., Pultau, V., Vandenberg, S., Vereecken, L., 2007. *J. Phys. Chem. A* 111, 1618.
- Peeters, J., Boullart, W., Pultau, V., Vandenberg, S., Vereecken, L., 2007. *J. Phys. Chem. A* 111, 1618.
- Pfrang, C., King, M.D., Canosa-Mas, C.E., Wayne, R.P., 2006. *Atmos. Environ.* 40, 1180.
- Rissanen, M.P., Kurtén, T., Sipilä, M., Thornton, J.A., Kangasluoma, J., Sarnela, N., Junninen, H., Jørgensen, S., Schallhart, S., Kajos, M.K., Taipale, R., Springer, M., Mentel, T.F., Ruuskanen, T., Petäjä, T., Worsnop, D.R., Kjaergaard, H.G., Ehn, M., 2014. *J. Am. Chem. Soc.* 136, 15596.
- Sadezky, A., Chaimbault, P., Mellouki, A., Römpp, A., Winterhalter, R., Le Bras, G., Moortgat, G.K., 2006. *Atmos. Chem. Phys.* 6, 5009.
- Sadezky, A., Winterhalter, R., Kanawati, B., Römpp, A., Spengler, B., Mellouki, A., Le Bras, G., Chaimbault, P., Moortgat, G.K., 2008. *Atmos. Chem. Phys.* 8, 2667.
- Sakamoto, Y., Inomata, S., Hirokawa, J., 2013. *J. Phys. Chem. A* 117, 12912.
- Sidebottom, H., Tracy, J., 1997. In: Le Bras, G. (Ed.), *Chemical Processes in Atmospheric Oxidation*, vol. 3. Springer Berlin Heidelberg, p. 218.
- Stewart, D.J., Almbrok, S.H., Lockhart, J.P., Mohamed, O.M., Nutt, D.R., Pfrang, C., Marston, G., 2013. *Atmos. Environ.* 70, 227.
- Taft, R., 1956. *Steric Effects in Organic Chemistry*. John Wiley & Sons, Inc., New York.
- Tkacik, D.S., Presto, A.A., Donahue, N.M., Robinson, A.L., 2012. *Environ. Sci. Technol.* 46, 8773.
- Tolocka, M.P., Jang, M., Ginter, J.M., Cox, F.J., Kamens, R.M., Johnston, M.V., 2004. *Environ. Sci. Technol.* 38, 1428.
- Treacy, J., Elhag, M., O'Farrell, D., Sidebottom, H., 1992. *Ber. Bunsen Phys. Chem.* 96, 422.
- Treacy, J., Curley, M., Wenger, J., Sidebottom, H., 1997. *J. Chem. Soc. Faraday Trans.* 93, 2877.
- US Environmental Protection Agency, 2014. 4.11 ed., Washington DC, USA.
- Vereecken, L., Francisco, J.S., 2012. *Chem. Soc. Rev.* 41, 6259.
- Wiedensohler, A., Birmili, W., Nowak, A., Sonntag, A., Weinhold, K., Merkel, M., Wehner, B., Tuch, T., Pfeifer, S., Fiebig, M., Fjåraa, A.M., Asmi, E., Sellegri, K., Depuy, R., Venzac, H., Villani, P., Laj, P., Aalto, P., Ogren, J.A., Swietlicki, E., Williams, P., Roldin, P., Quincey, P., Hüglin, C., Fierz-Schmidhauser, R., Gysel, M., Weingartner, E., Riccobono, F., Santos, S., Gröning, C., Faloon, K., Beddows, D., Harrison, R., Monahan, C., Jennings, S.G., O'Dowd, C.D., Marinoni, A., Horn, H.G., Keck, L., Jiang, J., Scheckman, J., McMurry, P.H., Deng, Z., Zhao, C.S., Moerman, M., Henzing, B., de Leeuw, G., Löschau, G., Bastian, S., 2012. *Atmos. Meas. Tech.* 5, 657.
- Yee, L.D., Craven, J.S., Loza, C.L., Schilling, K.A., Ng, N.L., Canagaratna, M.R., Ziemann, P.J., Flagan, R.C., Seinfeld, J.H., 2013. *Atmos. Chem. Phys. Discuss.* 13, 10859.
- Zahradis, J., Petrucci, G.A., 2007. *Atmos. Chem. Phys.* 7, 1237.